

*A Study of Nitronyl and Imino Nitroxide
Radicals Attached to Heterocyclic Cores.
High Spin Building Blocks Towards
Organic Magnets.*

Dissertation zur Erlangung des Grades
„Doktor der Naturwissenschaften“
am Fachbereich Chemie und Pharmazie
der Johannes Gutenberg-Universität in Mainz

vorgelegt von

Giorgio Zoppellaro
geb. in Cassano Magnago, Italien

Mainz, 19.11.2004

Dekan: Herr Prof. Dr. R. Zentel

1. Berichterstatter: Herr Prof. Dr. K. Müllen

2. Berichterstatter: Herr Prof. Dr. H. Meier

Tag der mündlichen Prüfung: 19.11. 2004

Die vorliegende Arbeit wurde in der Zeit von November 2001 bis September 2004 am Max-Planck-Institut für Polymerforschung in Mainz unter Anleitung von Herrn P.D. Dr. M. Baumgarten und Herrn Prof. Dr. K. Müllen durchgeführt.

Non chiederci la parola che squadri da ogni lato
l'animo nostro informe, e a lettere di fuoco
lo dichiari e risplenda come un croco
perduto in mezzo a un polveroso prato.
Ah l'uomo che se ne va sicuro,
agli altri ed a se stesso amico,
e l'ombra sua non cura che la canicola
stampi sopra uno scalcinato muro!
Non domandarci la formula che mondi possa aprirti,
sì qualche storta sillaba e secca come un ramo.
Codesto solo oggi possiamo dirti,
ciò che non siamo, ciò che non vogliamo.

Eugenio Montale, *Ossi di seppia*, 1923
1975 Nobel Laureate in Literature

Zusammenfassung

Stabile organische Radikale mit zusätzlichen Funktionalitäten wie Donor/Akzeptor Eigenschaften und Ligandeneignung für Übergangsmetallkomplexierung repräsentieren eine synthetische Herausforderung beim Streben nach der Konstruktion hochdimensionaler heterospin Strukturen. In diesem Hinblick wurden acht neue Hochspinbiradikal-Moleküle zusammen mit ihren Monoradikal- Pendanten in dieser Arbeit hergestellt. Die Wahl der Liganden als organische Distanzhalter der Radikaleinheiten wurde auf stickstoffhaltige Heterozyklen (Pyridin und Pyrazol) gelenkt. Diese wurden weiterhin mit den stabilen Spinträgern Nitronylnitroxid- (NN) und Iminonitroxidfragmenten (IN) dekoriert. Ihre Synthese beinhaltete mehrstufige Umsetzungen (Brominierung, Iodierung, N- und Carbaldehyd Schutzgruppen, Stille-Kupplung, Grignard Reaktion, etc.) um die Mono- und Dicarbaldehyd-heterocyclenderivate als Schlüsselvorläufer der Radikaleinheiten zu gewinnen. Die Carbaldehyd-Zwischenstufen wurden Kondensationsreaktionen mit 2,3-Dimethyl-2,3-bis(hydroxylamino)-butan unterworfen (üblicherweise in Dioxan unter Argon für ~ 7 Tage), gefolgt von der Oxidation der Bis-hydroxylimidazolidin-Vorläufer unter Phasentransferkatalyse ($\text{NaIO}_4/\text{H}_2\text{O}$). Die Radikalmoleküle wurden mit verschiedenen spektroskopischen Methoden untersucht (FT/IR, UV/Vis/ EPR etc.) und ihre Einkristalle mit Röntgenstrahlbeugung gemessen. Die UV/VIS- Lösungsspektren zeigten in einem breiten Bereich verschiedener Lösungsmittelpolaritäten keine spezifische Wechselwirkung zwischen Lösungsmittel und Radikaleinheit, während ihre Stabilitäten in protischen Lösungsmitteln wie MeOH stark abnahmen. Als Pulver konnten sie jedoch im Kühlschrank an der Luft für eine Jahr gelagert werden, ohne sich zu zersetzen. Die spektroskopischen Fingerabdrücke der Radikale wurden eindeutig identifiziert und erschienen stark abhängig vom Typ des π -Ringsystems an das die Spinträger gekoppelt wurden. Basierend auf diesen Informationen wurde ein schnelles Protokoll etabliert, das eine direkte Zuordnung der Art der Radikale und ihrer Anzahl ermöglicht, sowie ihre Reinheit und Verunreinigungen zu definieren. In Lösung bestätigte die Analyse der EPR Spektren der Biradikale die starke Austauschwechselwirkung J zwischen den Radikalfragmenten über die Kopplungseinheiten ($J \gg a_n$, a_n ist die Stickstoffhyperfinekopplungskonstante). Dies wurde weiter unterstützt durch die Beobachtungen in gefrorener Lösung über die Nullfeldaufspaltungen und verbotenen Halbfeldübergänge ($\Delta m_s = 2$). Die Temperaturabhängigkeiten der $\Delta m_s = 2$ - EPR Signale wurden bis herunter auf 4 K gemessen und das exakte Vorzeichen und die Größe von J ermittelt. Diese Arbeit unterstreicht die Möglichkeit über synthetische Chemie eine Feineinstellung der „through bond“ Austauschwechselwirkung zwischen verwandten π - und σ - konjugierten Heterozyklen zu erreichen, in denen der $S = 1$ Grundzustand angenommen wird. Zusätzlich zeigten diese Resultate, dass die Übertragung der Spinpolarisation durch verschiedene Koppler sehr effektiv war.

Abstract

Stable organic radicals with additional functionalities such as donor/acceptor properties and ligand capabilities to transition metal ions represent a synthetic challenge in the quest of constructing highly dimensional heterospin structures. In this frame, eight novel high spin biradical systems were prepared in this work, together with their monoradical counterparts. The choice of the ligands, as organic spacer for the radical entities, was directed towards nitrogen containing heterocycles (pyridine and pyrazole). Those were further decorated with the stable spin carrier's nitronyl nitroxide (NN) and imino nitroxide fragments. Their synthesis involved multi-step procedures (bromination, iodination, N- and carbaldehyde protecting groups, Stille coupling, Grignard reaction, etc.) in order to assemble the mono and bis-carbaldehyde hetero-derivatives, the key precursors for the radical entities. Such intermediates were subjected to condensation reaction with 2,3-dimethyl-2,3-bis(hydroxylamino)-butane (generally in dioxane under argon for ~ 7 days), followed by oxidation of the bis-hydroxyimidazolidyn precursor under phase transfer conditions ($\text{NaIO}_4 / \text{H}_2\text{O}$). The radical molecules were studied using different spectroscopic techniques (FT/IR, UV/Vis, EPR) and on the single crystals, by X-ray diffractions. The UV/Vis solution spectra witnessed no specific interaction between solvent and radical moieties, in a broad range of solvent polarities, while their stabilities strongly decreased in protic solvents, especially in THF and methanol. As powders, however, they could be stored in cold under air for a year without decomposition. The spectroscopic fingerprints of the radical entities were unambiguously identified and appeared strongly dependent on the type of π -ring system in which the spin carriers were attached to. Based on these information's, a quick protocol was established that allowed to assign straightforwardly the type of radical and their numbers (monoradical, biradical), to define their purities and the nature of the contaminants. In solution, the EPR analysis in the biradical systems confirmed the strong exchange interaction, J , between the radical fragments through the couplers ($J \gg a_N$, with a_N the nitrogen hyperfine interaction), further supported by the observation in frozen state of both zero-field-splitting (zfs) and forbidden half-field transitions ($\Delta m_s = 2$). These findings were consistent with dipolar couplings accounting for $S = 1$ state species. The temperature dependencies of the $\Delta m_s = 2$ EPR signals were followed down to cryogenic temperature (4 K), and the exact sign and magnitude of J were derived. This work underlined the opportunity *via* synthetic chemistry to fine tune the through-bond exchange interaction among closely related π - and σ -conjugated hetero-systems, in which the $S = 1$ ground state were preferentially adopted. In addition, these results showed that the propagation of the spin polarization were effective through different couplers. Therefore those constitute unprecedented findings as compared with the limited number of similar systems known in literature in which no comparable effects were observed.

Table of Contents

Chapter 1- Prelude	p.1
1.1. Organic molecular magnetism.	p.1
1.2. Anticipated properties of organic magnetic materials, <i>pros</i> and <i>cons</i> .	p.2
1.3. Classes of organic magnetic molecules, their design and thesis objectives.	p.2
References.	p.6
Chapter 2- Synthesis of Pyridine and Pyrazole containing Radicals	p.11
2.1. Pyridine containing radicals.	p.12
2.2. Pyrazolopyridine containing radicals.	p.25
References.	p.46
Chapter 3- The Radical's Optical Properties	p.49
3.1. The UV/Vis absorption spectra of the radical systems.	p.49
3.2. Theoretical predictions of the UV/Vis absorption spectra in the biradical systems.	p.53
3.3. The IR absorption spectra of the radicals.	p.58
Chapter 4- EPR Analysis	p.62
4.1. The EPR analysis of monoradical systems in solution.	p.62
4.2. The EPR of biradical systems in solution.	p.69
4.2.1 The spectral EPR analysis of the biradical systems in solution.	p.72
4.2.2 The determination of thermally activated spin-states in the biradical systems.	p.74
4.3. The observed EPR spectra of the π - conjugated biradicals in solution.	p.75
4.4. The EPR spectra of the σ - conjugated biradicals in solution.	p.82
4.5. The EPR of mono and biradical systems in frozen solutions.	p.85
4.6.1 The observed EPR spectra of the monoradical systems in frozen solutions.	p.87
4.6.2 The observed EPR spectra of the biradical systems in frozen solutions.	p.88
4.7. The EPR saturation behaviour of mono and biradical systems in frozen solutions.	p.92
4.8. Determination of the electronic ground state in the magnetically dilute biradical systems.	p.96
4.8.1. The terpyridine based biradicals.	p.96
4.8.2. The bispyrazolopyridine based biradicals.	p.99

Table of Contents

4.8.3. The pyrazolylbipyridine based biradicals.	p.101
4.8.4. The σ - conjugated biradicals.	p.102
4.9. Conclusion.	p.102
References.	p.108
Chapter 5- Crystal Structures of the Radicals	p.111
5.1. The structure of 5,5''-bis(1-oxyl-3-oxo-4,4,5,5-tetramethyl-imidazolidin-2-yl)2,2':6',2''-terpyridine (12) and the supramolecular π -stacking chain formation.	p.111
5.2. The structure of 2,6-bis[4'-(3-oxide-1-oxyl-4,4,5,5-tetramethylimidazolin-2-yl)pyrazol-1'-yl]-pyridine (26) and the zig-zag chain formation.	p.114
5.3. The structure of 4'',5'-bis[3-oxide-1-oxyl-4,4,5,5-tetramethylimidazolin-2-yl]-6-(pyrazol-1''yl)-2,2'-bipyridine (33) and the dimers formation.	p.116
5.4. The structure of 6-bromo-5'[3-oxide-1-oxyl-4,4,5,5-tetramethylimidazolidin-2-yl]-2,2'-bipyridine (8) and the dimers formation.	p.117
5.5. Conclusion.	p.118
Chapter 6- Summary and Outlook	p.120
Chapter 7- Experimental Session	p.126
7.1. Materials and Methods.	p.126
7.2. Data treatment.	p.127
7.2.1. Synthesis of 6-bromo-3-pyridinecarbaldehyde (1).	p.128
7.2.2..Synthesis of 2-bromo-5-[1,3]dioxolan-2-yl-pyridine (2).	p.129
7.2.3. Synthesis of 2-tributylstannyl-5-[1,3]dioxolan-2-yl-pyridine (3).	p.130
7.2.4. Synthesis of 2-tributylstannyl-6-bromopyridine (4).	p.130
7.2.5. Synthesis of 6'-bromo-[2,2]'-dipyridinyl-5'-carbaldehyde (5).	p.131
7.2.6. Synthesis of 2,3-dimethyl-2,3-bis(hydroxylamino)-butane (6).	p.132
7.2.7. Synthesis of 6-bromo-5'[1,3-dihydroxy-4,4,5,5-tetramethylimidazolidin-2-yl]-2,2'-bipyridine (7).	p.133
7.2.8. Synthesis of 6-bromo-5'[3-oxide-1-oxyl-4,4,5,5-tetramethylimidazolidin-2-yl]-2,2'-bipyridine (8).	p.134
7.2.9. Synthesis of 6-bromo-5'[1-oxyl-4,4,5,5-tetramethylimidazolidin-2-yl]-2,2'-bipyridine (9).	p.134
7.2.10. Synthesis of 5, 5''-diformyl-2,2':6',2'' terpyridine (10).	p.135
7.2.11.Synthesis of 5,5''-bis(1,3-dihydroxy-4,4,5,5-tetramethylimidazolidin-2-yl)2,2':6',2''-terpyridine (11).	p.136

Table of Contents

7.2.12. Synthesis of 5,5''-bis(1-oxyl-3-oxo-4,4,5,5-tetramethylimidazolidin-2-yl)2,2':6',2''-terpyridine (12).	p.137
7.2.13. Synthesis of 5,5''-bis(1-oxyl-4,4,5,5-tetramethylimidazolidin-2-yl)2,2':6',2''-terpyridine (13).	p.138
7.2.14. Synthesis of triformylmethane (14).	p.139
7.2.15. Synthesis of 4-formyl-1(H)-pyrazole (15)(Method A).	p.139
Synthesis of 4-formyl-1(H)-pyrazole (Method B).	p.140
7.2.16. Synthesis of 4-iodo-pyrazole (16).	p.140
7.2.17. Synthesis of 1-(1-ethoxyethyl)-4-iodo-pyrazole (17).	p.141
7.2.18. Synthesis of 4-formyl-1(H)-pyrazole (18).	p.141
7.2.19. Synthesis of 2,6-bis(4'-formylpyrazol-1'-yl)-pyridine (19).	p.142
7.2.20. Synthesis of 2,6-bis-pyrazol-1-yl-pyridine (20).	p.143
7.2.21. Synthesis of 2,6-bis-(4-iodo-pyrazol-1-yl)-pyridine (21).	p.144
7.2.22. Synthesis of 2,6-bis-(4-bromo-pyrazol-1-yl)-pyridine (22).	p.145
7.2.23. Synthesis of 2,6-bis-(4-trimethylsilamylethynyl-pyrazol-1-yl)-pyridine (23).	p.146
7.2.24. Synthesis of 2,6-bis-(4-ethynyl-pyrazol-1-yl)-pyridine (24).	p.147
(See 7.2.19) Synthesis of 2,6-bis(4'-formylpyrazol-1'-yl)-pyridine by Grignard reaction.	p.148
7.2.25. Synthesis of 2,6-bis[4'-(1,3-dihydroxy-4,4,5,5-tetramethylimidazolidin-2-yl)pyrazol-1'-yl]-pyridine (25).	p.148
7.2.26. Synthesis of 2,6-bis[4'-(3-oxide-1-oxyl-4,4,5,5-tetramethylimidazolin-2-yl)pyrazol-1'-yl]-pyridine (26).	p.149
7.2.27. Synthesis of 2,6-bis[4-(1-hydroxy-4,4,5,5-tetramethylimidazolin-2-yl)pyrazolyl]-pyridine (27).	p.149
7.2.28. Synthesis of 2,6-bis[4-(1-oxyl-3-4,4,5,5-tetramethylimidazolin-2-yl)pyrazolyl]-pyridine (28).	p.150
7.2.29. Synthesis of 2-bromo-6-hydrazinopyridine (29).	p.151
7.2.30. Synthesis of 6-bromo-2-[4'-formylpyrazol-1'-yl]-pyridine (30).	p.151
7.2.31. Synthesis of 6'-(4-formyl-pyrazol-1-yl)-[2,2']-bipyridinyl-5-carbaldehyde (31).	p.152
7.2.32. Synthesis of 4'',5'-bis[1,3-dihydroxy-4,4,5,5-tetramethylimidazolidin-2-yl]-6-(pyrazol-1''-yl)-2,2'-bipyridine (32).	p.153
7.2.33. Synthesis of 4'',5'-bis[3-oxide-1-oxyl-4,4,5,5-tetramethylimidazolin-2-yl]-6-(pyrazol-1''-yl)-2,2'-bipyridine (33).	p.154
7.2.34. Synthesis of 4'',5'-bis[1-oxyl-4,4,5,5-tetramethylimidazolin-2-yl]-6-(pyrazol-1''-yl)-2,2'-bipyridine (34).	p.155
7.2.35. Synthesis of 2-(4-formylpyrazolyl)pyridine (35).	p.155
7.2.36. Synthesis of 2[4-(1-hydroxy-3-oxyl-4,4,5,5-tetramethylimidazolin-2-yl)pyrazolyl]-pyridine (36).	p.156

Table of Contents

7.2.37. Synthesis of 2[4-(1-oxide-3-oxyl-4,4,5,5-tetramethylimidazolin-2-yl)-pyrazolyl]-pyridine (37).	p.157
7.2.38. Synthesis of 2[4-(1-oxyl-4,4,5,5-tetramethylimidazolin-2-yl)pyrazolyl]-pyridine (38).	p.157
7.2.39. Synthesis of 2,6-bis(4-formylpyrazolylmethyl)pyridine (39).	p.158
7.2.40. Synthesis of 2,6-bis[4-(1,3-dihydroxy-4,4,5,5-tetramethylimidazolidin-2-yl)-pyrazolylmethyl]-pyridine (40).	p.159
7.2.41. Synthesis of 2,6-bis[4-(1-oxyl-3-oxide-4,4,5,5-tetramethylimidazolin-2-yl)-pyrazolylmethyl]-pyridine (41).	p.159
7.2.42. Synthesis of 2,6-bis[4-(1-oxyl-4,4,5,5-tetramethylimidazolin-2-yl)pyrazolylmethyl]-pyridine (42).	p.160
Acknowledgements	p.161
Curriculum Vitae	p.162

List of Symbols

$ \psi(0) ^2$ – Unpaired electron density at the nucleus	a - Hyperfine coupling
\mathbf{A} - Hyperfine splitting tensor	a_H - Proton hyperfine splitting
a_{iso} - Isotropic hyperfine splitting (Fermi contact term)	a_N - Nitrogen hyperfine splitting
c - Concentration	C - Curie constant
d - Distance	
D - Zero-field-splitting	DI- Double Integrated EPR signal intensity
\mathbf{g} - g tensor	g_e - Electron g factor
g_n - Nuclear g factor	h - Plancks constant
H - magnetic field strength	\hat{H} - Spin Hamiltonian
$\hat{\mathbf{I}}$ - Nuclear spin operator	I - Nuclear spin quantum number
J - Spin-spin exchange coupling energy	J - Total angular momentum
K_B - Boltzmann constant	L/G - Lorentzian- Gaussian ratio
\mathbf{m} - Distance vector	M - Magnetization
M_I - Nuclear spin quantum number	M_s - Electron spin quantum number
N_A - Avogadro's number	\mathbf{r} - Distance between two atoms
$\hat{\mathbf{S}}$ - Electron spin operator	S - Spin quantum number
T - temperature	T_c - Curie temperature
β_e - Bohr Magneton	β_n - Nuclear Magneton
ΔB_{PP} - Difference in peak to peak width	ΔE - Difference in energy
ΔE_{ST} - Singlet-Triplet energy difference	$\Delta \nu$ - Frequency shift in wavenumber
ε - Extinction coefficient	Θ - Torsional angle
Θ - Weiss constant	μ_{eff} - Effective magnetic moment
ν - Frequency	ρ - Spin density of electron
χ_M - Molar susceptibility	χ - Susceptibility

List of Abbreviations

Å - Armstrong	AF – Antiferromagnetic coupler
AO - Atomic orbital	b.p. - Boiling point
cm - Centimeter	CW - Continuous wave
CHCl_3 - Chloroform	CH_2Cl_2 - Dichloromethane
DMF - Dimethylformamide	ENDOR – Electron nuclear double resonance
EPR - Electron paramagnetic resonance	FC - Ferromagnetic coupler
g - gram	h - Hour
<i>hfc</i> - Hyperfine coupling	IN - Iminonitroxide
IR - Infrared	m.p. - Melting point
MeOH - Methanol	min - Minute
MO - Molecular orbital	mol - Mole
mW - MilliWatt	NN - Nitronylnitroxide
nm - Nanometer	NMR - Nuclear magnetic resonance
RT - Room temperature	THF - Tetrahydrofuran
TLC - Thin layer chromatography	UV/Vis - Ultraviolet/visible
<i>zfs</i> - Zero-field-splitting	

Table of Contents

Table I

Conversion factors (EPR)

dB	μWatt	$\sqrt{\mu\text{Watt}}$	dB	μWatt	$\sqrt{\mu\text{Watt}}$
40	20.1	4.4833	23	1010	31.7805
39	25.3	5.02991	22	1270	35.63706
38	31.9	5.64801	21	1600	40
37	40	6.32456	20	2000	44.72136
36	50.4	7.0993	19	2530	50.29911
35	63.6	7.97496	18	3180	56.39149
34	80	8.94427	17	4000	63.24555
33	101	10.04988	16	5040	70.99296
32	127	11.26943	15	6350	79.68689
31	160	12.64911	14	8010	89.4986
30	201	14.17745	13	10100	100.49876
29	250	15.81139	12	1270	35.63706
28	320	17.88854	11	16000	126.49111
27	400	20	10	20100	141.77447
26	510	22.58318	9	25300	159.05974
25	640	25.29822	8	31800	178.32555
24	800	28.28427	7	40100	200.24984
		--	6	50400	224.49944
dB	μWatt	$\sqrt{\mu\text{Watt}}$	dB	μWatt	$\sqrt{\mu\text{Watt}}$

Table II

Conversion factors for Energy Units

	cm^{-1}	MHz	aJ	eV	kJ/mol	kcal/mol	K (Kelvin)
cm^{-1}	1	2.997925×10^4	1.986447×10^{-5}	1.239842×10^{-4}	1.196266×10^{-2}	2.85914×10^{-3}	1.438769
MHz	3.33564×10^{-5}	1	6.626076×10^{-10}	4.135669×10^{-9}	3.990313×10^{-7}	9.53708×10^{-8}	4.79922×10^{-5}
aJ	50341.1	1.509189×10^9	1	6.241506	602.2137	143.9325	7.24292×10^4
eV	8065.54	2.417988×10^8	0.1602177	1	96.4853	23.0605	1.16045×10^4
kJ/mol	83.5935	2.506069×10^6	1.660540×10^{-3}	1.036427×10^{-2}	1	0.239006	120.272
kcal/mol	349.755	1.048539×10^7	6.947700×10^{-3}	4.336411×10^{-2}	4.184	1	503.217
K (Kelvin)	0.695039	2.08367×10^4	1.380658×10^{-5}	8.61738×10^{-5}	8.31451×10^{-3}	1.98722×10^{-3}	1

Chapter 1 - Prelude

It was in 1856 when W. H. Perkin discovered his famous colorant “mauvein” serendipitously [1], and since then organic compounds have played an important role in industrial and material chemistry [2], especially in the field of dyes [3] and pigments [4]. However, it was only after 1950 that in some organic compounds normally having insulating properties, electrons have been found to have conducting properties [5], i.e., several kinds of organic semi-conductors, conductors and even superconductors have been discovered and developed [6]. Compared with the advances in organic conducting materials, the more recent development of organomagnetic materials is rather similar in the sense that even the most sophisticated properties can be rationally designed by a systematic modification of the organic molecular structures. The notion of organomagnetic materials showing metallic properties, such as electron conductivity and ferromagnetism [7], began several decades ago. The goal was to create an assembly of organic molecules or macromolecules containing only light elements (C,H,N,O,S, etc.), and yet possessing the electron/hole mobility or spin alignment that is inherent to metals or their oxides.

1.1. Organic molecular magnetism.

The progresses towards obtaining organomagnetic materials have been triggered by the advance in the chemistry of organic radicals [8]. With the notation of “organic radical”, we refer to molecules that contain “unpaired” electrons, each one formally associated with different atomic centers in the isolated molecular unit. In order to achieve magnetic properties in these organic molecules, it is necessary to obtain cooperative interactions among their unpaired electrons, i.e. to keep the unpaired spins parallel to each other. However, the control of such long-range spin interactions turned out to be extremely hard to accomplish [9]. It is consequently not surprising that only a decade or so has passed since high-spin molecules with parallel spin alignment in the bulk have been developed, although the theoretical possibility of organic based magnetic materials was suggested as early as 1963 [10], when McConnell proposed through-space models for building up bulk ferromagnetic interactions among spin carriers. As originally postulated, the assemble of such long range interactions among spin carriers consist of the following sequence of events: (1) the design of the isolated molecular unit, with one, two, or more already interacting entities; (2) a large molecule with several interacting entities; (3) mesoscopic-size molecules with added complexities; and (4) assembly of molecules to supramolecular clusters, monomolecular layers, or bulk solids. The goals of such an approach through rational design and synthesis of molecules and molecular

assemblies, are to prepare either materials with superior properties compared to their existing “natural” or artificial counterparts, or to gain better insight to more complex systems [11]. From the preparative organic chemist’s perspective, the first point is crucial. This implies the research of novel spin-containing building blocks (i.e. free radicals and radical ions) and the definition of their exchange coupling. These issues are addressed in this work.

1.2. Anticipated properties of organic magnetic materials, *pros* and *cons*.

The first application would be the replacement of existing bulk magnets or magnetic recording devices. Values of the saturation magnetisation, M_s , for molecular organic based magnets are comparable to metallic magnets on a molar basis. The inherently large molecular weight (per magnetic moment) of organomagnetic material and their low density, however, result in a smaller saturation magnetisation on either a volume or a mass basis, i.e. the spin concentration is low. As a consequence, they feature lower magnetisations, small exchange energies (because of large interspin distances), and low temperature of transition (T_c , the Curie-temperature) to the ferromagnetic state. This means that organic magnets are unlikely to compare with existing magnets. Further disadvantages are the inherent chemical instability of many organic materials and their “aging” with time. They might offer, however, several advantages with respect to their inorganic counterparts: (1) organomagnetic materials are transparent in nature, therefore a variety of optical properties may be expected, i.e. photomagnetic switches and polarized light manipulation in integrated optical devices; (2) the biocompatibility of such materials may lead to application in magnetic imaging and transducers for medical implants; (3) tuning properties *via* organic chemistry, processability, low environmental contamination; (4) electronic/magnetic molecular devices for applications in modern computer technology.

Other than commercial opportunities, the future realization of the potential of organic ferromagnetism is significant from a basic point of view, in which extended ferromagnetic exchange interactions through s and p orbitals may provide a better insight into the phenomenon of magnetism, far beyond of being fully understood.

1.3. Classes of organic magnetic molecules, their design and thesis objectives.

Several spin carrying units are currently in active use towards building organic based magnets. Some examples are the nitronylnitroxide, NN, iminonitroxide, IN, tbutylnitroxide, NO, verdazyl radicals, VZ, carbenes, nitrenes, phenoxides, ArO, ketyl radicals, and triphenyl methyl radical, TPM. These spin units are shown together in Figure 1.1. However, NN, IN, NO, VZ constitute one of the rare classes of radicals capable being handled under ordinary

conditions on the laboratory bench, allowing their isolation and purification as stable substances. The choice of the spin carriers in this thesis was directed towards the NN and IN radical's type. They offer multiple opportunities such as H-bond formation, π -stacking, and even extension to mixed organic-inorganic hybrid structures, thanks to the chelating properties of both N and NO moieties that readily provide coordination sites for metal acetylacetonates.

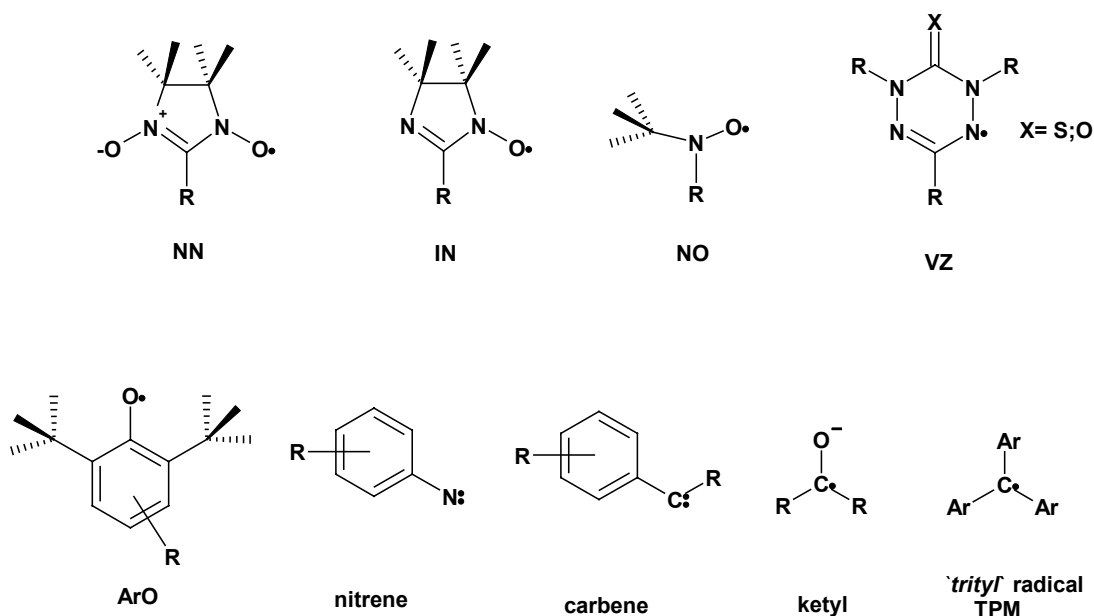
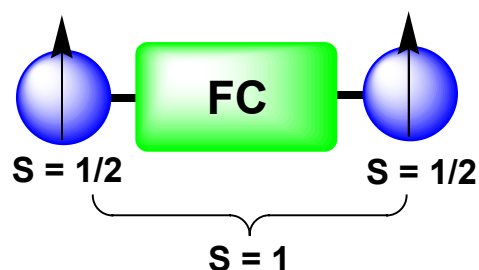


Figure 1.1: The most often encountered radical units used for organic molecular magnets.

For assembling a high spin molecule, the spin alignment in the organic compound must be arranged in such a way that interactions between the spins are allowed to be parallel (ferromagnetic, $S \geq 1$). This appears to work against nature, because organic compounds with unpaired electrons normally have a strong tendency to bind together with antiparallel spins (antiferromagnetic, $S=0$) or they do not interact at all, behaving as independent spin units. It is therefore necessary to use a "*ferromagnetic couple*" (FC) or spacer, which still allows interactions between two or more unpaired electrons but prevents their pairing [12].



Conceptually, the interactions among unpaired spins can be regarded as the fine balance of three physical mechanisms [13]:

- (i) direct coupling;
- (ii) indirect coupling;
- (iii) spin polarisation.

The design of the molecular backbone allows to decrease the effect of direct coupling, and to tune the indirect coupling (so called through-bond interaction), upon choosing the type of bonds involved (connectivity) and molecular topology. Then, the nature of the radical defines the strength of the spin polarisation contribution [14].

The endeavour of chemists *via* synthetic design would be, in principle, to gain full control of these three factors. In reality, the most used synthetic tool to accomplish a high spin molecule relies on shaping at least the through-bond interaction between/among unpaired spins, leading to so called non-Kekulé structures, as in *m*-xylene, where no double bond between the unpaired electrons can possibly be formed (Figure 1.2A). The *p*- and *o*-xylene, in contrast, allow spin pairing toward the more stable quinoid structures in the Kekulé forms as shown in Figure.1.2 B, and therefore the low spin state ($S = 0$) might be expected.

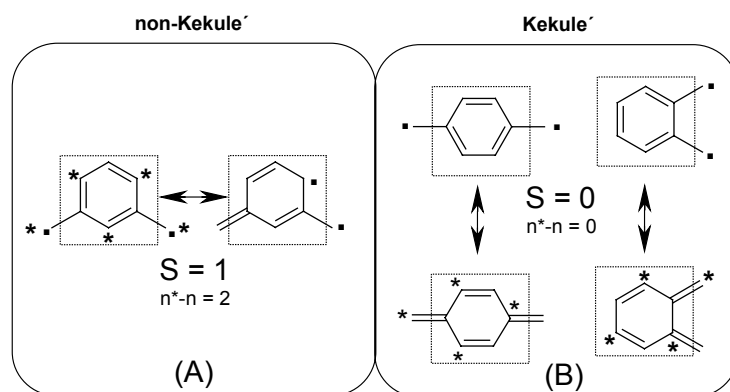


Figure 1.2. non-Kekulé versus Kekulé structures.

In case of *m*-xylene (non-Kekulé), the ground state is thought to be a triplet ($S = 1$). This is due to the presence of degenerate non-bonding molecular orbitals (NBMOs) of a non-disjoint type. In 1950, Longuet-Higgins [16a] proposed a rule, the topological model, to predict the ground spin state in a π -conjugated molecule on the basis of the Hund's rule. This relation is given by equation (1),

$$[n\text{NBMO} = (N-2T); S = 0.5 (N-2T)] \quad (1)$$

Where, N is the number of π -centres and T the number of double bonds. Later, Ovchinnikov [16c] using valence bond theory and a Pariser-Parr-Pople Hamiltonian, proposed a different model (spin polarization). In this case, if the conjugated carbon framework can be divided in alternant “starred” n^* and “unstarred” n (spin polarized) centres, in such a way that each starred atom faces contacts with only unstarred ones, then through equation (2), and by counting half of the difference between n^* and n , the value of the net spin S in the system can be anticipated.

$$S = 0.5 (n^* - n) \quad (2)$$

Because the spin multiplicity is expressed as $2S+1$, the Ovchinnikov rule also predicts triplet ground state for non-Kekulé molecules. Following these approaches many high spin molecules connected by different FC units have been designed and synthesized [15]. Such theoretical guidelines [16], on the other hand, cannot be straightforwardly extended neither to hetero-systems containing radicals (like in NN and IN) and couplers, nor clearly to non-alternant systems (e.g. five member rings). In these cases, several factors such as the specific molecular geometry of the molecule [17], the nature and position of the substituents in the organic spacer [18], and the heteroatom influence [19] seem to influence strongly the ground spin state. To put this thesis work on molecular magnetism into perspective, and to address the other points raised in the introduction, namely how to arrange each single-unit into a supramolecular network [20], the choice of both radicals and type of couplers are therefore determinant. One possible approach to achieve such a goal was based on intermolecular interaction via H-bonding, or stacking among pure organic carriers, and this led to the attainment of bulk ferromagnetism (T_c) where the *p*-nitrophenyl-nitronyl nitroxide made in the Kinoshita group [21] and the 1,3,5,7-tetramethyl-2,6-diazaadamantane-*N,N'*-dioxyl by Rassat [22] represent two among other outstanding examples [23] (Figure 1.3 A and 1.3 B, respectively).

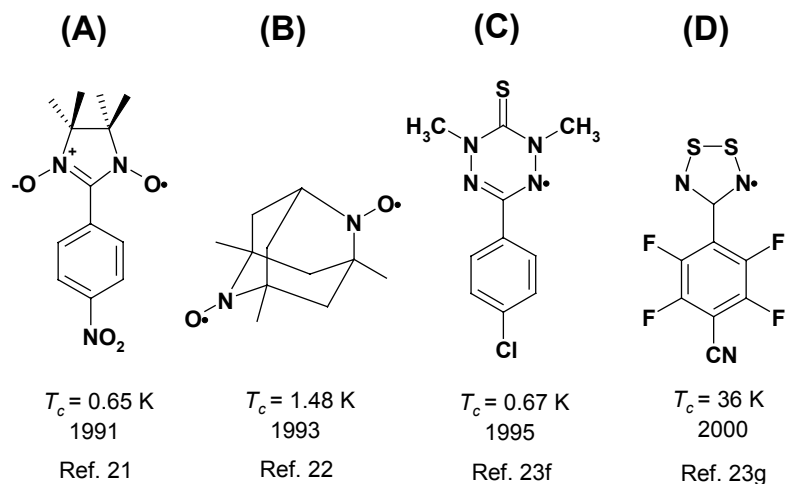


Figure 1.3: Examples of pure organic based magnets.

Another approach relies on the combination between paramagnetic metal ions and pure organic radicals, leading to a new class of hybrid organic-inorganic materials [24]. Two of such examples are shown in Figure 1.4 and 1.5.

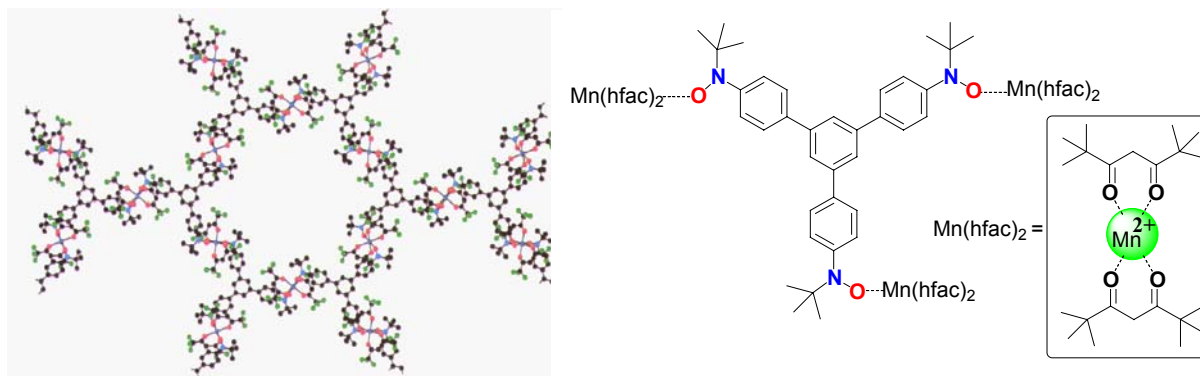


Figure 1.4: The Inoue and Iwamura's 2D honey-comb metallo-organic higher dimensional compound [Ref.24g].

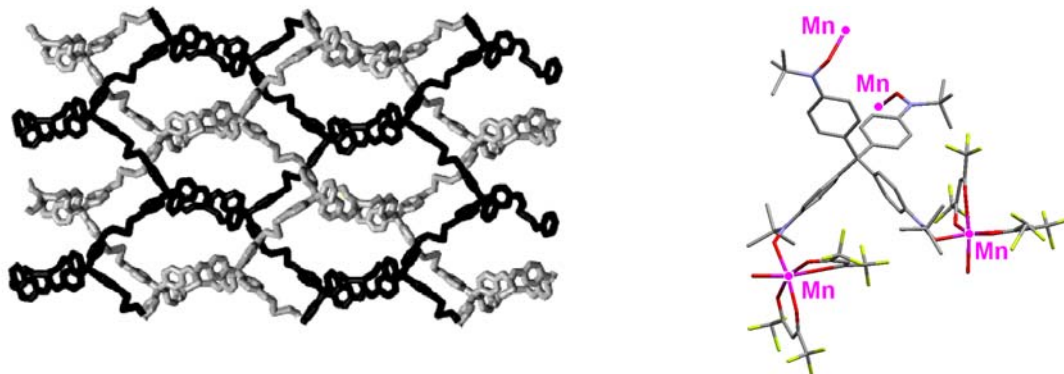


Figure 1.5: The Mathevet and Luneau's 3D polymeric metal-radical network [Ref.24h].

A note of caution should be made, nevertheless, about the prospects of purely organic molecular magnets. So far, despite much research effort, the highest T_c recorded is 36 K. There appears to be some barrier to high T_c s, and it is therefore likely that further progress can be made with a high-spin metal organic hybrid complex crystal or polymer. Therefore, the hybrid approach has been pursued within this research work, by making accessible novel synthetic routes towards chelating coupling unit cores (terpyridine, bipyridine, pyrazolopyridine), followed by their functionalisation with stable nitronyl- and iminonitroxide radical moieties.

Through this thesis, the reader will find in Chapter 2 the synthetic strategies towards such molecular entities, which in turn set up flexible routes for further extension on analogous heterosystems. Besides synthesis, the full characterization of the radical systems and their intermediates are needed. Therefore, a comprehensive study of their optical properties (absorption and IR spectroscopy) is given in Chapter 3. Some practical tools for assessing the precursor/radical fingerprints and their purities are provided. The Chapter 4 presents the whole EPR analysis of the monoradical and biradical systems. When more than one spin unit (i.e. biradicals) is connected to the organic core, the theoretical and experimental steps necessary to define their molecular ground state spin multiplicity are described in detail. Finally, in Chapter 5, the molecular structures of one monoradical and three biradical systems are analysed, together with a perspective of their supramolecular assemblies.

References

- [1] W.H. Perkin, Br. Pat., 1984, 1856.
- [2] K. Ziegler and G. Natta, *Nobel Lecture*, December 12, **1963**.
- [3] J. F. W. A. von Baeyer (**1905**), *Nobel Lecture, Chemistry, 1901-1921*, Elsevier Publishing Group, Amsterdam **1966**.
- [4] R. M. Willstätter (**1915**), *Nobel Lecture, Chemistry, 1901-1921*, Elsevier Publishing Group, Amsterdam **1966**.
- [5] (a) H. Shirakawa, E.J. Louis, A.G. MacDiarmid, C.K. Chiang, A.J. Heeger, *Chem. Commun.*, **1977**, 578. (b) C.K. Chiang, C.R. Jr. Fincher, Y. W. Park, A.J. Heeger, H. Shirakawa, E.J. Louis, *Phys. Rev Lett.*, **1977**, 39, 1098. (c) B. Rándy, In *Cojugated Polymers and Related Materials: The Interconnection of Chemical and Electronic Structures*, W.R Salaneck, I. Lündström, B. Rándy, Eds., Oxford University Press: Oxford, UK, **1993**, Chapter 3. (d) A.J. Heeger, *J. Phys. Chem. B*, **2001**, 36, 8475.
- [6] M. R. Bryce, *Chem. Soc. Rev.*, **1991**, 20, 355. (b) J. M. Williams, A.J. Schultz, U. Geiser, K. D. Carlson, A. M. Kini, H.H. Wang, W.-K. Kwok, M.-H. Whangbo, J. E. Sreiber, *Science*, **1991**, 252, 1501.
- [7] (a) H.K.J., Bushow, E.P. Wohlfart, *Ferromagnetic Materials*, Eds., North Holland: Amsterdam, **1980-1990**, Vols. 1-5. (b) K.H. Fisher, J.A. Hertz, *Spin Glasses*, Cambridge University Press: Cambridge, **1991**. (c) D.R. Tilley, J. Tilley, *Superfluidity and Superconductivity*, Hilger, Bristol, **1986**.
- [8] (a) G. Herzberg, *Nobel Lecture*, December 11, **1971**. (b) A. R. Forrester, J. M. Hay, R. H. Thomson, *Organic Chemistry of Stable Free Radicals*, Academic Press, New York, **1968**. (c) E. G. Rozantsev, *Free Nitroxyl Radicals*, Plenum Press, New York, **1970**. (d) E. G. Rozantsev, V. D. Sholle, *Synthesis* **1971**, 190, 401. (e) . Sayre, *J. Am. Chem. Soc.* **1955**, 77, 6689. (f) M. Lamchen, T. W. Mittag, *J. Chem. Soc.* **1966**, 2300. (g) E. F. Ullman, J. H. Osiecki, D.G.B. Boocock, *J. Am. Chem. Soc.* **1972**, 94, 7049. (h) J. F. W. Keana, *Chem. Rev.* **1978**, 78, 37; (i) L. B. Vordarsky, *Imidazoline Nitroxides*, CRC Press, Boca Raton, Florida, **1988**, Vol. I-II. (l) H. G. Aulich in *Nitrones, Nitronates and Nitroxides*, S. Patai and Z. Rappoport (Eds.) John Wiley and Sons, New York, **1989**, p. 313. (m) M.-E. Brik, *Heterocycles* **1995**, 41, 2827.
- [9] (a) O. Kahn, *Magnetism: A Supramolecular Function*, Eds., Kluwer, Dordrecht, **1996**. (b) J. S. Miller, M. Drillon, *Magnetism: Molecules to Materials III*, Wiley-VCH, Weinheim, **2001**. (c) J. S. Miller, M. Drillon, *Magnetism: Molecules to Materials I, II, IV*, Wiley-VCH, Weinheim, **2003**.
- [10] H. M. McConnell, *J. Chem. Phys.* **1963**, 39, 1916.
- [11] (a) J. S. Miller and A. Epstein, *Angew. Chem. Int. Ed.* **1994**, 106, 399. (b) S. Nakatsuji and H. Anzai, *J. Mat. Chem.* **1997**, 7, 2161. (c) J. A. Crayston, J. N. Devine, J. C. Walton, *Tetrahedron* **2000**, 56, 7829. (d) U. Hartmann, *Ann. Rev. Mat. Sci.*, **1999**, 29, 53. (e) R.J. Bushby, J.-P. Paillaud, *Introduction to Molecular Electronics*; M.C. Petty, M.R. Brice, D. Bloor,

- Eds., Edward Arnold: London, **1995**, Chapter 4. (f) J.A. Crayston, J. N. Devine, J.C. Walton, *Tetrahedron*, **2000**, 56, 7829.
- [12] P. Lafenete, J.J. Nova, M.J. Bearpark, P. Celani, M. Olivucci, M.A. Robb, *Theor. Chem. Acc.* **1999**, 102, 309.
- [13] (a) Y. Molin, K. M. Salikhov, K. I. Zamaraev, *Spin Exchange*, Springer Verlag, Berlin, **1980**, p.11. (b) E. Coronado, B. S. Tsukerblat, R. Georges, in: E. Coronado et al. (Eds), *Molecular Magnetism: From Molecular Assemblies to the Device*, NATO ASI Series E, vol. 321, **1996**, p. 65.
- [14] J. E. Wertz, J. R. Bolton, *Electron Spin Resonance, Elementary Theory and Practical Applications*, Chapman & Hall, **1986**.
- [15] (a) A. Calder, A.R. Forrester, P.G. James, G.R. Luckhurst, *J.Am.Chem.Soc.* **1969**, 91, 3724. (b) K. Inoue, H. Iwamura, *Angew.Chem.Int.Ed.* **1995**, 34, 927. (c) T. Ishida, H. Iwamura, *J.Am.Chem.Soc.* **1991**, 113, 4238. (d) F. Kanno, K. Inoue, N. Koga, H. Iwamura, *J.Phys. Chem.* **1993**, 97, 13267. (e) K. Inoue, H. Iwamura, *J.Am.Chem.Soc.* **1994**, 116, 3173. (f) T. Itoh, K. Matsuda, H. Iwamura, *Angew.Chem.* **1999**, 111, 1886. (g) T. Itoh, K. Matsuda; H. Iwamura, K. Hori, *J.Am.Chem.Soc.* **2000**, 122, 2567. (h) D. Shiomi, M. Tamura, H. Sawa, R. Kato, M. Kinoshita, *Synt.Met.* **1993**, 56, 3279. (i) L. Catala, P. Turek, J. Le Moigne, A. De Cian, N. Kyrisakas, *Tetrahedron Lett.* **2000**, 41, 1015. (j) F. Mathevet, D. Luneau, *J.Am.Chem.Soc.* **2001**, 123, 7465 - 7466.
- [16] (a) H. C. Longuet-Higgins, *J. Chem. Phys.* **1950**, 18, 265. (b) W. T. Borden, E. R. Davidson, *J. Am. Chem. Soc.* **1977**, 99, 4587. (c) A. A. Ovchinnikov, *Theor. Chim. Acta* **1978**, 47, 297. (d) P. M. Lahti, *Magnetic Properties of Organic Materials*, Marcel Dekker, New York, **1999**.
- [17] K. Okada, T. Imakura, M. Oda, M. Baumgarten, *J. Am. Chem. Soc.* **1996**, 118, 3047
- [18] (a) M. Dvornitzki, R. Chiarelli, A. Rassat, *Angew. Chem. Int. Ed. Engl.* **1992**, 31, 180. (b) F. Kanno, K. Inoue, N. Koga, H. Iwamura, *J. Am. Chem. Soc.* **1993**, 115, 847.
- [19] (a) A.P. Jr. West, S.K. Silverman, D.A. Dougherty, *J. Am. Chem. Soc.* **1996**, 118, 1452. (b) S.V. Chapyshev, R. Walton, J.A. Sanborn, P.M Lahti, *J. Am. Chem. Soc.* **2000**, 122, 1580-1588. (c) M. Rule, A.R. Matlin, D.E. Seeger, E.F. Hilinski, D.A. Dougherty, J.A. Berson, *Tetrahedron*. **1982**, 38, 787. (d) Y. Liao, C. Xie, P.M. Lahti, R.T. Weber, J. Jiang, D.P. Barr, *J. Org. Chem.* **1999**, 64 (14), 5176-5182.
- [20] (a) J. S. Miller, A. Epstein, W. M. Reiff, *Chem. Rev.* **1988**, 88, 201. (b) A. Rajca, *Chem. Rev.* **1994**, 94, 871. (c) J. S. Miller, *Inorg. Chem.* **2000**, 39,4392.(d) D. Luneau, *Curr. Op. in Sol. State Mat. Sci.* **2001**, 5, 123. (e) for a collection of the recent progresses in the field see *Proceedings of the 8th International Conference on Molecule-Based Magnets (ICMM 2002)*, *Polyhedron* **2003**, 22, 1725-2584.

- [21] M. Tamura, Y. Nakazawa, D. Shiomi, K. Nozawa, Y. Hosokoshi, M. Ishikawa, M. Takahashi, M. Kinoshita, *Chem. Phys. Lett.* **1991**, 186, 401.
- [22] R. Chiarelli, M. A. Novak, A. Rassat and J. L. Tholence, *Nature (London)* **1993**, 363, 147.
- [23] (a) T. Sugawara, M. M. Matsushita, A. Izuoka, N. Wada, N. Takeda, M. Ishikawa, *J. Chem. Soc. Chem. Commun.* **1994**, 1723. (b) J. Cirujeda, M. Mas, E. Molins, F. L. dePhantou, J. Laugier, J. G. Park, C. Paulsen, P. Rey, C. Rovira, J. Veciana, *J. Chem. Soc. Chem. Commun.* **1995**, 709. (c) J. Veciana, J. Cirujeda, C. Rovira, J. Vidal-Gancedo, *Adv. Mater.* **1995**, 7, 221. (d) A. Caneschi, F. Ferraro, D. Gatteschi, A. Ielirzin, M. A. Novak, E. Rentschler, R. Sessoli, *Adv. Mater.* **1995**, 7, 476. (e) Y. Pey, O. Kahn, M. A. Aebersold, L. Ouahab, F. LeBerre, L. Pardi, J. L. Tholence, *Adv. Mater.* **1994**, 6, 681. (f) K. Mukai, K. Konishi, K. Nedaki, K. Takeda, *J. Magn. Mater.*, 1995, 140, 1449. (g) P. Carretta, D. Gatteschi, A. Lascialfari, *Physica B.* **2000**, pp. 94-105.
- [24] (a) J. Cirujeda, L. E. Ochanko, J. M. Amigo, G. Rovira, J. Rius, J. Veciana, *Angew. Chem.* **1995**, 107, 99-102; *Angew. Chem. Int. Ed. Engl.* **1995**, 34, 55-57. (b) D. A. Shultz, S. H. Bodnar, K. E. Vostrikova, J. W. Kampf, *Inorg. Chem.* **2000**, 39, 6091-6093. (c) H. O. Stumpf, L. Ouahab, Y. Pei, D. Grandjean, O. Kahn, *Science* **1993**, 261, 447-449. (d) K. Inoue, T. Hayamizu, H. Iwamura, D. Hashizume, Y. Ohashi, *J. Am. Chem. Soc.* **1996**, 118, 1803. (e) G. Ballester, E. Coronado, C. Giménez-Saiz, F. Romero, *Angew. Chem.* **2001**, 113, 814. *Angew. Chem. Int. Ed. Engl.* **2001**, 40, 792. (f) K. Fegy, D. Luneau, T. Ohm, C. Paulsen, P. Rey, *Angew. Chem.* **1998**, 110, 1331. *Angew. Chem. Int. Ed. Engl.* **1998**, 37, 1270. (g) C. Benelli, D. Gatteschi, *Chem. Rev.* **2002**, 102, 2369. (h) K. Inoue, H. Iwamura, *J. Am. Chem. Soc.* **1994**, 116, 3173-3174. (i) F. Mathevet, D. Luneau, *J. Am. Chem. Soc.* **2001**, 123, 7465.

Chapter 2 - Synthesis of Pyridine and Pyrazole containing Radicals

Nitronyl (NN) and imino nitroxide (IN) free radicals were described in the 1970's by Ullman in his pioneering work [1-3], and since then they have attracted much attention with a revival in the 1990's. This increasing interest mainly stems from the use of these paramagnetic species as building blocks for designing molecular magnetic materials [4]. Successful achievements in this field such as purely organic ferromagnetically ordered solids and metal-organic exchange-coupled complexes that exhibit versatile magnetic properties have triggered the synthesis of hundreds of these free radicals [5]. The synthesis of nitronyl- and imino nitroxides relies almost exclusively [6] on the condensation of 2,3-bishydroxylamino-2,3-dimethylbutane [7a] with an aldehyde, and oxidation of the condensation product to afford the radical derivatives. However, from either the preparative synthetic and physical chemist's perspectives, the challenge is dual [8]. It consists not only on building carbaldehyde derivatives anywhere, but also to topologically control the position such that it allows ferromagnetic intramolecular interactions among the spin carriers through the organic backbone (coupling unit, **CU**). The synthetic choice for the coupling unit cores in this thesis were directed towards the synthesis of hetero-ligands based on terpyridines and pyrazolylpyridines. Both are known for their rich coordination chemistry [9] and have been used widely in supramolecular assemblies [10], in molecular biology [11] optical devices [12] spin-crossover compounds [13] and even in photochemistry [14]. Unfortunately substituted terpyridines and bispyrazolylpyridines [15] were limited by tedious multistep synthesis. In addition, carbaldehyde-functionalised pyridines and pyrazoles are overall the less known derivatives. In this 2nd Chapter are described the synthetic pathways that led to novel protocols for the nitronyl- and imino nitroxide radicals (**R**) attached to terpyridine, bispyrazolylpyridine and pyrazolylbipyridine cores as heterocyclic functional coupling unit (**CU**)(Figure 2.1).

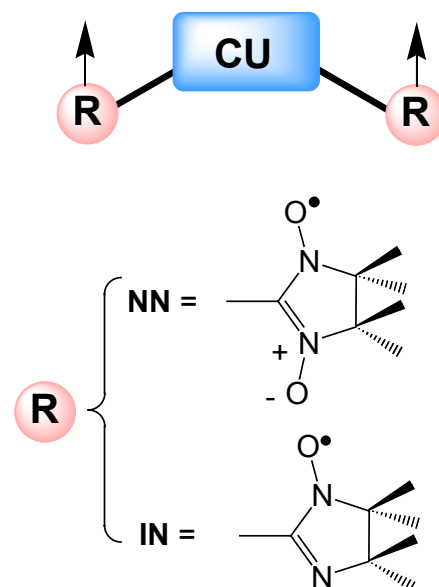
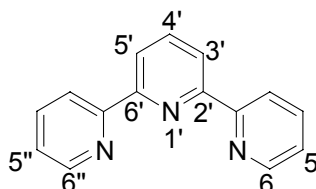


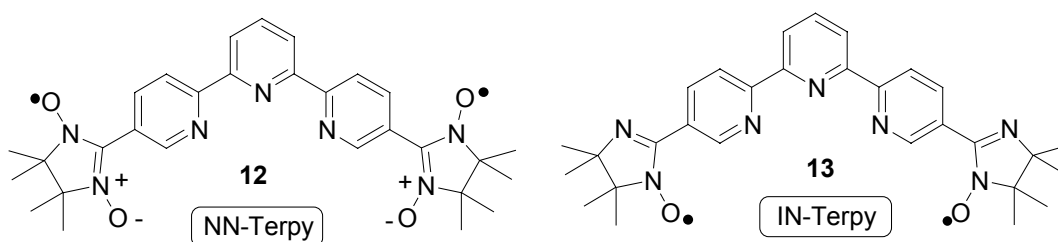
Figure 2.1: Schematic sketch of the heterocyclic functional coupling unit core (**CU**) functionalized with radical moieties (**R**).

2.1. Pyridine containing radicals

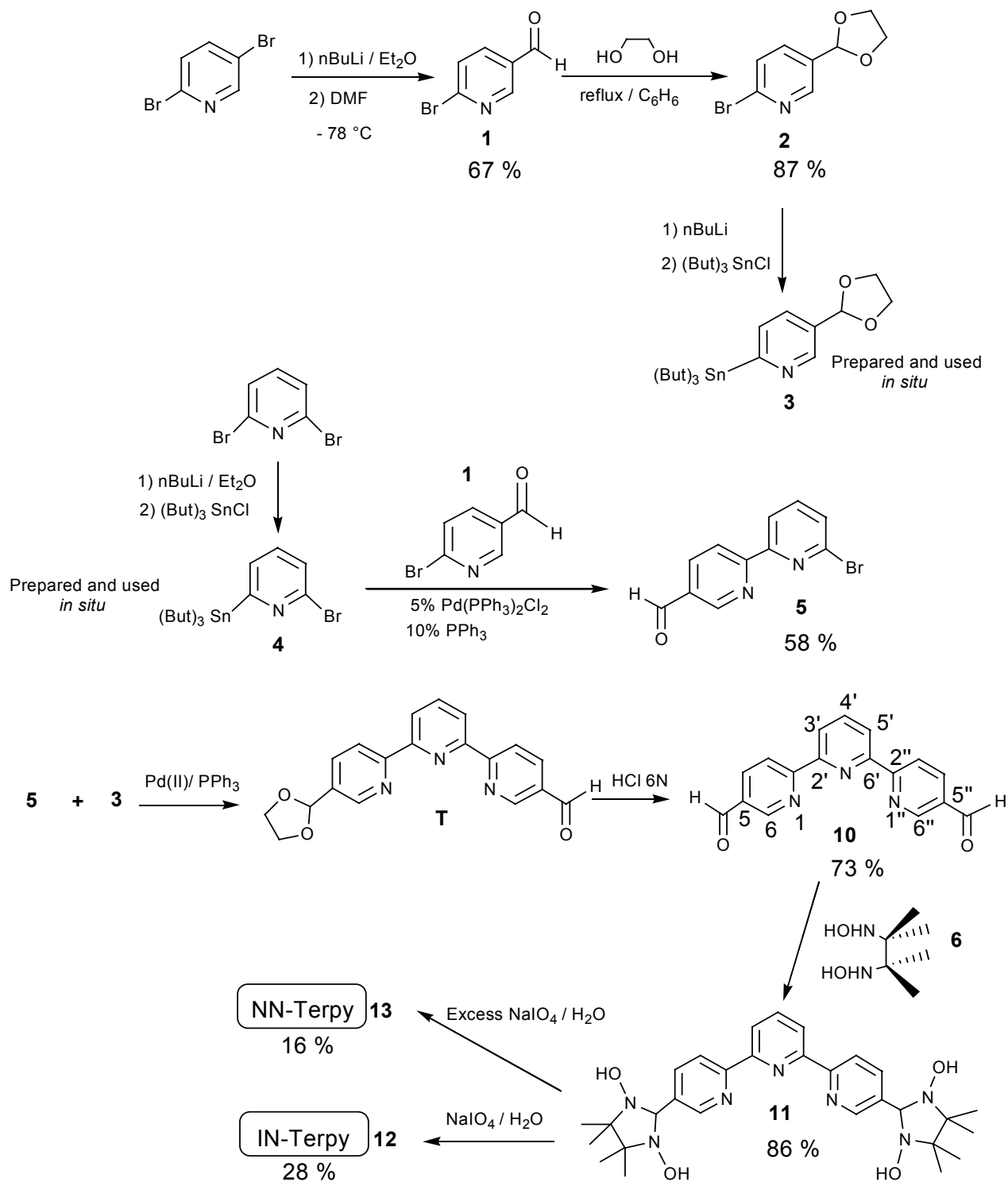
Only three terpyridine ligands bearing Ullman radicals were synthesized so far [16]. Those included functionalisations either in the positions 6-6'' of the terminal pyridine rings or in the 4' position of the central pyridine ring.



None of them showed to encompass a triplet ground state. Our target was to combine into the terpyridine core two Ullman radicals in position 5-5'' namely 5,5''-bis(1-oxyl-3-oxo-4,4,5,5-tetramethylimidazolin-2-yl)2,2':6',2''-terpyridine (**12**) and 5,5''-bis(1-oxyl-4,4,5,5-tetramethylimidazolin-2-yl)2,2':6',2''-terpyridine (**13**). In these positions the spin carriers would feature intramolecular ferromagnetic interaction with formation of triplet (S=1) ground state.

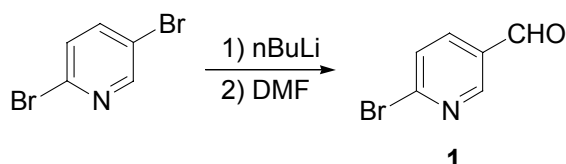


Two recent reports described the bis-carbaldehyde terpyridine **10** functionalised in 5-5'' [17], and both afforded the product in low amount (from 45 to 290 mg per run) after a multistep synthesis. We therefore searched for a different route that could leave open further synthetic extensions. The synthetic path is described in Scheme 2.1.



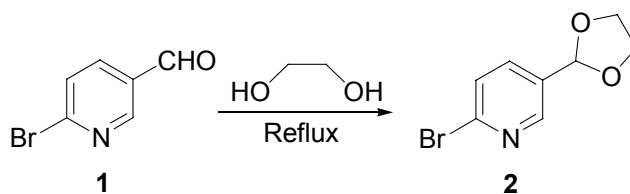
Scheme 2.1

The first step relies on building the 6-bromo-3-pyridinecarbaldehyde (**1**), starting from the commercially available 2,5-dibromo-pyridine. This bromo-derivative can be selectively mono-lithiated in position 5 upon working at -78°C using ether as reaction solvent (Scheme 2.2). The reaction in ether is heterogeneous, due to the poor solubility of the 2,5-dibromopyridine in this solvent at low temperature ($< 40^{\circ}\text{C}$). Nevertheless the lithium derivative is completely soluble at -78° . As reported in the short description found in literature [18], the two bromine groups in position 5 and 2 feature different reactivity towards lithium exchange. In particular the bromine in position 5 seems kinetically more reactive, while the bromine in position 2 is thermodynamically more stable. Thus, long aging of the reaction mixture with the lithiating agent should lead to substitution in 2, and short aging (< 60 min) should give major substitution in 5. As pointed out by the authors [18], also the solvent plays a role. Polar solvents (e.g. toluene) favor substitution in position 2, while apolar solvents favor substitution in position 5. Even though the authors suggested either ether or THF, several trials made by using THF or other solvents like glyme in which the starting material is far more soluble, led to much less overall yield. Also the concentration of the starting pyridine halide is important for achieving a successful reaction, and should be kept within 0.1-0.2 M. The quenching of the 5-lithio-2-bromo-pyridine with N-N-dimethylformamide (DMF) gave straightforwardly the corresponding 6-bromo-3-pyridinecarbaldehyde (**1**) (yield 67%) [19], after hydrolysis in NH_4Cl and chromatographic separation on silica column.



Scheme 2.2

The second step consisted in the protection of the carbaldehyde group in **1** (Scheme 2.3). It was easily achieved by formation of the correspondent dioxolane 2-bromo-5-[1,3]dioxolan-2-yl-pyridine (**2**) using toluene-4-sulfonic-acid as catalyst ($\text{CH}_3\text{C}_6\text{H}_4\text{SO}_3\text{H} \times \text{H}_2\text{O}$, 8% mol) with ethyleneglycole as protecting group. The benzene proved to be the best solvent for this reaction. The product **2** was obtained as yellowish oil that became solid on standing (yield 87%).



Scheme 2.3

Lehn and co-workers [19] suggested a different procedure for this reaction, using Amberlist-15 as acid catalyst (yield 82%), but without providing any synthetic explanation. In a later report they recommended a different protecting group based on propanediol and PPTS ($C_5H_5N^+HtsO^-$, yield 80%) [16b]. Our procedure might offer an easier alternative route.

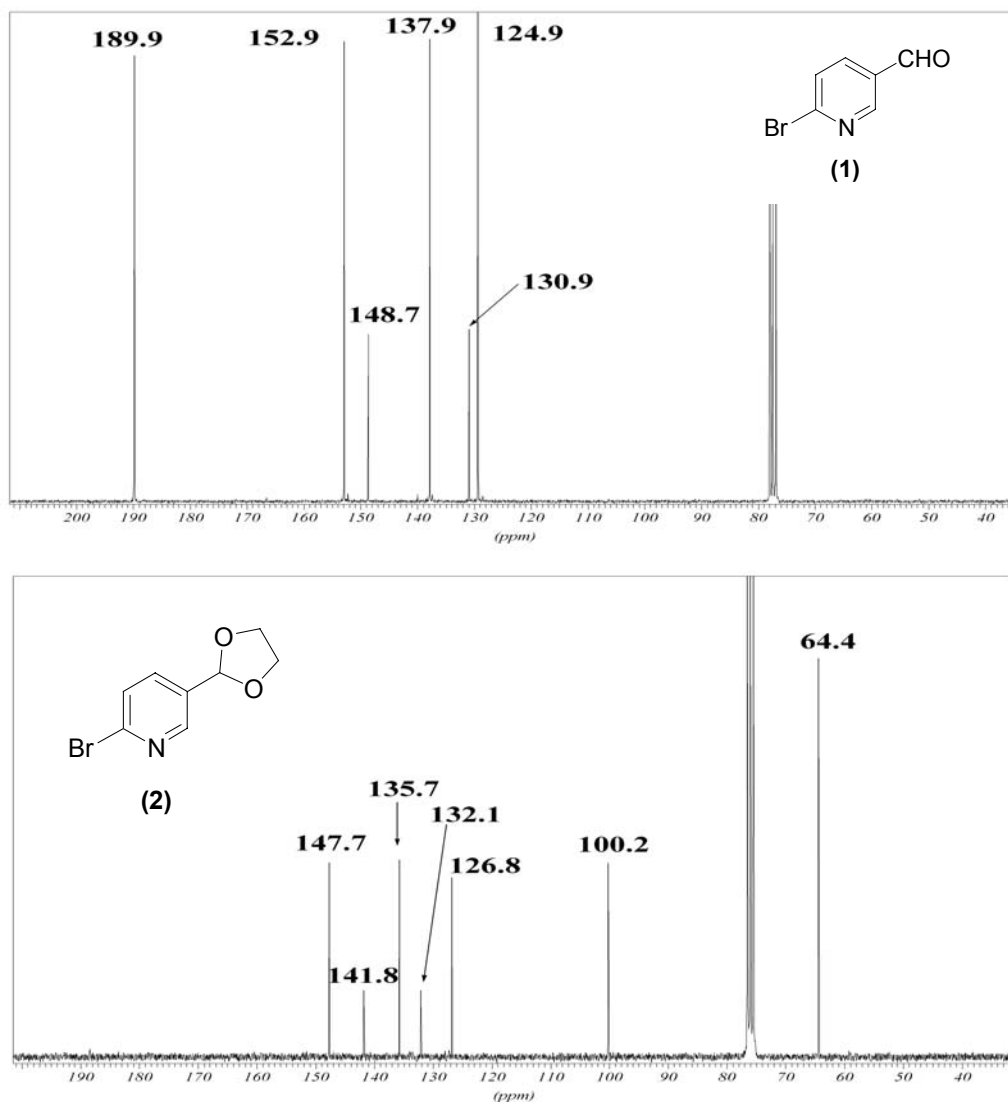
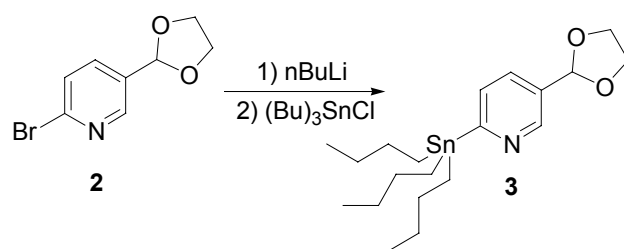
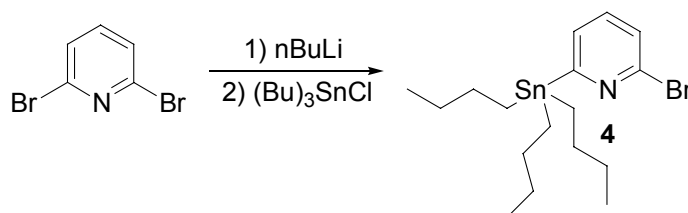


Figure 2.2: ^{13}C -NMR (250 MHz, r.t.) spectra of **1** and **2** recorded in $CDCl_3$.

Further, the lithium exchange of the bromine in position 2 [20] followed by quenching with Bu_3SnCl afforded 2-tributylstannyl-5-[1,3]dioxolan-2-yl-pyridine (**3**) (Scheme 2.4). The compound **3** was used later for Stille coupling reaction with derivative **5** (6-bromo-2,2'-dipyridine-5'-carbaldehyde). The next synthetic part illustrates the preparation of the monostannyl-derivative starting from commercially available 2,6-dibromopyridine. The 2,6-dibromopyridine was initially mono-lithiated working at $-40^\circ C$ in ether (Scheme 2.5). The subsequent quenching with tributyltin-chloride (Bu_3SnCl) was achieved by lowering the temperature at $-78^\circ C$ and yielded 2-tributylstannyl-6-bromopyridine **4** as pale yellowish oil.

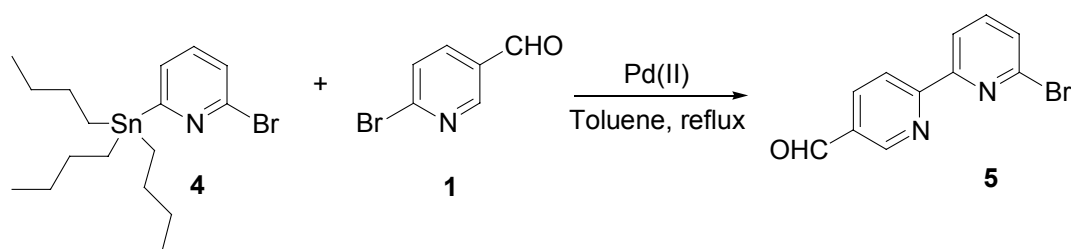


Scheme 2.4



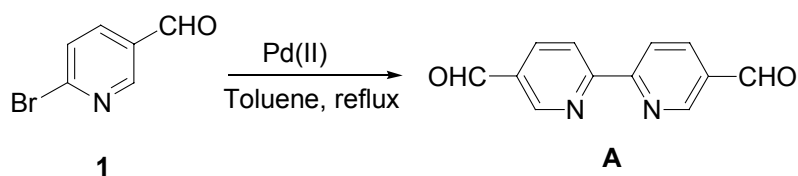
Scheme 2.5

The stannyl-compounds **3** and **4**, apart from the known toxicity of similar compounds [21], cannot be chromatographed either in alumina and silica column without substantial decomposition. Although they seemed quite stable at room temperature, they cannot be stored for long time even under argon. Thus they were prepared and used in situ. The Stille coupling between **4** and 6-bromo-3-pyridinecarbaldehyde (**1**) (Scheme 2.6) in anhydrous toluene under argon gave the first precursor for the synthesis of the biscarbaldehyde terpyridine, 6-bromo-[2,2']-dipyridinyl-5'-carbaldehyde (**5**). The optimized conditions obtained for the coupling reaction were achieved by using an excess of **1** (2.4 eq) with respect to **4** (1 eq), together with Pd(PPh₃)₂Cl₂ (5% mol) and PPh₃ (10% mol) as catalyst, without addition of the additive CuI (yield 58%). Trials made in the presence of CuI in catalytic amount (<5% with respect to **4**) did not improve the yield, while higher amounts (up to 10% with respect to **4**) led to a drastic decrease on the whole yield (< 30%). Although it is reported that CuI can generally raise the reaction rate (>10²) due to its free ligand scavenging ability, strong ligands in solution (e.g. polypyridines) may compete and inhibit the rate-limiting transmetalation step [22].



Scheme 2.6

A side product obtained from the Stille reaction consisted in the homo-coupling of **1** to afford the [2,2']bipyridinyl-5,5'-dicarbaldehyde (**A**) (Scheme 2.7).



Scheme 2.7

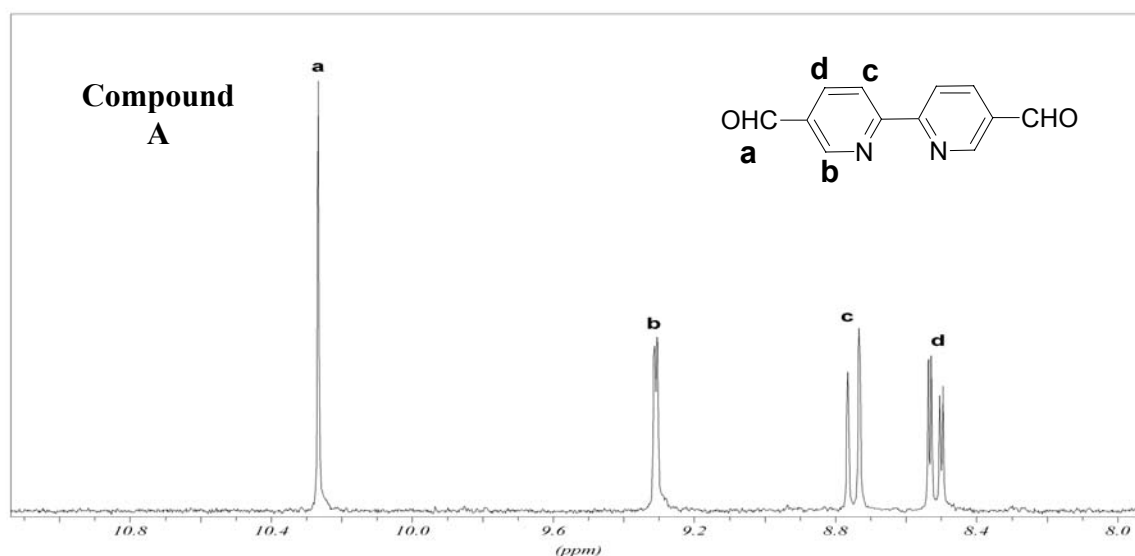
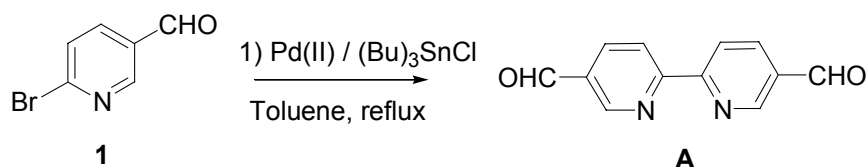


Figure 2.3: $^1\text{H-NMR}$ (250 MHz, r.t.) spectrum recorded in $\text{DMSO-}d_6$; note that the signals (**d**) and (**b**) are further splitted (doublet-doublet) by through space interaction with the carbaldehyde proton (**a**).

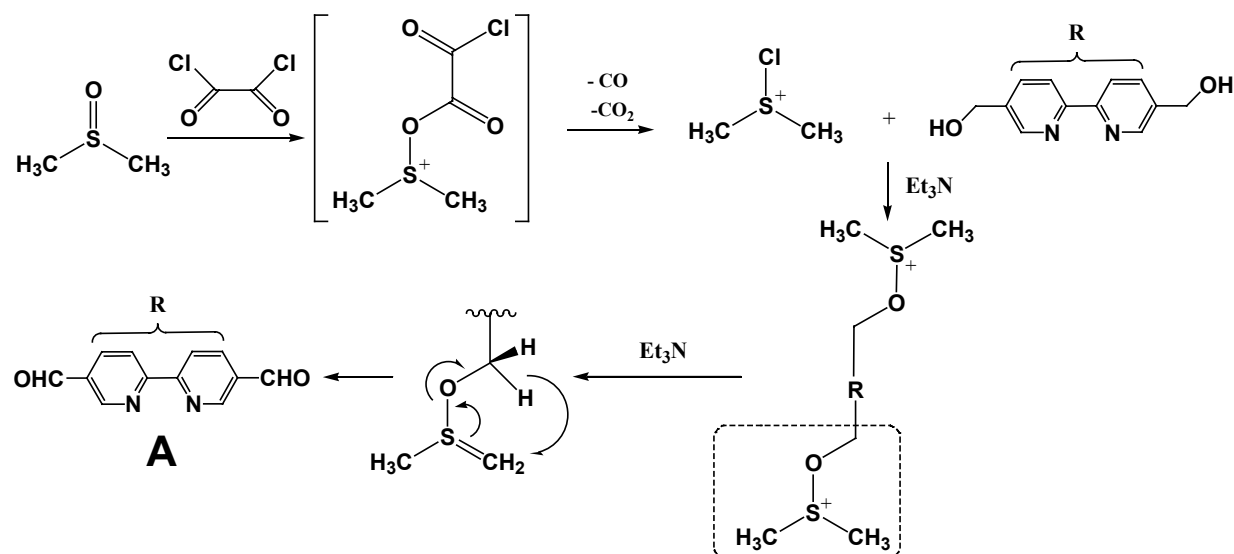
This reaction, whose mechanism is not known, was substantiated by using **1** (2 eq.), $\text{Pd}(\text{PPh}_3)_2\text{Cl}_2$ (5% mol) and PPh_3 (10% mol) as catalyst and tributyltin-chloride (Bu_3SnCl , 0.3 eq.), without coupling partner. After 60 hours of reaction the compound **A** was obtained in an unexpectedly good yield (60%) after chromatographic purification on silica column (Scheme 2.8).



Scheme 2.8

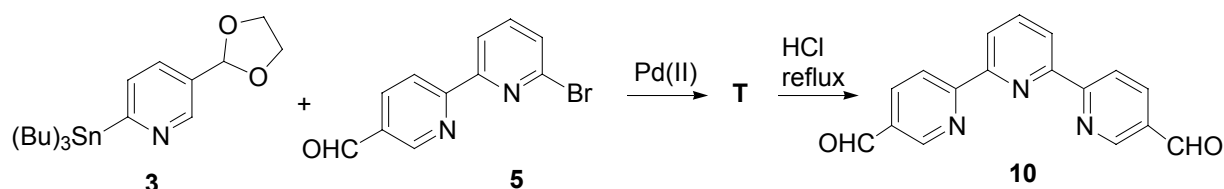
It is worth to notice that similar reports on homocoupling under Stille conditions can be found in literature [15i]. In addition one report based on homocoupling induced by hexa-*n*-butyldistannane compound (e.g. on 2,5-dibromopyridine leading to 5,5'-dibromo-bipyridine)

recently appeared [23]. Although deeper investigation on **A** was not conducted, the reaction 2.8 may represent an alternative synthesis of **A** with respect to that one reported [24] based on Swern oxidation of the alcohol 5,5'-hydroxymethyl-[2,2']bipyridine as shown in Scheme 2.9. It is also interesting to point out that the more classical nickel (II) catalyzed homocoupling largely employed for aryl halides has never been tested in the case of aldehyde substituted pyridine halides [25].



Scheme 2.9

Finally, the Stille-coupling reaction between **3** and **5** gave the 5,5''-diformyl-2,2':6',2''-terpyridine (**10**) (yield 73%)(Scheme 2.10). This reaction occurred in degassed and dry toluene under argon, in a similar way as found for **1** and **4**, by heating the reaction mixture to reflux for 60 hours; further hydrolysis of the dioxolane **T** in the presence of HCl (6 N) followed by basification provided the dialdehyde **10**.

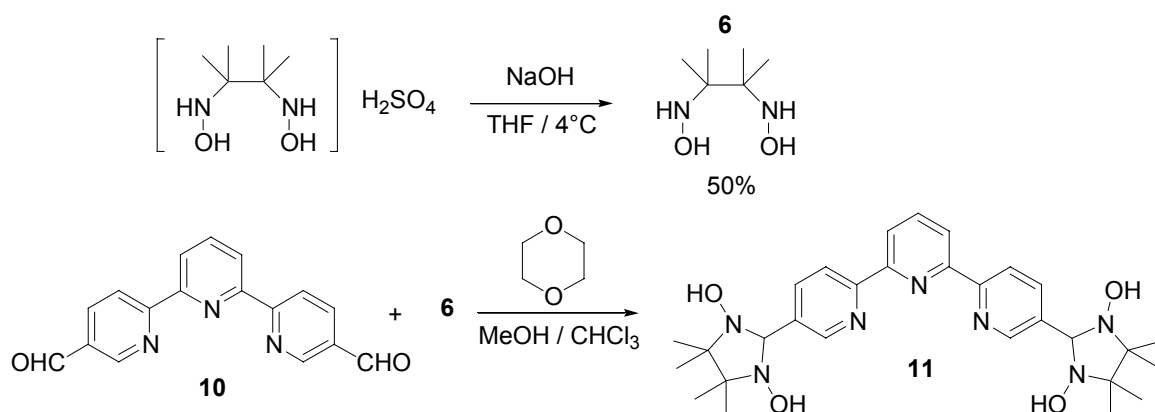


Scheme 2.10

Some comments may be useful at this point. A major consideration in working up reaction mixtures from Stille coupling is the removal of the tin byproducts. While trimethyltin chloride is water soluble and rather volatile, tributyltin chloride has a low volatility and is

soluble in most organic solvents. Separation on silica gel is difficult due to the tendency of tributyltin to elute even under non polar conditions, and to streak on the column. However, with basic compounds, e.g. oligopyridines, the workup of the reaction mixture is somehow easy. While oligopyridines are soluble in concentrated hydrochloric acid, the tin-byproducts can be removed by extraction with dichloromethane. Neutralisation of the acid phase gives the free oligopyridine ligands. In presence of sensitive groups like carbaldehydes, the basification needs to be carried out with sodium or potassium carbonate rather than sodium hydroxide in order to prevent Cannizzaro reactions that lead to the formation of the diacid. This derivative, very soluble in water, was on the other hand, not completely characterized.

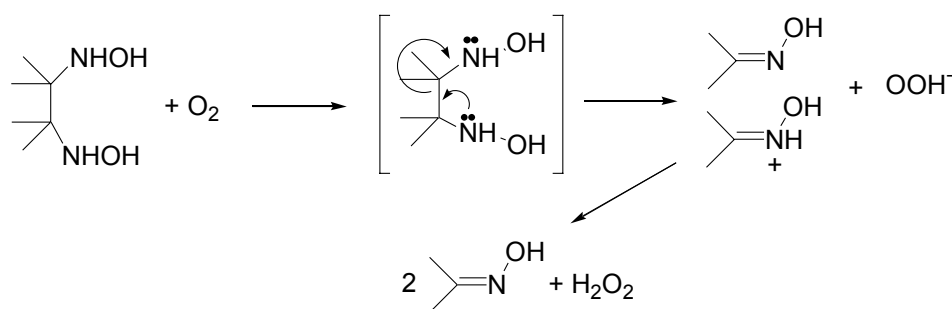
The organic compounds which contain no trace of tin byproducts can be extracted with CH_2Cl_2 and purified by chromatography. The diformyl derivative **10** (1 eq) was finally subjected to Ullman coupling with 2,3-bishydroxylamino-2,3-dimethyl-butane (**6**, 3 eq) using a mixture of 1,4-dioxane, trichloro-methane and methanol (4/3/3) as solvents for 7 days, under argon at room temperature to afford the white precipitate 5,5"-bis(1,3-dihydroxy-4,4,5,5-tetramethylimidazolidin-2-yl)2,2':6',2" terpyridine (**11**) as radical precursor (yield 86%)(Scheme 2.11).



Scheme 2.11

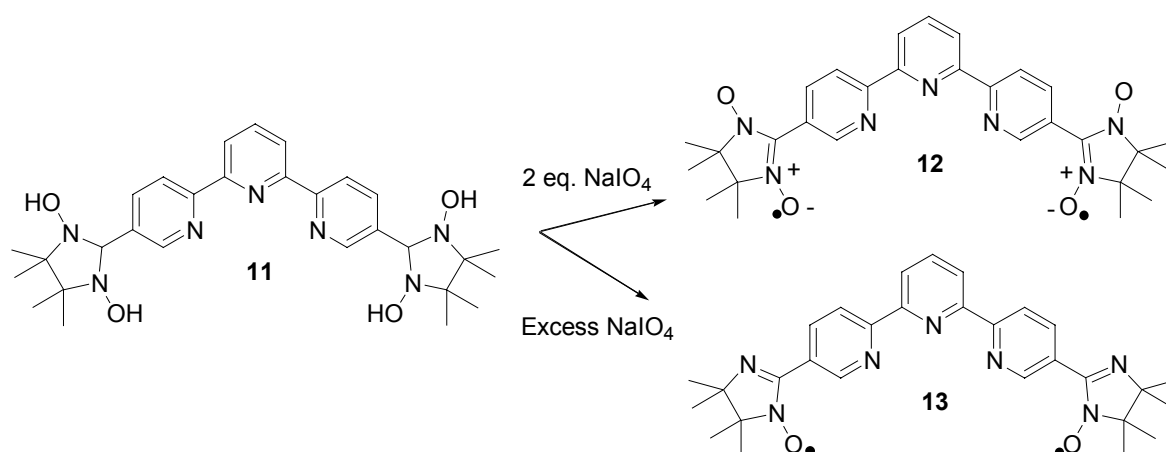
Heating of the reaction mixture (50°C) in order to speed up the condensation induced fast decomposition either of **6** and **11**, and no precipitate was obtained. Only an oily mixture was recovered (the solution turned into pale orange after 1 day) that afforded a very small amount of the biradical **12** or **13** after oxidation with NaIO_4 (*vide infra*). It is worth to notice that when part of the tin-biproducs were left in the dialdehyde **10**, they catalyzed fast decomposition (oxidation) of the 2,3-bishydroxylamino-2,3-dimethylbutane **6**. A very small amount of the radical precursor **11** was obtained after the condensation reaction, indicative for the presence of two competitive mechanisms. A pale rose colour of the reaction mixture was observed in this case. The decomposition of **6** occurs slowly in presence of oxygen to acetone

oxyme (pale rose, see Experimental Session) according to a mechanism similar to the synchronous *trans*-elimination [7b] (Scheme 2.12). Since the presence of O₂ in the medium is ruled out and the condensation reaction between **6** and **10** appeared rather slow, any tin-residues left should act somehow faster on **6** with a mechanism similar to the hydrogen abstraction induced by dioxygen. Therefore only very pure **10** and careful exclusion of O₂ could lead to successful formation of **11**.



Scheme 2.12

The compound **11** was oxidized at room temperature (Scheme 2.13) working under phase transfer conditions (CHCl₃/CH₂Cl₂/H₂O), by using slight excess of NaIO₄ (2.5 eq) with respect to **11** (1.0 eq) for 30 min using argon saturated solution. After column chromatography 5,5"-bis(1-oxyl-3-oxo-4,4,5,5-tetramethylimidazolidin-2-yl)2,2':6',2"-terpyridine (**12**) was obtained as deep-green powder (yield 16%). Similarly but using an excess of NaIO₄ (4 eq) with respect to **11** (1.0 eq) and warming the mixture up to 40 °C, the 5,5"-bis(1-oxyl-4,4,5,5-tetramethylimidazolidin-2-yl)2,2':6',2"-terpyridine (**13**) was obtained as orange-red powder (yield 28%).



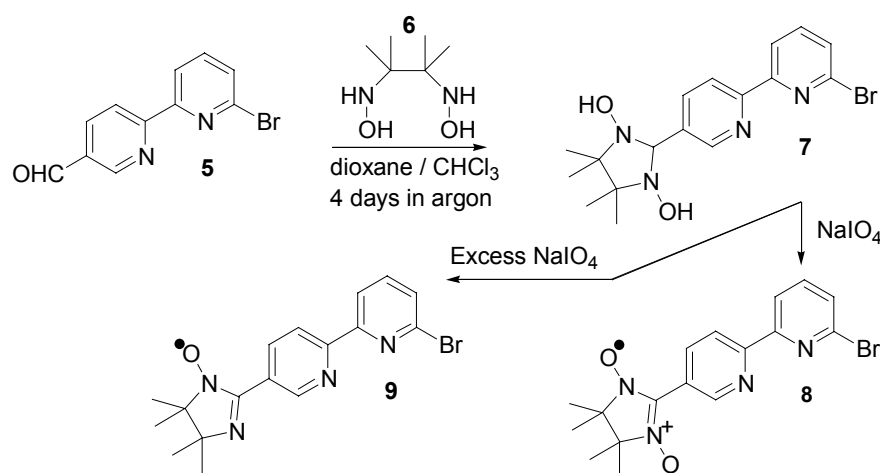
Scheme 2.13

One of the by products identified after prolonged oxidation carried under argon at room temperature (2 hours) with stoichiometric amount of NaIO₄ with respect to **11** (2 eq./1 eq.) was 5,5"-bis-(4,4,5,5-tetramethyl-4,5-dihydro-1H-imidazol-2-yl)-[2,2';6',2'']terpyridine. This

terpyridine derivative could only be eluted through alumina column upon using MeOH as polar solvent. Therefore the major problems encountered in obtaining compounds **12** and **13** were avoiding the loss of one or both oxygen groups respectively (dehydration) by balancing the amount of oxidizing agent and the reaction time.

The nitronyl nitroxide derivative **12** was obtained always in smaller amount with respect to the imino radical **13**. This result arises by the fact that the oxidation reaction with NaIO_4 occurs at the interface between H_2O and CHCl_3 , leading to a statistical mixture of monoxidized, fully oxidized and overoxidised/decomposed **11**.

The use of another oxidizing agent largely employed in the case of precursors for nitroxide radicals (PbO_2) showed to be far less effective in controlling side reactions. The 6-bromo-[2,2']-dipyridinyl-5'-carbaldehyde (**5**) was used for the synthesis of the monoradicals 6-bromo-5'[3-oxide-1-oxyl-4,4,5,5-tetramethylimidazolidin-2-yl]-2,2'-bipyridine (**8**) and 6-bromo-5'[1-oxyl-4,4,5,5-tetramethylimidazolidin-2-yl]-2,2'-bipyridine (**9**) according to the Scheme 2.14.



Scheme 2.14

The condensation with 2,3-bis(hydroxyamino)-2,3-dimethyl-butane (**6**) afforded the radical precursor 6-bromo-5'[1,3-dihydroxy-4,4,5,5-tetramethylimidazolidin-2-yl]-2,2'-bipyridine (**7**) (yield 85%). In Figure 2.4 and 2.5 are shown the $^1\text{H-NMR}$ spectra of **5** and **7**. Subsequent oxidation of **7** with sodium periodate afforded either **8** (yield 25%) or **9** (yield 28%) depending on the amount of oxidant used. As previously mentioned in the case of **11**, heating the reaction mixture should be avoided. In fact, while in principle we might increase the amount of at least the imino compound **9**, in practice the dehydration process of **7** made it hard to control the radical oxidation with NaIO_4 and almost no imino nitroxide radical was recovered after this step. Also in this case, the use of the other types of oxidizing agents (PbO_2) that allowed to avoid the phase transfer conditions, gave a smaller overall yield for both **8** and **9** (< 15%). In the $^1\text{H-NMR}$ spectra, the precursors of the Ullman radicals showed always characteristic peaks associated with the imidazolyl moiety. As reported for compound **7** in

Figure 2.5, and compound **11** in Figure 2.6C, the C-H proton of the imidazolyl ring featured a well defined resonance around 4.5- 4.6 ppm, while the two cis/trans methyl carbons –CH₃ gave two singlet at ~1.0 ppm. In solution all the pyridine-based radicals were very sensitive in presence of traces of acids. The following order of stability **9** > **8** > **13** > **12** (from more stable to less stable) can be drawn. These have been defined by monitoring the decrease of the double integration of their EPR signals at room temperature *versus* time. In solvents like toluene or hexane they all showed high stability (up to a year), and unexpectedly also in ethylacetate and 2-propanol. They should not be kept for long time in acetone, CH₂Cl₂ and CHCl₃ although they feature high solubility in these solvents. Other solvents like MeOH and EtOH or ethereal solvents like THF destroyed the biradical **12** and **13** very fast (~ one day, see Table 2.1 at the end of this Chapter) while the monoradicals **8** and **9** were completely lost in approximately one week. The solvent effect on the radical stabilities could be easily monitored by observing a fading in the blue or red colour being accompanied with the absence of EPR signal either in solution or in frozen state. The purifications of these radicals were always carried out on neutral alumina (Al₂O₃) since they showed same trend of decomposition when silica (SiO₂) was used.

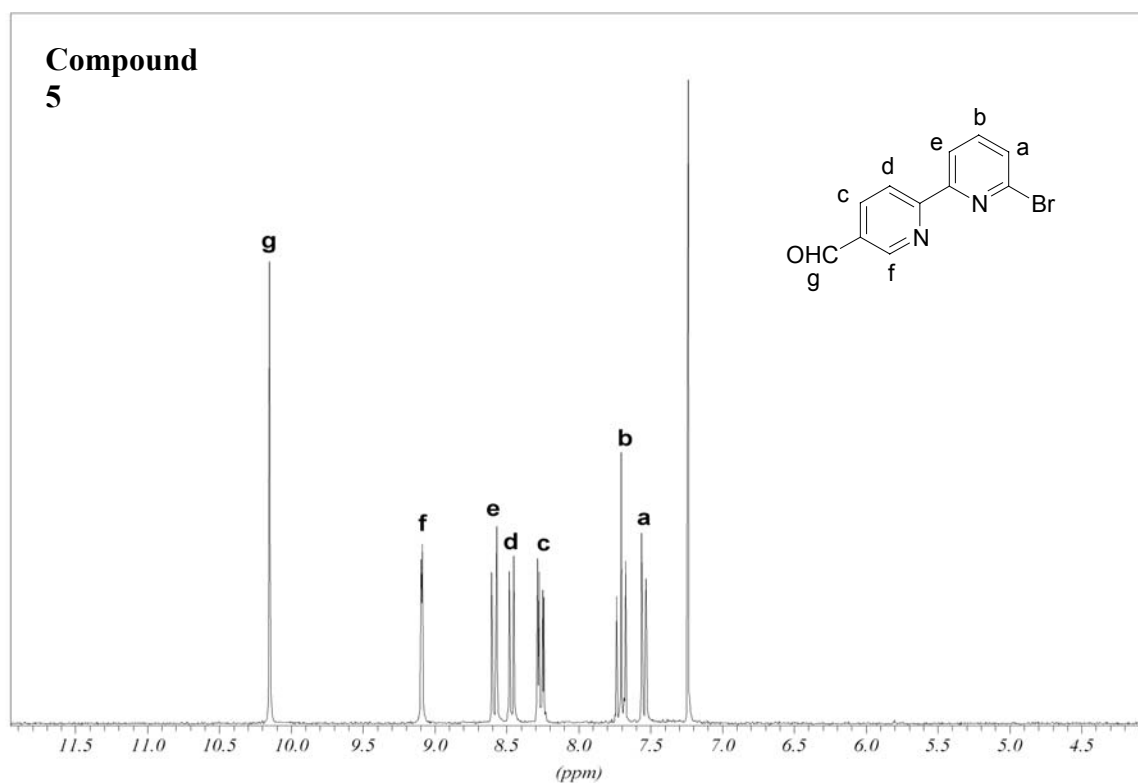


Figure 2.4: $^1\text{H-NMR}$ (250 MHz, r.t.) spectrum recorded in CDCl_3 . Note that the signals (c) and (f) are further splitted in doublets by (g) as found previously in compound **A** (see its $^1\text{H-NMR}$ spectrum in Figure 2.3).

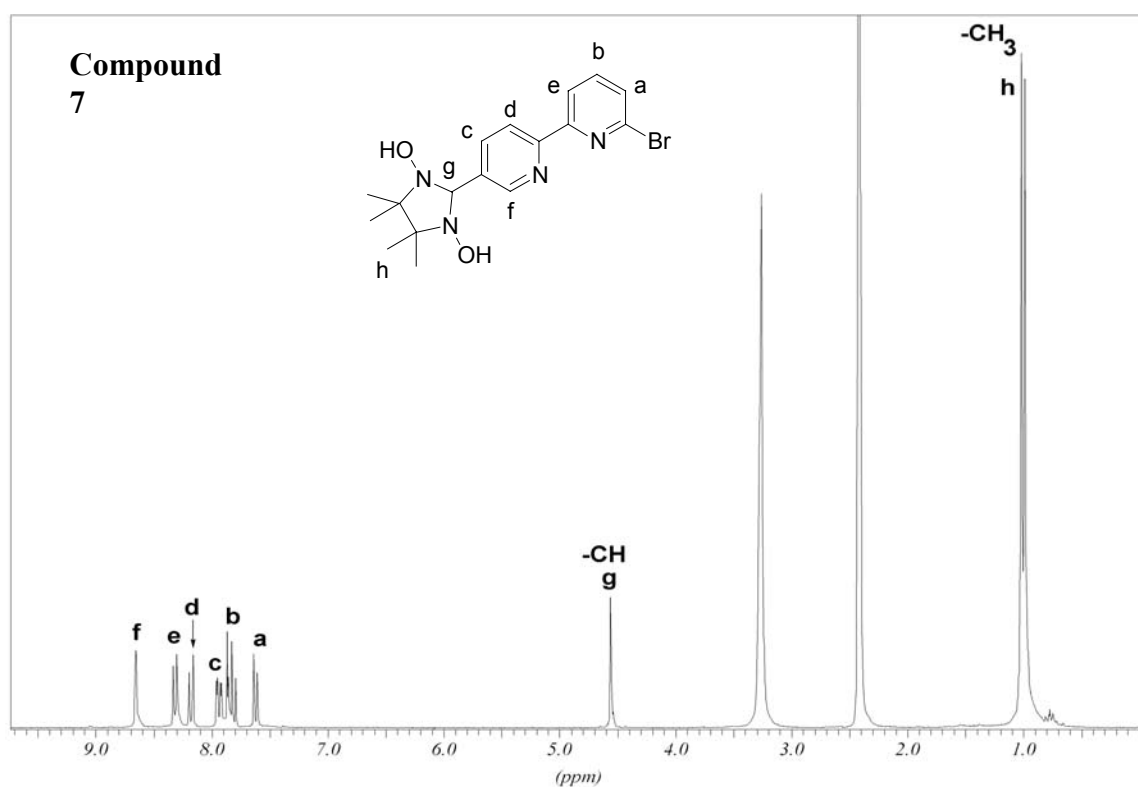


Figure 2.5: $^1\text{H-NMR}$ (250 MHz, r.t.) spectrum recorded in $\text{DMSO-}d_6$.

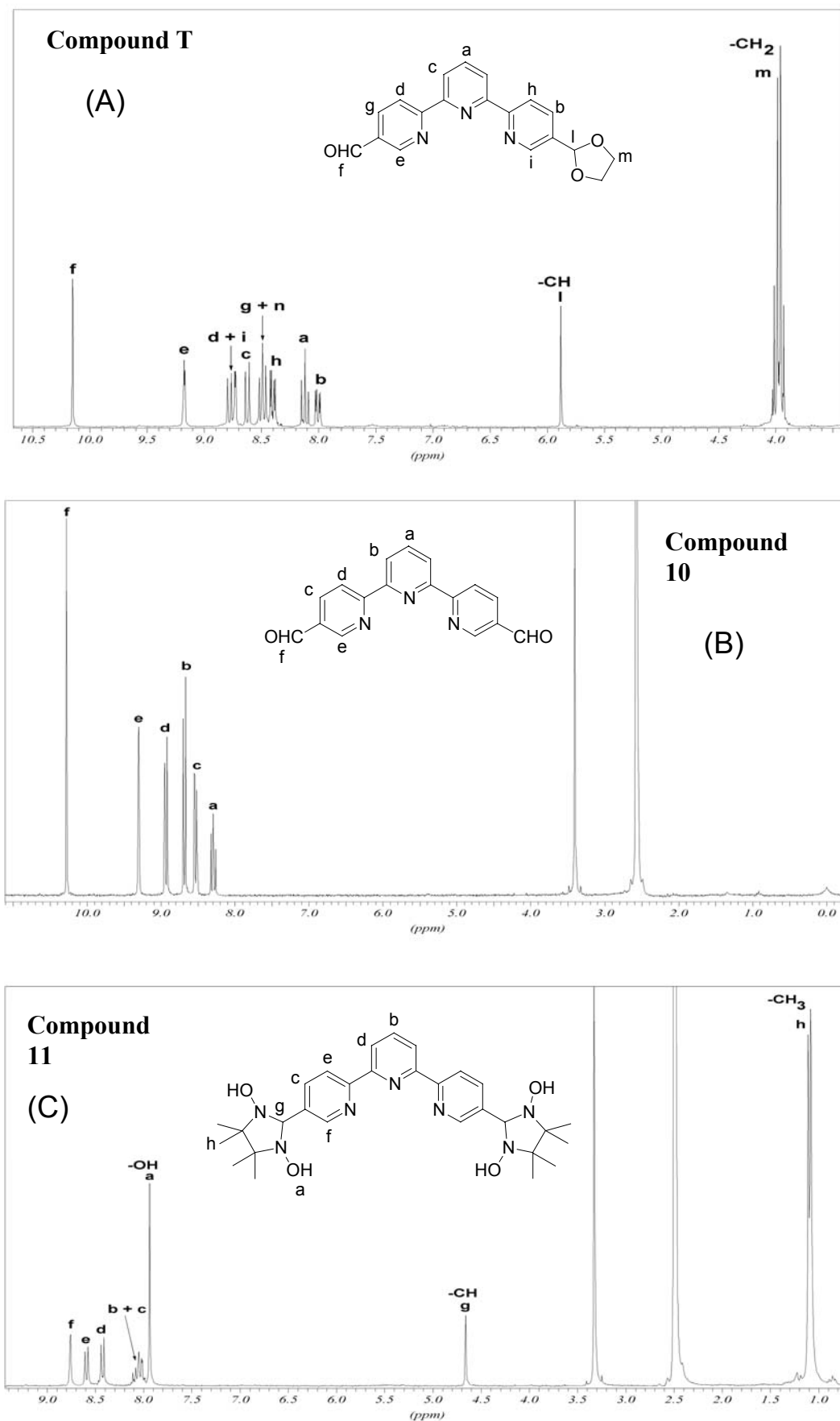
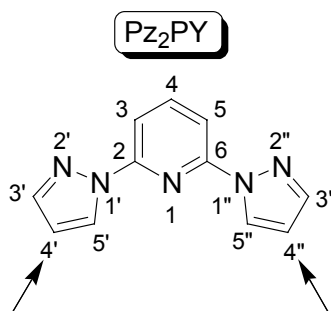


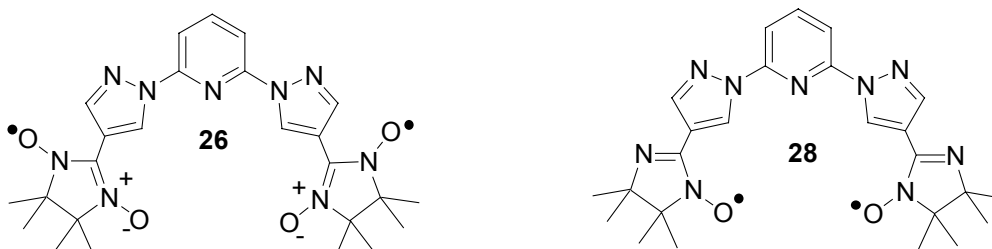
Figure 2.6: ¹H-NMR (250 MHz, r.t.) spectra of the terpyridine derivatives recorded in DMSO-*d*₆.

2.2. Pyrazolypyridine containing radicals

In order to extend the work from the terpyridine to a similar hetero-system, the 2,6-bispyrazolypyridine core was then considered. Pz₂Py can be regarded as a terpyridine-analogue, since it reproduces the tridentate nitrogen binding motif of the terpyridine core. The final target was to attach in the positions 4',4'' two NN or IN radical fragments.

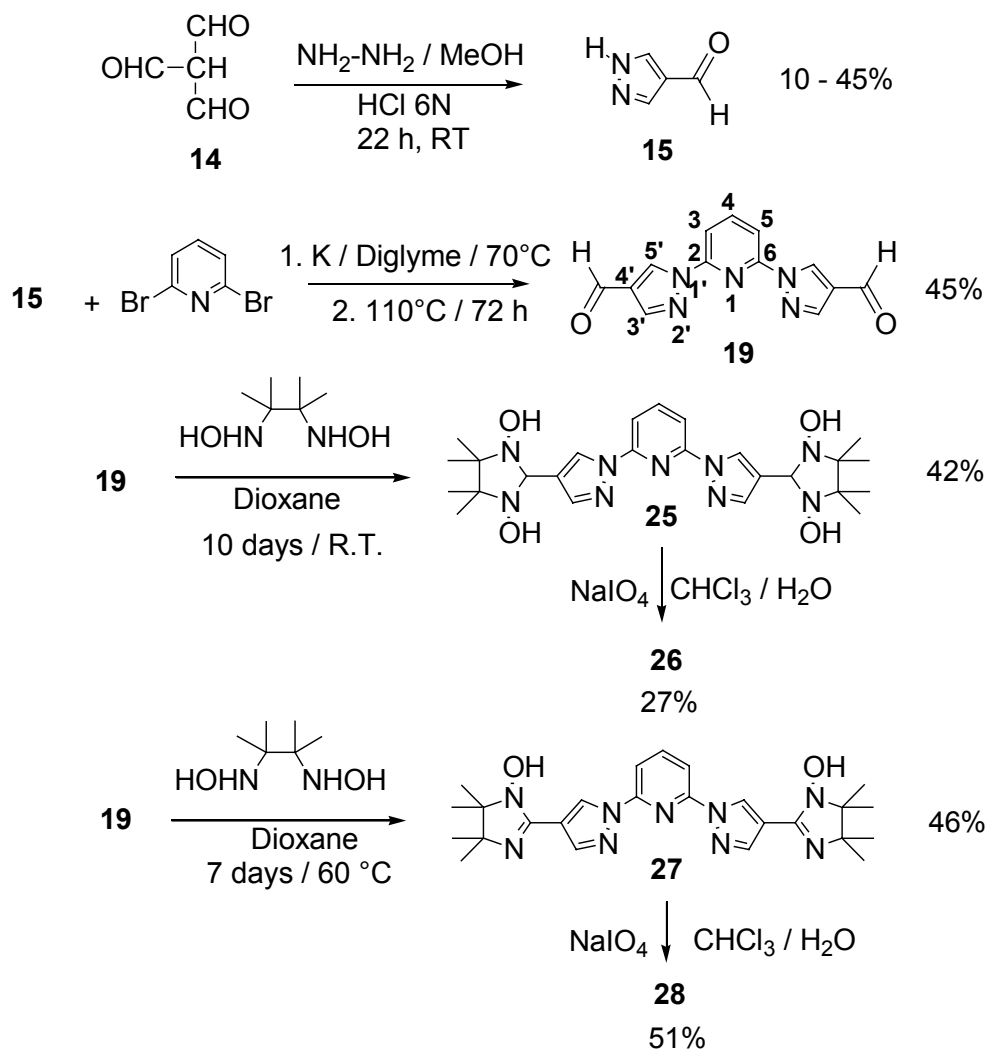


Such design led to the novel symmetric biradical derivatives 2,6-bis[4'-(3-oxide-1-oxyl-4,4,5,5-tetramethylimidazolin-2-yl)pyrazol-1'-yl]-pyridine (**26**) and 2,6-bis[4-(1-oxyl-3-4,4,5,5-tetramethylimidazolin-2-yl)pyrazolyl]pyridine (**28**).



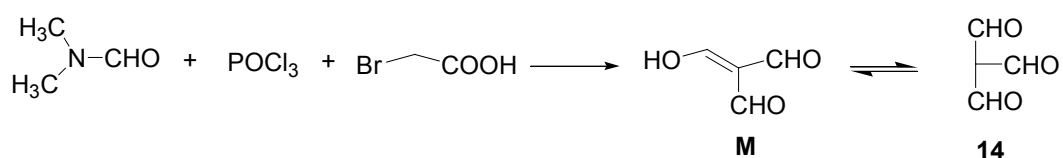
Unfortunately we did not find in literature either established synthetic routes towards the 4',4''-biscarbaldehyde functionality, that represents the key precursor for the Ullman radicals, nor any type of radical units appended anywhere on the 2,6-bispyrazolypyridine backbone. In order to justify the synthetic effort the following considerations have been taken into account. (1) The synthetic development of novel functionalities in position 4',4'', besides the radical units, might in principle enable easier metal complexation without the hindrance induced by the usually encountered substituents for the terminal pyrazoles (methyl, phenyl, etc.) in the positions 3',3'' or 5',5''. In order to attain coordination of the metal in 3',3'' or 5',5' bispyrazolypyridine derivatives often are required prolonged reaction time with the metal salt and high temperatures. (2) Novel functionalizations of 4',4'' substituted bispyrazolypyridines are promising precursors for spin-crossover complexes and optoelectronics. (3) The presence of the two pyrazolyl fragments renders the systems **26** and **28** non-alternant.

Therefore, the clear definition of the ground spin state multiplicity must be explored. Furthermore, they will offer valuable model systems for the synthetic development of other cores based on non-alternant heterocyclic unit. Based on these motivations, the synthetic strategy towards the biradicals **26** and **28** is outlined below as Scheme 2.15.



Scheme 2.15

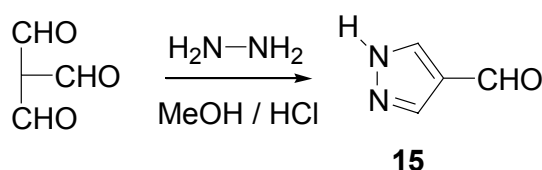
The first synthetic step consisted on the preparation of the triformylmethane (**14**), according to a very brief description reported in literature [26](Scheme 2.16) using N,N dimethylformamide, phosphorus oxychloride and bromoacetic acid.



Scheme 2.16

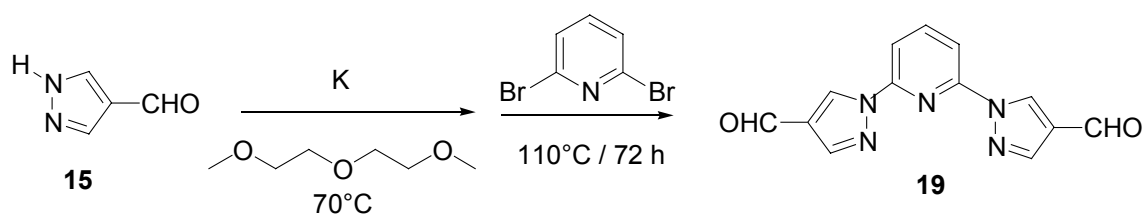
The course of this reaction, as suggested by the authors, seems very complex where the triformylmethane obtained is in equilibrium with 2-hydroxymethylene-malonaldehyde (**M**) [26]. As underlined in the experimental section, the delicate point consisted on the pre-reaction between DMF and POCl₃ (this is the formylating agent) and then, once the reaction with bromoacetic acid is completed, the decomposition (in ice) and basification of the very acid mixture needed to be performed fast, without reaching too basic environment (up to pH ~8). The product **14** (variable yield 10-45%) infact appeared very sensitive to oxidize to the acid under air (Cannizzaro type reaction) in basic environment.

Since basification cannot be avoided, this represented the major draw back for such reaction that led to the variable yields as above reported. Then, the condensation of triformylmethane (**14**) (1 eq) with hydrazine-monohydrate (1 eq) was sucesfull only when the hydrazine was added very slowly, over 3 hours. It was additionally carried out in acidified alcoholic medium [27] (Scheme 2.17). The reaction occurred simply at room temperature, by stirring for 20 hours, followed by basification and separation of **15** over silica column. The pyrazol-4-carboxaldehyde **15** (yield 52%) was finally obtained as yellowish solid. Its ¹H-NMR and ¹³C-NMR spectra are shown both in Figure 2.7A and 2.7B respectively.



Scheme 2.17

The 2,6-bis(4-formyl-pyrazolyl)-pyridine (**19**), that represents the key precursor towards the biradical systems, was synthesized in one step reaction according to Scheme 2.18, by condensation between the nucleophilic potassium-salt of **15** with 2,6-dibromopyridine in diethylene glycol dimethyl ether (diglyme) as reaction solvent (yield 45%). The choice of diglyme was mostly dictated by the fact that the first bromine group in the 2,6-dibromopyridine is usually replaced relatively easily (70°C, 48h) [15m], however substitution of the strongly inactivated second bromine group requires higher temperature and prolonged reaction time.



Scheme 2.18

As advantages the diglyme offers with respect to the other most often used ethereal solvents (e.g. THF, Et₂O) the higher boiling point (162°C at 760 mmHg) and stability at high temperature. In addition, its ability to chelate cations (the potassium cation in this case) left the nucleophile much more active. The figure 2.8 shows the ¹H-NMR spectra of the dialdehyde **19**.

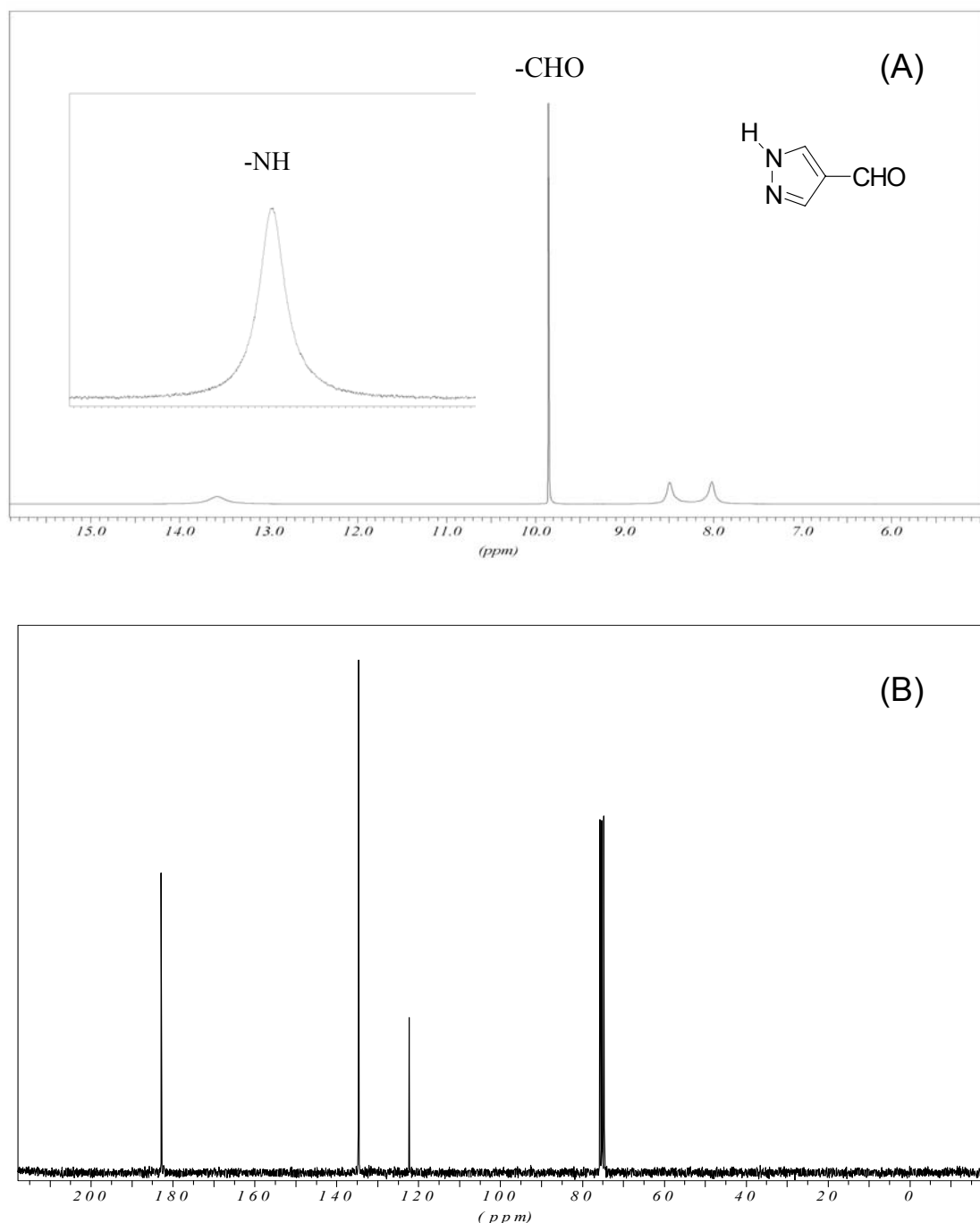


Figure 2.7: (A) ¹H-NMR (250 MHz, r.t.) spectrum for compound **15** recorded in DMSO-*d*₆ and (B) its ¹³C-NMR (63 MHz, r.t.) spectrum recorded in CDCl₃.

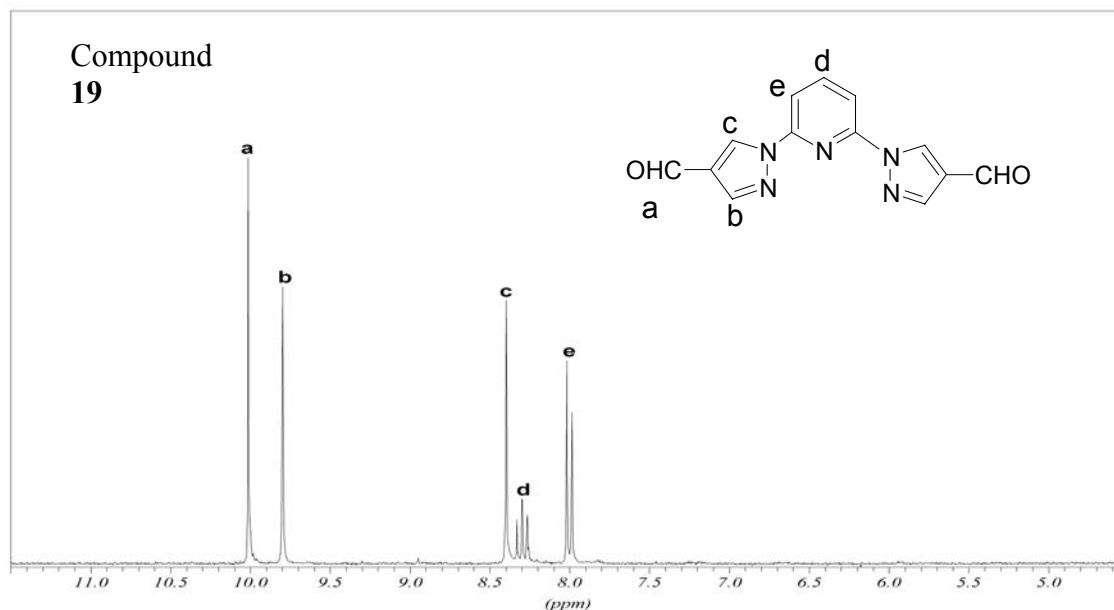
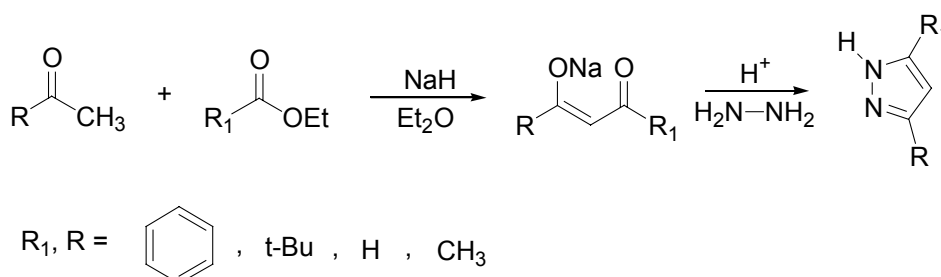


Figure 2.8: $^1\text{H-NMR}$ (250 MHz, r.t.) spectrum for compound **19** recorded in $\text{DMSO-}d_6$.

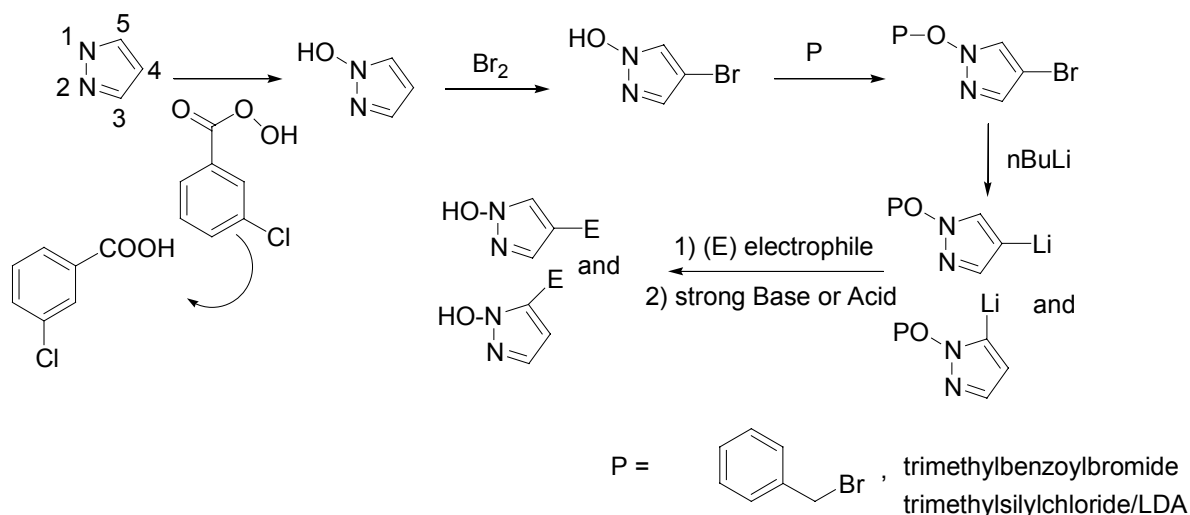
We explored two other possibilities in order to obtain compound **19**. One relied on building the pyrazol-4-carboxaldehyde (**15**) starting from the commercially available pyrazole, and the second method consisted in synthesizing at first the bispyrazolopyridine backbone followed by functionalisation of the terminal pyrazoles in positions 4. While pyrazole 3,5 disubstituted derivatives are readily generated via a Claisen condensation to form a 1,3-dicarbonyl followed by condensation with hydrazine [15m,28] as shown in scheme 2.19, those pyrazoles functionalised in position 4 are much less common and often required tedious multi-step approaches.



Scheme 2.19

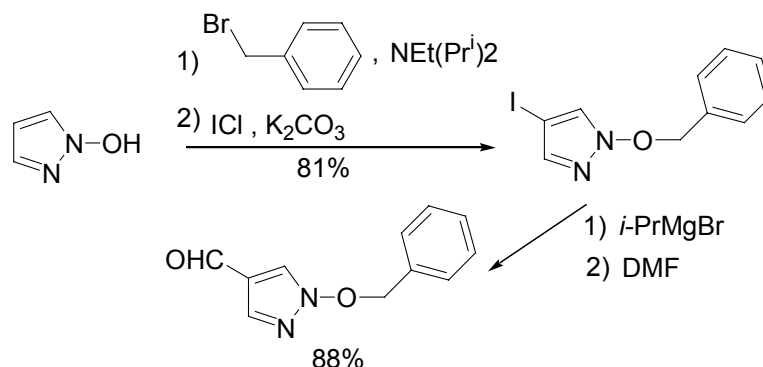
Since only 4-substituted pyrazole were needed, one method would be the reaction of 4-lithiopyrazoles with electrophiles [29]. The 4-halogen substituted pyrazoles are readily generated by N-protection followed by electrophilic halogenation [30] (or nitration [31]). However, there are only few examples of pyrazole C-4 lithiation [32], all based on bromine-lithium exchange and obviously as mentioned above required a protecting group in position 1 (N-protection). Such reaction proceeds with low chemoselectivity due to competing

deprotonation at C-5 [32a] or isomerization of the 4-lithiopyrazole to the corresponding 5-lithiopyrazole [33] (Scheme 2.20). Obviously this problem can be avoided upon introduction of a second protecting group in the C-5 position, making this procedure even more tedious [32f].



Scheme 2.20

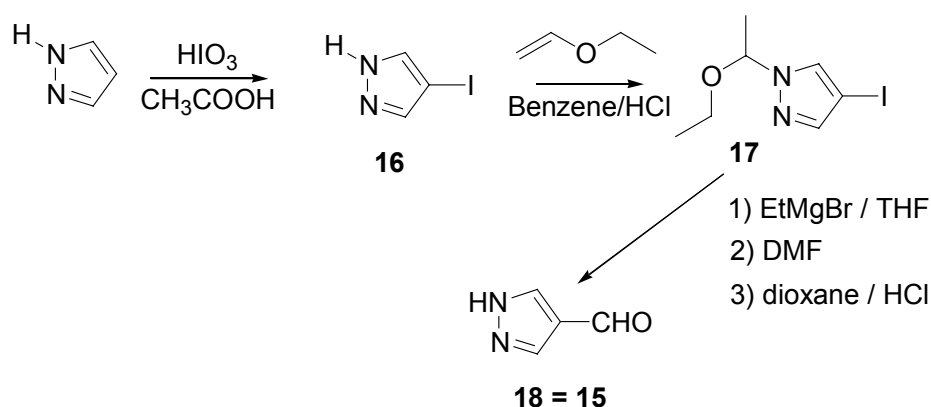
We decided to avoid the lithiation procedure. One report [34a] described the regioselective monoiodination of 1-benzyloxy pyrazole [34b] without protecting group at C-5 followed by magnesium-iodine exchange. Subsequent reaction with DMF produced the corresponding 4-formyl-1-benzyloxy pyrazole in good yield (88%). Hydrolysis in acid environment gave the 1-hydroxypyrazole. Further deprotection of the nitrogen 1 was not described. This reaction is shown in Scheme 2.21.



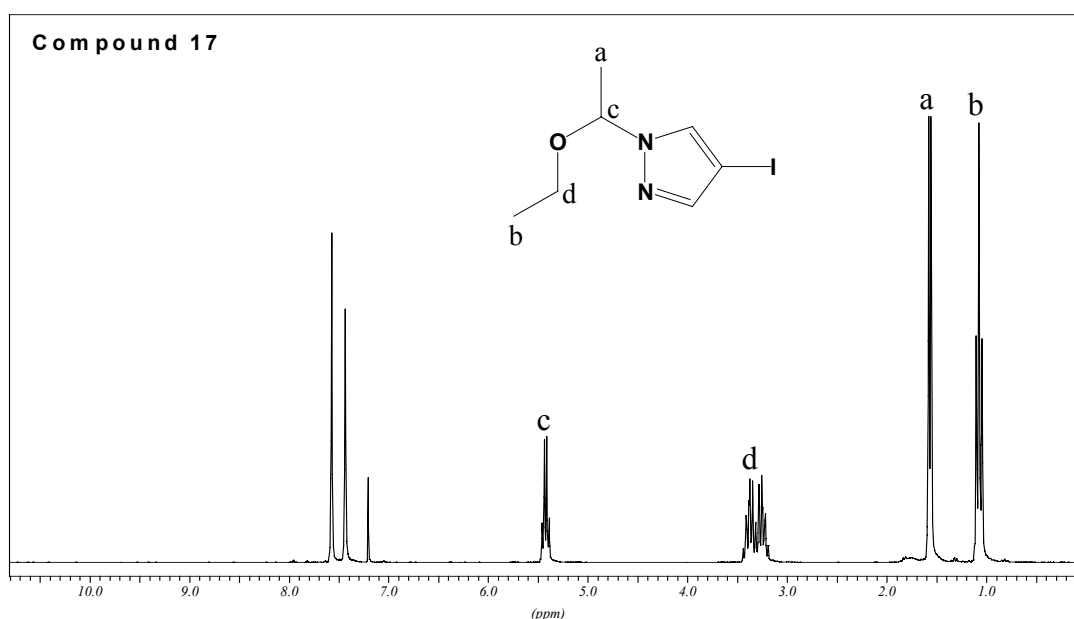
Scheme 2.21

In attempts to avoid initial N-protection, a mixture of NaI/I₂ in sodium acetate/water or KI/I₂ was used as iodinating agents for the pyrazole. However, the product obtained in both

cases consisted of a mixture of all three isomers (3, 4 and 5 iodo-pyrazole). The following protocol appeared recently as alternative route by using a mixture of HIO_3/I_2 in acetic acid [35]. On the other hand, attempts to reproduce the procedure as reported led also to a mixture of products plus unreacted starting material. While the pyrazole can be easily recovered (water soluble) separation of the isomers is very difficult to achieve. As pointed out in the experimental part, the key point consisted in the slow addition of the iodinating agent (drop by drop); kinetically only the position 4 is favoured, and since the 4-substituted iodo pyrazole (**16**) is not very soluble even in acetic acid, its precipitation drives the reaction to completion (yield 88%). As reported in Scheme 2.22, the subsequent step consisted in the N-protection of the pyrazolyl-nitrogen in position 1 using ethylvinylether in slightly acidified medium (HCl) followed by chromatographic separation on alumina (Al_2O_3 , yield > 94%). The product 1-(1-ethoxyethyl)-4-iodo-pyrazole (**17**) collected is a pale yellowish oil. The $^1\text{H-NMR}$ spectrum of **17** is shown in Figure 2.9.

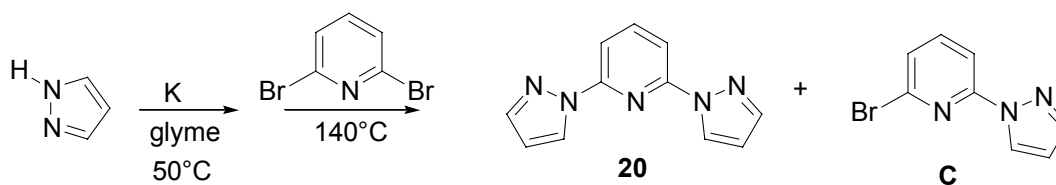


Scheme 2.22

Figure 2.9: $^1\text{H-NMR}$ (250 MHz, r.t.) spectrum for compound **17** recorded in CDCl_3 .

The final step towards the synthesis of **15** consisted in the formation of the correspondent Grignard derivative. Reaction of 1-(1-ethoxyethyl)-4-iodo-pyrazole with magnesium wire was ineffective either in THF and glyme, even upon heating over 90°C and in presence of CuI [similar to Note 17 in Reference 34a]. As an alternative, the reaction with a stronger Grignard reagent (ethylmagnesium bromide) proceeded very well. The Grignard derivative of **17** was not soluble and at the end of the reaction a solid paste was formed. This intermediate is unstable and should be kept below 4°C. Nevertheless, slow addition of the electrophile DMF led to the resolubilization of the solid. After hydrolysis and column chromatography (ethylacetate/hexane) the pyrazol-4-carboxaldehyde (**18**) is obtained in a very good yield (80%). Although this route is longer than that previously suggested (reactions 2.16 and 2.17) was always very successful.

The second route for building the bis-carbaldehyde derivative **19** relies on an even more simplified procedure, and further allows flexibility in developing novel functionalisations for the bispyrazolylpyridine core that can be used for different cross-coupling reactions. The pyrazolylpyridine core was easily built by nucleophilic substitution between the pyrazole anion prepared by reacting pyrazole (1 eq.) with potassium metal (1 eq.) and 2,6-dibromo-pyridine (Scheme 2.23).



Scheme 2.23

This reaction as discussed in Scheme 2.18 is rather slow (4 days) and afforded **20** in moderate yield (~50%) after chromatographic separation on silica ($R_f = 0.1-0.5$ in $\text{CHCl}_3/\text{hexane}/\text{ethylacetate}$, 6/2/1). A side product consisted in the mono-substituted 2-bromo-6-pyrazolyl-1-yl-pyridine (Compound **C**, $R_f = 0.8$) that was easily separated from **20**. In Figure 2.10 and 2.11 are shown their respective $^1\text{H-NMR}$ spectra.

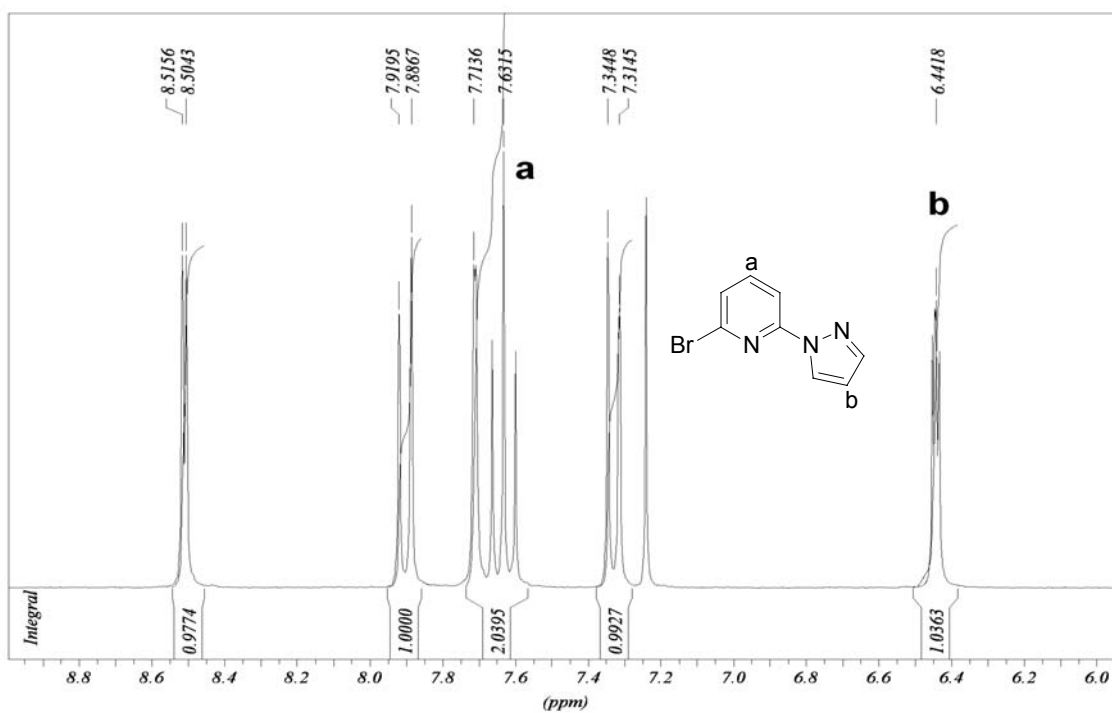


Figure 2.10: ¹H-NMR (250 MHz, r.t.) spectrum for compound (C) recorded in CDCl₃.

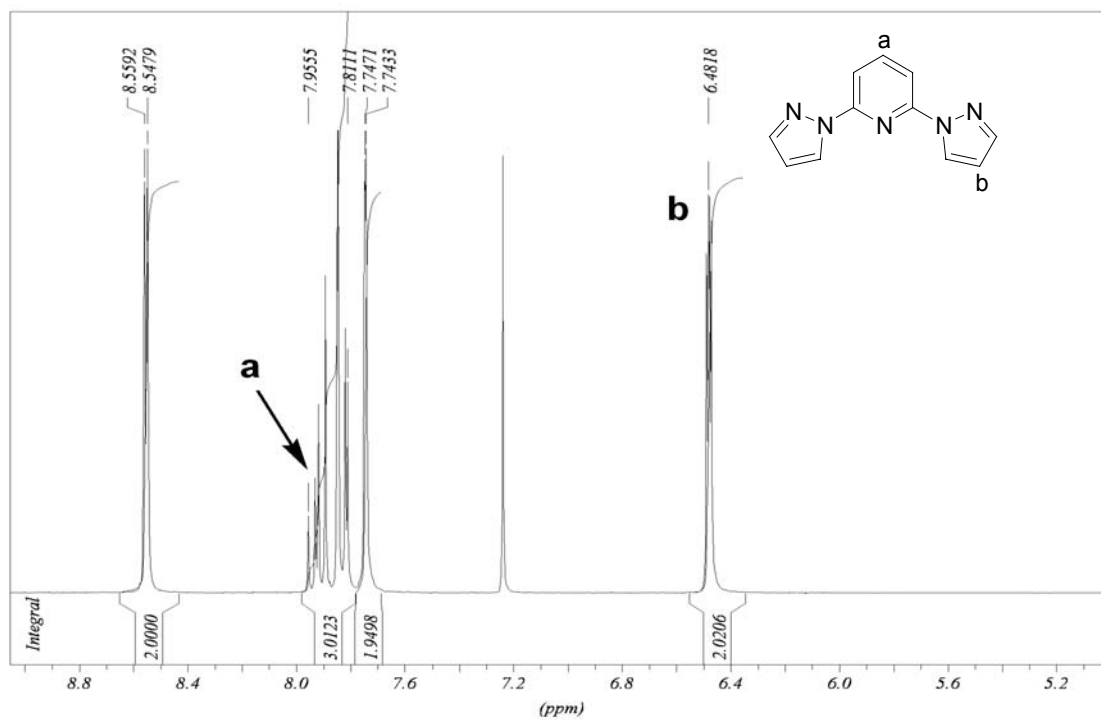
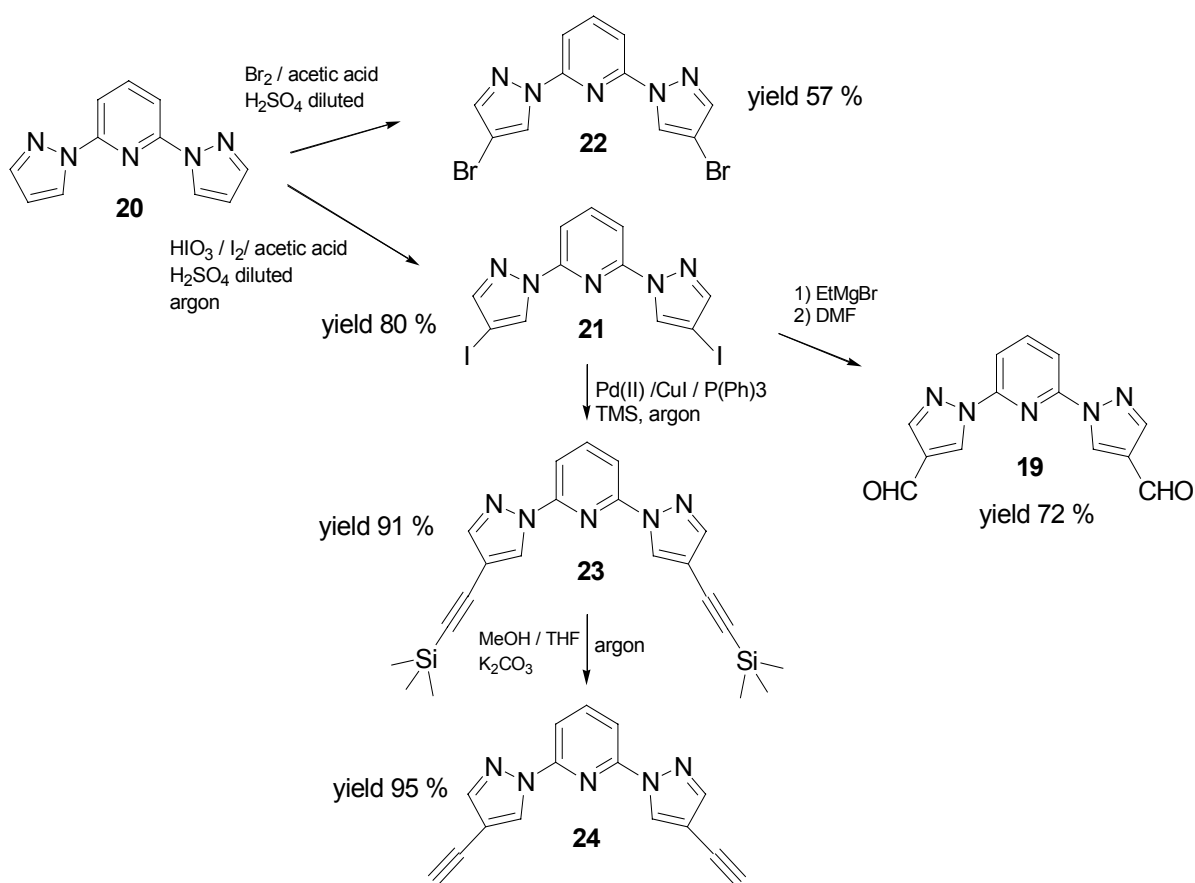


Figure 2.11: ¹H-NMR (250 MHz, r.t.) spectrum for compound 20 recorded in CDCl₃.

The next step consisted in the functionalisation of the terminal pyrazoles in position 4. An old report described some electrophilic reactions (e.g. bromination, chlorinations, nitrations) carried out on various 2-(pyrazolyl-1'-yl)-pyridines but we did not find any report of similar reactions on **20** [36]. As shown in Scheme 2.24 the symmetric 2,6-bis-(4-Iodo-pyrazolyl-1-yl)-pyridine (**21**) and 2,6-bis-(4-Bromo-pyrazolyl-1-yl)-pyridine (**22**) were obtained from very good (**21**, >80%) to good yield (**22**, 57%). This opened the way to access a large number of derivatives which are shown in Scheme 2.24. The Grignard exchange on **21** was very successful, and allowed the synthesis of the bis-carbaldehyde **19** easily. The ^{13}C -NMR spectra for compounds **21**, **22**, and **24** are reported in Figure 2.12



Scheme 2.24

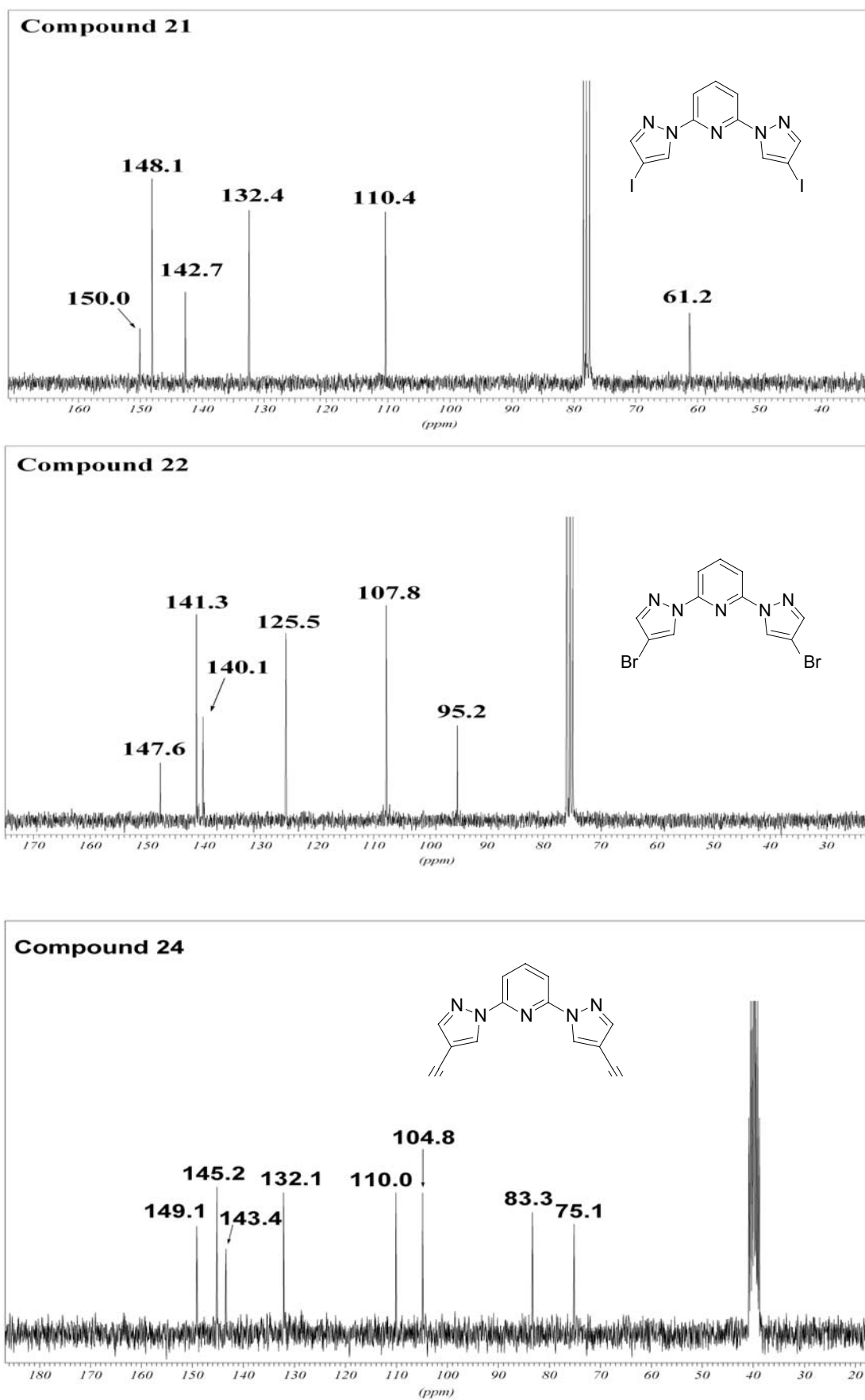
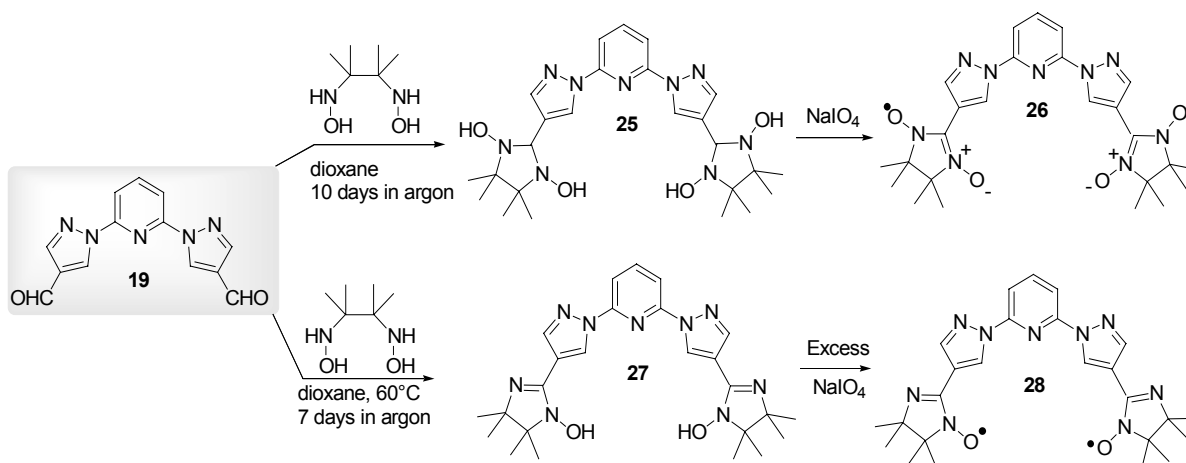


Figure 2.12: ^{13}C -NMR (63 MHz, r.t.) spectra for compounds **21** and **22** recorded in CDCl_3 and **24** in $\text{DMSO}-d_6$.

The Scheme 2.25 illustrates the subsequent steps towards the nitronyl nitroxide and iminonitroxide biradicals. The condensation between the diformyl-derivative **19** with 2,3-bishydroxylamino-2,3-dimethylbutane (**6**) in dioxane occurred while stirring at room temperature under argon over ten days, and afforded the radical precursor 2,6-bis[4-(1,3-dihydroxy-4,4,5,5-tetramethylimidazolidin-2-yl)-pyrazolyl]-pyridine (**25**) as yellowish powder (yield 42%). Heating the reaction mixture increased the decomposition of the hydroxyl-derivative in solution, and led to the formation of compound 2,6-bis[4-(1-hydroxy-4,4,5,5-tetramethylimidazolin-2-yl)pyrazolyl]-pyridine (**27**). The sodium-periodate oxidation of **25** carried under phase transfer conditions ($\text{CHCl}_3/\text{H}_2\text{O}$) gave the crude biradical 2,6-bis[4'-(3-oxide-1-oxyl-4,4,5,5-tetramethylimidazolin-2-yl)pyrazol-1'-yl]-pyridine (**26**) in the organic phase. The side products (i.e mono nitronyl nitroxide, mono imino nitroxide) were easily separated by column chromatography (silica gel, acetone/light petroleum ether, b.p. 30-40°C, 2/8) and highly pure **26** was collected ($R_f = 0.34$) and recrystallised from CHCl_3 (blue crystals, yield 27%).



Scheme 2.25

Similarly, the oxidation of the radical precursor **26** under phase transfer conditions ($\text{CHCl}_3/\text{H}_2\text{O}$) afforded the crude biradical 2,6-bis[4-(1-oxyl-3-4,4,5,5-tetramethylimidazolin-2-yl)pyrazolyl]pyridine (**28**) in the organic phase. The purification of the crude mixture was carried out by column chromatography (silica gel, acetone/light petroleum ether, b.p. 30-40°C, 2/8, $R_f = 0.46$), then recrystallisation from CH_2Cl_2 gave pure **28** (orange powder, yield 51%). As expected, the biradical **28** was obtained in larger yield with respect to **27**. Once isolated, the biradicals are stable as powder over several months, while in protic solvents (e.g. CH_2Cl_2 or CHCl_3), that may catalyze loss of water molecules, a clear decrease of their stability was observed upon prolonged storage. However, in aprotic solvents like toluene, as previously found for the terpyridine and the bispyridine based radicals, the compounds **26** and **28** could safely be kept for long time. Even when they were heated up to 60°C for several hours, no hint

of decompositions was observed, providing that the medium was maintained oxygen free. In Figure 2.13 are reported for comparison the ^{13}C -NMR spectra of the biscarbalddehyde **19** and the radical precursor **25**.

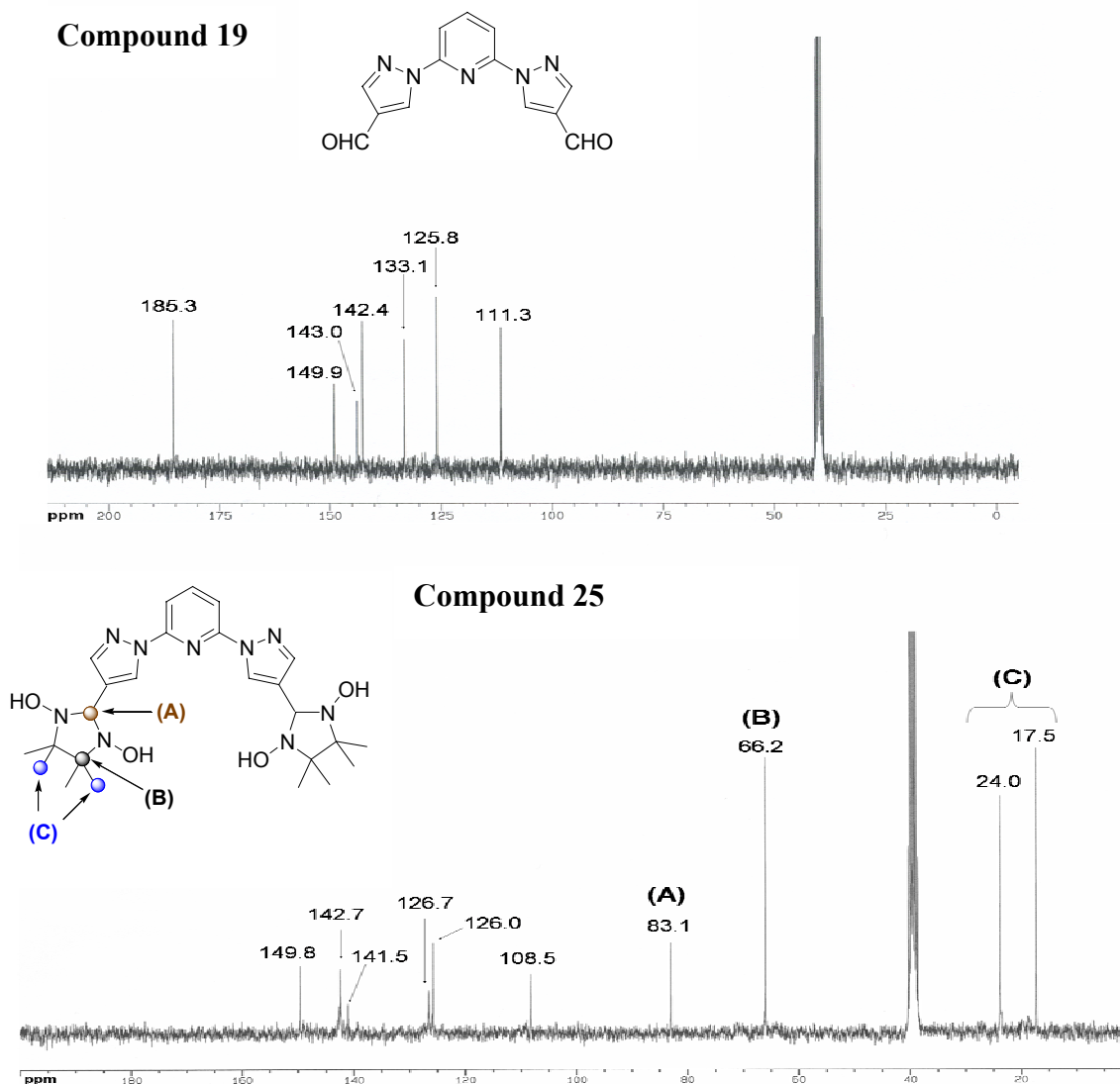
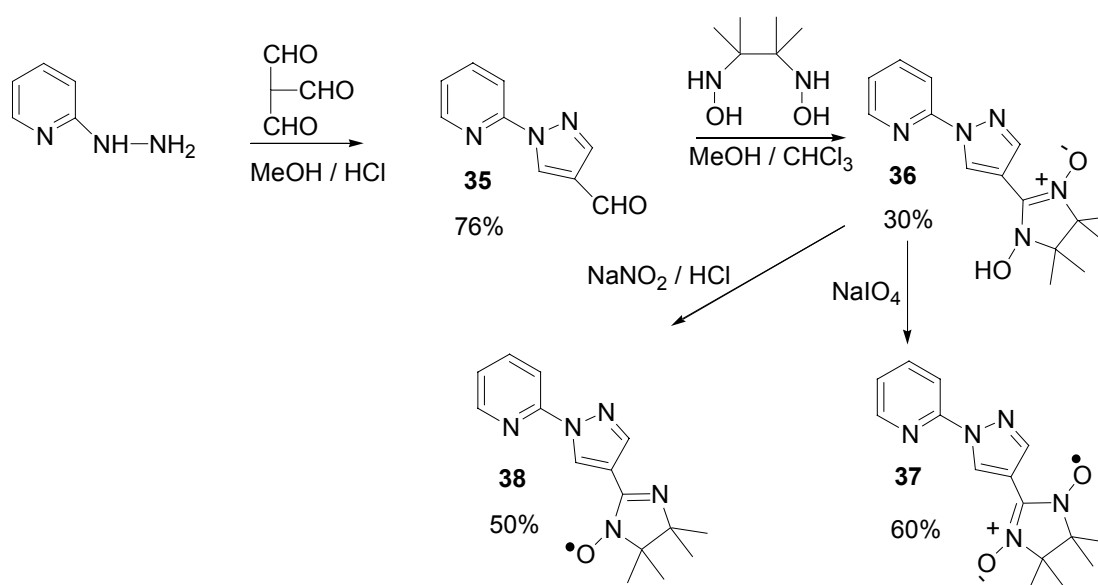


Figure 2.13: ^{13}C -NMR (63 MHz, r.t.) spectra for compounds **19** and **25** recorded in $\text{DMSO}-d_6$.

The precursors of the Ullman base radicals feature always characteristic peaks associated with the imidazolyl moiety. As an example, the C-H carbon of the imidazolyl ring in compound **25**, marked with (A) in Figure 2.13, exhibits a well defined resonance around 83 ppm, while the two cis/trans methyl carbons (C) fall at ~ 17 and ~ 24 ppm respectively. The quaternary carbon (B) instead gives constantly a sharp peak around 66 ppm.

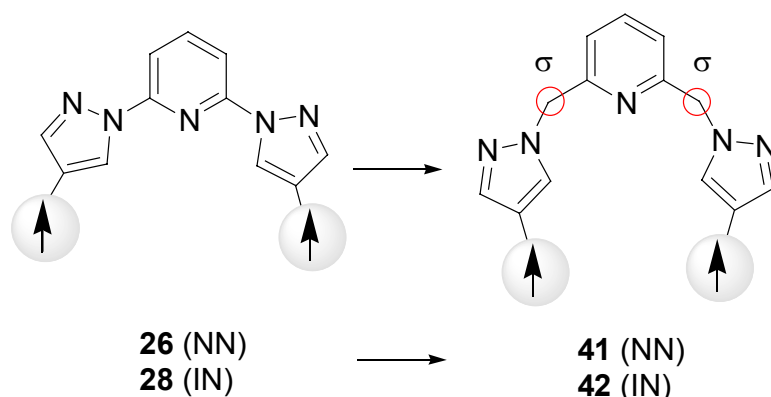
The similar synthetic procedures used to assemble the biradical derivatives **26** and **28** have been employed also for the synthesis of the two pyrazolyl-based monoradical systems, the 2[4-(1-oxide-3-oxyl-4,4,5,5-tetramethylimidazolin-2-yl)pyrazolyl]-pyridine (**37**) (NN) and 2[4-(1-oxyl-4,4,5,5-tetramethylimidazolin-2-yl)pyrazolyl]-pyridine (**38**) (IN). Their synthesis were necessary in order to obtain either suitable references for the pyrazole based biradical systems (**26** and **28**), and to probe up to which extent the electronic properties of the radical fragments (NN and IN) are influenced upon connection to different types of π -hetero rings (pyrazole based radicals *versus* pyridine based radicals).

The Scheme 2.26 describes the reaction steps. The condensation between hydrazinopyridine with triformylmethane afforded in very good yield the 2-(4-formylpyrazolyl)-pyridine (**35**). Then, further condensation with 2,3-bishydroxylamino-2,3-dimethylbutane (**6**) in methanol/trichloromethane mixture under argon gave the air sensitive monoradical precursor 2[4-(1-hydroxy-3-oxyl-4,4,5,5-tetramethylimidazolin-2-yl)pyrazolyl]-pyridine (**36**). The nitronyl nitroxide radical **37** was obtained by usual NaIO_4 oxidation under phase transfer conditions (water/chloroform) carried on the precursors **36**. However, excess of NaIO_4 did not provide the correspondent imino nitroxide radical **38**, even when the reaction mixture was heated up to 50°C . Thus, it has been used a much stronger oxidizing agent (NaNO_2/HCl). Both radicals were obtained in a very good yield after purifications on silica column, and this represents a relevant difference with respect to the radicals directly attached to pyridine moieties that suffer of fast over-oxidation processes and decomposition, even within the purification in column when silica have been used. Furthermore, the overall yields of both mono- and biradical systems directly linked to pyrazole (**26**, **28**, **37** and **38**) are much higher with respect to those connected to pyridine units.

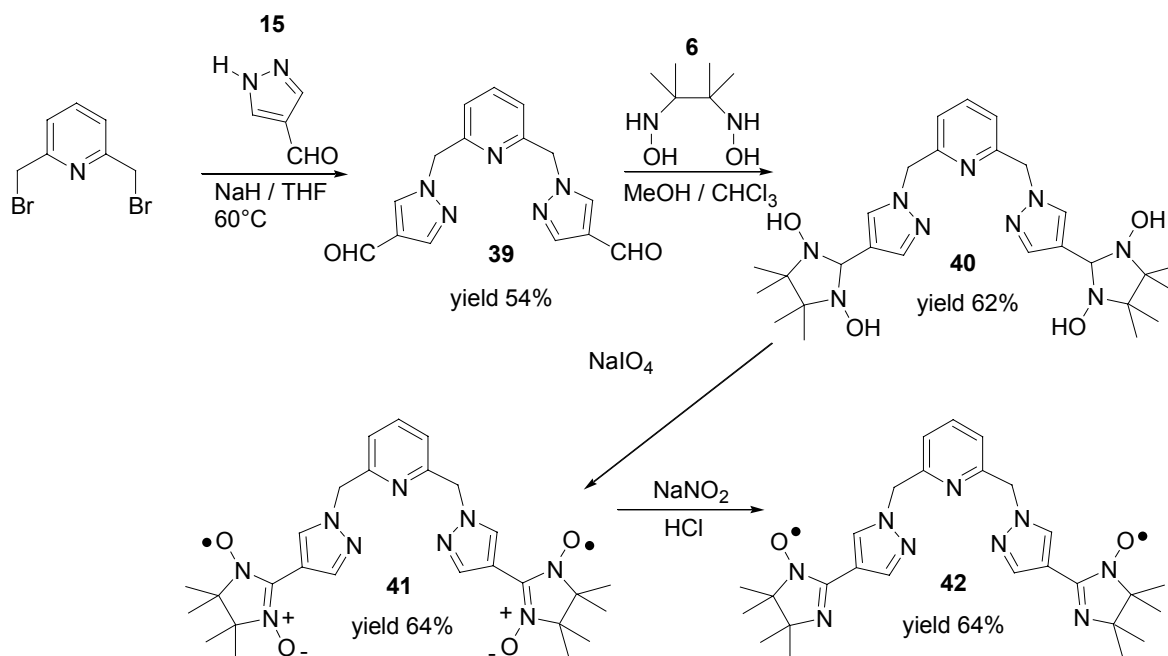


Scheme 2.26

A decrease in the π -conjugation between radical moieties in a biradical system should induce a decrease in their through-bond interaction. However, while such decrease is expected, it would be extremely difficult to assess quantitatively this effect by using theoretical predictions. Therefore, we decided to synthesize two model systems by taking as reference the biradicals **26** (NN) and **28** (IN), and introducing two σ -bonds between the pyrazolyl-imidazolidin moieties and the central pyridine ring, in order to attain their related σ -conjugated radicals 2,6-bis[4-(1-oxyl-3-oxide-4,4,5,5-tetramethylimidazolin-2-yl)pyrazolylmethyl] pyridine (**41**) and 2,6-bis[4-(1-oxyl-4,4,5,5-tetramethylimidazolin-2-yl)pyrazolylmethyl] pyridine (**42**).



The synthetic steps are described below as Scheme 2.27, and provided the radicals **41** and **42** in a very good yield.



Scheme 2.27

The 2,6-bis(4-formylpyrazolylmethyl)pyridine (**39**) was made accessible by reacting the commercially available 2,6-dibromomethylpyridine with 4-formylpyrazole (**15**) and sodium hydride in THF. The nucleophilic substitution occurred very fast (3 hours), and gave the

biscarbaldehyde **39** in good yield (54%). Further condensation with 2,3-bishydroxylamino-2,3-dimethylbutane (**6**) in methanol/trichloromethane mixture under argon gave within 2 days the biradical precursor 2[4-(1-hydroxy-3-oxyl-4,4,5,5-tetramethylimidazolin-2-yl)pyrazolyl]-pyridine (**40**). The NN radical **41** was obtained by usual NaIO_4 oxidation under phase transfer conditions (water/chloroform), and separated as blue powder. However, as previously found for the monoradicals **38**, using excess of NaIO_4 in **40** did not provide the desired imino nitroxide biradical **42**. Therefore both **40** and **41** appeared very resistant towards over-oxidation processes. Thus, the stronger oxidizing agent NaNO_2/HCl was employed on the precursor **41**, and the biradical **42** was cleanly obtained as orange-red powder. Also in this case, the purifications of the radicals have been performed easily on silica column, without showing any trend of decomposition. The ^{13}C NMR spectra of **39** and the radical (NN) precursor **40** are shown in the Figure 2.14.

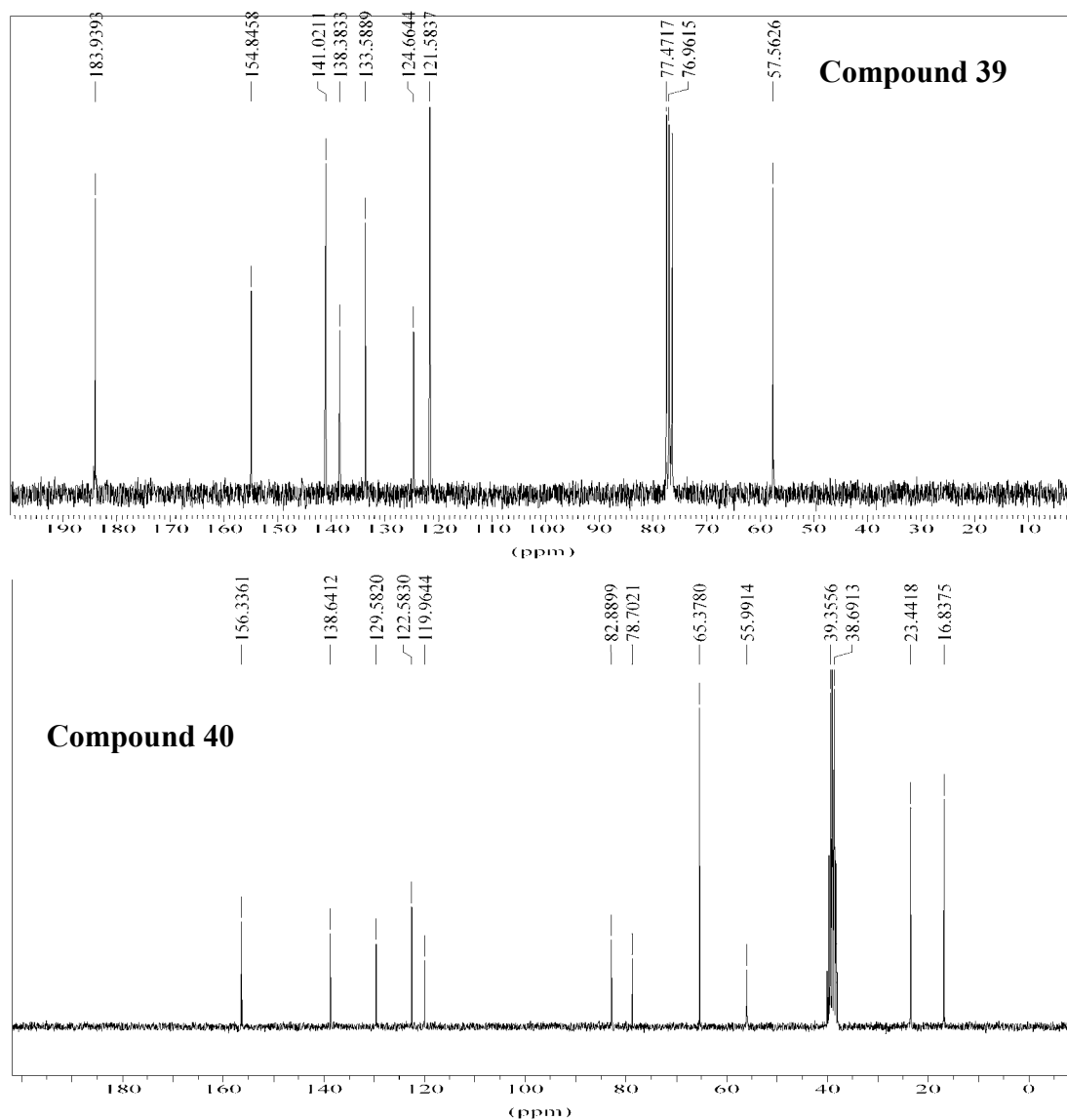
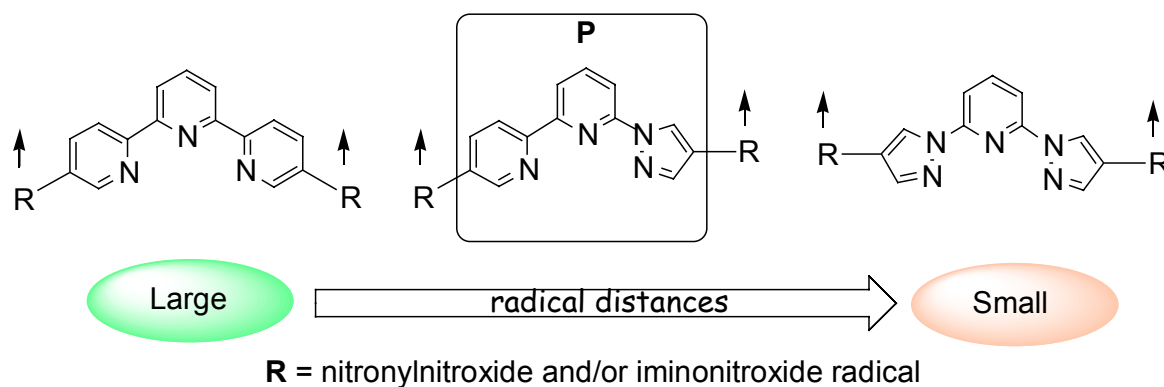
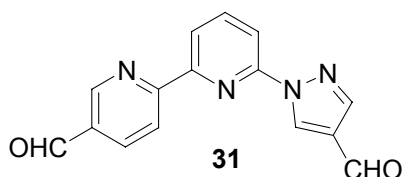


Figure 2.14: ^{13}C -NMR (63 MHz, r.t.) spectra for compounds **39** (CDCl₃) and **40** (DMSO-*d*₆).

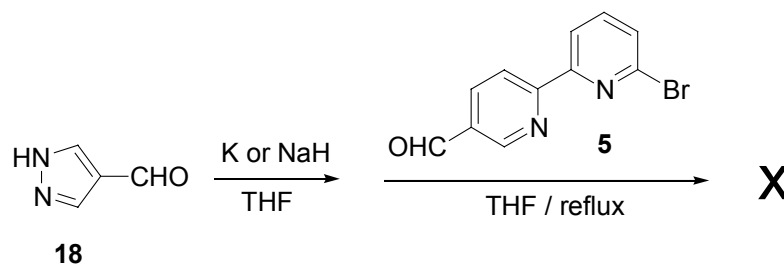
In order to provide an intermediate case (radical distances vs exchange pathways) for the π -conjugated N-heterocyclic cores, which could stay in between the terpyridine and the bispyrazolylpyridine units, it was necessary to synthesize a non symmetric nitrogen-based ligand. The choice was straightforwardly directed to the pyrazolylbipyridine element (**P**).



The successful synthetic path that led to the biradicals based on **P**, required the preparation of the derivative 4'',5'-diformyl-6-(pyrazol-1''-yl)-2,2'-bipyridine (**31**). This was obtained using the combined knowledge gained on the terpyridine and bispyrazolylpyridine systems. The necessary synthetic steps are outlined in the following section.

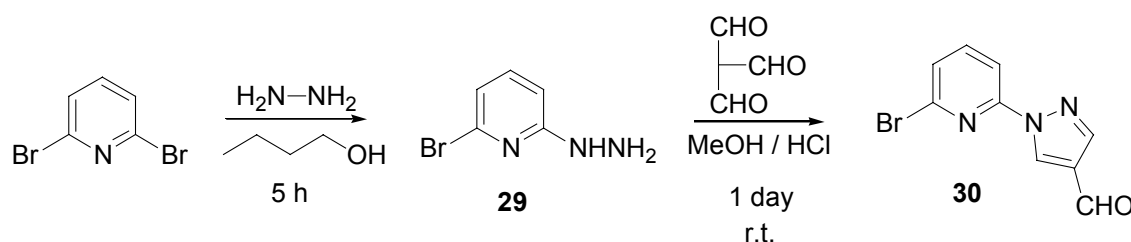


The coupling reaction between 6-bromo-2,2'-dipyridine-5'-carbaldehyde (**5**) as previously prepared with either the potassium or the sodium hydride salt of pyrazol-4-carboxaldehyde (**18**) in THF was almost ineffective, and led to a complex mixture of by-products, where the major loss of the carbaldehyde group in **5** was observed (Scheme 2.28).



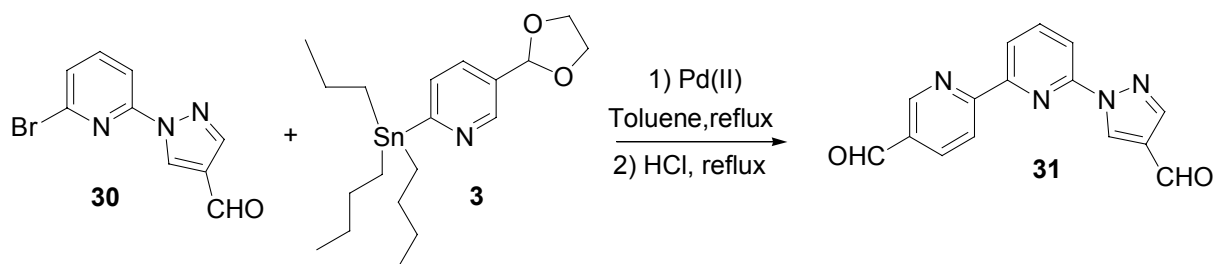
Scheme 2.28

This failure seemed consistent with the poor reactivity of the bromine group in position 6 due to lack of activation towards nucleophilic substitutions. In addition the protection of the carbaldehyde group in **5** turned to be surprisingly difficult to achieve by using ethyleneglycole with either toluene-4-sulfonic-acid or Amberlist-15 as acid catalyst. This represents a substantial difference with the previous protection of the 6-bromo-3-pyridinecarbaldehyde (**1**). The successful reaction path for **31** was then carried out as follows: the 2,6-dibromopyridine was reacted in alcoholic medium (ButOH) with excess of hydrazine-monohydrate (solution in THF), and gave the 2-bromo-6-hydrazinopyridine (**29**) as yellowish crystals (yield 57% - 63%). The condensation between **29** and triformylmethane (**14**) was achieved in acidified alcoholic medium (MeOH/HCl), and afforded the 6-bromo-2-[4'-formylpyrazol-1'-yl]-pyridine (**30**). It was obtained as fine precipitate after neutralization with aqueous Na_2CO_3 solution and chromatographic separation on silica column ($\text{CHCl}_3/\text{Hexane}/\text{Ethylacetate}$, 1/3/1, $R_f = 0.67$) (yield 70%).



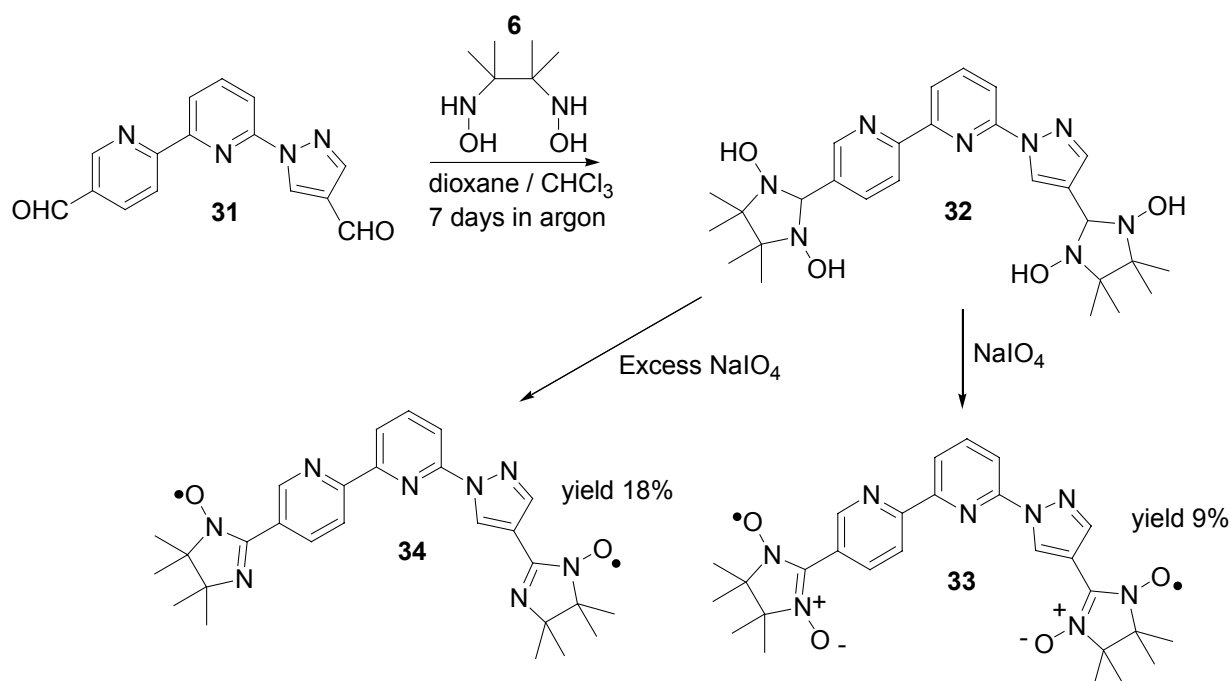
Scheme 2.29

As an alternative, **30** can be obtained as well by reacting the 2,6-dibromopyridine (1.eq.) with the potassium salt of pyrazol-4-carboxaldehyde (**18**) (1.2 eq) in THF under argon, and heating the mixture for 60 h at 70° (yield 60%) followed by purification on silica column using the same procedure reported above. Both routes provided comparable yields but the one shown in Scheme 2.29 was somehow faster. Then, the Stille coupling reaction between **30** and 2-tributylstannyl-5-[1,3]dioxolan-2-yl-pyridine (**3**) was achieved in toluene under rigorous argon atmosphere for 60 hours, in presence of $\text{Pd}(\text{PPh}_3)_2\text{Cl}_2$ (5%), PPh_3 (10%) and copper iodide (CuI) as catalyst. The presence of CuI was essential, since the use of the $\text{Pd}(\text{II})/\text{PPh}_3$ catalyst itself led to a drastic decrease in the overall yield (from 46% to ~ 20%). This effect is exactly opposite to that one previously observed for the similar Stille coupling reaction between **5** and **3**. Further hydrolysis of the dioxolane in presence of HCl (6 N) followed by basification gave 4'',5'-diformyl-6-(pyrazol-1''-yl)-2,2'-bipyridine (**31**) as shown in Scheme 2.30.



Scheme 2.30

The bisformyl-derivative **31** (1 eq) was then subjected to Ullman coupling with 2,3-bishydroxylamino-2,3-dimethylbutane (**6**, 3.5 eq) using a mixture of 1,4-dioxane and trichloromethane (1/1) as solvents for 7 days, under argon at room temperature as depicted in Scheme 2.31.



Scheme 2.31

The reaction mixture showed no hint of precipitate formation. This was consistent with the partial dehydration of the bis(N,N')-hydroxy-imidazolidine to N-hydroxy-imidazolidine. The use of the FTIR technique proved to be very useful in this case. In fact, upon collecting aliquots of the reaction mixture at various times, we could monitor the proceeding of the condensation reaction just by observing the disappearance of the carbaldehyde peak (with $\nu_{C=O}$ at 1689 cm⁻¹). The yellowish powder obtained, upon solvent removal, contained the crude 4'',5'-bis[1,3-dihydroxy-4,4,5,5-tetramethylimidazolidin-2-yl]-6-(pyrazol-1''-yl)-2,2'-bipyridine (**32**) (crude yield 73%) and this powder was oxidized, working under phase transfer conditions (CHCl₃/H₂O) at room temperature, by using slight excess of NaIO₄ (2.5 eq) with respect to **32**

(1.0 eq) for 20 min. After collection of the organic phase side products (mono- nitronyl nitroxide and mono imino nitroxide radicals) were separated by column chromatography (aluminum-oxide, acetone/light petroleum ether) while the non-oxidized and/or decomposed hydroxy-imidazolidine **32** was not eluted at all, and remained strongly retained at the top of the column. Then, pure 4'',5'-bis[3-oxide-1-oxyl-4,4,5,5-tetramethylimidazolin-2-yl]-6-(pyrazol-1''-yl)-2,2'-bipyridine (**33**) was obtained as deep-blue powder. In a similar manner, the 4'',5'-bis[1-oxyl-4,4,5,5-tetramethylimidazolin-2-yl]-6-(pyrazol-1''-yl)-2,2'-bipyridine (**34**) was synthesized by using excess of oxidant (NaIO₄, 4.0 eq) with respect to **32** (1.0 eq) followed by chromatographic separation on neutral alumina, to afford **34** as orange-red powder. Unfortunately, was not possible to increase the yield of the nitronyl nitroxide biradical **33** since, as reported previously, the NN radicals attached to pyridine moieties are far more sensitive towards over-oxidation processes with respect to those appended on the pyrazole rings. Finally, in Table 2.1, is shown a comparative outlook of the radical stabilities in solution for the nitronyl nitroxide (NN) series.

Table 2.1. The NN radical stabilities in solution.

NN radicals	hexane	toluene	THF	acetone	CH ₂ Cl ₂	MeOH	CHCl ₃
12 biradical	Stable (~ 1 year) ~[10 ⁻³ M]	Stable (~1 year) ~[10 ⁻³ M]	Not stable (< day) >[10 ⁻³ M]	Stable (~6 months) >>[10 ⁻³ M]	Stable (~3 months) >>[10 ⁻³ M]	Not stable (< day) >[10 ⁻³ M]	Stable (~ 1 month) >>[10 ⁻³ M]
8 monoradical	Stable ~[10 ⁻³ M]	Stable (~1 year)* ~[10 ⁻³ M]	Not stable (~ week) >[10 ⁻³ M]	Stable (~8 months) >>[10 ⁻³ M]	Stable (~4 months) >>[10 ⁻³ M]	Not stable (< week) >[10 ⁻³ M]	Stable (< 2 months) >>[10 ⁻³ M]
26 biradical	Stable (~ 1 year) < [10 ⁻³ M]	Stable (~1 year)* ~[10 ⁻³ M]	Not stable (~ 1 day) >[10 ⁻³ M]	Stable (~9 months) >>[10 ⁻³ M]	Stable (~6 months) >>[10 ⁻³ M]	Not stable (< 1 day) >[10 ⁻³ M]	Stable (<4 months) >>[10 ⁻³ M]
36 monoradical	Stable (~ 1 year) > [10 ⁻³ M]	Stable (~1 year)* >[10 ⁻³ M]	Not stable (~ week) >[10 ⁻³ M]	Stable (~ 1 year) >>[10 ⁻³ M]	Stable (~7 months) >>[10 ⁻³ M]	Not stable (~ week) >[10 ⁻³ M]	Stable (<6 months) >>[10 ⁻³ M]
33 biradical	Stable (~ 1 year) < [10 ⁻³ M]	Stable (~1 year) ~[10 ⁻³ M]	Not stable (<< day) >[10 ⁻³ M]	Stable (~6 months) >>[10 ⁻³ M]	Stable (~2 months) >>[10 ⁻³ M]	Not stable (<< day) >[10 ⁻³ M]	Stable (~1 month) >>[10 ⁻³ M]
41 biradical	Stable (~ 1 year) > [10 ⁻³ M]	Stable (~1 year)* >[10 ⁻³ M]	Less stable (> week)* >[10 ⁻³ M]	Stable (~ 1 year) >>[10 ⁻³ M]	Stable (~7 months) >>[10 ⁻³ M]	Less stable (> week) >[10 ⁻³ M]	Stable (<7 months) >>[10 ⁻³ M]

The asterisk (*) indicates that the radical can be heated up to 60°C without apparent decomposition for three hours even in presence of NaH under argon. The numbers in brackets [x] indicates the relative solubility in the specific solvent. The imino nitroxide radicals showed comparable or slightly higher stabilities in these solvent series. In addition, two other solvents (ethylacetate and 2-propanol) were recently tested in which the radicals featured similar stabilities as compared with, for example, acetone. All the solvents were purchased as spectrophotometric grade, and used as received with the exception of THF that was distilled in presence of sodium under argon.

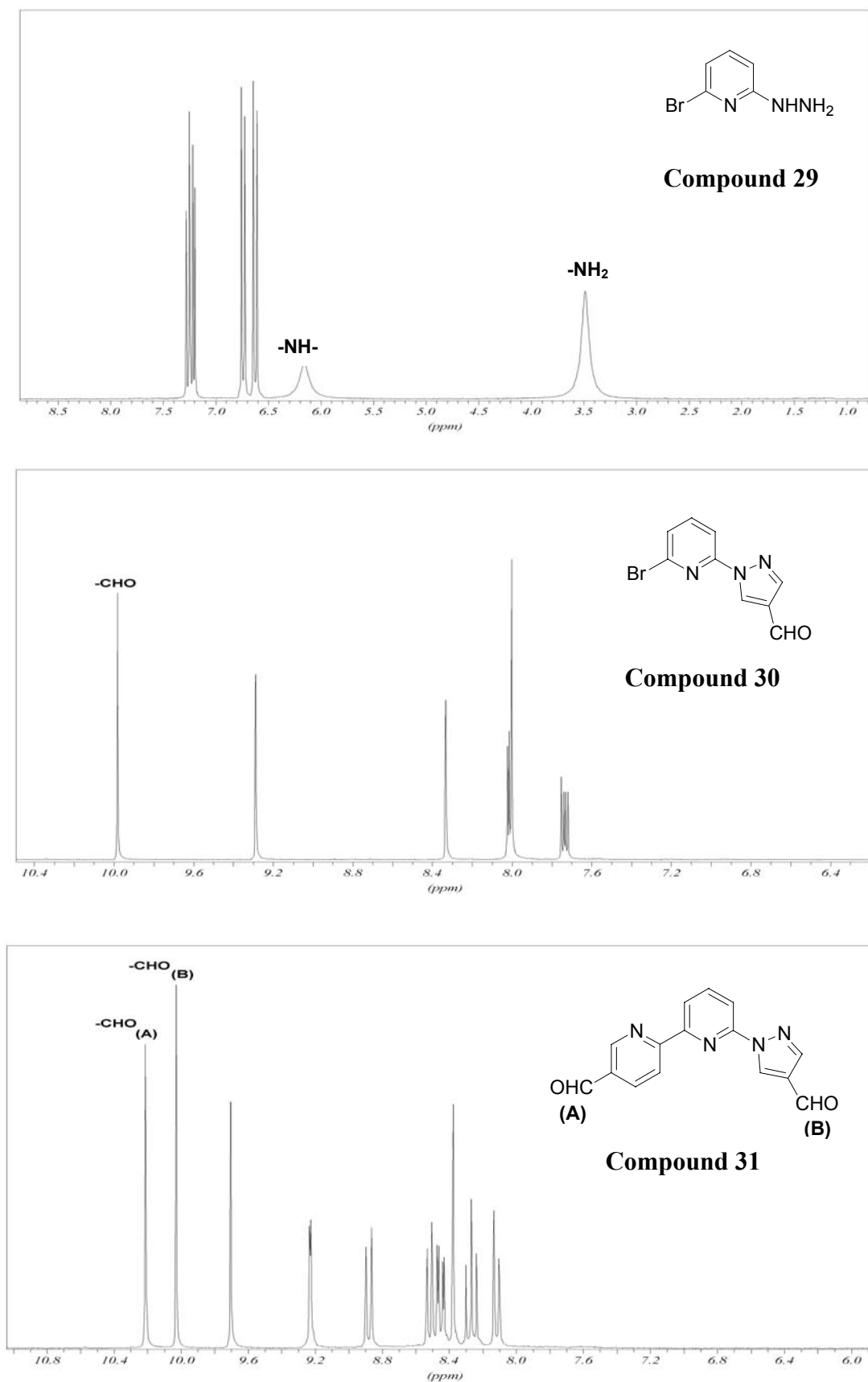


Figure 2.15: ¹H-NMR (250 MHz, r.t.) spectra for compounds **29** recorded in CDCl₃, **30** and **31** recorded in DMSO-*d*₆.

References

- [1] Osiecki J.H. and Ullman E.F., *J. Am. Chem. Soc.*, 90 (4) **1968**, 1078.
- [2] Ullman E.F., Call L., Osiecki J.H., *J. Org. Chem.* 35 (11), **1970**, 3623.
- [3] Ullman E.F., Osiecki J.H., Boocock D.G.B., Darcy R., *J. Am. Chem. Soc.* 94 (20), **1972**, 7049.
- [4] (a) O. Kahn, *Magnetism: A Supramolecular Function*, Eds., Kluwer, Dordrecht, **1996**. (b) J. S. Miller, M. Drillon, *Magnetism: Molecules to Materials III*, Wiley-VCH, Weinheim, **2001**. (c) J. S. Miller, M. Drillon, *Magnetism: Molecules to Materials I, II, IV*, Wiley-VCH, Weinheim, **2003**.
- [5] For a collection of the recent progresses in the field see *Proceedings of the 8th International Conference on Molecule-Based Magnets (ICMM 2002)*, *Polyhedron* **2003**, 22, 1725-2584.
- [6] Formation of 2-phenyl imidazoline from 2,3-diamino-2,3-dimethylbutane and phenylthioamide followed by oxidation with NaWO₄/H₂O₂ has been reported by Aurich H.G., Czepluch H., Hahn K., *Tetrahedron Lett.* 50, **1977**, 4373.
- [7] (a) Hirel C., Vostrikova E.K., Pécaut J., Ovcharenko V.I., Rey P., *Chem. Eur. J.* 7 (9), **2001**, 2007. (b) G. V. Shustov, N. B. Tavakalyan, L. L. Shustova, A. P. Pleshkova, R. G. Kostianovskii, *Bull. Acad. Sci. URSS, Div. Chem. Sci.*, **1982**, 31 (Engl. transl.)
- [8](a) J. S. Miller and A. Epstein, *Angew. Chem. Int. Ed.*, 106, **1994**, 399. (b) S. Nakatsuji and H. Anzai, *J. Mat. Chem.* 7, **1997**, 2161. (c) J. A. Crayston, J. N. Devine, J. C. Walton, *Tetrahedron*, 56, **2000**, 7829.
- [9] (a) Chelucci G., Thummel R.P., *Chem. Rev.* 102, **2002**, 3129. (b) Cargill Thompson A.M.W., *Coord. Chem. Rev.* 160, **1997**, 1. (c) Lehmann U., Henze O., Schlüter A.D., *Chem. Eur. J.* 5, **1999**, 854. (d) Romanenko G.V., El'tsov I.V., Ovcharenko V.I., *J. of Struct. Chem.*, 43, **2002**, 700. (e) Solanki N.K., McInnes E.J.L., Mabbs F.E., Radojevic S., McPartlin M., Feeder N., Davies J.E., Halcrow M.A., *Angew. Chem. Int. Ed.*, 37, **1998**, 2221.
- [10] (a) J. P. Sauvage, J. P. Collin, J. C. Chambron, S. Guillerez, C. Coudret, V. Balzani, F. Barigelletti, L. De Cola, L. Flamigni, *Chem. Rev.*, 94, **1994**, 993. (b) J.-M. Lehn, *Supramolecular Chemistry. Concepts and Perspectives*, Wiley VCH, Weinheim, Germany, 1995. (c) Drain C.M., Lehn J.-M., *J. Chem. Soc. Chem. Commun.*, **1994**, 2313. (d) Loi M, Hosseini M.W., Jouaiti A., De Cian A., Fisher J., *Eur. J. Inorg. Chem.*, **1999**, 1981. (e) Jouaiti A., Loï M., Hosseini M.W., De Cian A., *J. Chem. Soc. Chem. Commun.*, **2000**, 2085.
- [11] Trawick B.N., Daniher A.T., Bashkin J.K., *Chem. Rev.*, 98, **1998**, 939.
- [12] E. Coronado, P. Delhaés, D. Gatteschi, J. S. Miller, Eds., *Molecular Magnetism: From Molecular Assemblies to the Devices*, NATO ASI Series E 321, Kluwer Academic Publishers, Dordrecht **1996**.

- [13] Edwin C. Constable, Gerhard Baum, Eckhard Bill, Raylene Dyson, Rudi van Eldik, Dieter Fenske, Susan Kaderli, Darrell Morris, Anton Neubrand, Markus Neuburger, Diane R. Smith, Karl Wieghardt, Margareta Zehnder, Andreas D. Zuberbühler, *Chem. Eur. J.*, 5 (2), **1999**, 498. (b) Kremer S., Henke W., Reinen D., *Inorg. Chem.*, 21, **1982**, 3013. (c) Figgis B.N., Kucharski E.S., White A.W., *Aus. J. Chem.*, 36, **1983**, 1537. (d) Money V.A., Evans I.R., Halcrow M.A., Goeta A.E., Howard J.A.K., *Chem. Commun.* **2003**, 158.
- [14] A. Harriman, R. Ziessel, *Coord. Chem. Rev.*, 171, **1998**, 331.
- [15] Constable E.C., Ward M.D., Corr S., *Inorg. Chim. Acta*, 141, **1988**, 201. (b) Dietrich-Buchecker C.O., Marnot P.A., Sauvage J.P., *Tetrahedron Lett.*, **1983**, 5291. (c) Bell, T.W., Firestone A.J., *J. Org. Chem.*, 51, **1986**, 764. (d) Schubert U.S., Eschbaumer C, Georg Hochwimmer, *Synthesis*, 5, **1999**, 779. (e) Ziener U., Lehn J.-M., Mourran A., Moller M, *Chem Eur. J.*, 8 (4), **2002**, 951. (f) Kelly TR, Lebedev R.L., *J. Org. Chem.* 67 (7), **2002**, 2197. (g) El-Ghayoury A., Ziessel R., *J. Org. Chem.*, 65, **2000**, 7757. (h) Halcrow M.A., Brechin E.K., McInnes E.J.L., Mabbs F.E., Davies J.E., *J. Chem. Soc., Dalton Trans.*, **1998**, 2477. (i) Lehmann U., Henze O., Schlüter A.D., *Chem. Eur. J.*, 5 (3), **1999**, 854. (l) Constable E.C., Ward M.D., *J. Chem. Soc. Dalton Trans.*, **1990**, 1405. (m) Jameson L. D., Goldsby K.A., *J. Org. Chem.*, 55, **1990**, 4992. (n) Mukherjee R., *Coord. Chem. Rev.*, 203, **2000**, 151.
- [16](a) M. A. Halcrow, E. K. Brechin, E. J. L. McInnes, F. E. Mabbs, J. E. Davies, *J. Chem. Soc., Dalton Trans.*, **1998**, 2477. (b) C. Stroh, R. Ziessel, *Tetrahedron Lett.* 40, **1999**, 4543. (c) C. Stroh, P. Turek, P. Rabu, R. Ziessel, *Inorg. Chem.* 40, **2001**, 5334.
- [17] (a) Sasaki I., Daran J.C., Balavoine G.G.A., *Synthesis*, 5, **1999**, 815. (b) Goral V., Nelen M.I., Eliseev A.V., Lehn J.-M., *PNAS*, 98 (4), **2001**, 1347.
- [18] X. Wang, P. Rabbat, P. O'Shea, R. Tiller, E. J. J. Grabowski, P. J. Reider *Tetrahedron Lett.*, 41, **2000**, 4335.
- [19] F. J. Romero-Salguero, J.-M. Lehn *Tetrahedron Lett.*, 40, **1999**, 859.
- [20] D. Cai, D. L. Hughes, T. R. Verhoeven, *Tetrahedron Lett.*, 37, **1996**, 2537.
- [21] For the toxicity of stannyl-compounds see for example: A. G. Davies, P. J. Smith, *Comprehensive Organometallic Chemistry* (Ed. E. W. Abel) Pergamon, Oxford 2, **1982**, 608.
- [22] See for example "On the nature of the "Copper Effect" in the Stille Cross-Coupling". Farina V. Kapadia S. Krishnan B., Wang, C; Liebeskind L.S., *J. Org. Chem.*, 59, **1994**, 5905.
- [23] Schwab P.F.H., Fleischer F., Michl J., *J. Org. Chem.*, 67 (2), **2002**, 443.
- [24] J. de Mendoza, E. Mesa, Juan-Carlos Rodríguez-Ubis, P. Vázquez, F. Vögtle, Paul-Michael Windscheif, K. Rissanen, J.-M. Lehn, D. Lilienbaum, R. Ziessel, *Angew. Chem. Int. Ed. (Engl.)* 30 (10), **1991**, 1331.
- [25] (a) Iyoda M., Otsuka H., Sato K., Nisato N., Oda M., "Homocoupling of aryl halides using Nickel(II) complex and Zinc in presence of Et₄Ni. An efficient method for the synthesis of

biaryls and bipyridines”, *Bull. Chem. Soc. Jpn*, 63, **1990**, 80. (b) Jolly P.V., “Nickel catalyzed coupling of organic halides and related reactions” in “*Comprehensive Organometallic Chemistry*” Ed. G. Wilkinson, Pergamon Press., Oxford, Vol. 8, **1982**, p.713.

[26] Z. Arnold Z., *Coll. Czech. Chem. Commun.* 26, **1961**, 3051.

[27] Takagi K., Bajnati A., Hubert-Habart M., *Bull. Soc. Chim. Fr.*, 127, **1990**, 660.

[28] (a) Sorrel T.N., *Tetrahedron*, 45, **1989**,3.(b) Trofimenko S., Calabrese J.C., Thompson J.S., *Inorg. Chem.* 26, **1987**, 1507. (c) Almirante N., Cerri A., Fedrizzi G., Marazzi G., Santagostino M., *Tetrahedron Letters*, 39, **1998**, 3287.

[29] Grimmet M., Iddon B. *Heterocycles*, 37, **1994**, 2087.

[30] (a) Hüttel, R., Schäffer O., Jochum P., *Liebigs Ann. Chem.*, 593, **1955**, 200. (b) Lipp M., Dallacker F., Munnes S., *Liebigs Ann. Chem.*, 618, **1958**, 110.

[31] Hüttel R., Büchele F., Jochum P., *Chem. Ber.* 88, **1955**, 1577.

[32] (a) Hüttel, R., Schön M.E., *Liebigs Ann. Chem.*, 625, **1959**, 55. (b) Hahn M., Heinisch G., Holzer W., Schwarz H., *J. Heterocycl. Chem.* 28, **1991**, 1189. (c) Iwata S., Qian C.-P, Tanaka K., *Chem. Lett.* **1992**, 357. (d) Sakamoto T., Shiga F., Uchiyama D., Kondo Y., Yamanaka H., *Heterocycles*, 22, **1992**, 813. (e) Elguero J., Jaramillo C., Pardo C., *Synthesis*, **1997**, 563. (f) Balle T., Per Vedsø, Begtrup M., *J. Org. Chem.* 64 (15), **1999**, 5366.

[33] Tertov B.A., Morkovnik A.S., *Chem. Heterocycl. Compd. (Engl. Transl.)* 11, **1975**, 343.

[34] (a) Felding J, Kristensen J., Bjerregaard T., Sander L., Per Vedsø, Begtrup M., *J. Org. Chem.*, 64 (11), **1999**, 4196. (b) Begtrup M. Per Vedsø, *J. Chem. Soc. Perkin Trans. 1* **1995**, 243.

[35] Vasilevsky S.F., Klyatskaya S.V., Tretyakov E.V., Elguero J., *Heterocycles*, 60 (4), **2003**, 879.

[36] Khan M.A., Pinto A.A.A., *J. Heterocyclic Chem.*, 18, **1981**, 9.

Chapter 3 - The Radical`s Optical Properties

The nitronyl nitroxide (**NN**) and imino nitroxide (**IN**) radical systems feature clear differences in their UV/Vis and IR optical properties. The spectroscopic fingerprints of the radical entities have been unambiguously identified and appeared strongly dependent on the type of π -ring system in which the radicals have been attached on. Based on these information's, we established a quick protocol that allows to assign straightforwardly the type of radical and their numbers (monoradical, biradical), to define their purities and the nature of the contaminants.

3.1. The UV/Vis absorption spectra of the radical systems.

The nitronyl nitroxide (**NN**) derivatives show light blue colour in solution (Figure 3.1), with a broad absorption band characterized by several vibronic components in the visible region of the spectra. These bands have been associated to the $n \rightarrow \pi^*$ transitions of the aminoxyl-oxide residues (at ~ 600 nm) and their assignement were assessed by theoretical calculations on the absorption envelope (vide Section 3.2). Their intensities and spectral distributions did not show appreciable dependence upon changing solvent polarities (e.g for **12** in hexane λ_{\max} at 605 nm and in nitromethane λ_{\max} at 603 nm, see Figure 3.2.) but indeed strongly depend on which type of hetero-ring the spin carriers have been grafted on. The NN pyridine based radicals present always a weak but distinctive vibronic band around 740 nm ($\epsilon \leq 70 \text{ M}^{-1} \times \text{cm}^{-1}$), that is missing when the radicals are connected to the pyrazolyl-moiety. In addition, within the pyridine based NN, the terpyridine biradical **12** shows a remarkable blue shift of the absorption envelope in the visible region with respect to the bipyridyl monoradical **8**, being accompanied by a weakening in the molar extinction (ϵ). This hampering effect is not present in the pyrazole-based radical systems, in which for example the biradical **26** features just twice the molar extinction of the monoradical **37**. The second distinctive absorption of NN falls in the UV region of the spectrum (<400 nm) and represents another fingerprint that allows to distinguish pyridine and pyrazole NN radicals. In the formers case this absorption is red-shifted over 380 nm, while in the latter is blue shifted (> 10 nm). This band is always very strong, and arises from $\pi \rightarrow \pi^*$ transition of the aminoxyl-oxide residues. In the non-symmetric radical **33**, in which pyrazole and pyridine moieties are both present, such effect is particularly clear. The transition at 373 nm ($\epsilon = 17510 \text{ M}^{-1} \times \text{cm}^{-1}$) originates from the radical connected to the pyrazole ring; in fact in the biradical system **26** this transition occur at 375 nm, $\epsilon = 16960 \text{ M}^{-1} \times \text{cm}^{-1}$ while in the monoradical **37** occur at 368 nm, $\epsilon = 11100 \text{ M}^{-1} \times \text{cm}^{-1}$. The similar transition at 392 nm ($\epsilon = 10685 \text{ M}^{-1} \times \text{cm}^{-1}$) originates from the radical connected to

the pyridine ring since in the monoradical **8** it occurs at 394 nm with $\epsilon = 8960 \text{ M}^{-1} \times \text{cm}^{-1}$ and in the biradical **12** occurs at 387 nm with $\epsilon = 13100 \text{ M}^{-1} \times \text{cm}^{-1}$. In the case of **41** this transition is strongly blue-shifted ($\sim 20 \text{ nm}$) due to the broken symmetry that results in less aromatic character of the molecule induced by the presence of $\sigma(\text{-CH}_2)$ bonds. However it appears as the most enhanced within the NN radical series.

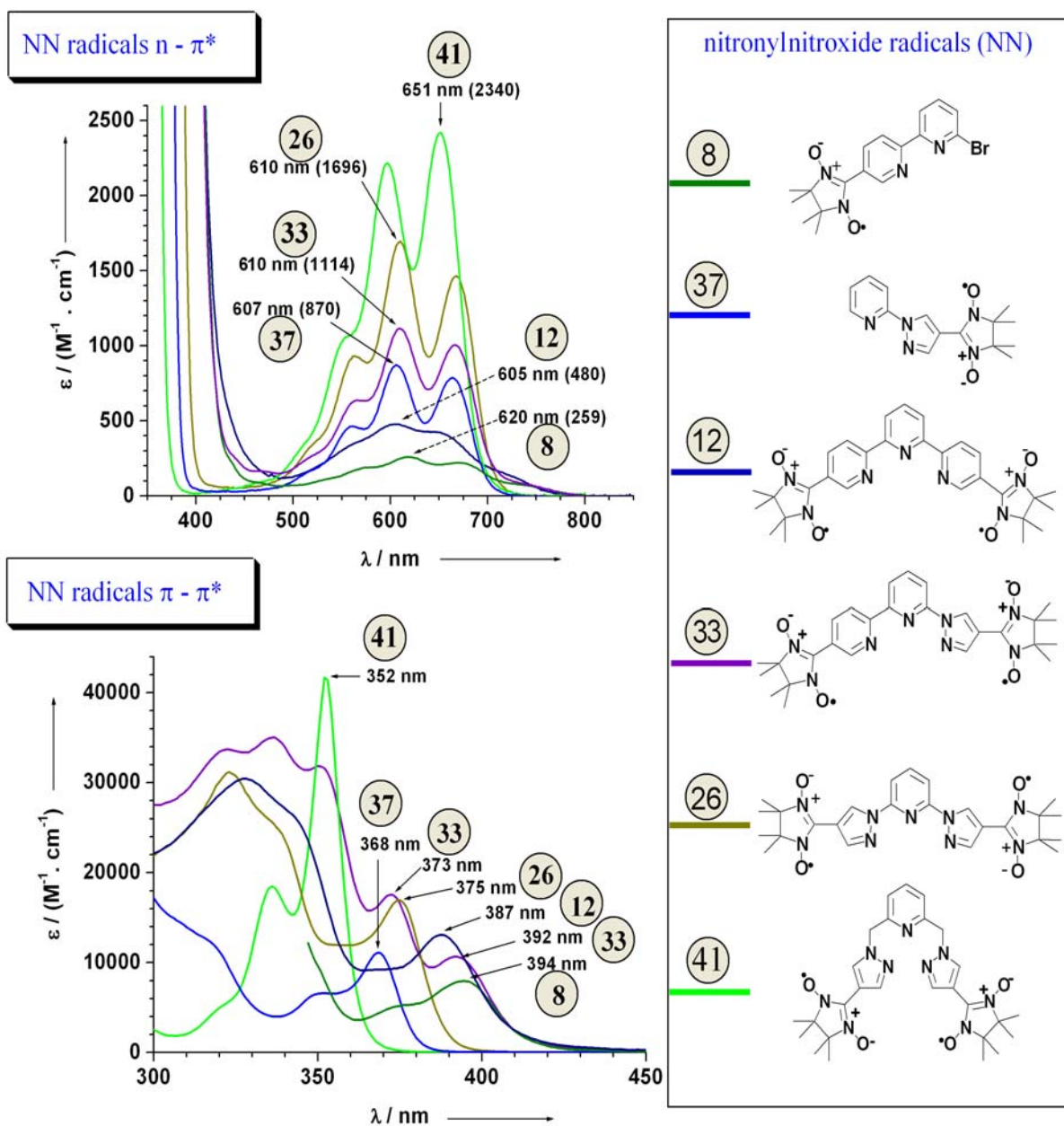


Figure 3.1: The absorption spectra of the NN radicals recorded in dilute toluene solutions at r.t.

The imino nitroxide (**IN**) derivatives feature a light orange-red colour in solution (Figure 3.3), with a broad absorption band around ~ 470 nm ($n \rightarrow \pi^*$ transitions). Likewise as previously discussed for the NN radicals, also in the INs the intensities and spectral distributions of the $n \rightarrow \pi^*$ transitions did not present appreciable dependence upon changing solvent polarities but strongly depend on the type of hetero-ring in which they have been connected (the pyridine rings hamper in a similar manner the radical optical properties as compared with those pyrazolyl-based). As shown in the case of **12** also the terpyridine biradical **13** shows a similar blue-shift on λ_{\max} . This effect arises from the increased aromatic character of the molecule once compared with its related monoradical **9**. However, the absorption envelope of **13** in the visible is accompanied by a weakening in vibronic components, and a more remarkable quenching of the molar extinction (ϵ). The pyrazolyl-based radicals instead follow a somewhat simpler trend where the biradical **28** (λ_{\max} at 468 nm, $\epsilon = 1400 \text{ M}^{-1} \times \text{cm}^{-1}$) exhibits close to twice the extinction of the monoradical **38** (λ_{\max} at 469 nm, $\epsilon = 768 \text{ M}^{-1} \times \text{cm}^{-1}$), and the biradical **34** (λ_{\max} at 467 nm, $\epsilon = 1082 \text{ M}^{-1} \times \text{cm}^{-1}$) in which both moieties are present shows an overall absorption very close to the superposition of the isolated monoradical envelopes **9** (λ_{\max} at 464 nm, $\epsilon = 321 \text{ M}^{-1} \times \text{cm}^{-1}$) and **38**, in excellent agreement with the observed properties of the parent NN system **37**. As previously observed in the case of **41**, also in **42** the broad absorption in the visible appeared the most enhanced within this series of radical. The other distinct absorption of the radical moieties ($\pi \rightarrow \pi^*$ transition of the aminoxyl-residues) is here strongly blue-shifted and cannot be discriminated from the $\pi \rightarrow \pi^*$ transition of the organic backbone. Nevertheless the UV/Vis analysis represented a complementary and quick tool that allowed to identify the presence of different radical impurities (within the limit of 5%); in the IN based radical an absorption around 370 nm indicates the presence of left NN radical, vice versa an absorption in a solution of NN radical around 470 nm is consistent with the presence of an IN impurity.

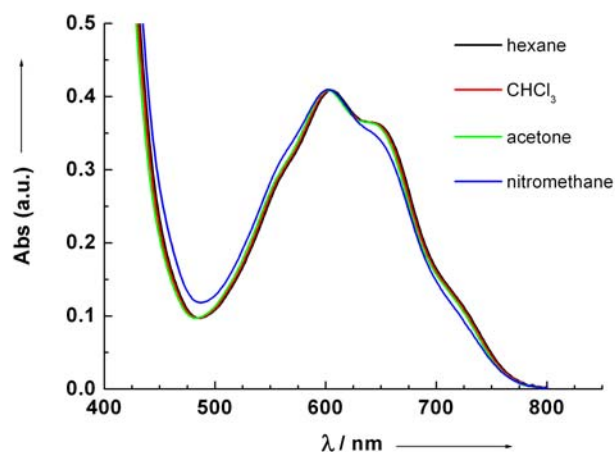


Figure 3.2: The absorption spectra of the 12 as function of the solvent polarity recorded at r.t.

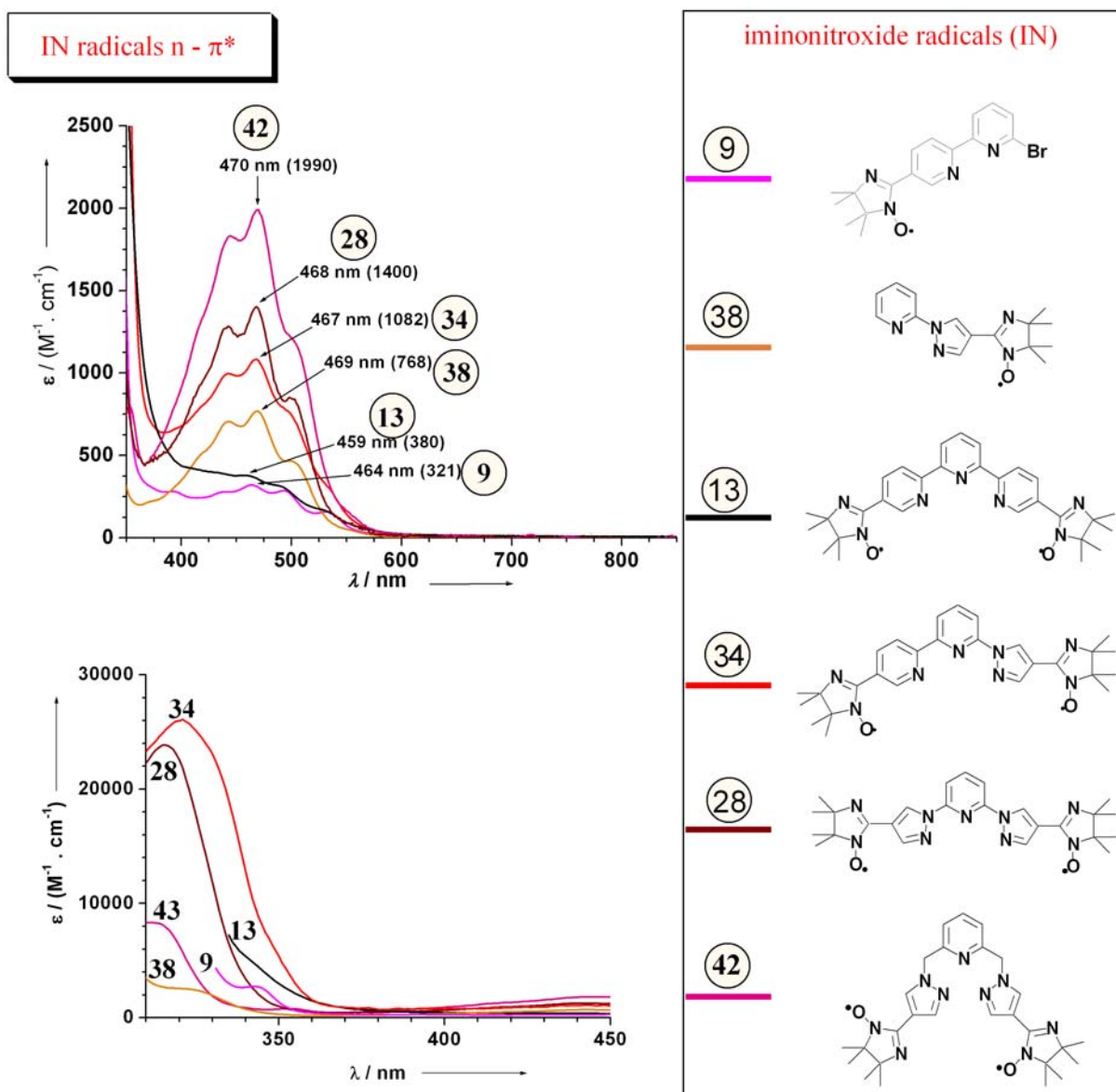


Figure 3.3: The absorption spectra of the IN radicals recorded in dilute toluene solutions at r.t.

3.2. Theoretical predictions of the UV/Vis absorption spectra in the biradical systems.

The semiempirical approach ROHF/AM1 (Austin Model) including CIS (20,20) (20 electrons in 20 molecular orbitals) has been used to simulate the absorption spectra of three selected biradicals **12**, **13**, and **26**. This would verify the applicability of the computational procedure for theoretical prediction of the absorption spectra of similar compounds, and furthermore allow assignment of the observed experimental transitions. It is worth to note that the simulations were based on the optimised geometry for the triplet-ground state. Therefore the nitronyl nitroxide biradical based on pyridine **12**, the other one based on pyrazolylpyridine **26** and the imino nitroxide biradical **13** were selected. These radicals feature fairly large ΔE_{ST} gap (see Chapter 4). The calculated absorption spectra are summarised in Table 3.1 and in the Figure 3.4 and are expressed in function of the calculated oscillator strength. In order to explain the results reported in table 3.1 some points are therein clarified.

An atom or molecule can be stimulated by light to change from one energy state to another. An atom or molecule in an excited energy state can also decay spontaneously to a lower state. The probability of an atom or molecule changing states depends on the nature of the initial and final state wavefunctions, how strongly light can interact with them, and on the intensity of any incident light. To a first approximation, transitions strengths or simply the probability that a certain type of transition is occurring, are governed by selection rules which determine whether a transition is allowed or disallowed. Practical measurements of transitions strengths are usually described in terms of the Einstein A and B coefficients or the oscillator strength (f).

1. Selection Rules

1. The parity of the initial and final wavefunctions must be different.
2. The spin can not change, $\Delta S = 0$.
3. The change in orbital angular momentum can be $\Delta L = 0, \pm 1$, but $L=0$ to $L=0$ transitions are not allowed.
4. The change in total angular momentum can be $\Delta J = 0, \pm 1$, but $J=0$ to $J=0$ transitions are not allowed.

2. Transition Probability

The transition probability is R^2 with units of J (Joule) cm^3 , where R is the transition moment given by (a)

$$R = \langle X | u | X \rangle \quad (a)$$

with u is the dipole moment operator and X the wavefunction. Basically what this equation indicates is that the strength of a transition is relative to how strongly the dipole moment of a resonance between energy states can couple to the electric field of a light wave.

3. Einstein coefficients

For a two-level system (ground-state level i and upper level j), the rate of an upward stimulated transition (absorption, $-dN_i/dt$ or dN_j/dt) is:

$$-dN_i/dt = N_i B_{ij} U_\nu$$

where N_i is the number density of atoms in the ground state, U_ν is the light intensity, and the proportionality factor B_{ij} is the Einstein B coefficient for absorption:

$$B_{ij} = 8 \pi^3 R^2 / 3 h g_i$$

For stimulated emission the Einstein coefficient becomes:

$$B_{ji} = B_{ij} g_i / g_j$$

where g_i and g_j are the degeneracies of the ground and excited states, respectively. Atoms in the excited state can decay without the presence of an external light field due to stimulation due to "zero-point fluctuations." Zero-point fluctuations are the dynamic variations in the shape of an electronic orbital at any instant in time. These instantaneous orbitals can be described by a linear combination of the wavefunctions of the system, which provides the mechanism for transitions between different states of the system. The spontaneous decay rate:

($-dN_j/dt$ or dN_i/dt) change into:

$$-dN_j/dt = N_j * A_{ji}$$

where A_{ji} is the Einstein coefficient for spontaneous emission:

$$A_{ji} = 8 \pi h B_{ij} g_i / g_j \lambda_m^3 = 64 \pi^4 R^2 / 3 h g_j \lambda_m^3$$

Since atoms in the upper level can decay by both spontaneous and stimulated emission, the total downward rate ($-dN_j/dt$ or dN_i/dt) is given by:

$$-dN_j/dt = N_j (A_{ji} + B_{ji} U_\nu)$$

4. Oscillator strength

The oscillator strength of a transition is therefore a dimensionless number that is useful for comparing different transitions. It is defined as the ratio's strength of an atomic or molecular transition with respect to the theoretical transition strength of a single electron, using a harmonic-oscillator model. For absorption:

$$f_{ij} = 4 \epsilon_0 h c m_e B_{ij} / e^2 \lambda_m$$

and for emission:

$$f_{ji} = f_{ij} g_i/g_j$$

Oscillator strengths can range from 0 to 1, or a small integer. A strong transition will have an f close to 1. Oscillator strengths greater than 1 result from the degeneracy of real electronic systems.

Based on the computation, the predicted transition wavelengths correspond fairly well to the experimental values. The longest wavelength transitions in both **12** and **13** originate from the radical. In **13** this is an $n \rightarrow \pi^*$ transition at 440 nm from the radical SOMO to an anti-bonding π^* MO. In **12**, however, there are two degenerate transitions (at 611 nm and 610 nm) between the radical HOMO and one of its anti-bonding σ^* -type MOs. Unexpectedly, these two transitions are rather intensive. The second characteristic transition for nitronyl nitroxide (<415 nm) is reproduced as well. However, the predicted wavelength is higher than the experimental value of 387 nm. The calculated $\pi \rightarrow \pi^*$ transitions arising from the terpyridine core follow a reasonable trend. The wavelength in **13** (286 nm) corresponds to the one measured for pure terpyridine (see experimental session). A bathochromic shift of ~ 70 nm is observed in **12** due to the enhanced conjugation. This is also in line with the experimentally measured spectra. In the case of the radical **26** a hypsochromic shift at 584 nm (HOMO (NN) \rightarrow POMO (NN) and HOMO-1 (NN) \rightarrow POMO (NN)) was calculated for the first fingerprint of the radical moiety. This is not more intense as compared with **12**, and therefore does not reproduce the trend experimentally observed (pyridine hamper and pyrazole enhance) suggesting the presence of limits in this type of computation when singlet-triplet states are both thermally populated (see selection rules, point 2). The second fingerprint indeed is well reproduced (372 nm, $\pi \rightarrow \pi^*$ transition from the core to the radical, observed 375 nm) and it is in line with the hypsochromic shift experimentally observed in all the pyrazolyl-based radicals.

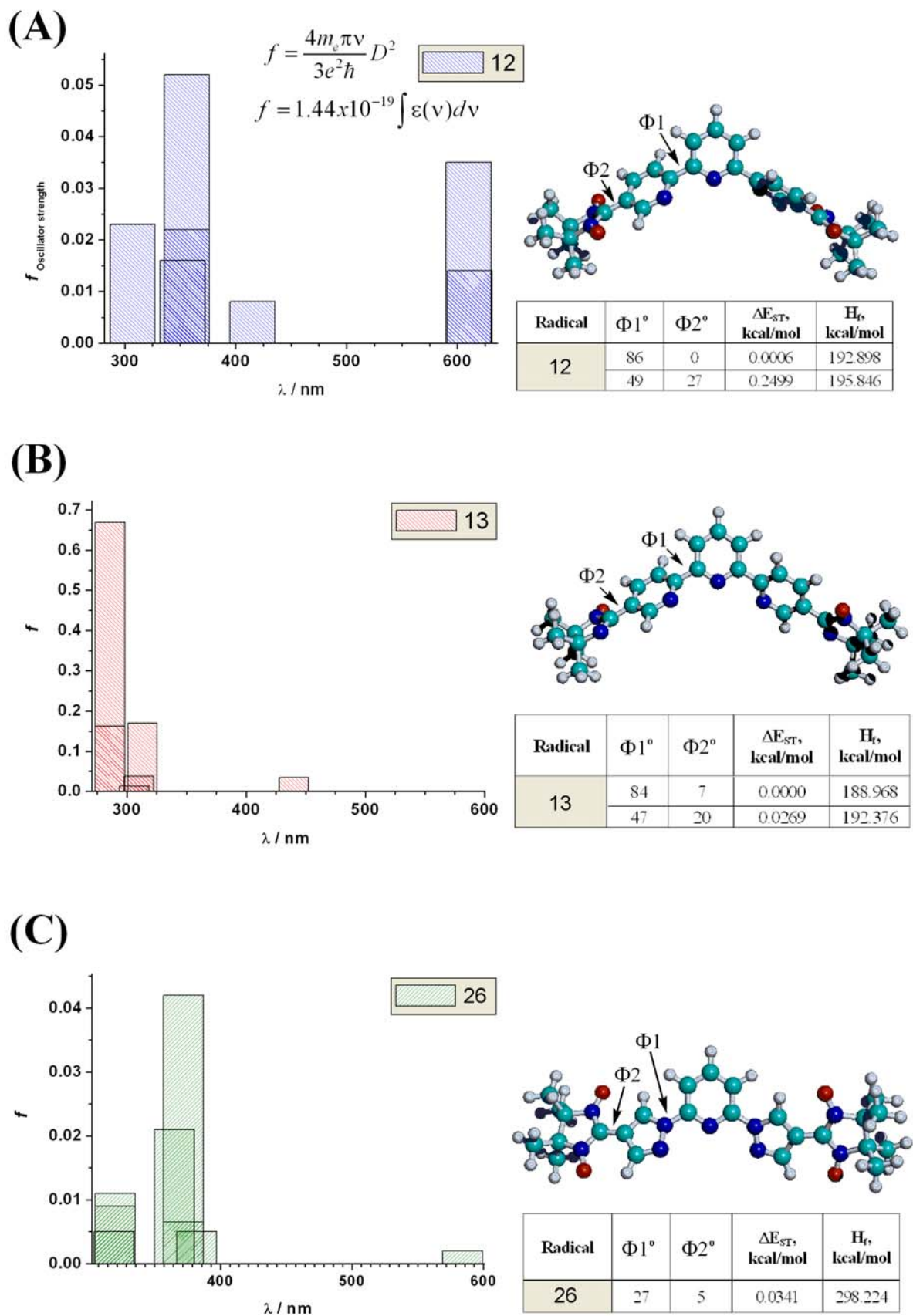


Figure 3.4. Pictorial view of the calculated UV/vis transitions in **12** (A), **13** (B) and **26** (C) by ROHF/AM1/CIS(20,20). The singlet-triplet gap on the optimised molecular geometry is collected in the small Table depicted on the right.

Table 3.1. UV/VIS spectra simulated by ROAM1 / CIS(20,20) for triplet ground state.

Transitions for 12	λ , nm	Oscillator strength	MOs involved	Comment
1	611	0.014	HOMO (NN) \rightarrow LUMO+1 (NN)	$\pi \rightarrow \sigma^*$ transition involving only the spin bearing part of the radical
2	610	0.035	HOMO (NN) \rightarrow LUMO+1 (NN)	$\pi \rightarrow \sigma^*$ transition involving only the spin bearing part of the radical
3	415	0.008	HOMO (NN) \rightarrow LUMO+3 (terpy)	$\pi \rightarrow \pi^*$ transition from the radical to the terpyridine core
4	356	0.022	HOMO (terpy) \rightarrow LUMO (terpy) HOMO-1 (terpy) \rightarrow LUMO (terpy)	$\pi \rightarrow \pi^*$ transition from the terpyridine core
5	356	0.052	HOMO (terpy) \rightarrow LUMO+1 (terpy) HOMO (terpy) \rightarrow LUMO (terpy)	$\pi \rightarrow \pi^*$ transition from the terpyridine core
6	352	0.016	HOMO-* (terpy) \rightarrow LUMO+* (terpy)	$\pi \rightarrow \pi^*$ transition from the terpyridine core
7	307	0.023	POMO (NN) \rightarrow LUMO+2 (terpy) POMO (NN) \rightarrow LUMO+3 (terpy)	$n \rightarrow \pi^*$ transition from the radical to the terpyridine core
Transitions for 13	λ , nm	Oscillator strength	MOs involved	Comment
1	440	0.035	POMO (IN) \rightarrow LUMO (IN)	The $n \rightarrow \pi^*$ transition involving only the spin bearing part of the radical
2	313	0.170	HOMO (terpy) \rightarrow LUMO+1 (terpy) HOMO-1 (terpy) \rightarrow LUMO (terpy)	$\pi \rightarrow \pi^*$ transition from the terpyridine core
3	310	0.038	HOMO (terpy) \rightarrow LUMO (terpy) HOMO-1 (terpy) \rightarrow LUMO+1 (terpy)	$\pi \rightarrow \pi^*$ transition from the terpyridine core
4	306	0.013	HOMO-3 (IN) \rightarrow POMO (IN) HOMO-3 (IN) \rightarrow POMO (IN)	$\pi \rightarrow n$ transition from the radical
5	286	0.669	HOMO (terpy) \rightarrow LUMO+1 (terpy) HOMO-1 (terpy) \rightarrow LUMO (terpy)	$\pi \rightarrow \pi^*$ transition from the terpyridine core
6	286	0.162	HOMO (terpy) \rightarrow LUMO (terpy) HOMO-1 (terpy) \rightarrow LUMO+1 (terpy)	$\pi \rightarrow \pi^*$ transition from the terpyridine core
Transitions for 26	λ , nm	Oscillator strength	MOs involved	Comment
1	584	0.002	HOMO (NN) \rightarrow POMO (NN) HOMO-1 (NN) \rightarrow POMO (NN)	$\pi \rightarrow n$ transition involving only the spin bearing part of the radical
2	382	0.005	HOMO-3 (pyr) \rightarrow LUMO +1 (pyr)	$\pi \rightarrow \pi^*$ transition involving only the pyrazolyl core
3	372	0.065	HOMO (pyr) \rightarrow LUMO (NN) HOMO-1 (pyr) \rightarrow LUMO (NN)	$\pi \rightarrow \pi^*$ transition from the core to the radical
4	372	0.042	HOMO (pyr) \rightarrow LUMO (NN) HOMO-1 (pyr) \rightarrow LUMO (NN)	$\pi \rightarrow \pi^*$ transition from the core to the radical
5	365	0.021	HOMO-1 (pyr) \rightarrow LUMO+3 (pyr) HOMO (pyr) \rightarrow LUMO (pyr)	$\pi \rightarrow \pi^*$ transition from the pyrazolyl core
6	320	0.009	POMO (NN) \rightarrow LUMO (pyr)	$n \rightarrow \pi^*$ transition from the radical to the pyrazolyl core
7	320	0.011	POMO (NN) \rightarrow LUMO (pyr)	$n \rightarrow \pi^*$ transition from the radical to the pyrazolyl core
8	319	0.005	HOMO-3 (NN) \rightarrow LUMO +1 (pyr)	$\pi \rightarrow \pi^*$ transition from the radical to the core

3.3. The IR absorption spectra of the radicals.

Clear differences between NN and IN radicals were witnessed if one compares their respective IR absorption envelopes. This technique represents a quick complementary tool in order to monitor the process of condensation reactions between the different aldehydes with the 2,3-dimethyl-2,3-bis(hydroxylamino)-butane. It is worth to note that all the isolated radical precursors (e.g **7**, **11**, **26**, **36** and **41**) could not be purified either on alumina or silica columns due to their quick decomposition, but only by rapid washing with different solvents (see Experimental Session). The IR analyses was very helpful when, within the condensation reaction, the mixture showed no hint of precipitate formation and the radical precursor could not be isolated from the reaction medium due to its partial dehydration from the bis-N,N'-hydroxy-imidazolidine to N-hydroxy-imidazolidine as for **32**. In the Figure 3.4 is shown the spectrum of the isolated free base 2,3-dimethyl-2,3-bis(hydroxylamino)-butane.

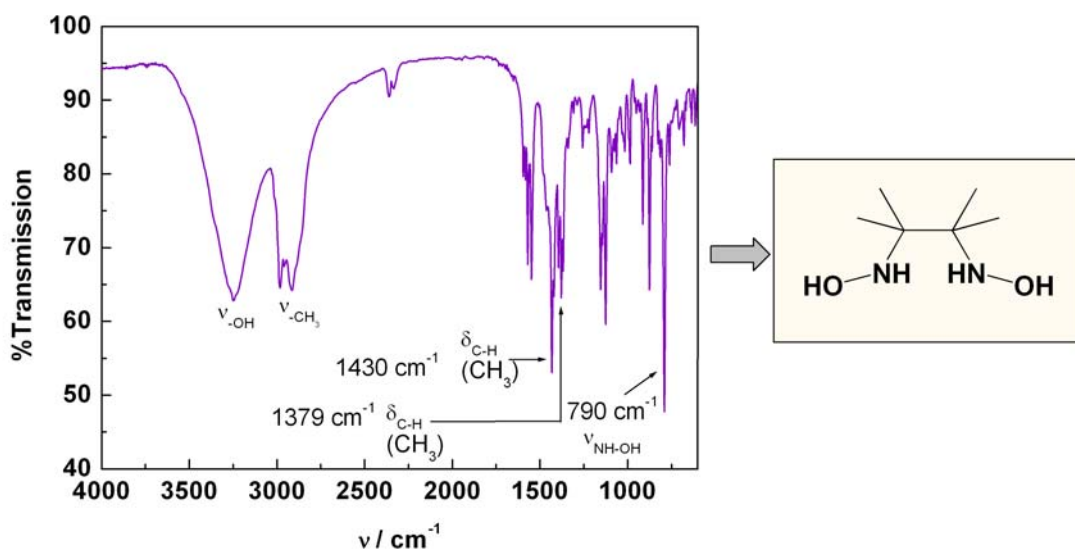


Figure 3.4: FT-IR spectrum of the free base recorded in KBr pellet at r.t.

For comparison, in Figure 3.5 are reported the infrared spectra of 5, 5''-diformyl-2,2':6',2'' terpyridine (**10**) the precursor 5,5''-bis(1,3-dihydroxy-4,4,5,5-tetramethylimidazolidin-2-yl)2,2':6',2'' terpyridine (**11**), the nitronyl nitroxide biradical **12** and the imino nitroxide biradical **13**. The complete conversion of the dicarbaldyde **10** into the radical precursors **11** clearly implied the disappearance of the strong signal at 1693 cm^{-1} ($\text{C}=\text{O}$) being accompanied with the formation of another strong and broad signal around 3252 cm^{-1} for **11** originating from the OH stretching-mode. After the oxidation process with NaIO_4 and purifications of the radicals the OH signals disappeared in **12** and **13** being accompanied, in the case of **12**, by an

unusually strong signal at 1351 cm^{-1} . This was assumed to arise from the N-O stretching of the imidazolidin moiety. In the case of **13** the novel signal, absent in **11**, is shifted to longer wavenumbers (1378 cm^{-1}) and accompanied by the appearance of a strong signal at 1554 cm^{-1} that may be tentatively attributed to the C=N stretching mode. In Figure 3.6 is reported a case in which isolation of the radical precursor **32** was not possible. Therefore the IR technique was applied in order to follow the condensation reaction between **31** and the 2,3-dimethyl-2,3-bis(hydroxylamino)-butane, by collecting aliquots of the reaction mixture at different times until complete disappearance of the carbaldehyde signal ($\nu_{\text{C=O}}$ appeared at 1689 cm^{-1}). Upon oxidation of the precursor **32**, the difference between the nitronyl and imino-nitroxide radicals is visible in the shift at longer wavenumbers associated with the N-O stretching frequency (from 1352 cm^{-1} in NN **33** to 1371 cm^{-1} in IN **34**) together with a clear decrease in the relative signal intensities. These differences were found consistent in all the radicals purified. The NN radicals always featured the N-O stretching frequency around $1350\text{--}1360\text{ cm}^{-1}$ with a very strong signal, while in the IN radicals such resonance is shifted (around 1370 cm^{-1}), much less intense and, in the case of **28** and **43**, appeared embedded in the spectra and could not be unambiguously identified. In Figure 3.7 those traces are reported together to allow quick comparison.

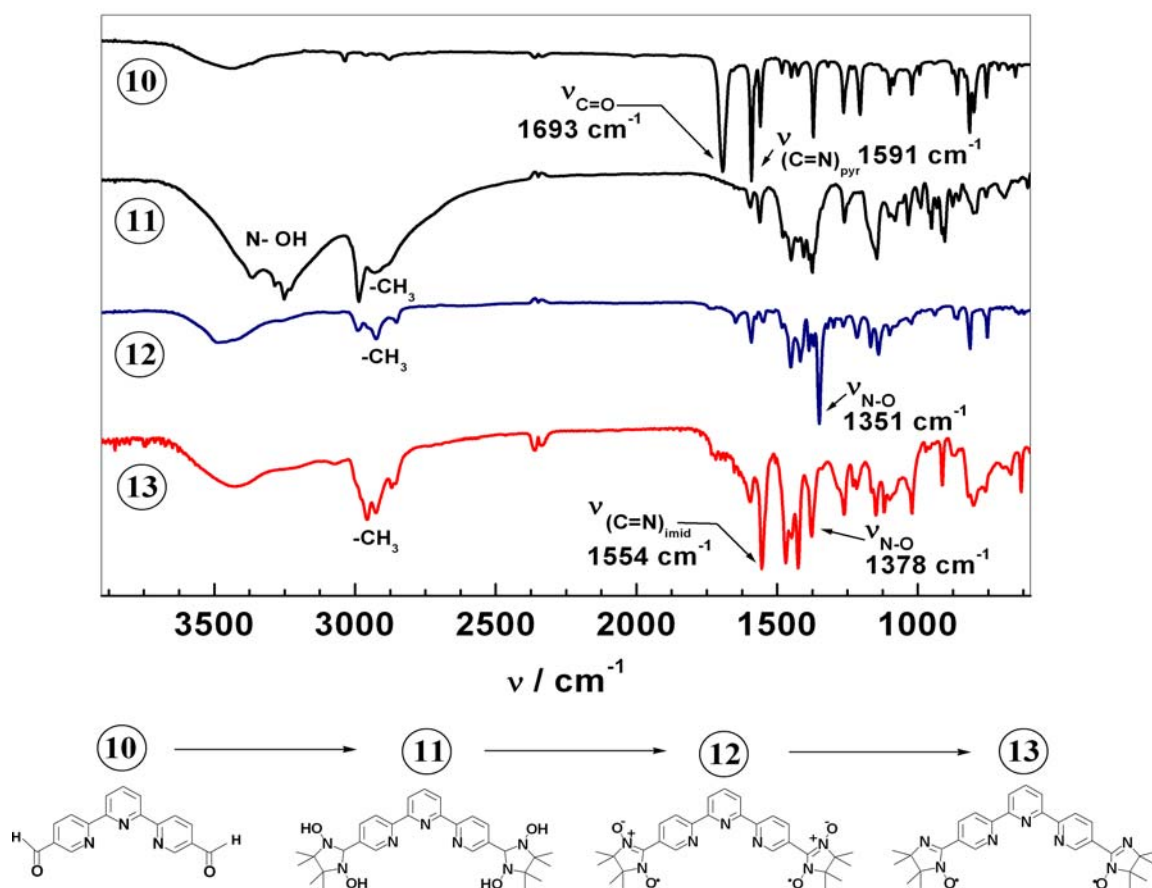


Figure 3.5: FT-IR spectra in KBr pellet recorded at r.t. for the terpyridine derivatives.

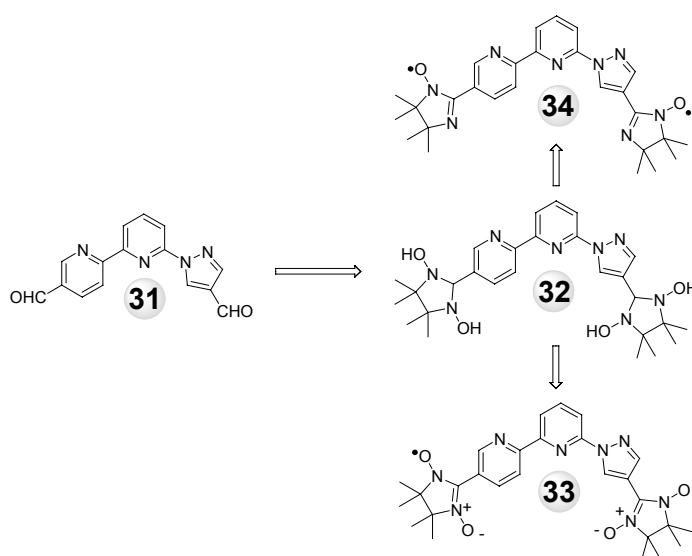
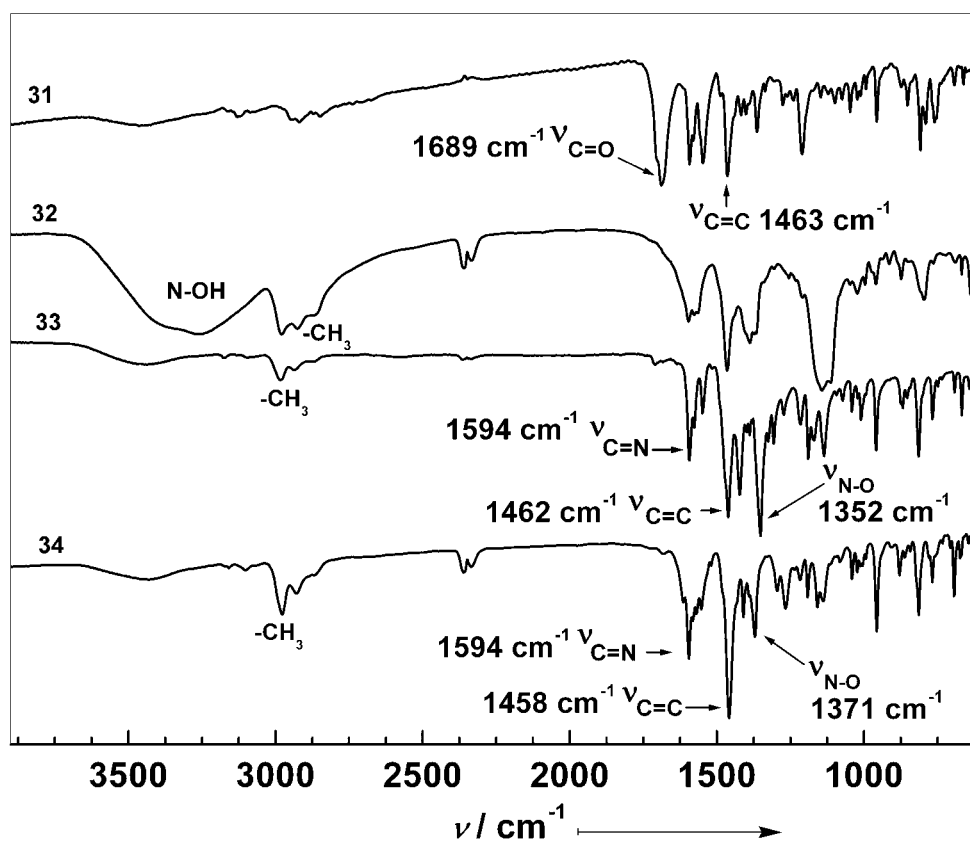


Figure 3.6: FT-IR spectra in KBr pellet recorded at r.t. Note the asymmetric peak at 1689 cm^{-1} in **31** originating from the two slightly different carbaldehyde groups (one attached to the pyridine and the other to the pyrazole moiety).

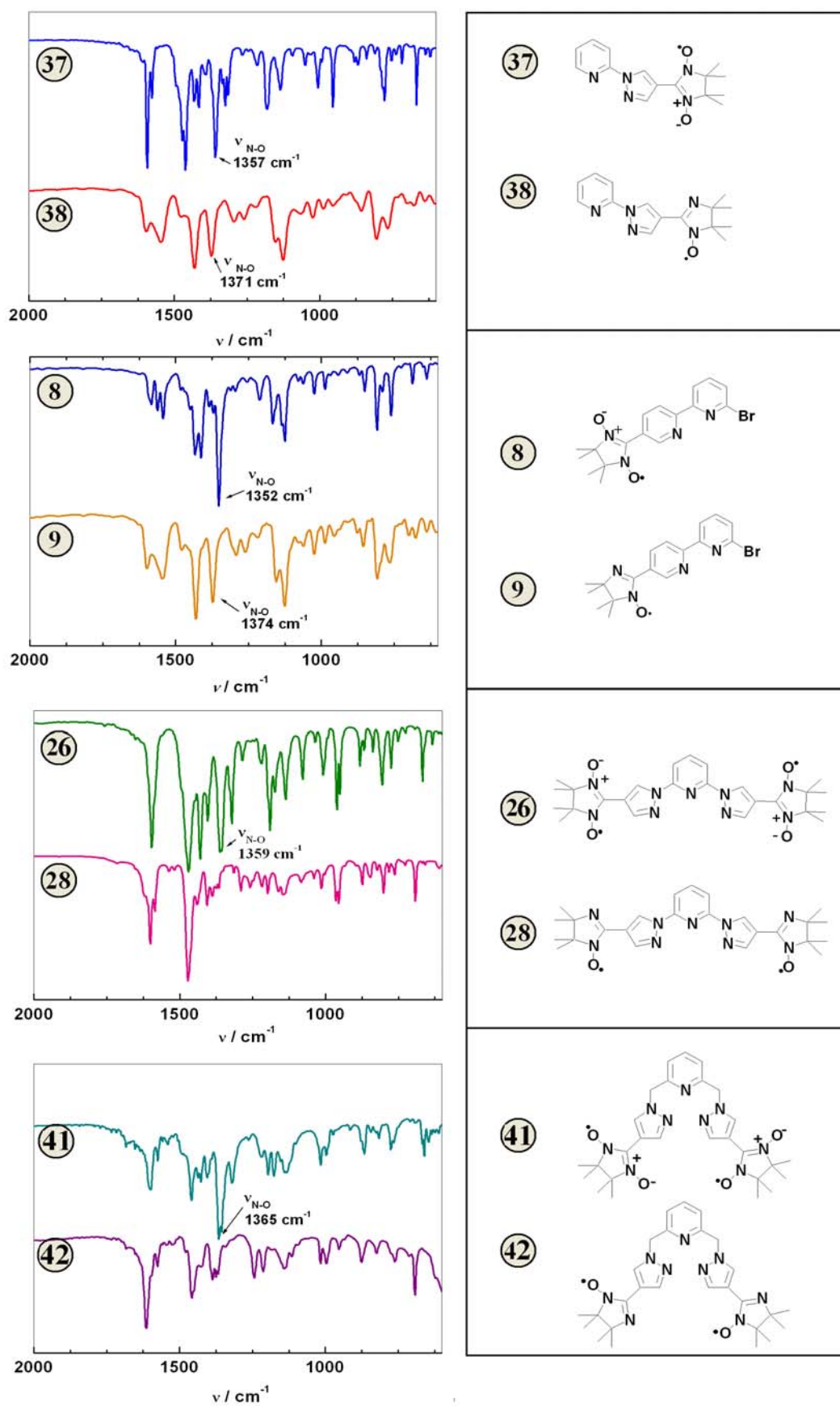
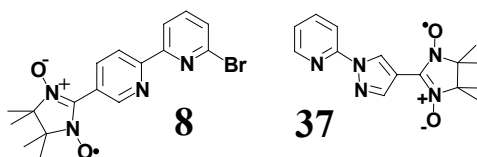


Figure 3.7: FT-IR spectra magnified in the region of the N-O stretching vibration (ν , cm⁻¹) for NN and IN radicals, recorded in KBr pellet at r.t.

Chapter 4 - EPR Analysis

4.1. The EPR analysis of monoradical systems in solution.

The EPR spectra in dilute ($\leq 10^{-4}$ M) and oxygen free toluene solutions of the nitronyl nitroxide monoradicals **8** and **37** exhibit clear isotropic five line pattern at $g_{\text{iso}} = 2.0066(1)$ and $2.0065(1)$ respectively. The spectra are shown in Figure 4.1 for **8** and 4.2 for **37**.



Such five lines spectra originate from the interaction of the unpaired electron with the two equivalent nitrogen nuclei of the imidazolyl moiety. The relative intensity of each line follows the expected 1:2:3:2:1 ratio. The spin energy levels for the $S=1/2$ system, as for the radicals **8** and **37**, are described by the spin-Hamiltonian \hat{H} (1), in which are reported the contributions from the electron-Zeeman (\hat{H}_{EZ}) and the hyperfine interaction (\hat{H}_{HF}). Higher order terms such as nuclear Zeeman and Quadrupole are usually not considered [1].

$$\hat{H} = \hat{H}_{\text{EZ}} + \hat{H}_{\text{HF}} + \text{higher order terms} \quad (1)$$

$$\hat{H} = g\beta_e\hat{S}_i\mathbf{B}_o + \sum a_{ij}\hat{S}_i\hat{I}_j \quad (2)$$

The electron-Zeeman term ($\hat{H}_{\text{EZ}} = g\beta_e\hat{S}_i\mathbf{B}_o$) describes the interaction between the electron spin operator \hat{S}_i and the applied external magnetic field tensor \mathbf{B}_o , β_e is the Bohr magneton ($|eh/4\pi m_e| = 9.2740 \times 10^{-24}$ J/T, written also as μ_B). Here the g value is the observable, and any deviations from g_e (the free electron in vacuum with resonance value at 2.0023) result from the so called spin-orbit coupling between the unpaired spin (\hat{S}_i) and the orbital angular momentum (\mathbf{L}). This coupling can be described by the Hamiltonian (3)

$$\hat{H} = \lambda\mathbf{L}\hat{S}_i \quad (3)$$

Where λ represents the spin-orbit coupling constant (sometimes expressed as $\xi = 2\hat{S}_i\lambda$). The spin orbit coupling is influenced by the admixture of other orbitals, e.g. lone pair orbitals, to the singly occupied orbitals; λ is constant for a particular shell in a particular atom, and increases sharply with the atomic mass. For organic radicals, such as the nitronyl- and imino nitroxide objects of this thesis, the spin-orbit coupling constant is usually very small and therefore the

observed deviation of the g value from g_e for both **8** and **37** is small ($\Delta g = g_{\text{obs}} - g_e \sim 0.005$). In the spin-Hamiltonian (2) the hyperfine term ($\hat{H}_{\text{HF}} = \sum a_{ij} \hat{S}_i \hat{I}_j$) describes the interaction between the magnetic moment of the electron spin (\hat{S}_i) and the magnetic moment of a nucleus in the vicinity (\hat{I}_j), and the coefficient a_{ij} represents the hyperfine coupling constant (hfc). Thus, the best fitting for the observed EPR lines in **8** has been achieved by applying the spin-Hamiltonian (2), with the parameters $a_N = 0.748(2)$ mT, $\Delta B_{\text{pp}} = 0.105$ mT, Lorentzian/Gaussian line-width ratio = 1/3 [1a, 1d], and $g_{\text{iso}} = 2.0066$ (1). The fitting is shown in Figure 4.1 as dashed-dotted line. The L/G ratio is taken into account because the intensity of the EPR transition is a lineshape-function according to equation (a)

$$I(\nu, B) = C \nu |P_{ij}|^2 f[(\nu - \nu_0)^2, \sigma_\nu] \quad (\text{a})$$

where C is a constant dependent on the type of microwave cavity and its temperature, ν_0 is the frequency required for resonance at any particular magnetic field \mathbf{B} (see the Zeeman term $\nu = g\beta_e \hat{S}_i \mathbf{B}_0 / h$), f is the line-shape function (Gaussian, Lorentzian or a mixture of both), σ_ν is the line-width parameter (in frequency units) and $|P_{ij}|^2$ is the time-independent part of the transition probability between the state i and j .

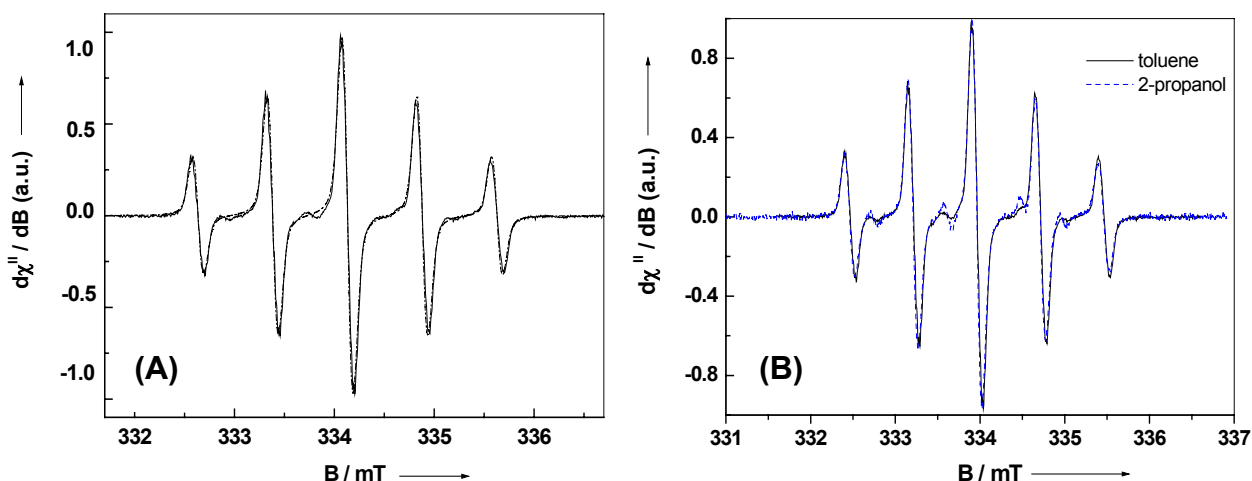


Figure 4.1: (A) EPR spectrum for the radicals **8** recorded in toluene solution (black lines) at 293 K with concentrations of 8×10^{-5} M. Experimental parameters: 9.39987 GHz, 100 kHz modulation frequency, 0.03 mT, 21 msec time constant, 42 sec sweep time, 2.0 mW microwave power, 10^5 gain, 4 scan were accumulated and averaged. The dashed-dotted line represents the computer simulations with parameters given in the text. (B) Comparison between the EPR spectrum of **8** recorded in toluene (solid line) and then in 2-propanol (dashed-line, -----) in which no clear solvent effect on a_N has been observed. Experimental parameters as those reported in (A).

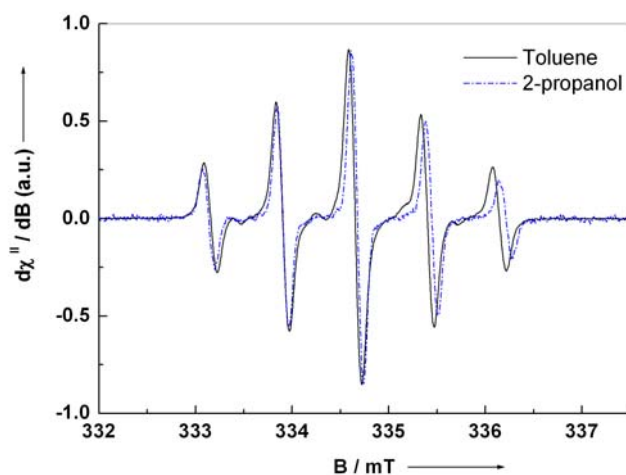


Figure 4.2: EPR spectrum for the radicals **37** recorded in toluene (black line) and in 2-propanol (dotted blue line) solutions at 293 K with concentration of 10^{-4} M. Experimental parameters (toluene) 9.40021 GHz, (2-propanol) 9.40026 GHz, then 100 kHz modulation frequency, 0.03 mT, 21 msec time constant, 42 sec sweep time, 1.0 mW microwave power, 10^5 gain, 4 scan were accumulated and averaged. The two spectra show the solvent effect in which a_N increases from $\sim 0.755(3)$ mT in Toluene up to $\sim 0.767(3)$ mT in 2-propanol.

In the monoradical **8**, in addition to the major five lines, the high resolution spectra reveals a more complex pattern (Figure 4.3, bold blue line) with at least 13 visible additional splittings overlapped on each N *hfc*.

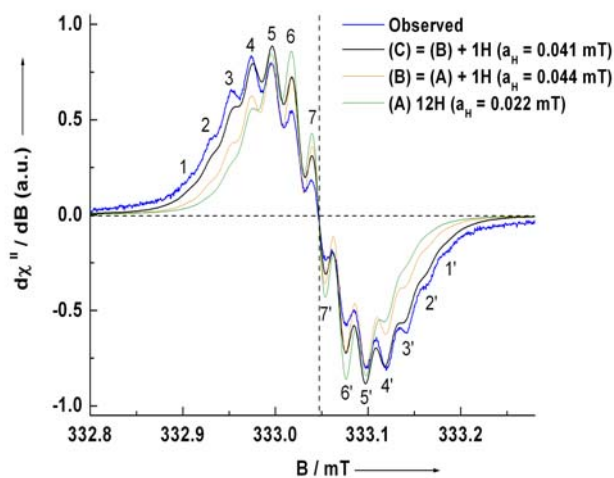


Figure 4.3: The high resolution EPR spectrum of **8** (blue line, 8×10^{-5} M in toluene) for the $M_i = +1$ line, recorded with the following parameters: 9.39759 GHz, 100 kHz modulation frequency, 0.01 mT modulation amplitude, 41 msec time constant, 84 sec sweep time, 0.8 mW microwave power, 8×10^4 gain, temperature 293 K, 10 scan were accumulated and averaged. The other lines represent the computer simulations with parameters given in the text.

These superimposed lines originate from the presence of additional couplings of the single unpaired electron ($S = 1/2$) with twelve hydrogen nuclei ($I = 1/2$), of the four methyl groups ($a_H = 0.022(1)$ mT), the 4' ($a_H = 0.041(1)$ mT) and 6' hydrogens ($a_H = 0.044(2)$ mT) of the pyridyl moiety, therefore experimentally demonstrate that non "zero spin density" resides also in the pyridine ring. Such effect is known as spin-polarization [Reference 1b, and Chapter 4 in 1c]. These lines rapidly saturate at relatively low powers (< 5 mW) at room temperature, while the major five lines hardly saturate even at 20 mW at room temperature. The parameters employed for the simulation of the H-*hfc* agree well with the estimated H-*hfc* found for similar systems in the literature. These references are collected in Figure 4.5.

Similarly to what has been shown previously in **8**, also for the monoradical **37** in addition to the major five lines, the high resolution spectra of the central transition line ($M_I = 0$) recorded in 2-propanol reveals a complex pattern (Figure 4.4A) with at least 17 visible additional splittings overlapped on each N *hfc*. These transitions originate again from extra couplings with the imidazolyl protons of the four methyl groups and the two hydrogens of the pyrazole ring. However, the spectrum is not symmetric with respect to the centre, once compared with the similar one for **8** reported in Figure 4.3. In particular, the third line (enclosed in a red circle in the figure 4.4A) is not well resolved. The identical effect has been observed in the nitronylnitroxide monoradical based on the pyrazole **P** (Figure 4.4B).

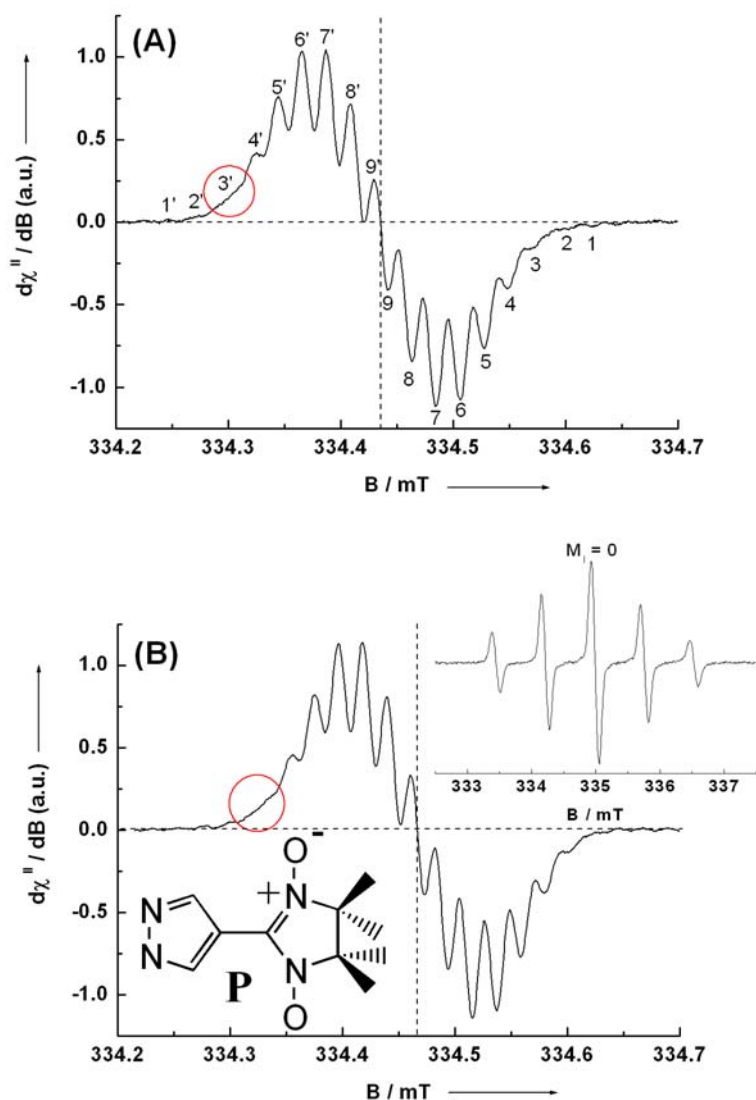
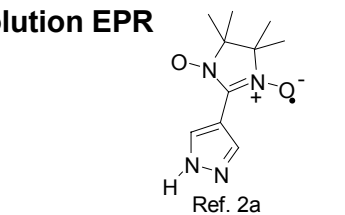


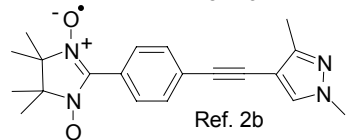
Figure 4.4: (A) The high resolution EPR spectrum of **37** (7×10^{-5} M in 2-propanol) for the $M_I = 0$ line, recorded with following parameters: 9.41021 GHz, 100 kHz modulation frequency, 0.01 mT modulation amplitude, 41 msec time constant, 84 sec sweep time, 0.5 mW microwave power, temperature 293 K. (B) The high resolution EPR spectrum of **P** for the $M_I = 0$ line recorded under identical conditions as in **37**. The small inset in (B) shows the total EPR spectrum of **P**.

Solution EPR



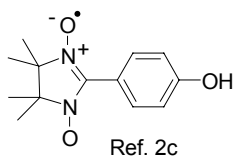
Solvent	a_N	a_{Me}	$a_{Hpyrazole}$	$a_{Npyrazole}$
H ₂ O	8.33	0.185	0.315	0.094
H ₂ O/NaOH	8.45	0.205	0.279	0.064

hfc in Gauss T = 293 K



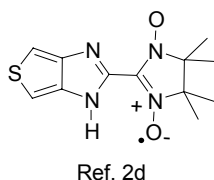
Solvent	a_N	a_{Me}	$a_{Hbenzene}$
hexane	7.40	0.21	0.54 only <i>ortho</i> -protons

hfc in Gauss T = 293 K



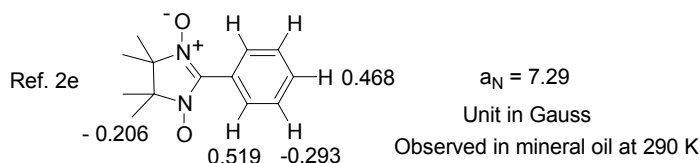
Solvent	a_N	a_{Me}	$a_{Hbenzene}$	a_{OH}
CCl ₄	7.50	0.207	0.499	0.177 < 0.02

ortho-H meta-H
hfc in Gauss T = 293 K



Solvent	a_N	a_{Me}	a_N thienoimidazole =N-	a_N thienoimidazole -N-H	a_H , (N)H
Benzene/ methanol	7.15	0.20	0.47	0.12	0.16
Benzene/ methanol- <i>d</i> ¹	7.18	0.20	0.47	0.12	

hfc in Gauss T = 293 K

¹H-ENDOR

¹H-NMR (CDCl₃, RT)

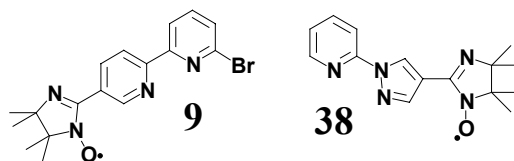
Ref.	ΔH	$a_{H-ortho}$	ΔH	a_{H-meta}	ΔH	a_{H-para}	ΔH	a_{Me}
Ref. 2f	-3.31	+0.446	+1.31	-0.177	-2.83	+0.382	+1.485	-0.201
Ref. 2f	-2.20	+0.296	+1.00	-0.135	-2.20	+0.296	+1.415	-0.196
Ref. 2f	-3.63	+0.490	+0.92	-0.125			+1.450	-0.191
Ref. 2f	-3.21	+0.435	+1.40	-0.189	-3.21	+0.435	+1.440	-0.194

 ΔH in KHz, a in Gauss

$$\Delta H = -a (\gamma_e \gamma_N) g \beta H / 4kT$$

Figure 4.5: The proton and nitrogen hyperfine coupling (a_H , a_N) constants obtained experimentally in nitronyl nitroxide radicals as found in the literature.

The EPR spectra in dilute and oxygen free toluene solutions of the imino nitroxide monoradicals **9** and **38** feature seven line patterns at $g_{\text{iso}} = 2.0061(1)$ and $2.0060(1)$ respectively.



These lines originate from the interaction of the unpaired electron with the two non equivalent nitrogen nuclei of the imidazolyl moiety, with intensities ratio 1:1:2:1:2:1:1, since two of the N - hfc splittings overlap each other. The spectrum of **9** is shown in Figure 4.6, together with the best simulation (dashed-dotted line) obtained with parameters $a_{N1} = 0.885(2)$ mT, $a_{N2} = 0.430(3)$ mT, $\Delta B_{pp} = 0.106$ mT, and assuming pure Lorentzian line.

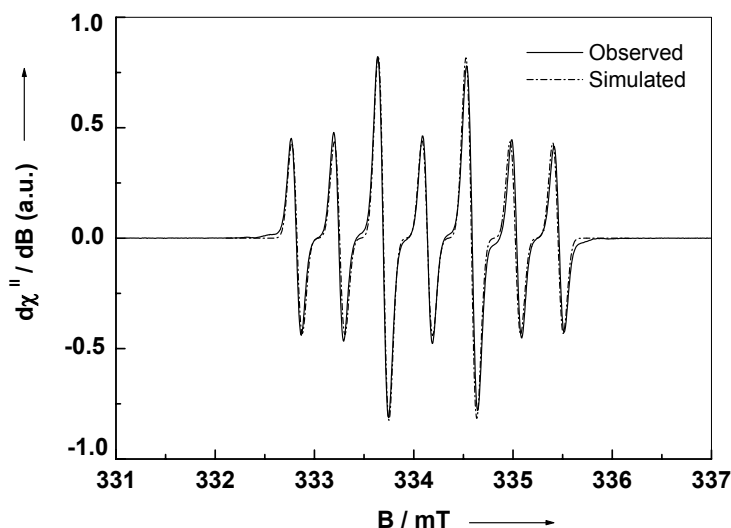


Figure 4.6: EPR spectrum of the radical **9** recorded in dilute (10^{-4} M) and oxygen free toluene solution at 293 K. Experimental parameters: 9.400210 GHz, 100 kHz modulation frequency, 0.03 mT modulation amplitude, 21 msec time constant, 42 sec sweep time, 2.0 mW microwave power (0.8 mW for B), 10^5 gain, 4 scan were accumulated and averaged.

The nitronyl nitroxide and imino nitroxide monoradicals followed nicely the Curie-law in solution with linear increase of the signal intensities (DI) upon lowering the temperature according to equation (6). This is clearly expected for isolated $S = \frac{1}{2}$ spin systems.

$$DI = \chi_{\text{EPR}} \propto (N_a/3k_bT) \times \mu_B^2 g^2 S(S+1) = C/T \quad (6)$$

In equation (6) N_a represents the Avogadro number, k_b Boltzman constant, μ_B the Bohr magneton and χ_{EPR} the magnetic susceptibility. Note that χ is actually the sum of $\chi(\text{para}) + \chi(\text{dia}) + \chi(\text{TIP})$ where only the paramagnetic contribution $\chi(\text{para})$ (large and positive) is temperature dependent, $\chi(\text{dia})$ is small and negative ($\leq 0.001 \times \chi(\text{para})$), and $\chi(\text{TIP})$ is small and positive. Although the double integration of the EPR absorption line discharges the

diamagnetic part, in practice extrapolation of the linear fit in the Curie Plot for $T \rightarrow \infty$, should provide a negative intercept; this corresponds to the $\chi(\text{dia})$ term. All the recorded solution EPR spectra for the monoradical systems **8**, **9**, **37** and **38** feature a very small increase in the peak-to-peak line-width upon cooling. This is shown in two examples for the radical **8** (NN) and **9** (IN) (Figure 4.7A and 4.7B respectively) along with the related Curie-behaviour for **8** (Figure 4.8A and 4.8B).

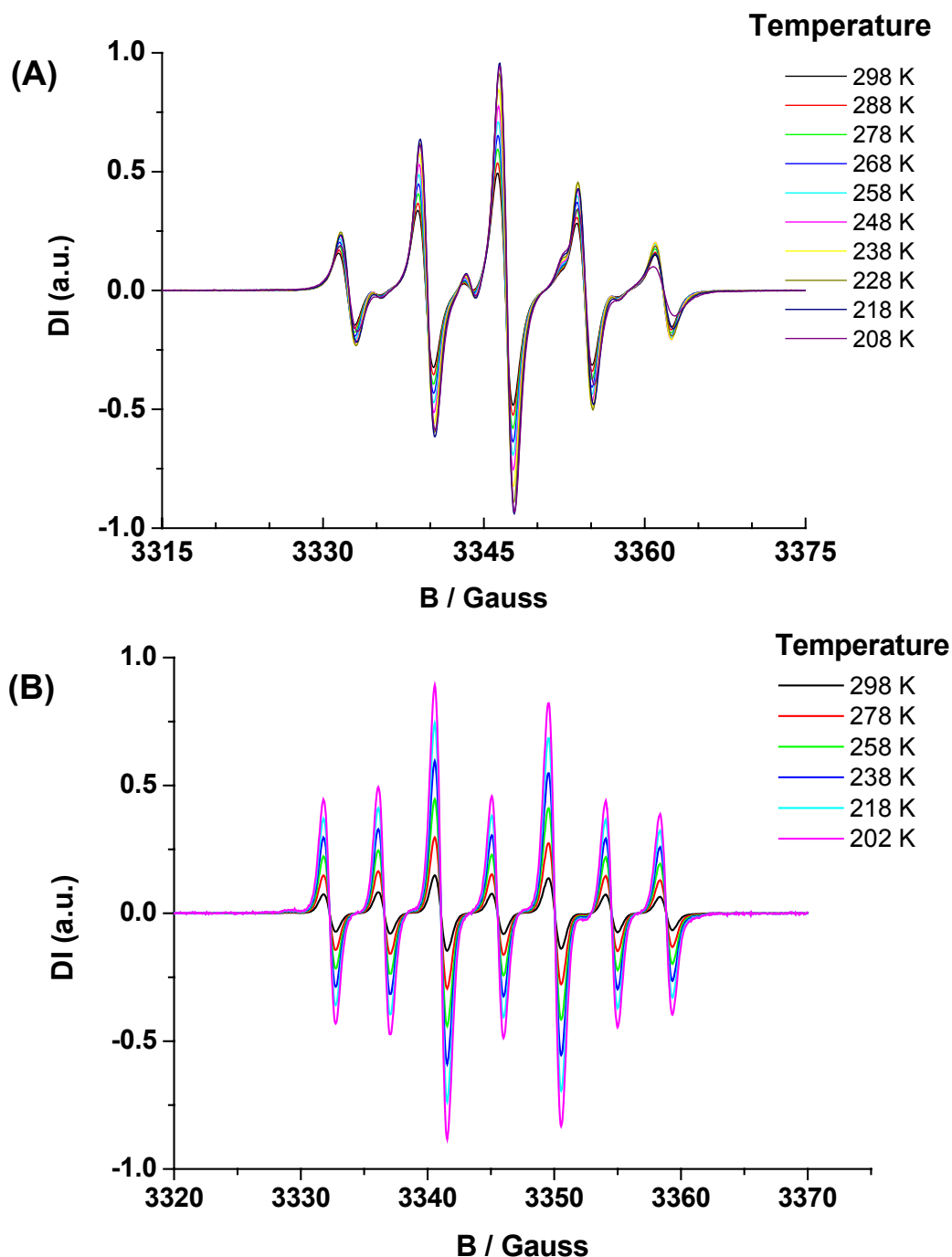


Figure 4.7: EPR spectra of the NN monoradical **8** (A) and the IN monoradical **9** (B), recorded as a function of the temperature. The samples were allowed to equilibrate in the cavity-cell at the fixed temperature for over 10 min. Each spectrum was both base-line and centre-field corrected. The error in the temperature setting was found to be within $\pm 1\text{K}$.

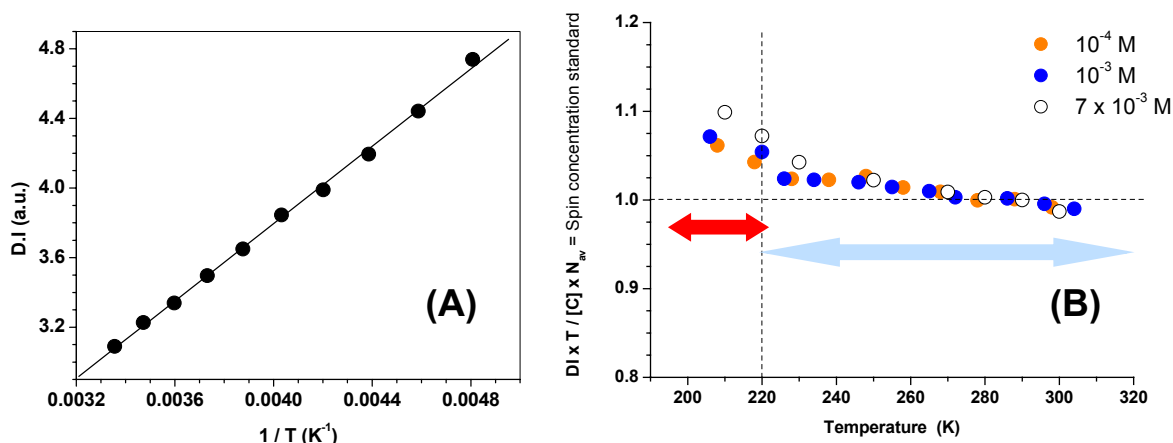


Figure 4.8: (A) The Curie-behaviour in solution of radical **8**. The closed circles (\bullet , DI) represent the double integration of the EPR signals recorded at various temperatures. All the spectra were base-line corrected prior to their double integration. The solid line shows the theoretical linear fitting according to the Curie equation (6) with the Curie constant, C , large and positive ($C = + 1113.6$, from the linear fitting) and the diamagnetic term small and negative (-0.6). In the Curie constant is also included the temperature independent paramagnetism $\chi(\text{TIP})$. (B) The product $\text{DI} \times T$ vs T for **8** recorded with different radical concentrations. The light blue arrow underlines the suitable range in which the monoradical unit can be used as spin-standard. The red arrow shows the temperature range where a large deviation from the linearity in $\text{DI} \times T$ vs T is observed. This effect corresponds to a phase change in the fluid toluene solution.

4.2. The EPR of biradical systems in solution.

The EPR spectra of the biradicals in solution feature a pattern very different from those observed in the simple $S = \frac{1}{2}$ systems, and therefore the theoretical background is therein treated in few more details. The low lying excited states of a magnetic system are generally described in terms of a spin-Hamiltonian as earlier shown in the case of $S=1/2$ systems. For two interacting spins the phenomenological spin-Hamiltonian (1) is modified into (7):

$$\hat{H} = g\beta\mathbf{B}_o\hat{S}_{a,b} - 2J\hat{S}_a\hat{S}_b + \sum_{ij} a_{Nij} \times (\hat{S}_a\hat{I}_{Nij} + \hat{S}_b\hat{I}_{Nij}) \quad (7)$$

The term $2J\hat{S}_a\hat{S}_b = \hat{H}_{\text{exch}}$ represents the electron-exchange interaction, also termed Heisenberg-Dirac-van Vleck Hamiltonian, HDVV [3,4], \hat{S}_a and \hat{S}_b the electron-spin operators and J the isotropic electron-exchange coupling constant. When the EPR spectra are analyzed in terms of (7), the spin exchange parameter plays the role of numerical fitting parameter needed to reproduce the experimental data. At first approximation in (7) the contributions arising from slow molecular interconversion in solution are neglected. Those are responsible for the sometimes observed strong temperature dependence in the linewidth-broadening. In fact in exchange-coupled systems the ESR linewidth is determined by both the fluctuation of the (t)-dependent exchange interaction $J(t)$ around its time averaged $\langle J \rangle$ (the main exchange

term in equation (7)), while the resonance positions of each line are determined mainly by $\langle J \rangle$. Thus, if the time dependent term is considered, the exchange term in the spin-Hamiltonian (7) from $\hat{H} = -2J\hat{S}_a\hat{S}_b$ needs to be changed into (8)

$$\hat{H} = 2 \sum_{a,b} [J_{a,b}(t) - \langle J_{a,b} \rangle] \hat{S}_a \hat{S}_b \quad (8)$$

The theoretical and conceptual bases for understanding spin exchange interactions were laid out by Anderson [5], by Löwdin [6], by Nesbet [7], by Hai, Thibeault and Hoffmann [8], by Kahn and Briat [9], by Noodleman [10], Noodleman and Davidson [11]. A quantitative description of spin-exchange interaction from the theoretical perspective represents however a challenging task, since it requires state-of-the-art computational efforts on the basis of either configuration interaction wave functions (CI) [12-14] or density functional theory DFT [15-17]. Recently Illas et al. have provided a comprehensive review on the conceptual and theoretical issues concerning these quantitative approaches [18].

The HDVV model Hamiltonian $2J\hat{S}_a\hat{S}_b$ acts in spin space only and, hence, assumes that the spatial part of the wave functions involved in magnetic coupling is the same for all the neutral spin configurations. This treatment is discussed in details in some advanced books [20]. For a two electron spin system, the spin space has a dimension of four, and the basis for this space is simply given by the combination between α and β spin (α for spin up, β for spin down). This leads to $|\alpha\alpha\rangle$, $|\beta\beta\rangle$, $|\alpha\beta\rangle$, and $|\beta\alpha\rangle$. Since in the HDVV model, the total square spin operator S^2 , and its z-component S_z^2 , commute with each other, it is possible to find a set of eigenfunctions common to the operators. The eigenfunctions of S^2 and S_z^2 are denoted $|S, M_s\rangle$ and lead to the description of the four spin states as $|1,1\rangle = |\alpha\alpha\rangle$, $|1,-1\rangle = |\beta\beta\rangle$, $|0,0\rangle = |\alpha\beta\rangle$, and $|1,0\rangle = |\beta\alpha\rangle$. Therefore the spin states are combined in singlet $|S\rangle$ $|0,0\rangle$ and triplet $|T\rangle$ with its three S_z components. The singlet and triplet states are also eigenfunctions of the HDVV Hamiltonian with energies $(3/2)J$ and $(-1/2)J$ [21,22].

Therefore the magnetic coupling constant is given by the energy difference between $|S\rangle$ - $|T\rangle=2J$ corresponding to the singlet-triplet energy gap (ΔE_{ST}) as shown in Figure 4.9 for a singlet ground state.

This was the procedure that has been adopted when numerical diagonalization of the spin-Hamiltonian (7) was used for the simulation of the entire solution EPR envelopes in the biradical systems. The exchange interaction J however cannot be fully exploited for structural

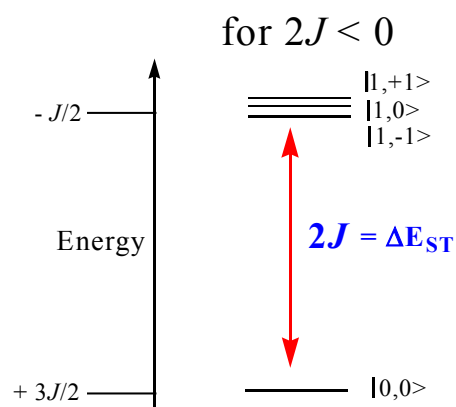


Figure 4.9: The singlet-triplet energy gap for $S = 1$ system when $2J < 0$.

investigation because it depends on several contributions, such as the radical distance and the number, nature, geometry and topology of the bonding involved between the radical entities. However, the contributions to J can be broadly classified into through-bond and through-space.

The through-bond contribution is regarded as an electrostatic interaction, and decreases quite rapidly if the bondings are single σ bonds. A general expression for radical centers connected with n number of σ bonds was proposed several years ago [23] in the form:

$$J \text{ [MHz]} = (-1)^n (3 \times 10^{-6-n}) \quad (9)$$

The through-bond interaction originates from spin-polarisation effects of the molecular bonding involved within the coupling unit. Such effect is expressed as a function of $(\zeta) = \rho^\uparrow - \rho^\downarrow / \rho_T$, where the symbols indicate ρ^\uparrow spin up densities (positive, α , spin up, parallel to the applied field) and spin down ρ^\downarrow densities (negative, β , spin down, antiparallel), and ρ_T the total spin densities (e.g. in the isolated biradical molecule $\rho_T = 1$, and in the general case $\rho_T = S_T$). We might depict the spin-densities in the form (10)

$$\rho(\mathbf{r}) = \sum_I \rho_I \psi_I(\mathbf{r}) \psi_I^*(\mathbf{r}) = 1 \quad (10)$$

With

$$J \propto f \rho(\mathbf{r}) = f_\rho(\theta, r) \quad (11)$$

The exchange energy term J is linked with $(\rho(\mathbf{r}))$ with a non-univocal direct correlation (*vide infra*). In equation (10) $\rho_I(r)$ and ψ_I are the local spin-densities on the i^{th} atoms, ψ_I its atomic wave-functions and (\mathbf{r}) its distribution in the space (spin-densities distribution). The sum indicates that this distribution is normalized to one (over the entire molecule) and each atom will retain a fraction of it. By writing $\psi_I = \sum_J c_{ij} \Phi_j$ in which the molecular function of the unpaired electron can be expressed as linear combination of atomic functions Φ_j through the coefficients c_{ij} we get the relation (12) [24-25]:

$$\rho(\mathbf{r}) = |c_{ij}|^2 \quad (12)$$

Thus ρ_I simply indicate the probability that the electron in the molecular orbital ψ_I resides in the atomic orbital Φ_j , and measures the unitless unpaired π -electron population ρ_I on the atom J when this atom bears only a single orbital occurring in ψ_I .

It is intuitive to suggest that a less efficient spin-polarization should lead to a decrease in the “communication” between radical sites through-bond, up to the limit in which no interaction occurs, and the radical entities behave as independent spins. In addition, increasing the dihedral θ angular torsions (i.e. when $\theta \neq 0^\circ$) between radical sites and coupling unit, as indicated in the general relation (11), leads to a decrease in the magnitude of J . Furthermore J may even change sign at angles $\theta \sim 80^\circ$ [26].

The second contribution to J is due to the so called through-space interactions, which varies with the radical separation, $\langle r \rangle$. This is a magnetic interaction in the real sense, and it is based on the magnetic dipole moment generated by the unpaired spins (dipolar spin-spin interaction). Although the functional dependence on $\langle r \rangle$ is also not well established, an exponential decrease with increasing $\langle r \rangle$ is generally assumed according to equation (13)

$$J = J_0 \exp [-\alpha (\langle r \rangle - d)] \quad (13)$$

Where d represents the minimum distance-approach, J_0 and α are empirical values [27]. However an estimation of J_0 can sometimes be obtained by applying Anderson’s theory [28a,b].

4.2.1 The spectral EPR analysis of the biradical systems in solution.

Considering the case of nitronyl and imino nitroxide biradical systems, according to the relative size of J with respect to $\langle a \rangle$, three cases could be encountered in the observed solution EPR envelopes:

- 1) Case $|J| \gg |a|$

the line positions in the observed spectrum are given by equations (14), (15) and (16) where $M_I (=m_I(a) + m_I(b))$ represents the z-component of the total nuclear spin angular momentum for the halves (a) and (b) carrying the radical units (the imidazolyl moieties), $\Delta m_I = |m_I(a) - m_I(b)|$, and $\varphi = \arctan (a_N \Delta m_I / 4J)$

$$h\nu(T) = g\beta\mathbf{B}_0 + (a_N/2) M_I \pm (a_N \Delta m_I / 2) \tan \varphi \quad (14)$$

$$h\nu(S) = g\beta\mathbf{B}_0 + (a_N/2) M_I \pm (a_N \Delta m_I / 2) \tan \varphi \pm 2J \quad (15)$$

$$\text{with } (T) = [1 / \sqrt{2(\alpha\beta + \beta\alpha)}] \text{ and } (S) = [1 / \sqrt{2(\alpha\beta - \beta\alpha)}] \quad (16)$$

When J is large compared to a (e.g. for $a_N \sim 0.75$ mT, $J > 7.5$ mT), $\varphi \rightarrow 0$ and equation (14) reduced into (17)

$$h\nu(T) = g\beta\mathbf{B}_0 + a_N/2 M_I \quad (17)$$

Thus one would anticipate $(2 \times 4 \times 1 + 1) = 9$ lines pattern for the nitronyl nitroxide and $(2 \times 2 \times 1 + 1) \times (2 \times 2 \times 1 + 1) = 25$ lines for the imino nitroxide biradical, with the observed a_N half of that featured by the related monoradical. Since most of the transition lines in the imino nitroxide biradical will overlap each other, a 13 lines pattern is practically observed. Simulation of the solution spectra can provide the lower limiting value of J . The total spread in magnetic field (spectral-width) of the observed EPR spectrum would be the same as that observed in the monoradical case.

2) Case $|J| \ll |a|$

In the spin-Hamiltonian (7) the exchange term almost vanishes leading to the limiting equation ($J \sim 0$) (18)

$$\hat{H} = g\beta\mathbf{B}_0(\hat{S}_{a,b}) + \sum_{ij} a_{Nij} \times (\hat{S}_a \hat{I}_{Nij} + \hat{S}_b \hat{I}_{Nij}) = g\beta_e \mathbf{B}_0 \hat{S}_i + \sum a_{ij} \hat{S}_i \hat{I}_j \quad (18)$$

Each radical centre behaves independently, and can be treated as uncorrelated spin-system (e.g. $S=1/2$ system). It follows that the total spread in the magnetic field of the observed EPR spectrum exactly matches that of a monoradical system with intensity doubled compared to the later.

3) Case $|J| \sim |a|$

The mixing between (T) and (S) through hyperfine interaction is possible. In the EPR spectrum the numbers of observed lines are determined by the ratio $a_N \Delta m_I / 4J$. Therefore in the limit of $J = a$

$$h\nu(T) = g\beta\mathbf{B}_0 + (a_N/2) M_I \pm (a_N \Delta m_I^2 / 8) \quad (19)$$

The numbers of observed lines will be more than nine for the nitronyl nitroxide and more than thirteen for the imino nitroxide biradicals. The total spectral-width in the observed EPR spectrum would be larger than that observed in the respective monoradical case. The simulation of the spectrum by EPR analyses studies would provide the exact size of $|J|$ and not only the relative magnitude.

4.2.2 The determination of thermally activated spin-states in the biradical systems.

The double integration (DI) of the EPR envelope of paramagnetic species is directly proportional to the concentration ($[C_S]$) of the unpaired electrons (spin-concentration) and, in absence of signal saturation DI is inversely proportional to the absolute temperature, according to the Curie-law (equation 6). Hence, comparison between the integrated intensities of the biradical system *versus* monoradical standards with known concentrations, recorded under identical conditions (filling factor, temperature, power, modulation amplitude, etc.) would provide the spin concentration of the biradical system. However, different spin-states contribute in different way according to the ratio $|J/k_bT|$. We therefore can encounter the two limiting cases **(A)** and **(B)** in which the relation (20) and (21) can be obtained by combining the Curie and the Bleaney-Bowers equations:

$$\text{(A)} \quad |2J/k_bT| \gg 1$$

$$DI_{(S=1)} = cN_A \times \{ \mathbf{4}\Delta E/3k_bT \} / [3 + \exp^{-\mathbf{2}J/k_bT}] \quad \text{(biradical)} \quad (20)$$

$$DI_{(S=1/2)} = cN_A \times \{ \mathbf{2}\Delta E/3k_bT \} / [3 + \exp^{-\mathbf{2}J/k_bT}] \quad \text{(monoradical)} \quad (21)$$

Here again N_A represents the Avogadro number, k_b the Boltzmann constant and DI the double integration of the signal intensities (for monoradical $S = 1/2$ or biradical $S = 1$); the coefficients written in bold in equation (20) and (21) simply indicate the total number of states (\hat{S}) (e.g four states for biradical, two states for monoradical), under the frame of Boltzmann distribution (*vide infra*). The DI ratio between the biradical systems against monoradical standard is obtained upon applying the limit:

$$J \rightarrow \infty \text{ (biradical) in equation (20), } J \rightarrow 0 \text{ (monoradical) in equation (21)}$$

Therefore:

$$DI_{(S=1)} / DI_{(S=1/2)} = [cN_A \times (4\Delta E/9k_bT)] / [cN_A \times (2\Delta E/12k_bT)] = 2.66666 \text{ spin} \quad (22)$$

Note that J is assumed large (∞) and positive. If $J \rightarrow -\infty$, then $[3 + \exp^{-\mathbf{2}J/k_bT}] \rightarrow \infty$ and $DI_{(S=1)} = 0$ at every temperature.

$$\text{(B)} \quad |2J/k_bT| \ll 1$$

The thermal energy is much larger than the exchange energy, and singlet-triplet states are in equilibrium and follow the Boltzmann distribution. The ratio of molecules in triplet state:

$$N_{\text{triplet}} / cN_A = \frac{3}{4} \times (\exp^{-2J/kbT}) = 75\% = 0.75 \quad (23)$$

And those in the singlet:

$$N_{\text{singlet}} / cN_A = \frac{1}{4} \times (\exp^{-2J/kbT}) = 25\% = 0.25 \quad (24)$$

The double integrated signal intensities compared with a monoradical standard would thus account for two doublets (2.0 spins):

$$[N_{\text{triplet}} / cN_A + N_{\text{singlet}} / cN_A] / [N_{S=1/2} / cN_A] = 0.75 \times 2.6666 + 0.25 \times 0 = 2.00 \text{ spin} \quad (25)$$

Therefore only when the thermal energy becomes smaller than the exchange energy ($k_bT < |J|$), the ground state starts to populate at the expense of the thermally excited state, until the equilibrium is fully shifted ($T \rightarrow 0$) to give in case of triplet ground state ($S=1$) DI = 2.6666 DI mono, or in the case of singlet ground state ($S=0$) DI = 0.

Consequently from the simulation of the diluted solution EPR spectrum, and the measure of the spin-concentration for a biradical system it is possible to obtain both lower and upper limits of the intramolecular exchange interaction J but not its sign.

4.3. The observed EPR spectra of the π - conjugated biradicals in solution.

The EPR spectra of the terpyridine-based biradical **12** (NN) and **13** (IN) are better resolved in dilute toluene solution [1×10^{-4} M] rather than in chloroform or dichloromethane, and are shown in Figure 4.9 and 4.10 respectively. The nitronyl nitroxide biradical **12** exhibits a well resolved nine line pattern, hence demonstrating that the intramolecular exchange interaction between the two radical fragments is much larger than the hyperfine terms ($2J/a_N \gg 1$, i.e. $2J \gg 7 \times 10^{-4} \text{ cm}^{-1}$). The observed line spacing (apparent hyperfine interaction, a_N) as pointed out in equation (17) would therefore correspond to half of that of the simple monoradical system (where $a_N = 0.748 \text{ mT}$). The observed spectrum (black line) is well reproduced by using the simple spin-Hamiltonian (2) with the apparent hyperfine interaction $a_N/2 = 0.374(1) \text{ mT}$ over four equivalent nitrogen nuclei, an average g value, $g_{\text{iso}} = 2.0066(1)$, pure Lorentzian line-shape for the single components and peak-to-peak line width, $\Delta B_{\text{pp}} = 0.135 \text{ mT}$. The simulation is shown with a magenta dotted line in Figure 4.10. An identical result is achieved by full diagonalization of the spin-Hamiltonian (7) with $a_N = 20.944 \text{ MHz} =$

0.748 mT, $|J/a_N| > 55$ (e.g. $|2J/k_b| = \Delta E_{ST} \geq 0.08 \text{ cm}^{-1}$ (Gaussian line-width = 3.194 MHz, 0.840 MHz modulation amplitude, weight factor = 1 for the averaged molecular conformations under strong exchange limit, (rms ≤ 0.3105)).

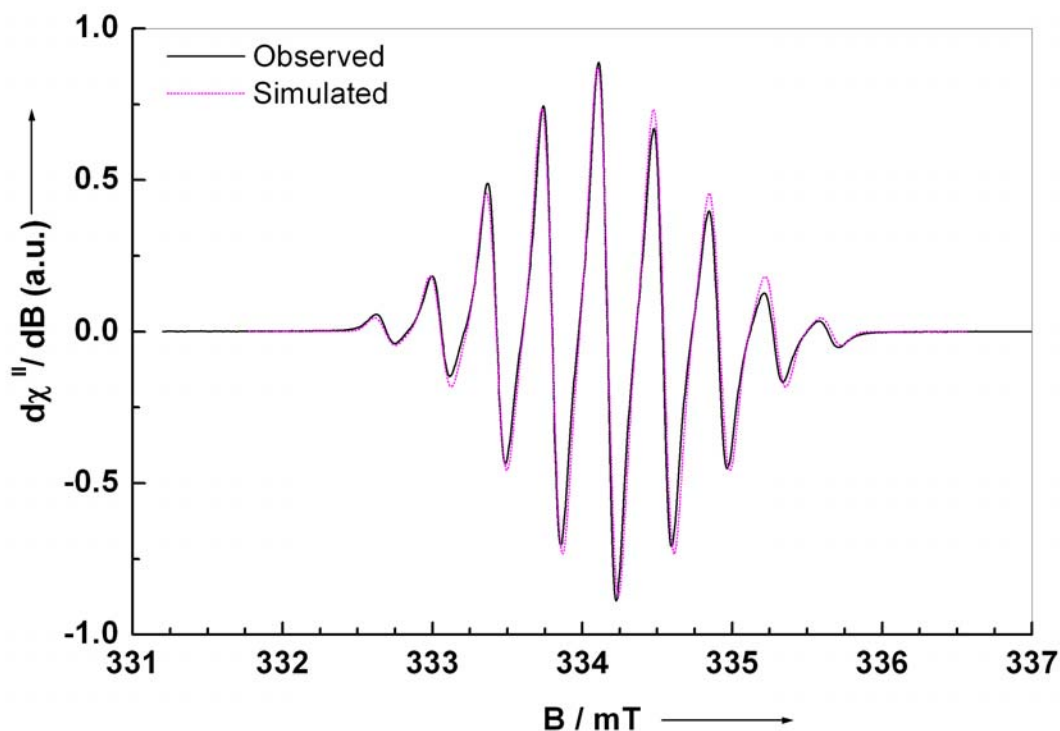


Figure 4.10. EPR spectrum of the nitronyl nitroxide biradical **12** (black line) recorded in dilute and oxygen free toluene solutions. Parameters: Frequency 9.40022 GHz, 100 KHz mod. frequency, 0.03 mT modulation amplitude, 21 msec time constant, 42 sec sweep time, 2.6 mW microwave power, 10^5 gain, temperature 260 K, 6 scan were accumulated and averaged. The dotted magenta line shows the spectrum simulation with parameters given in the text.

Similarly, the strong exchange-interaction between the radical fragments is observed in the imino nitroxide biradical **13** (Figure 4.11). The spectrum can also be reproduced by assuming the strong exchange limit ($J/a_N \gg 1$, i.e. $J \gg 4.2 \times 10^{-4} \text{ cm}^{-1}$) with the following parameters, $a_{N1}/2 = 0.430(1) \text{ mT}$, $a_{N2}/2 = 0.225(2) \text{ mT}$, $g_{\text{iso}} = 2.0061(1)$, the Lorentzian/Gaussian line-shape of 1/3 and the peak-to-peak line width, $\Delta B_{\text{pp}} = 0.200 \text{ mT}$ (red dotted line). The simple simulation according to the spin-Hamiltonian (2) however, although reproducing exactly the peak positions, is not completely satisfactory in reproducing the intensities of lines 1 and 13. A superior fitting can be achieved using again numerical diagonalization of the spin-Hamiltonian (7) with parameters $|2J/k_b| \geq 0.065 \text{ cm}^{-1}$ (rms ≤ 0.3544), $|a_{N1}|_{\text{iso}} = 11.679 \text{ MHz}$, $|a_{N2}|_{\text{iso}} = 25.573 \text{ MHz}$, Gaussian line-width = 2.216 MHz, 0.840 MHz modulation amplitude, weight factor = 0.97 for the averaged molecular conformations in strong exchange limit. This simulation corresponds to the blue dashed line in Figure 4.11.

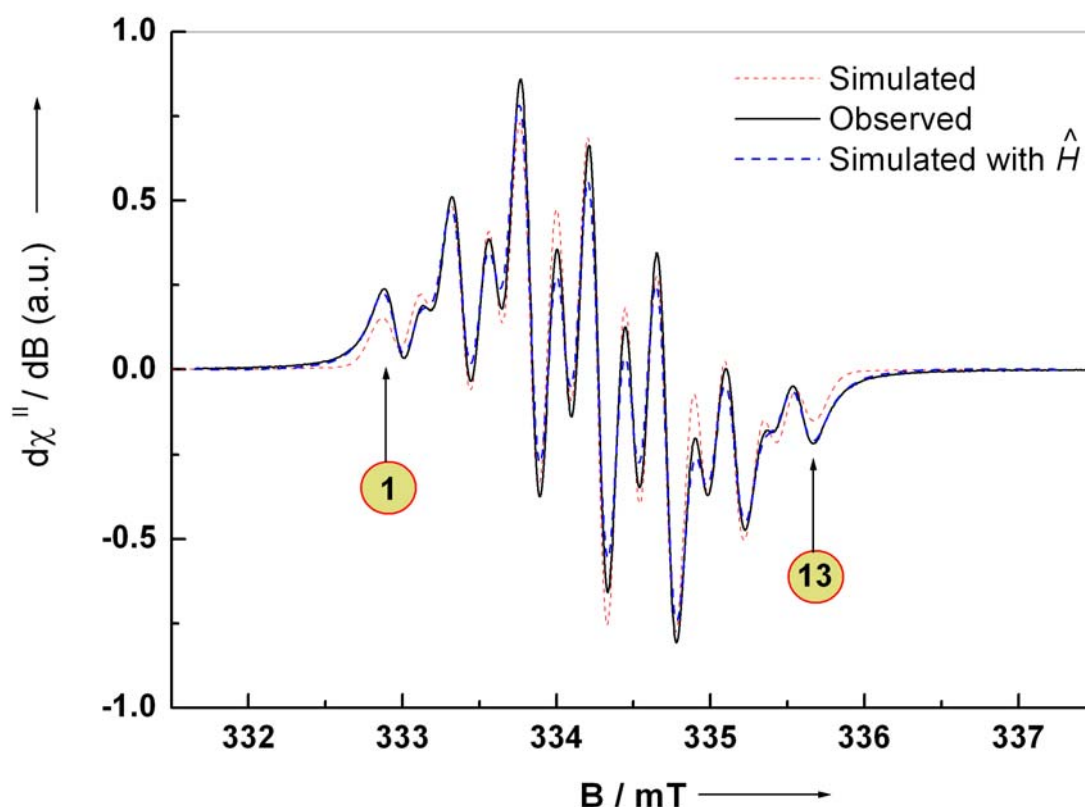


Figure 4.11. EPR spectrum of the imino nitroxide biradical **13** (black line) recorded in dilute and oxygen free toluene solutions. Parameters: Frequency 9.40240 GHz, 100 KHz mod. frequency, 0.3 Gauss modulation amplitude, 21 msec time constant, 42 sec sweep time, 5.0 mW microwave power, 4×10^4 gain, temperature 260 K, 4 scan were accumulated and averaged. The different lines in the figure (red and blue dashed line) show the spectra simulations with parameters given in the text.

Clearly the value of the exchange interaction $|J|$ evaluated from the simulation based on the spin-Hamiltonian (7) does not provide the sign (either positive or negative), but indeed its lower limiting value is obtained. The solution EPR spectra for the biradical systems **26** (NN), **28** (IN), **33** (NN) and **34** (IN) are analysed in the same frame as for **12** and **13**, since they all features $|J/a_N| \gg 1$. Their spectra are shown in Figure 4.12 (**26** and **28**) and 4.13 (**33** and **34**) together with their simulations and estimated parameters. The EPR analysis for the biradical system **41** and **42** (with a methylene-bridge between the pyrazole moieties and the central pyridine ring) are treated separately later in the chapter. The total spectral width and number of observed lines do not appreciable change upon changing the solvents (e.g. CH_2Cl_2 , CHCl_3 , acetone, THF, MeOH or toluene) for all these biradical. This implies that no specific interaction between the solvent and radical systems occurs. However, as mentioned earlier in Chapter 2 (Table 2.1) the radical stabilities in solution strongly decreased in protic solvents, and especially when THF and MeOH are used, they have been destroyed in a day. This effect is

shown in Figure 4.14 as one example for the case of the imino nitroxide biradical **28**. The biradical systems **12** (NN), **13** (IN), **26** (NN), **28** (IN), in diluted solutions feature clear Curie-like behaviour upon cooling, with linear increase of the double-integrated signal intensities with lowering the temperature. Some broadening in the peak-to-peak line width is observed in all cases upon cooling, without severe loss of the original nine and thirteen lines pattern. The spin-concentration accounts for $\sim 2.0 (\pm 0.1)$ uncorrelated spin, a indication of thermally activated spin states. The non-symmetric radicals **33** (NN) and **34** (IN) featured alternating line-width upon decreasing the temperature, together with small deviations from the linear Curie behaviour (within the 10% of the EPR limit in the double integration in the overall spectral resolution); for **33** this is particularly pronounced in a narrow temperature range (278 – 258 K), although recovering of the original nine line pattern is observed below 250 K. In **34** on the other hand, a homogeneous distortion of the thirteen lines spectrum recorded in the high temperature range occurs upon cooling, and leads to a broad dominating seven line pattern at 218 K. These spectra are shown in Figure 4.15 featuring both no solvent dependency and full reversibility (e.g. from low to high temperature both nine and thirteen line patterns are recovered even upon repeated cycles). The changes in the line-width are not easy to rationalize, but might be explained by the out-of phase rotation between the radicals attached on pyridine *versus* those connected to the pyrazole moiety. Although much work has been devoted to the analysis of the line-shape dependency *versus* temperature for monoradical systems, including nitronyl nitroxide [29], very little is still known about line-shape effects on spin-coupled systems. At concentrations higher than 8×10^{-3} M, all the radicals synthesized show very poorly resolved patterns in solutions, due to line-broadening arising from the interactions among unpaired electrons on surrounding centres. Therefore, in order to probe the pure intramolecular interactions between the unpaired spins, magnetically diluted samples with concentrations $\ll 8 \times 10^{-3}$ M are needed.

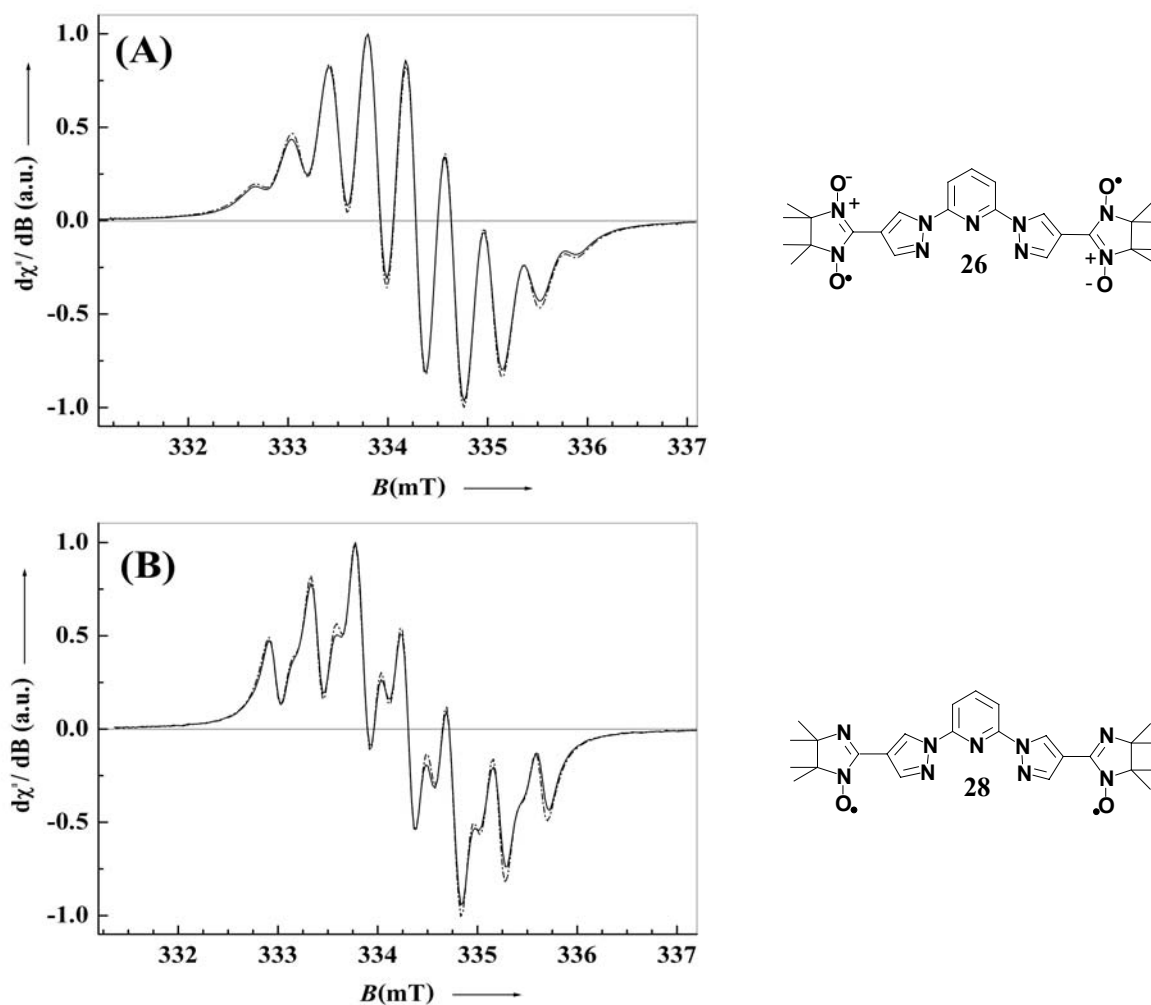


Figure 4.12. (A) EPR spectrum of **26** (solid line) recorded in dilute and oxygen free toluene solution at 298 K and its computer simulation (dashed-dotted line), with $g_{\text{iso}} = 2.0065(1)$, $|2J/k_B| \geq 0.07 \text{ cm}^{-1}$ ($\text{rms} \leq 0.31$), Gaussian line-width = 6.12 MHz, modulation amplitude = 0.84 MHz, $|\bar{a}_{\text{iso}}| = 21.44 \text{ MHz}$, weight factor 1.00, the other factors are kept the same as the experimentally recorded spectrum. Experimental parameters: 9.40334 GHz, 100 kHz modulation frequency, 4.0 mW power, 0.03 mT modulation amplitude, 21 ms time constant, 42 s sweep time, 10^4 gain, 4 scan were accumulated and averaged. **(B)** EPR spectrum of **28** (solid line) recorded in diluted and oxygen free toluene solution at 298 K and its computer simulation (dashed-dotted line), with $g_{\text{iso}} = 2.0060(1)$, $|2J/k_B| \geq 0.06 \text{ cm}^{-1}$ ($\text{rms} \leq 0.3795$), Lorentzian line-width = 4.78 MHz, modulation amplitude = 0.84 MHz, $|\bar{a}_{\text{iso}}| = 18.67 \text{ MHz}$ where $|\bar{a}_{\text{iso}}| = [|\bar{a}_{\text{N1}}| + |\bar{a}_{\text{N2}}| / 2]$ with $|\bar{a}_{\text{N1}}| = 11.62 \text{ MHz}$ and $|\bar{a}_{\text{N2}}| = 25.72 \text{ MHz}$, weight factor ≥ 0.73 for the averaged molecular conformations in strong exchange limit, the other factors are kept the same as the experimentally recorded spectrum. Experimental parameters: 9.40269 GHz, 100 kHz modulation frequency, 5.0 mW power, 0.03 mT modulation amplitude, 21 ms time constant, 42 s sweep time, 5×10^3 gain, 4 scan were accumulated and averaged.

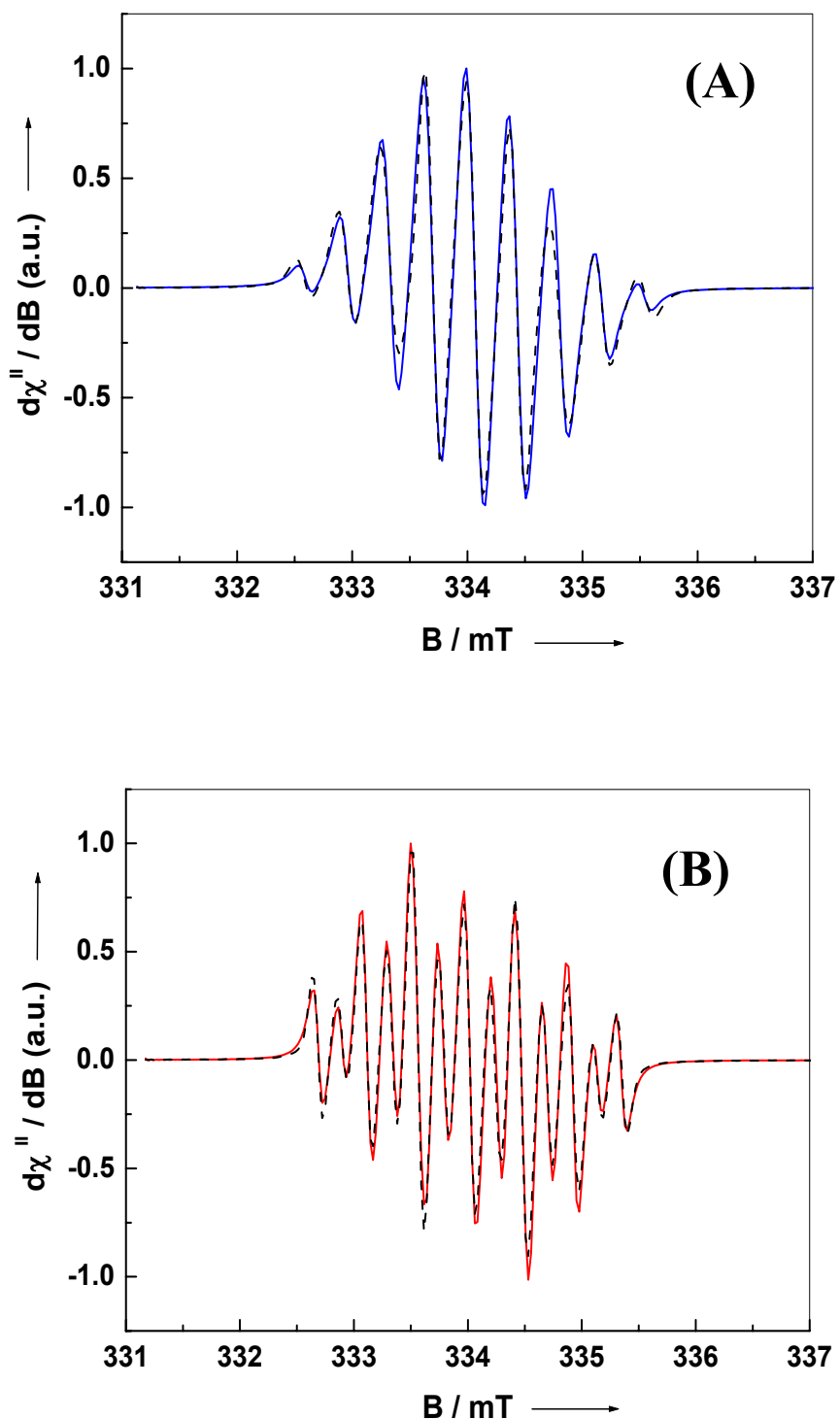


Figure 4.13. (A) EPR spectra of **33** (solid line), and (B) **34** (solid line), recorded in dilute (10^{-4} M) toluene solutions at 293 K. Parameters for: (A) $g_{\text{iso}} = 2.0066(1)$ at 9.4002 GHz, (B) $g_{\text{iso}} = 2.0061(1)$ at 9.40021 GHz, and 100 kHz mod. frequency, 0.3 Gauss modulation amplitude, 21 msec time constant, 42 sec sweep time, 2.6 mW microwave power, 10^5 gain, 4 scan were accumulated and averaged. The parameters used for the simulations (dashed lines) according to the spin-Hamiltonian (7) are reported in Table 4.2.

Table 4.2: Simulation parameters for the biradical **33** and **34** of the r.t. solution EPR spectra (see **Figure 4.13A** for **33** and **4.13B** for **34** obtained by numerical diagonalization of the spin-Hamiltonian \hat{H} (7)

Biradical	g_{iso}	$ 2J/k_B $	$ a_{N1} _{\text{iso}}$	$ a_{N2} _{\text{iso}}$	Gaussian line-width	Modulation amplitude	rms
33	2.0066(1)	≥ 0.069 cm^{-1}	6.876×10^{-4} cm^{-1}	-	1.065×10^{-4} cm^{-1}	2.802×10^{-5} cm^{-1}	≤ 0.806
34	2.0061(1)	≥ 0.061 cm^{-1}	3.896×10^{-4} cm^{-1}	8.530×10^{-4} cm^{-1}	7.393×10^{-5} cm^{-1}	2.802×10^{-5} cm^{-1}	≤ 0.696

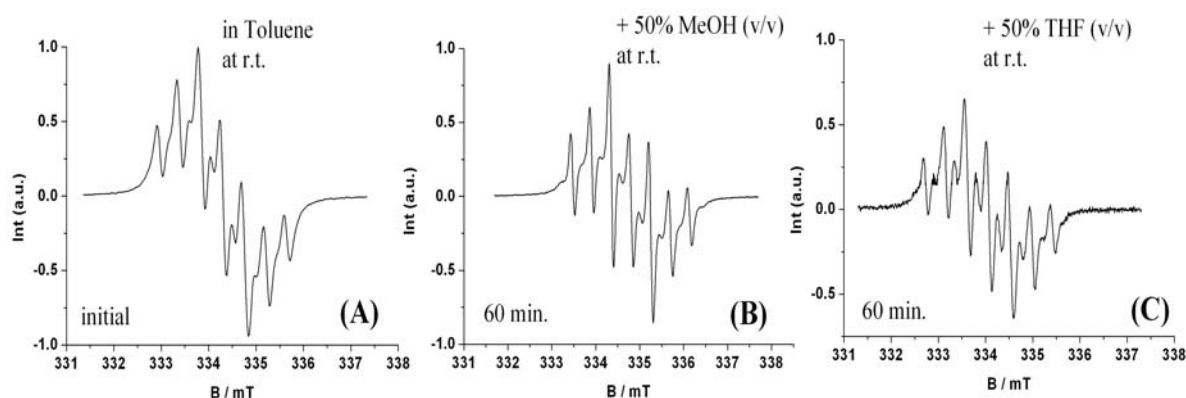


Figure 4.14. EPR spectra showing the solvent and stability effects of the imino nitroxide biradical **28**. Note that upon addition of MeOH (trace **B**), and after 1 hour of aging, approximately 20% of the biradical (**A**) is converted into monoradical. Upon addition of THF on (**A**) (see trace **C**), although the spectral resolution increased, the double integration of the signal intensities accounts for $\sim 50\%$ of biradical left in solution. After one day no signal could be detected by EPR either in (**B**) and (**C**) as indication for the completely loss of the radical system.

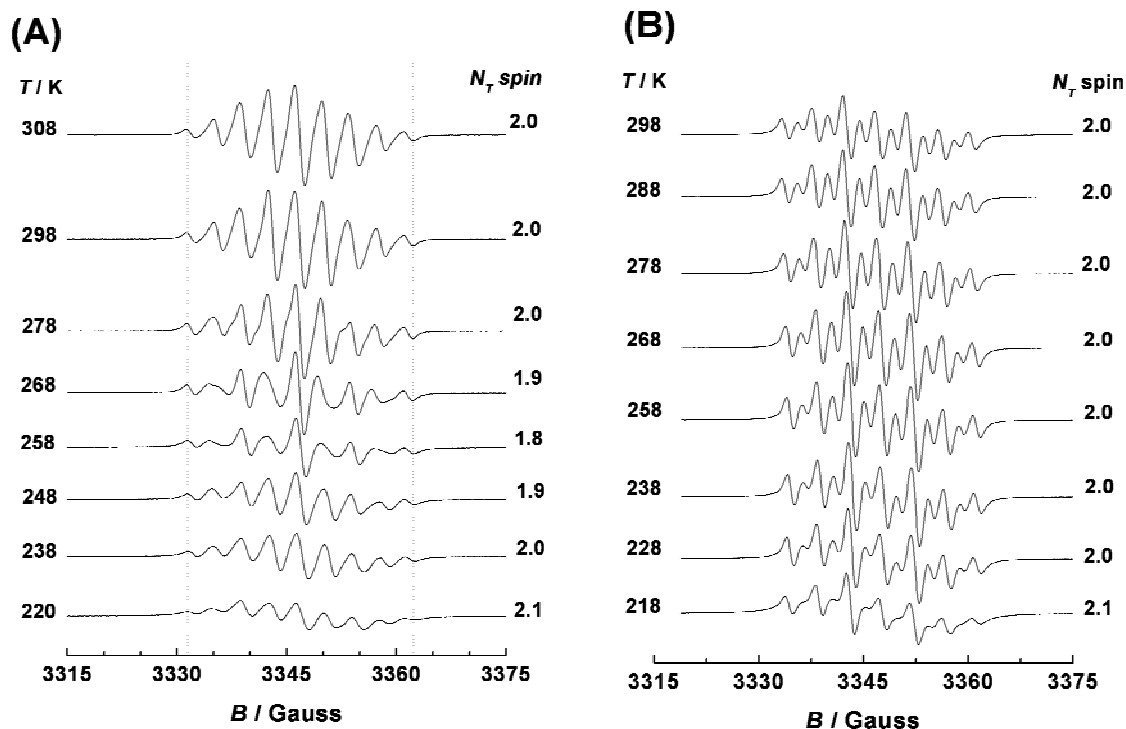
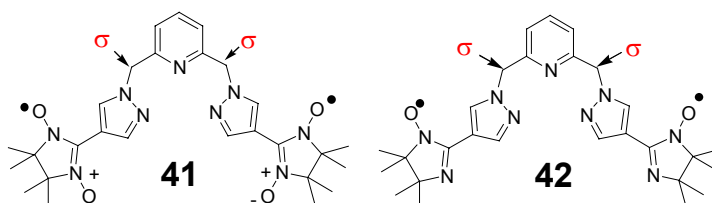


Figure 4.15. The alternating line-width effect in the EPR solution (toluene) spectra for the radicals **33** (A) and **34** (B) observed upon cooling. The numbers on the right of each spectrum indicates the spin-concentration of the biradical system at that temperature with ± 1 K in temperature error (T/K is written on the left of each series of spectra). The temperature-dependent spin concentrations have been obtained by comparison with the related monoradical standards **8** and **9**.

4.4. The EPR spectra of the σ - conjugated biradicals in solution.

The introduction of two σ bonds within the coupling unit clearly induced loss of the π -conjugation between the radical carriers.



Radicals **41** and **42** showed a strong temperature dependence of their EPR envelopes in diluted (10^{-4} M in toluene) solutions (Figure 4.16B and 4.17B respectively), although the observed dominating nine lines pattern for **41** and thirteen lines pattern for **42**, it suggested that still the strong exchange limit of $|J/a_N| \gg 1$ holds in both cases. As observed in the other biradical systems previously discussed, also in these cases the EPR features were

independent of the solvent used. The alternating line-width effect can be rationalized upon assuming the occurrence of different rotamers in solution (due to the σ bonds) [30], with a much easier interconversion from more planar to twisted radical-core conformations. No J modulation is involved in such process since the peak-positions and total spectral widths (apart from large broadening upon lowering the temperature) did not change in the temperature range analyzed (see Figure 4.16 B).

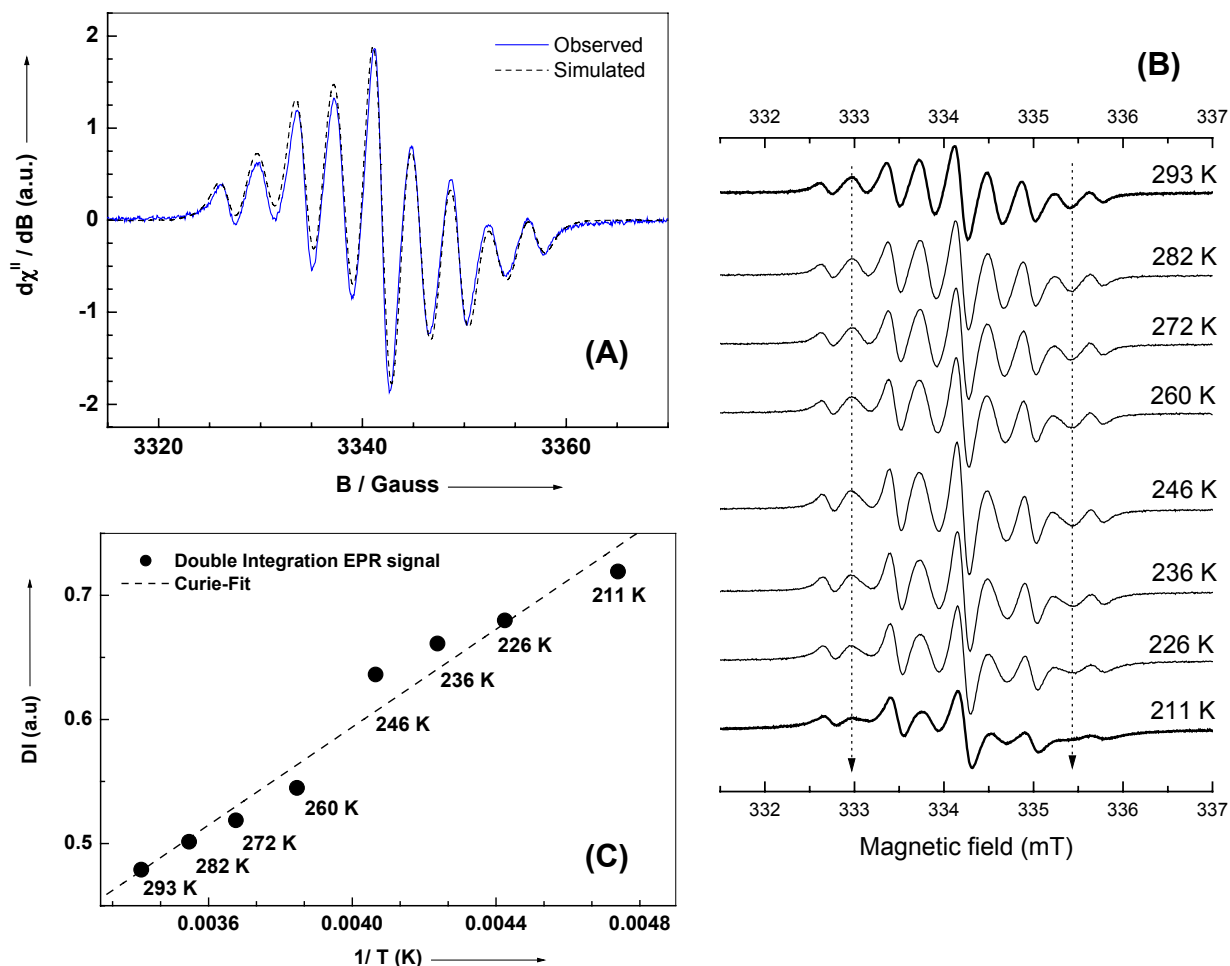


Figure 4.16: The alternating line-width effect in solution (toluene, **B**) observed upon cooling for the radical nitronyl nitroxide biradical **41**. Figure (**C**) shows the theoretical line (dashed line) for the Curie-like behaviour while the symbol (\bullet) represents the double integrated EPR envelope at the selected temperature. The spectra in (**A**) (solid line) report the observed biradical feature recorded at 293 K and its related computer simulation (dashed line). The spectra in (**A**) and (**B**) were base-line and frequency corrected. Experimental and spin-Hamiltonian parameters: 9.400086 GHz for (**A**) and (**B**), then 0.03 mT modulation amplitude, 2.0 mW power. $g_{\text{iso}} = 2.0065(1)$ and the apparent $a_N/2 = 0.374(2)$ mT.

The double integrated signal intensities increased either for **41** and **42** upon decreasing the temperature, with 2.0 ± 0.25 spins for **41** and 2.0 ± 0.15 for **42** in the full temperature range analyzed, showing however larger deviations from the theoretical linear Curie-plot especially for **41** (Figure 4.16C). The observed EPR spectrum of **41** recorded at

room temperature could be simulated only upon assuming a large percentage ($\sim 35\%$) of uncoupled biradical (with $|J| \ll 7 \times 10^{-4} \text{ cm}^{-1}$) superimposed on the biradical component ($\sim 65\%$) under strong exchange limit (with $|J/a| \geq 40$, i.e. $> 2J > 0.056 \text{ cm}^{-1}$ with $a_N = 20.94 \text{ MHz}$) (Figure 4.16A, dashed line). In the similar way, the simulation of the solution EPR spectrum of **42** (Figure 4.17A, black dashed-line) gave $\sim 25\%$ of uncoupled biradical (with $|J| \ll 7 \times 10^{-4} \text{ cm}^{-1}$) superimposed on the biradical component ($\sim 75\%$) under strong exchange limit (with $2J \geq 0.055 \text{ cm}^{-1}$ with $a_{N1} = 25.20 \text{ MHz}$ and $a_{N2} = 12.32 \text{ MHz}$).

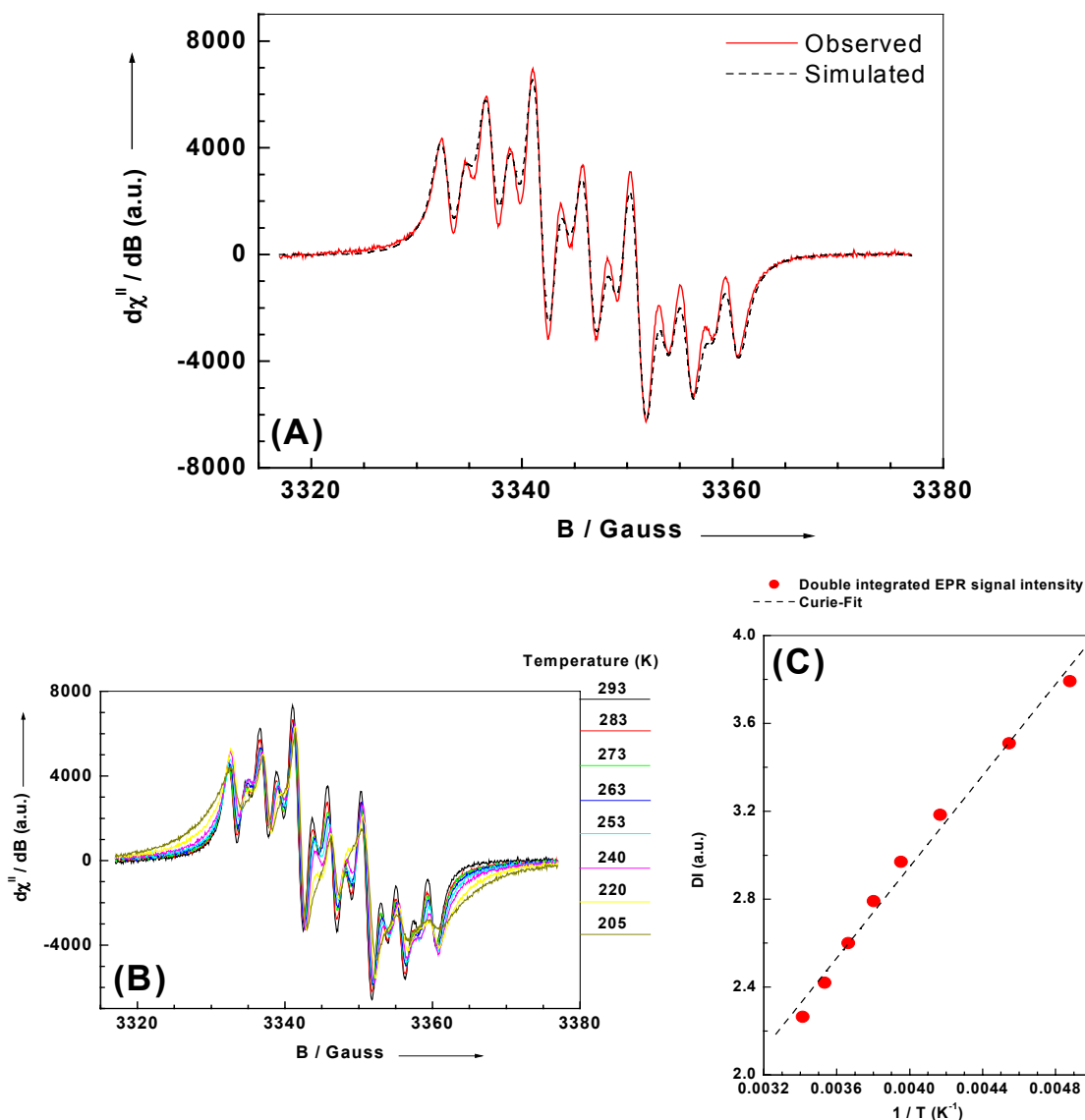


Figure 4.17. The alternating line-width effect in the solution EPR spectra observed upon cooling for the imino nitroxide biradical **42** (toluene, 10^{-4} M). The figure (C) shows the theoretical line for the Curie-like behaviour (dashed line) while the circles (\bullet) correspond to the measured double integrated EPR signals. In (A) is reported the thirteen line pattern of **42** recorded at 293 K together with its computer simulation (dashed line). The spectra in (A) and (B) were base-line and frequency corrected. Experimental and spin-Hamiltonian parameters: 9.402404 GHz , 0.03 mT modulation amplitude, 2.0 mW power. $g_{\text{iso}} = 2.0060(1)$, with the apparent $a_{N1}/2 = 0.450(2) \text{ mT}$, $a_{N2}/2 = 0.220(2) \text{ mT}$.

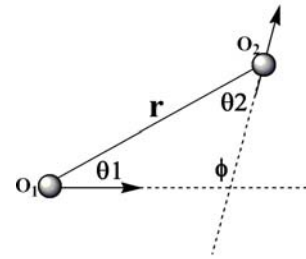
4.5. The EPR of mono and biradical systems in frozen solutions.

In frozen solution or in a powder the relevant spin-Hamiltonian describing the EPR transitions for monoradical and biradical systems are reported in equations (25) and (26) respectively:

$$\hat{H} = \beta_e \mathbf{g} \hat{S}_z \mathbf{B}_0 + \mathbf{S} \cdot \mathbf{A} \cdot \mathbf{I} \quad (25)$$

$$\hat{H} = \beta_e \mathbf{g} \hat{S}_{a,b} \mathbf{B}_0 - 2J \hat{S}_a \hat{S}_b + \mathbf{S} \cdot \mathbf{D} \cdot \mathbf{S} + \mathbf{S} \cdot \mathbf{A} \cdot \mathbf{I} \quad (26)$$

Where \mathbf{g} and \mathbf{A} are now tensors with different space components (anisotropy) such as $\mathbf{g} = (g_{xx} + g_{yy} + g_{zz} / 3)$, and $\mathbf{A} = (A_{xx} + A_{yy} + A_{zz} / 3)$ [22b,c]. The origin of the anisotropy in \mathbf{A} comes from the interaction between the magnetic moment of the electron and the nuclei, therefore it depends on $r^{-3} (\mu_e \mu_n [1 - 3 \cos^2 \theta] / r^3)$, with r being their distance, θ the angle between the μ vectors, and $\mu_e \mu_n$ electron and nuclear magnetic moments. In the general case for the dipole expression, when two $\mu_{A,B}$ vectors are not aligned mutually parallel to each other, it assumes the forms $(\mu_A \mu_B [\cos \phi - 3 \cos \theta_1 \cos \theta_2] / r^3)$ with r being the distance between the centres O_1 and O_2 . This is shown in the small figure on the right. Remarkably enough it is independent on the sign of r .



In $S \geq 1$ systems assuming that the \mathbf{D} - and \mathbf{g} -tensors have the same principal axis, the equation (26) reported above can be rewritten as (27):

$$\hat{H} = \mathbf{g} \beta_e \hat{S}_{a,b} \mathbf{B}_0 - 2J \hat{S}_a \hat{S}_b + D \{ \mathbf{S}_z^2 - S(S+1)/3 \} + E (\mathbf{S}_x^2 - \mathbf{S}_y^2) + \mathbf{S} \cdot \mathbf{A} \cdot \mathbf{I} \quad (27)$$

D and E are related to the principal values of the \mathbf{D} -tensor through $D = 3D_{zz}/2$ and $E = |D_{xx} - D_{yy}|/2$ and they represent the fine structure parameters (axial and rhombic) also called zero-field-splitting parameters. They originate from the electron-spin-electron-spin dipole interaction [20], and this causes the three fold degeneracy of the triplet state to be removed even in zero magnetic fields.

The \mathbf{D} , J and the Zeeman contributions expressed in the spin-Hamiltonian (27) are depicted in the Figure 4.18. Their in-depth theoretical descriptions are treated in several monographs [20, 22].

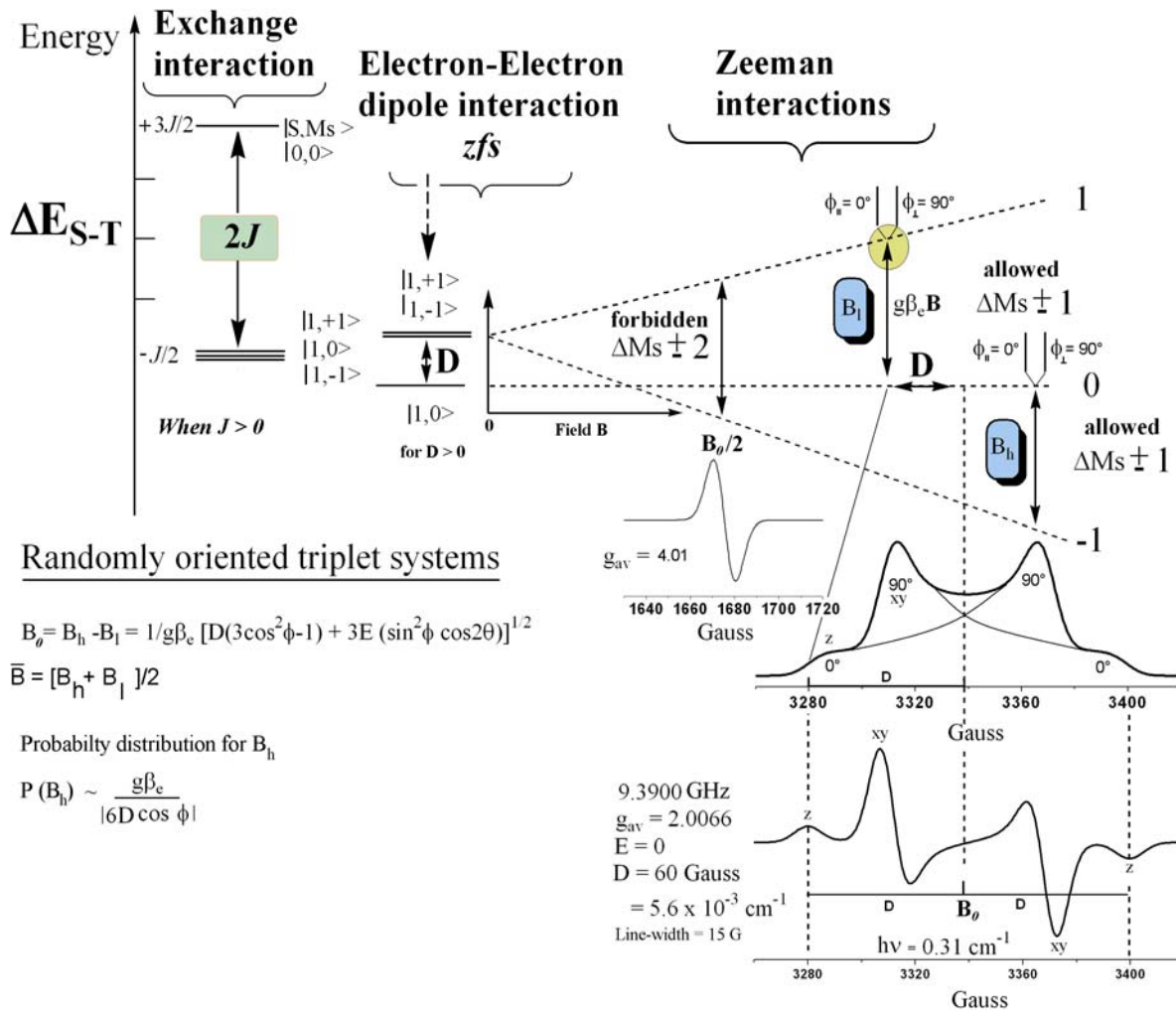
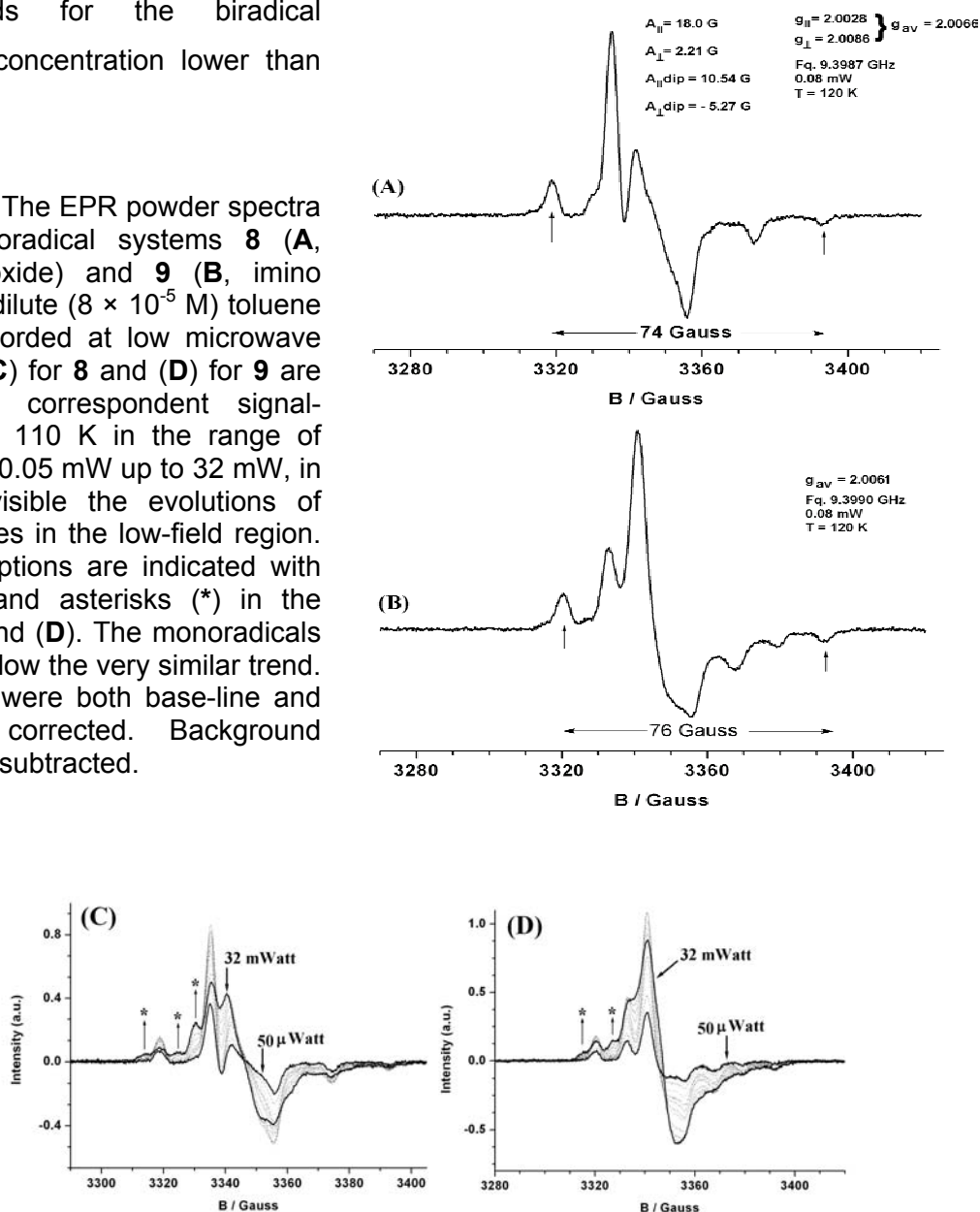


Figure 4.18. Energy diagram for the eigenstates of the spin-Hamiltonian (27) for two $S = \frac{1}{2}$ interacting spins. The term J is assumed as positive (ferromagnetic interaction); when it is negative (antiferromagnetic) the singlet lies below the triplet in energy. The zfs parameter D is also assumed as positive; when it is negative the transition $|1, 0\rangle$ lies higher in energy. The first-order perturbation theory is applied (e.g the Zeeman term is larger than the zfs terms). The powder spectrum (absorption) and its first derivative have been simulated with non zero line-width for a pure axial system ($E=0$). The terms B_h and B_l represent the high and low field components of the two allowed absorption lines. The forbidden half-field transition, $\Delta M_S = 2$, is also shown.

4.6.1 The observed EPR spectra of the monoradical systems in frozen solutions.

The monoradical spectra for the nitronyl- (NN) **8** ($g_{av} = 2.0066$) and imino nitroxide (IN) **9** ($g_{av} = 2.0061$) recorded at low power in diluted frozen solutions [10^{-4} M] are reported in Figure 4.19A and 4.19B respectively. The other two monoradical systems based on the pyridylpyrazolyl moieties (**37** and **38**) show the same EPR envelopes with respect to **8** and **9**, thus are not reported in the figure. However they feature slightly different g values with $g_{av} = 2.0065$ for **37** and $g_{av} = 2.0060$ for **38**. Note that the rhombic pattern (i.e. $g_{xx} \neq g_{yy} \neq g_{zz}$) of the monoradical systems cannot be resolved at X-band frequency [31] where they appear axial (with $g_{xx} = g_{yy} \neq g_{zz}$). All the monoradicals synthesized, followed nicely the Curie-Law, with linear increase of the double integrated signal intensities upon decreasing the temperature, and therefore they can be used as spin-standards for the biradical systems at concentration lower than 10^{-2} M.

Figure 4.19. The EPR powder spectra of the monoradical systems **8** (A, nitronyl nitroxide) and **9** (B, imino nitroxide) in dilute (8×10^{-5} M) toluene solutions recorded at low microwave powers. In (C) for **8** and (D) for **9** are shown their correspondent signal-saturation at 110 K in the range of powers from 0.05 mW up to 32 mW, in which are visible the evolutions of additional lines in the low-field region. Those absorptions are indicated with thin-arrows and asterisks (*) in the figures (C) and (D). The monoradicals **37** and **38** follow the very similar trend. The spectra were both base-line and centre-field corrected. Background signals were subtracted.



4.6.2 . The observed EPR spectra of the biradical systems in frozen solutions.

The EPR spectra in frozen solution (toluene) for the biradicals **12** (NN), **13**(IN), **26** (NN), **28** (IN), **33** (NN), and **34** (IN) are collected in Figure 4.20, to allow quick comparison, while the spectra for **41** (NN) and **42** (IN) are shown again separately in Figure 4.21. It is clear from the spectra, although part of the anisotropic patterns are retained, that most of the hyperfine couplings are not resolved. This effect arises from dipolar interactions characteristic of randomly oriented triplet species. Increasing the intramolecular radical distances led to a decrease in the magnitude of the zfs component, since the $|D|$ value in axial systems is related with the averaged radical distances according to equation (28)(the point-dipole approximation)

$$|D| \text{ (MHz)} = 77924 (g_{\text{obs}} / g_e) / r^3 \quad (28)$$

With r (in Angstrom, Å) considered as their averaged through-space separation. In Table 4.3 are collected for comparison the spin-Hamiltonian parameters for **12** (NN), **13**(IN), **26** (NN), **28** (IN), **33** (NN), and **34** (IN), together with their estimated r . In the biradical (NN) **33** the spectrum appeared quite complex (Figure 4.20 C) in which eleven resolved lines are observed ($\Delta B_{pp} = 0.75$ mT for the outermost pairs) with an unusual resolution of nitrogen hyperfine coupling. All the biradical systems even at ~ 120 K showed the forbidden ($\Delta m_s \pm 2$) half-field transition at $g \sim 4.01 - 4.02$, therefore supporting their biradical nature. For two biradical systems, **26** (NN), and **28** (IN), and perhaps also in **35** (IN) (*vide infra*), even after repeated purification steps through column chromatography or preparative TLC, a small amount of monoradical impurity ($\sim 3\%$ in **26** and $\leq 6\%$ in **28**) can be observed in the $\Delta m_s \pm 1$ transition in the recorded powder spectra. The monoradical-signal contributions are indicated with asterisks in Figure 4.20. Those impurities can be easily discriminated in **26** and **28**, because their saturation trends are much different from the major biradical absorption lines. This is shown in the Figure 4.21 for **28**, as one example in which the monoradical signal contribution is highlighted by enclosing it into a box. A double-quantum transition has to be ruled out because, it occurs, it requires far higher power [22d, 22e]. In **34** indeed, the overall EPR signal (including those marked with the asterisk in Figure 4.19 D) broadens in the same way when increasing microwave power has been applied. Upon subtraction of a small percentage ($\sim 5\%$) of monoradical contribution from the major biradical absorption line, the overall EPR envelope shows almost a full isotropic line, making very hard the estimation of $|2D|$. Although one might suggest that those extra signals are originating from the presence of different conformers in the powder spectra, with strongly twisted radical sites with respect to the coupling unit core, and not from monoradical impurities, this appears clearly in contradiction

with the fact that for **26** and **28** the solution spectra did not show strong line-width dependencies, upon decreasing the temperature. However, such hypothesis cannot be excluded for **34** in which such effect was observed.

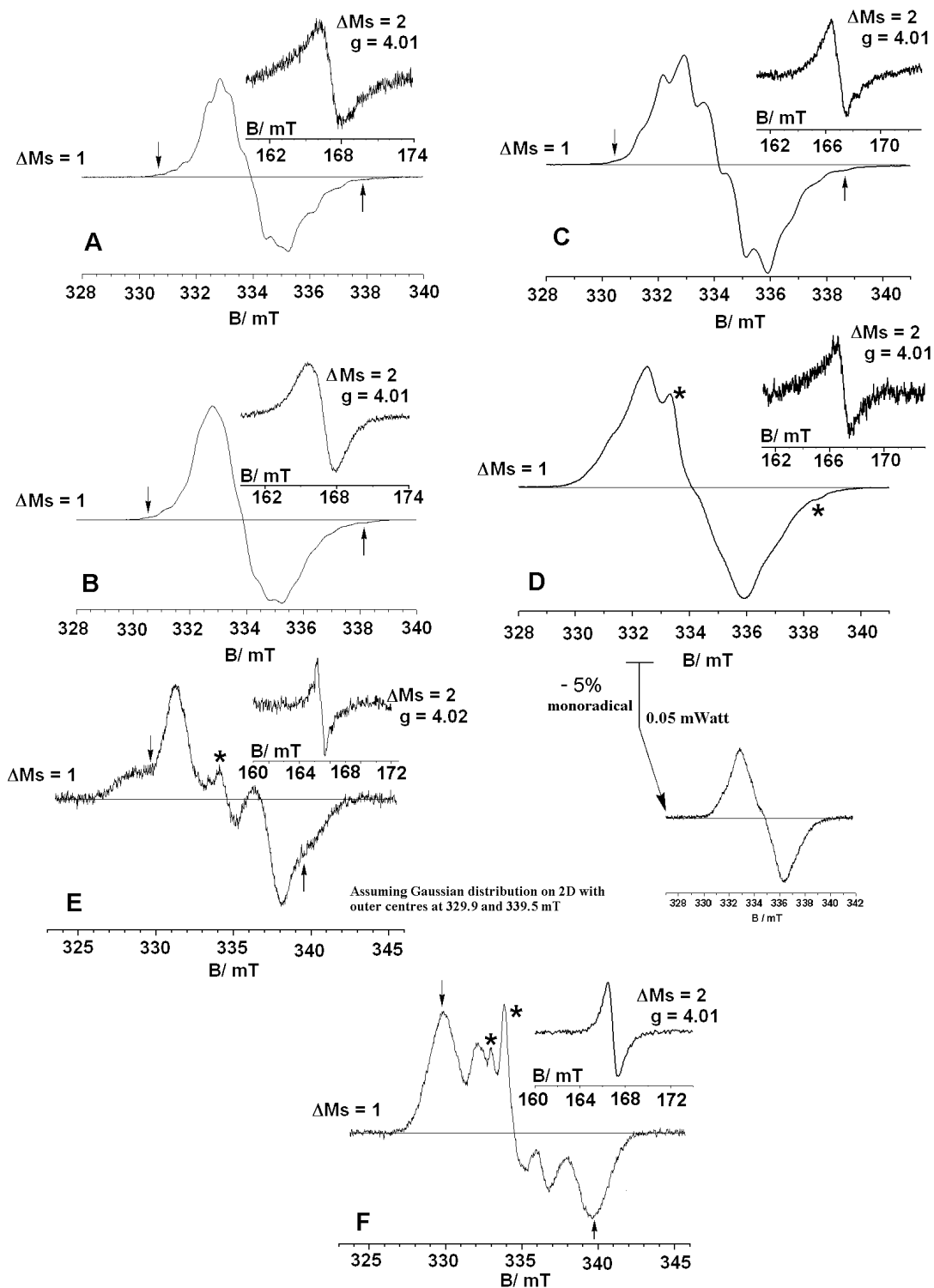
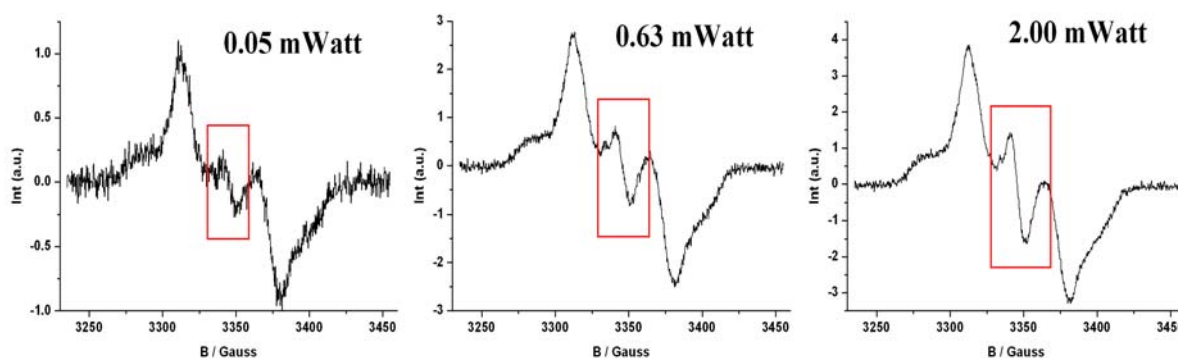


Figure 4.20. The EPR powder spectra of the biradical systems (A) **12**, (B) **13**, (C) **33**, (D) **34**, (E) **26** and (F) **28**. The relevant experimental parameters together with the estimated zfs are reported in Table 5.3. Note that the spectra were recorded at different powers, since the biradicals featured different saturation trends. The asterisks (\star) indicate a monoradical impurity and the arrows the estimated $|2D|$ range.

Table 4.3: The estimated zfs parameters for the biradical systems.

$\Delta m_s = 1$ transition	Microwave Power mWatt	T (K) [C] Solvent	Frequency GHz	g_{obs}	$ 2D $ Gauss	$ D/hc $ 10^{-3} cm^{-1}	r Å
12 (NN)	0.8	110 4×10^{-4} M toluene	9.3970	2.0066	74	3.46	9.1
13 (IN)	0.8	110 6×10^{-4} M toluene	9.4007	2.0061	79	3.69	8.9
33 (NN)	0.6	120 1.0×10^{-3} M toluene	9.3989	2.0066	81	3.79	8.8
34 (IN)	0.6	120 1.1×10^{-4} M toluene	9.4027	2.0061	~ 80	3.73	~ 8.8
26 (NN)	0.2	120 1.0×10^{-4} M toluene	9.4168	2.0065	~ 96	4.50	~ 8.3
28 (IN)	0.2	120 4×10^{-4} M toluene	9.4144	2.0060	102	4.78	8.2

**Figure 4.21.** The EPR powder spectra at 122 K for the biradical system **26** recorded at different microwave power. The red box encloses the signal coming from the monoradical impurity.

For the biradical **41** (NN) and **42** (IN), conformational interconversion towards strongly twisted radical sites with respect to the coupling unit core are more easily accessible. The zfs envelope for the pure biradical character in the $\Delta m_s \pm 1$ transition for **41** was obtained by subtracting a weighted percentage of uncoupled biradical (Figure 4.22 C). This was made possible by comparison with the saturation trend of the monoradical system **37**. The estimated zfs accounts for $|2D| \sim 62$ Gauss (i.e. $|D/hc| \sim 2.90 \times 10^{-3} \text{ cm}^{-1}$) corresponding to the

averaged distances between the radical fragments of 9.6 Å. This is the largest distance in the NN biradical series.

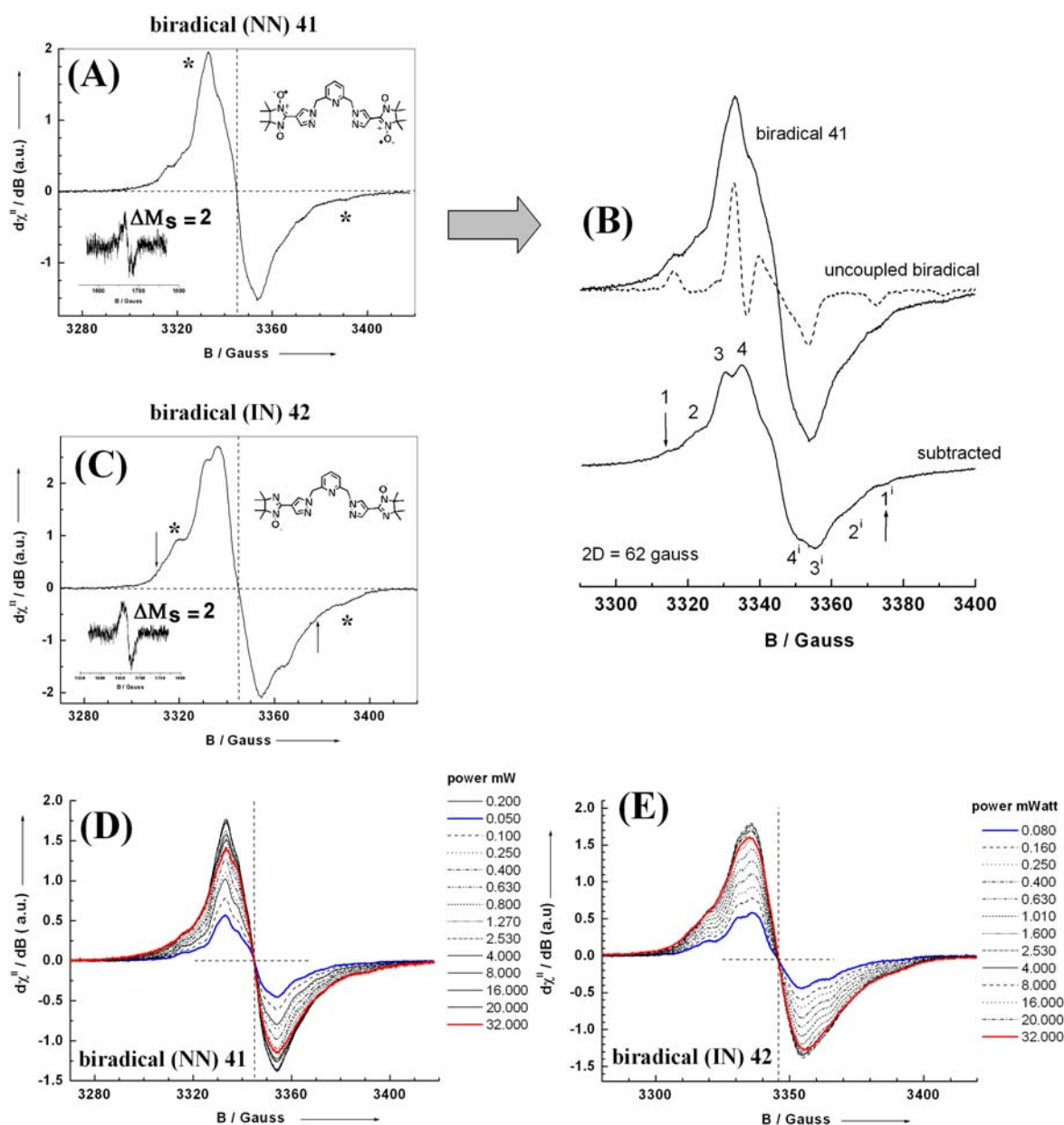


Figure 4.22: EPR spectra of the $\Delta M_s = 1$ transition for the nitronyl nitroxide radical **41** (A) and the imino nitroxide biradical **42** (C) with anelling procedures. The asterisks in (A) and (C) are fingerprints for more strongly twisted conformations vs coupling unit core for the radical moieties. Experimental parameters for (A): 9.41591 GHz, 100 kHz mod. frequency, 0.6 Gauss mod. amplitude, 2.0×10^4 gain, 84 sec sweep time, 41 msec t. constant, 122 K, 0.2 mWatt power, [concentration] = 4.5×10^{-4} M in toluene. Experimental parameters for (C): 9.41699 GHz, 100 kHz mod. frequency, 0.6 Gauss mod. amplitude, 4.0×10^4 gain, 84 sec sweep time, 82 msec t. constant, 0.16 mWatt power, 122 K, [C] = 4.9×10^{-4} M in toluene. Note that the filling factors were different for (A) and (C). The spectra were base-line corrected. Figure (B) shows in the lower traces (subtracted) the biradical EPR envelope for the planar conformer. (D) and (E) show the signal-saturation trends for **41** (D) and **42** (E) at 122 K. The insets in (A) and (C) represent the observed EPR half-field transition for **41** and **42** respectively. Note on anelling: fast cooling in N_2 bath at 77 K \rightarrow raise temperature at 170 K in the EPR cavity (keep for 20 min) \rightarrow lower the temperature slowly to 122 K.

However, in **42** since the overall absorption line broaden inhomogeneously at all available power (Figure 4.21 E), such a comparison was not possible. Therefore a very crude estimation of $|2D| \sim 68$ Gauss ($|D/hc| \sim 3.18 \times 10^{-3} \text{ cm}^{-1}$, $r = 9.4 \text{ \AA}$) has been obtained. A further comment might be useful at this point; one might suggest an indirect correlation between size of J and the zero-field-splitting $|D|$ by comparing equation (28) and (13).

As much as r is decreasing, J is increasing, hence J and $|D|$ should feature the same trend. From the values reported in Table 4.3, it seems that the nitronyl nitroxide biradical systems possess smaller or comparable $|D|$ once related with the imino nitroxide biradicals. Therefore J should be smaller or comparable (within the same coupling unit series). However, even taking under consideration errors in the estimation of the zfs parameters for the imino and nitronyl nitroxide biradicals, we shall see that larger $|D|$ does not imply larger J , and therefore correlation between $|D|$ and J based on the through-space interaction model would not be appropriate for discussing the strength of through-bond interaction between radical centers. As pointed out earlier by Ullman [33], the *cis* conformation of imino biradicals (e.g. in *meta*-phenylene derivatives) although seems to represent not the dominating conformers in frozen solutions, show larger zfs compared to the nitronyl nitroxides, even though the J value are smaller. All the biradical systems presented in this thesis, exhibit Curie-like behaviour also in their powder spectra, and the spin-concentration accounted for 2.0 ± 0.2 uncorrelated spins. These results indicate that thermally activated spin states still survive even at around 100 K, and therefore for all the biradical system the $\Delta E_{ST} < 100 \text{ K}$ (i.e. $< 69.5 \text{ cm}^{-1}$).

4.7. The EPR saturation behaviour of mono and biradical systems in frozen solutions.

Clear differences between mono and biradical systems are observed upon following the saturation trends of their $\Delta m_s = 1$ transitions in frozen solution. These results are collected together, for most of the spin systems synthesised, in Figure 4.23. The parameters obtained from fitting the variation of the double integration of the signal intensities (DI) *versus* applied microwave power (P) are reported in Table 4.4. The data of the EPR signal saturation were fitted using the empirical expression provided by Portis [36] and Castner [37], written in the following form:

$$DI = k \times \sqrt{P} / [(1+P/P_{1/2})]^{b/2} \quad (\text{a})$$

where b represents the relaxation factor ($b = 1$ for inhomogeneous line broadening and $b = 3$ for homogeneous line broadening) for a first derivative spectrum as it is usually acquired within common EPR experiment, $P_{1/2}$ the power at which half of the signal is being saturated

and k a normalization factor associated with the instrument. The logarithmic form of equation (a) is more often used to present the experimental data:

$$\text{Log}_{10} (DI / \sqrt{P}) = \text{Log}_{10} k - (b/2) \text{Log}_{10} [1 + (P / P_{1/2})] \quad (b)$$

If $[\text{Log}_{10} (DI / \sqrt{P})]$ is plotted versus $\text{Log}_{10} P$, two linear regions are obtained that intersect at $P = P_{1/2}$. The value of b depends on which mechanism is dominating within the relaxation process of the quanta being adsorbed, i.e. if the spin-lattice relaxation (T_L) represents the dominant factor, the power-dependent line broadening is inhomogeneous (Gaussian line) and b assumes the minimum value of 1. When T_s is dominant, the line broadening is homogeneous (Lorentzian line) and b assumes the maximum value of 3. The relaxation factor b is often allowed to fluctuate in the fitting in order to account for intermediate cases ($1 \leq b \leq 3$), when the line-shape observed is a mixture of Lorentzian and Gaussian line. This effect particularly holds for frozen solutions. In order to apply equation (a), the following experimental conditions must be satisfied: the samples should be in the region of the cavity with the maximum microwave field, H_1 , thus the filling factor has to be optimized, while the sample temperature, the Zeeman modulation amplitude, the frequency and possibly the gain must also be constant. Equation (a), on the other hand, is not strictly applicable when dipolar couplings are present in the system, because:

$$P_{1/2} = [\alpha / (T_s \times T_L)] \quad (c)$$

With $\alpha = 1/2 \times (V/Q \gamma^2)$ where V represents the cavity volume, Q the cavity quality factor ($Q = H_1^2 V / 2P$), P the power dissipated in the cavity and γ the gyromagnetic ratio. Equation (c) assumes that all spins at resonance saturate equivalently and hence they show the same product for $(T_L \times T_s)$. When dipolar interactions are present, the product $(T_L \times T_s)$ is no longer constant, and b is found sometimes smaller than 1, nevertheless a much more crude estimation of $P_{1/2}$ can be still obtained.

Therefore, from the trend in the saturation data and the corresponding theoretical fitting the following comments are drawn:

1) The monoradical systems start to saturate at very low power ($\ll 1$ mWatt), already at 122 K, with the clear tendency for the imino nitroxide radical to saturate at higher power with respect to the nitronyl nitroxide. The line-shapes are mostly described by a Gaussian-line ($b \sim 1$) although severe distortions occur at high power suggesting that the g_{zz} component saturates faster than the $g_{yy} \sim g_{xx}$ components.

2) The same trend is observed in the biradical systems with the exception of **28** (if we consider the estimated $P_{1/2}$ value) despite the additional contribution coming from dipolar interactions. The shape factor (b) is generally smaller in the case of the nitronyl- (NN) with respect to the imino nitroxide (IN) radicals with again the exception of **28** in which such trend is reversed. This should be related with the “magnitude” of the dipolar interaction (smaller $b \rightarrow$ larger D) in disagreement with the zfs parameters of the radical systems discussed previously (D seems usually smaller in NN with respect to IN).

3) No cross correlation among magnitude of $P_{1/2}$ or the shape factor (b) in similar biradical systems (e.g. all the nitronyl- and all the imino nitroxides) and corresponding strength of J can be made. For example in Figure 4.23 B the difference in saturation between radical **26** (NN) and **41** (NN) is negligible, and it is very small as compared with **28** (IN). However, **26** shows clear triplet ground state, while **41** and **28** feature almost singlet-triplet degeneracy (*vide infra*).

4) The use of the double integration (DI) of the $\Delta M_s = 1$ transition in these biradical systems down to cryogenic temperature (in order to estimate J) would be precluded, since already at less than 20 dB at 122 K ~10-15% signal saturation is observed.

5) The empirical correlation used to evaluate $|D|$ is based on the intensity ratios between the $\Delta M_s=2/\Delta M_s=1$ transition ($1:[D/B_0]^2$). This would be hardly applicable in these systems in whatever temperature range. Over 10 mWatt of microwave power, very much of the $\Delta M_s=1$ signal at 122 K is saturated, for the majority of these biradicals, while at such power hardly the $\Delta M_s=2$ can be observed; therefore no direct comparison can be made and no estimation of $|D|$ can be obtained.

Table 4.4: Saturation data at 122 K for the dilute (10^{-4} M) radical systems with simulation parameters according to $\text{Log}_{10} (\text{DI} / \sqrt{P}) = \text{Log}_{10} k - (b/2) \text{Log}_{10} [1 + (P / P_{1/2})]$. The k term represents the instrument constant. Upon normalization its value is ~1.000 and thus has not been included in the Table. Note that the estimated $P_{1/2}$ values in the biradicals are certainly approximated.

Radical	Type	Shape factor (b)	$P_{1/2}$ mWatt	R^2 >
41	NN biradical	0.467 ± 0.009	0.82 ± 0.06	0.999
42	IN biradical	1.078 ± 0.029	1.12 ± 0.11	0.999
8	NN monoradical	1.048 ± 0.013	0.71 ± 0.04	0.999
9	IN monoradical	1.017 ± 0.026	1.06 ± 0.10	0.999
33	NN biradical	0.802 ± 0.014	1.17 ± 0.08	0.999
34	IN biradical	0.918 ± 0.016	1.25 ± 0.08	0.999
12	NN biradical	0.287 ± 0.019	0.61 ± 0.19	0.991
13	IN biradical	1.217 ± 0.031	1.41 ± 0.13	0.999
26	NN biradical	0.524 ± 0.009	1.19 ± 0.07	0.999
28	IN biradical	0.450 ± 0.001	1.09 ± 0.10	0.996

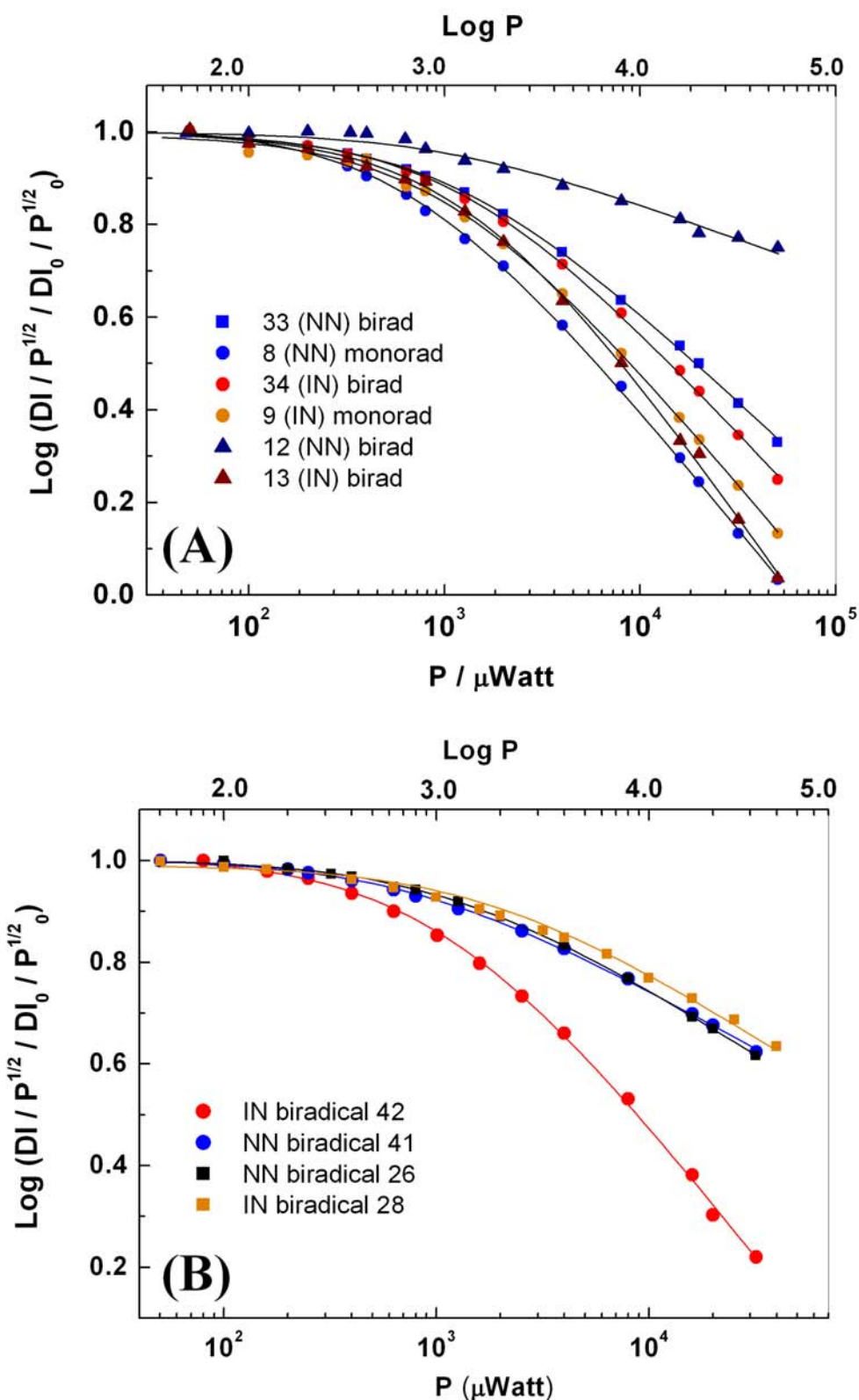


Figure 4.23: (A) and (B) Power saturation for the mono and biradical systems performed at 122 K. The radical concentrations were 10^{-4} M. The different symbols represent the double integration (DI) of the signal intensities and the solid lines the theoretical fit. Before performing the double integration of the signals, each spectrum was base-line corrected, and adjusted for frequency shift (diode current 200 μ A, lock offset to zero).

4.8. Determination of the electronic ground state in the magnetically diluted biradical systems.

4.8.1. The terpyridine based biradicals.

In order to analyze the trends in the magnetic properties of the isolated molecules, the temperature dependence of the $\Delta M_s = 2$ transitions have been followed down to cryogenic temperature. The microwave powers applied in the measurements were kept in such a way that the signals were proportional to the root of power, in order to avoid saturation effects. In the case of the terpyridine based biradicals **12** (NN) and **13** (IN) the double integration of the $\Delta M_s = 2$ signal increases upon decreasing the temperature for both (Curie Plot) as shown in Figure 4.24A and 4.24B. Moreover, the fact that also the product DI·T increases with decreasing temperature indicates that the ground states are certainly the triplets ($S=1$), and the singlets ($S=0$) have to be associated with thermally accessible excited states. Fitting the DI·T data according to the Bleaney-Bowers model [34a] for two interacting spins $S=1/2$ system where DI is expressed as

$$DI = \chi_{EPR} \propto \{(2Ng^2\beta^2/3k_bT) \times [1/3 + \exp(-2J/k_bT)]\} \quad (29)$$

it gave a separation for **12** of $|\Delta E_{ST}| = 2J/k_b$ of $15.4 \pm 2.0 \text{ cm}^{-1}$ between the magnetic ground ($S=1$) and the excited states ($S=0$) (Figure 4.24C), while a smaller singlet-triplet gap has been observed for **13** with $|\Delta E_{ST}| = 2J/k_b$ of $8.7 \pm 1.0 \text{ cm}^{-1}$ (Figure 4.24D).

In order to predict theoretically the ΔE_{ST} and compare it with the experimental findings, the ground spin-state for **12** and **13** has been obtained towards quantum chemical calculations, carried out by P.D. Dr. Martin Baumgarten and Dr. Anela Ivanova (University of Sofia, Bulgaria). The geometry of the biradicals was optimised both with UHF/AM1 and ROHF/AM1, the two methods yielding virtually identical lowest energy structures. Furthermore, no essential differences were witnessed between the geometry of the unrestricted singlet and triplet molecules. Therefore, the ROHF/AM1 structures of **12** and **13** were used further on for calculation of the spin-state energies. The imino nitroxide and the nitronyl nitroxide rings are essentially planar (intraring torsion angles $\leq 10^\circ$), with the N–O bonds about 15° out of the ring plane. The calculated bond lengths fall within the range of those measured for radicals of this class. The N–O bonds are slightly shorter than the most commonly encountered experimental value of 1.28 \AA , namely $R_{N-O} = 1.209$ and 1.204 for **12** and **13**, respectively. This result is similar to previous AM1 calculations. An interesting structural feature of the molecules are the torsional angles Θ_1 and Θ_2 and in the case of **12** those results might be compared with its X-ray structure (see Figure 4.25 for both spin densities distributions and optimized structure). Since angles Θ_1 and Θ_2 torsional angles reflect the possibility for free rotation around the two

single bonds, they can be used to measure the effective π -conjugation through the spacer. Therefore, a conformational search, i.e. systematic variation of Θ_1 and Θ_2 with calculation of the corresponding energy, was performed at the UHF/AM1 level. 92% of the conformations of **12** and 100 % of those of **13** differ in energy by less than 5 kcal/mol. This result indicates relatively high flexibility of the two molecules, the rotation barrier being lower in **13** than in **12**. The calculated singlet-triplet splitting and heats of formation of **12** and **13** are collected in Table 4.5. The simulations predict triplet ground states for both biradicals, as experimentally found, evidenced by the positive values of ΔE_{ST} . The triplet state is more stable with respect to the singlet in **12** than in **13**, which is probably due to more effective π -conjugation resulting from the less flexible structure of **12**. This is also in agreement with the experimental findings. It is apparent that the exchange coupling is extremely sensitive to rotation around the single bonds. Increase of Θ_1 to $\sim 90^\circ$ results in practically degenerate singlet and triplet states. This is an indication for hampered intramolecular coupling between the radical sites due to prevented spin transfer into the spacer. The calculated spin densities are presented in Figure 4.23. Both biradicals feature alternating signs of the spin densities at neighbouring atoms throughout the whole molecule. Thus, the main prerequisite for effective ferromagnetic exchange coupling is fulfilled. Increase of Θ_1 to $\sim 80^\circ$ (conformation **a** in Table 4.5) leads to zero value of the spin density at the carbon sites connecting the central pyridine ring to the two outer ones. A direct consequence is the inability for spin transfer and hence a breakdown in spin polarization. Although conformation **a** has slightly lower heat of formation in the gas phase, the small rotation barrier allows stabilization of more planarized structures like **b**. However, the optimised structure appears quite different from that observed in the crystal for **12** with an over-estimation of the singlet-triplet gap of $\sim 87 \text{ cm}^{-1}$ (i.e. $\sim 126 \text{ K}$), whereas in the case of **13** the estimated ΔE_{ST} gap of $\sim 9.4 \text{ cm}^{-1}$ ($\sim 13.5 \text{ K}$) is nearly identical to that one experimentally found. The intramolecular radical distances calculated using the approximation introduced by Mukai and co-workers [34b,c] defined as:

$$D = \frac{3}{4} g^2 \beta^2 \sum [r_{ij}^2 - 3m_{ij}^2] \rho_i \rho_j / r_{ij}^5 \quad (30)$$

Where r_{ij} is the distance between the atoms i and j , m_{ij} is the distance vector along the axis, which give rise to the largest dipole-dipole interaction, and ρ_i and ρ_j are the spin-densities on atom i and j . The relation (30) provides a better estimation of the averaged radical separation distances of $r = 0.83 \text{ nm}$ in case of **13** and $r = 0.88 \text{ nm}$ in case of **12**. Hence, larger D for **13** should be observed as compared with **12**. This is also in agreement with the experimental findings.

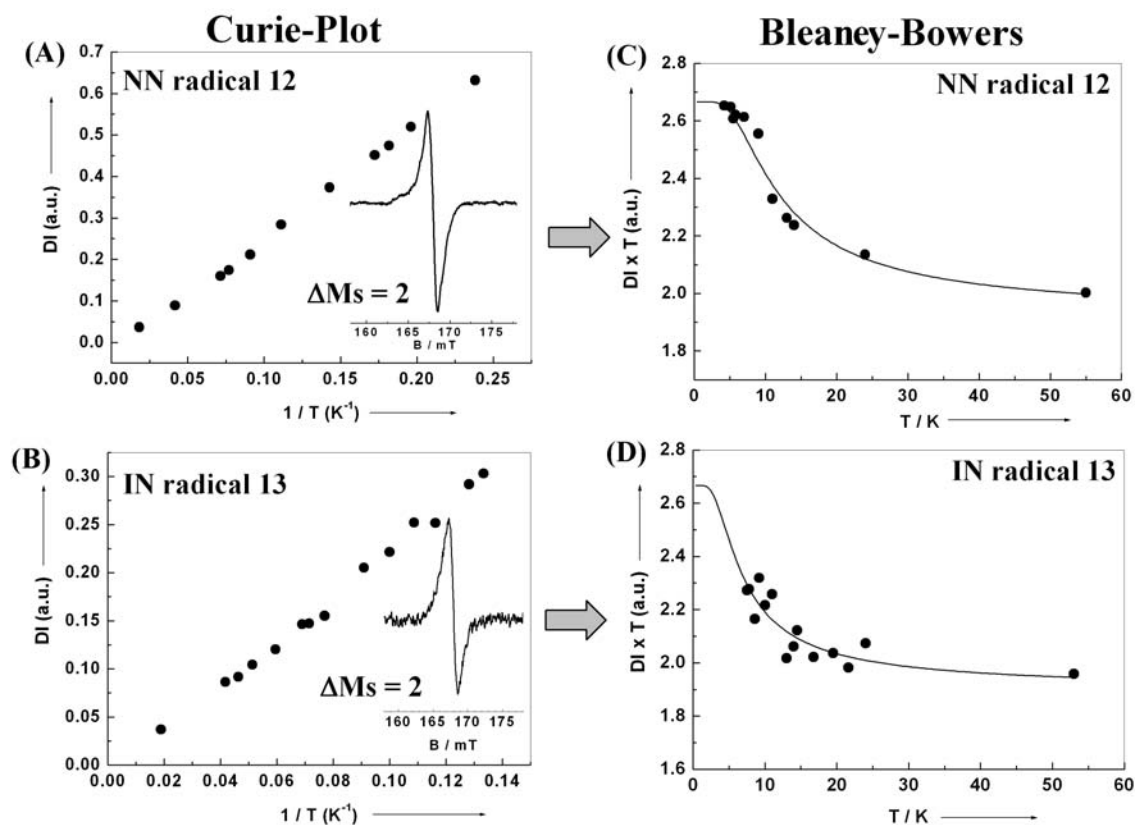


Figure 4.24: Curie-Plot for the terpyridine biradical systems: **(A)** nitronyl nitroxide **12** and **(B)** imino nitroxide **13** recorded in diluted (10^{-3} M) toluene solutions. DI represents the double integrated signal intensity of the half-field transition. The small inset in **(A)** and **(B)** show the observed half-field transition recorded 4.0 and 7.3 K respectively. **(C)** and **(D)** show the DI.T vs T plot; the best fitting according to the Bleaney-Bowers equation is shown as bold line with parameters given in the text.

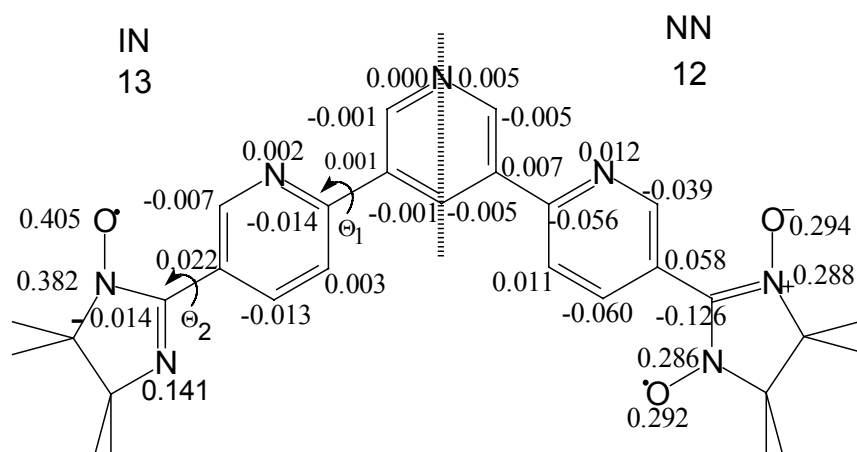


Figure 4.25. ROHF/AM1/CIS(20,20) calculated spin densities of conformation **b** of biradicals **12** (right) and **13** (left).

Table 4.5: ROHF/AM1/CAS [8,8] calculated singlet-triplet gap (ΔE_{ST}) and heat of formation (H_f) of biradicals **12** and **13** for different torsions Θ_1 and Θ_2 .

Radical	Conformation	$\Theta_1, ^\circ$	$\Theta_2, ^\circ$	$\Delta E_{ST}, \text{kcal/mol}$	$H_f, \text{kcal/mol}$
12	a	86	0	0.0006	192.898
	b	49	27	0.2499	195.846
13	a	84	7	0.0000	188.968
	b	47	20	0.0269	192.376

4.8.2. The bispyrazolopyridine based biradicals.

In the case of **26** (NN) the double integration (DI) of the $\Delta M_s=2$ signal increases upon decreasing the temperature (Figure 4.27A, ●, and 4.27C, ○) but also the quantity DI·T (Figure 4.27C, ●). Such findings indicate that in **26** the ground state is the triplet ($S=1$), and the singlet ($S=0$) represents a thermally accessible excited state.

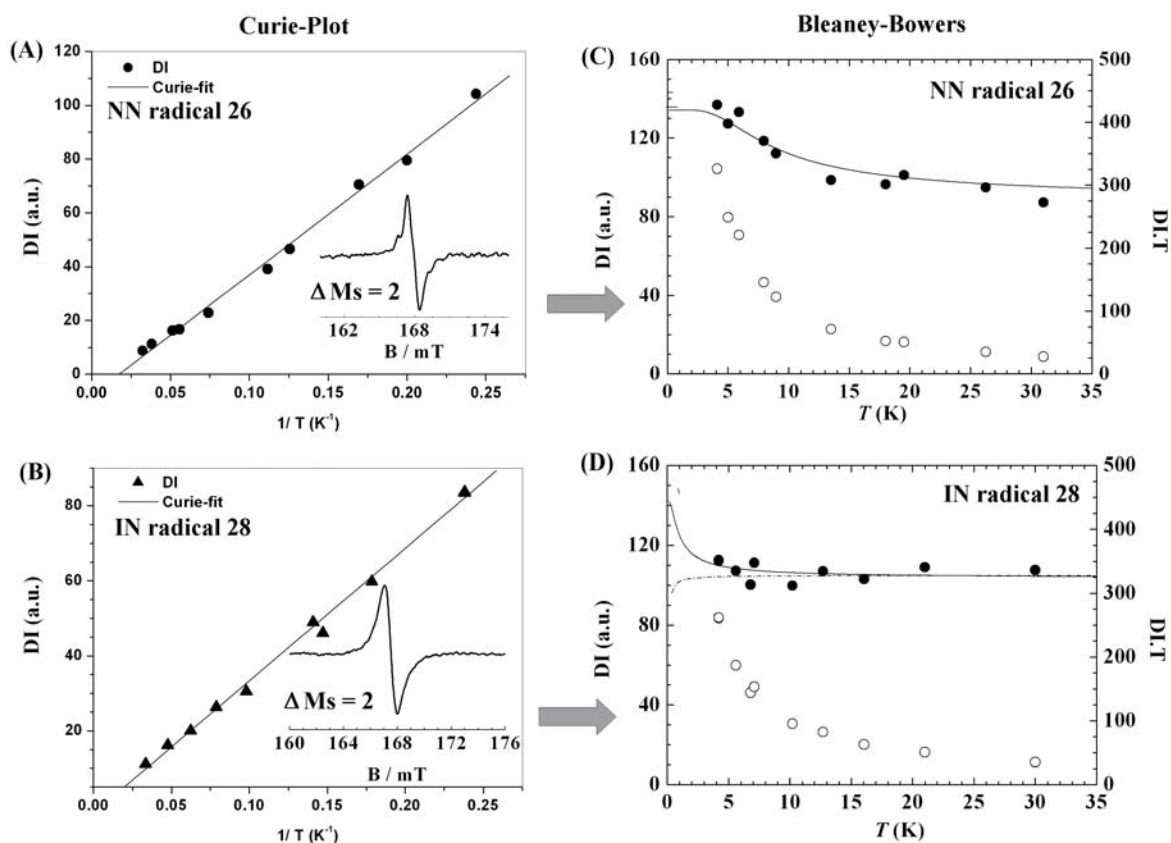


Figure 4.27: Curie-Plot for the bispyrazolopyridine biradical systems: **(A)** nitronyl nitroxide **26** and **(B)** imino nitroxide **28** recorded in dilute (10^{-3} M) toluene solutions. DI represents the double integrated signal intensity of the half-field transition. The small inset in **(A)** and **(B)** show the observed half-field transition recorded at 4.1 and 4.2 K respectively. **(C)** and **(D)** show the DI·T vs T plot; the best fitting according to the Bleaney-Bowers equation are described in **(C)** and **(D)** as bold line (for $S=1$) and dashed line (for $S=0$) with parameters given in the text. In **(D)** constraints in the fitting have been used according to the equations (32) and (33).

The fitting of the data according to the Bleaney-Bowers model for two interacting spins gives a separation $\Delta E_{ST} = 2J/k_b$ of $11.8 \pm 4.8 \text{ cm}^{-1}$ between the magnetic ground ($S=1$) and the excited states ($S=0$). However, in the imino nitroxide biradical system, **28**, while the $\Delta M_s=2$ signal clearly increased upon decreasing the temperature (Figure 4.27B, \blacktriangle , and 4.27D, \circ), the product $DI \cdot T$ appeared nearly constant (Figure 4.27D, \bullet), within the experimental error. Therefore, no thermal population or depopulation of the spin state of the molecules within the examined temperature range could be envisaged. In such case, either the triplet state ($S=1$) is the lowest-energy state separated from the singlet ($S=0$) by a substantial gap relative to the thermal energy ($|2J| \gg K_b T$), or the energy difference between triplet ($S=1$) and singlet ($S=0$) is extremely small leading to near degeneracy of those levels. Any change in temperature does not shift the thermal equilibrium between the two states, and they remain statistically populated according to the Boltzmann distribution ($\exp[-\Delta E/K_b T]$, e.g. 75% of the molecules occupies the triplet state and 25% the singlet).

Since from the solution and frozen state EPR studies discussed for **28**, it was clear that the energy gap between singlet and triplet cannot be large, such separation has to be very small, ranging far below the temperature available with a conventional experimental setting (4 K).

Fitting the $DI \cdot T$ data according to the Bleaney-Bowers model for two interacting spin systems, gave an upper limit for the singlet-triplet separation $\Delta E_{ST} = 2J/k_b$ of 0.7 cm^{-1} ($\sim 1 \text{ K}$) assuming triplet ground state ($J > 0$).

It is worth to emphasize that in this case in the fitting process, some assumptions have been made by using the limiting expressions (32) and (33)

$$\text{if } J > 0, \text{ then } \{[\lim_{T \rightarrow 0K} (D \cdot I_0)] / D \cdot I_T\} \rightarrow 0.333 \quad (32)$$

$$\text{if } J < 0, \text{ then } \{[\lim_{T \rightarrow 0K} (D \cdot I_0)] / D \cdot I_T\} \rightarrow 0 \quad (33)$$

Where DI_0 represents the double integrated $\Delta M_s = 2$ signal intensity extrapolated at $T = 0 \text{ K}$ and DI_T the double integration at the temperature in which the equilibrium between singlet and triplet state still satisfies the Boltzmann distribution (see equations 23 and 24). If the singlet ground state ($S=0$, $J < 0$) is considered, then the separation ΔE_{ST} is further reduced by a factor of ten ($2J/k_b$ of $\sim -0.07 \text{ cm}^{-1}$), in agreement with the lower limiting value obtained from the simulation of the solution EPR line. Because the complete spin reversal of the ground state multiplicity (from nitronyl- to imino nitroxide) seems improbable, although cannot be fully excluded, it is possible that also in **28** the ground state might be the triplet.

4.8.3. The pyrazolylbipyridine based biradicals.

Similarly as found in the previous cases for the terpyridine and bispyrazolylpyridine biradical systems, in the nitronyl nitroxide biradical **33** the ground state is the triplet with $\Delta E_{ST} = 2J/k_B$ of $13.3 \pm 4.9 \text{ cm}^{-1}$ ($19.0 \text{ K} \pm 7.0$) while in the imino nitroxide **34**, the smaller range of $-0.07 \text{ cm}^{-1} \leq \Delta E_{ST} \leq 0.7 \text{ cm}^{-1}$ has been obtained. These results are shown in Figure 4.28 with the related Curie and Bleaney-Bowers fitting. We might conclude that the nitronyl nitroxide biradicals in the π -conjugated coupling unit series posses stronger exchange interaction with respect to the imino nitroxide systems.

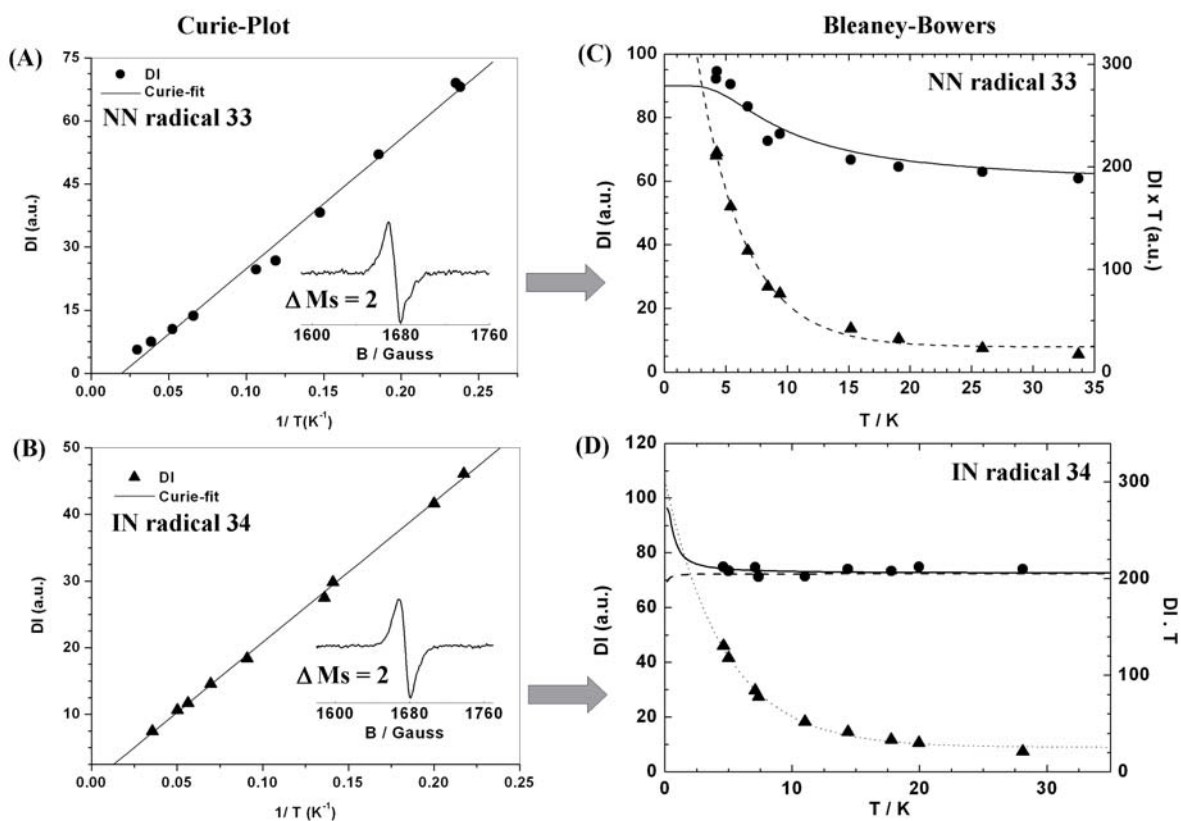


Figure 4.27: Curie-Plot for the bispyridylpyrazolyl biradical systems: **(A)** nitronyl nitroxide **34** and **(B)** imino nitroxide **35** recorded in diluted (10^{-3} M) toluene solutions. DI represents the double integrated signal intensity of the half-field transition. The small insets in **(A)** and **(B)** illustrate the observed half-field transition recorded at 4.2 and 4.6 K respectively. **(C)** and **(D)** show the DI.T vs T plot; the best fitting according to the Bleaney-Bowers equation are depicted in **(C)** as bold line (S=1), and in **(D)** bold line for S=1 and dashed line for S=0. The constraint equations used for the fitting in **(D)** correspond to the equations (32) and (33) with parameters given in the text.

4.8.4. The σ - conjugated biradicals.

The introduction of two σ bonds between the coupling unit and radical moieties in the NN biradical **41** (dipyrazolyldimethylpyridine) severely destabilizes the triplet state, with an upper limit for the singlet-triplet gap $\Delta E_{ST} = 2J/k_b$ of $2.8 \pm 0.8 \text{ cm}^{-1}$ (assuming triplet ground state). This is shown in the fitting of the DI.T data in Figure 4.29. Again, if the singlet ground state is considered, such gap has the size estimated from the solution EPR studies of $\sim -0.06 \text{ cm}^{-1}$. Judging from the data trend, still the triplet seems the ground state in **41**. However, in the imino nitroxide biradical **42**, most likely the singlet or its close degeneracy with the triplet is present.

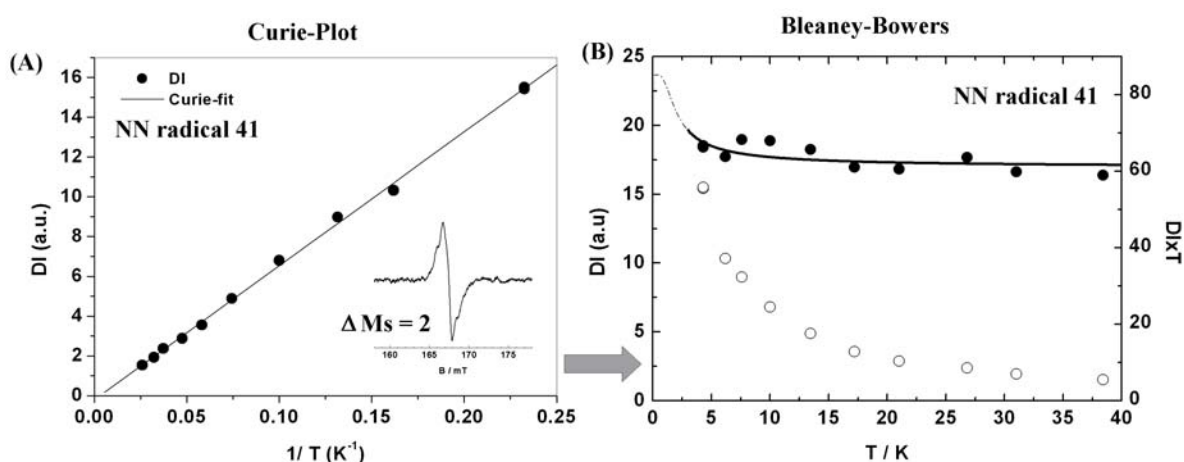


Figure 4.29: (A) Curie and (B) Bleaney-Bowers Plot for the bispyrazolyldimethyl-pyridine (NN) biradical **41** (10^{-3} M in toluene). DI represents the double integrated signal intensity of the half-field transition. The small inset in (A) shows the half-field transition recorded at 4.1 K and the solid lines the best fitting according to the Bleaney-Bowers equation with parameters given in the text.

4.9. Conclusion.

The detailed studies of nitronyl and imino nitroxide biradicals are scarce, fragmented and often contradictory to each other, as compared with the much more studied carbene, nitrene and nitroxide systems. Furthermore, in the plethora of the biradical derivatives found in literature, the unambiguous characterisation of the magnetic ground-states for the magnetically isolated molecule are, surprisingly, rarely treated, although such knowledge should constitute the essential prerequisite prior their use in extended magnetic structures. In this perspective, the literature available in the field makes very hard to compare the results obtained by different groups, since, very often, the experimental details and the procedures used for assessing the magnetic properties are not exhaustively reported. In this chapter much effort was thus devoted in presenting a comprehensive and detailed EPR analyses for

both the nitronyl and imino nitroxide mono- and biradical entities. We provided the necessary step-by-step methodologies for assessing the range of conditions in which the properties of the molecules were unambiguously analysed (radical purities, concentration range, presence or absence of solvent effects, radical stabilities, saturation trends), and then we clearly defined the ground spin state and the relative size of the exchange interactions for the biradical cases. In order to put this work into perspective, and to compare the results obtained with those available in literature, the following points need to be recollected.

- 1) In general, as discussed in Chapter 1, two unpaired electrons linked by *m*-phenylene bridge should afford triplet ground state ($S=1$).
- 2) However, heteroatomic substitution in the coupling unit core, like in pyridines, the presence of non alternant and competitive pathways for the spin polarization, like in the pyrazoles, the molecular conformations and the presence of substituents on coupling unit core, would affect strongly the ground spin state and the spin densities distribution in the molecule. This in turn would influence not only the size of the exchange term J but also its sign. Consequently the preference for $S=1$ state is not guaranteed.

The effect of the heteroatomic substitution in the coupling unit core is documented in literature by doubtful results. This is shown, as one example, by comparing the very simple biradical **a** (benzene core) versus **b** (pyridine core) and **c**, all reported in Figure 4.30.

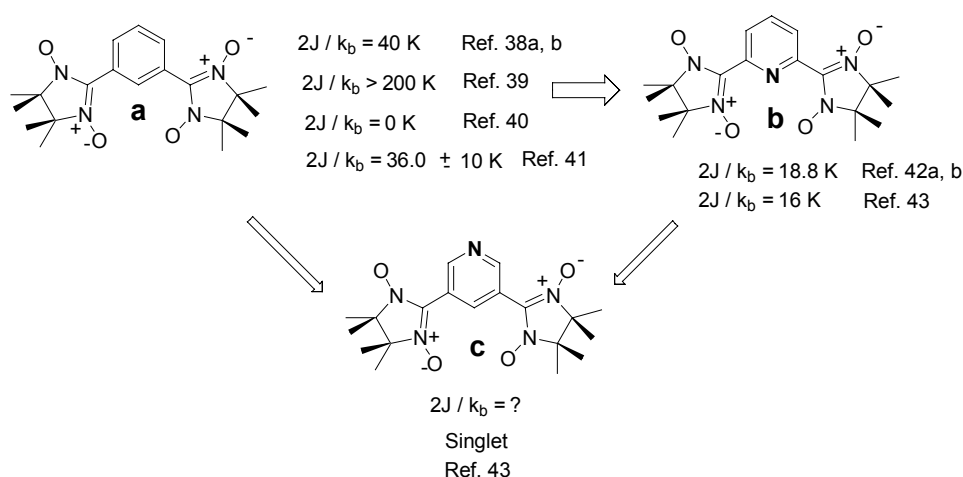


Figure 4.30: The estimated singlet-triplet energy gap (ΔE_{ST}) in a serie of NN biradical systems based on benzene (**a**), 2,6 pyridine (**b**), and 3,5- pyridine (**c**).

The reader can recognize that even for **a**, in which the isophthalaldehyde as key-radical precursor is commercially available, and therefore does not require much synthetic effort to access to large quantities for the radical system, at least four very different estimations of the

intramolecular exchange interaction J have been provided over the years (ranging from 0 up to $> 200\text{K}$) [38 - 41]. They were usually obtained by susceptibility measurements on powder samples. In only one reference [41] the EPR technique was applied in parallel with the magnetic susceptibility in the bulk, in order to evaluate and compare the strength of the through-bond interaction, J , with these two different techniques. The result reported in Figure 4.30 ($2J / k_b = 36 \pm 10\text{ K}$) was obtained from the low temperature EPR studies, and judged as the best estimation for the intramolecular interaction between the radical moieties. Nevertheless several doubts about the purity of the sample examined remain, especially if we consider that no EPR spectra in frozen solution were provided, together with the knowledge of the sample concentrations. Those are both crucial points that need to be documented. The intramolecular exchange interaction can only be probed in dilute solution ($\leq 8 * 10^{-3}\text{ M}$), and when no specific interactions with the solvent molecules are present. In concentrated phases, dipolar through space interactions among paramagnetic molecules are active, and therefore one would still analyse the cooperative effects coming from both inter- and intramolecular interactions. Also the sample purities needs to be specified, since as we emphasized in this chapter, monoradical impurities on biradical samples can be easily assessed by using the EPR technique. From the data reported in Figure 4.30, and supposing that **a** and **b** might adopt similar molecular conformation, one would conclude that the pyridine ring hamper the propagation of the spin-polarization induced by the two radical systems through the coupler, although J still is kept ferromagnetic in **b**. In contrast with this assessment, we showed indeed that non “zero-spin-densities” are delocalised from the radical moiety (NN) into either the pyridine ring (see EPR analyses of monoradical NN **8**) or even in the pyrazole (see EPR analyses of monoradical NN **37**). This is also in agreement with similar findings envisaged from other referenced data (Figure 4.4). More surprising are the results obtained for biradical **c** in which the ground spin-state is stated to be reversed [43], but no information about the magnitude of J was ever provided. In the section 4.2.2, we clearly showed that the spin concentration, once a suitable spin-standard is employed, combined with the EPR simulation in solution for the biradical envelope, can undoubtedly provide at least the upper and lower limit for the singlet-triplet energy gap. Very few examples of biradical systems attached on pyridine units are known, and are therein provided. These structures are collected in Figure 4.31. In all these biradicals systems (see structures from **d** to **i**) no significant intramolecular interactions were found by the authors. No $\Delta M_s = 1$ transition envelopes were ever reported, no estimation of the zero-field splitting terms, D and E , were ever made, nor any $\Delta M_s = 2$ transition were observed. From the literature results it appeared that a tremendous attenuation of the spin polarization effect is observed when a second or a third pyridine ring is present. However, it should be noted that for all of these NN pyridine derivatives, due to their topological design, the low spin ground states are expected. All the values reported in Figure

4.31 correspond to the Weiss (Φ) constant, accounting for only weak intermolecular antiferromagnetic interaction, although in the case of **g** the authors estimated a very crude through-bond interaction ~ -10 K. However, it is not understandable why no similar estimation was provided in **e**, which clearly should features in principle larger interaction, at least due to the shorter through-space radical distances.

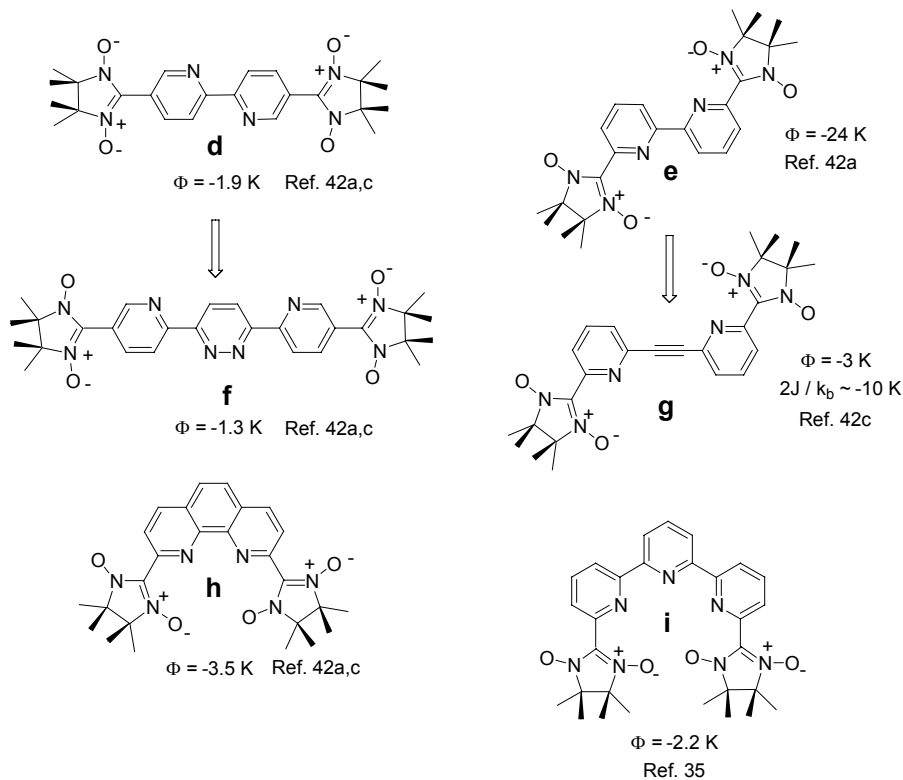


Figure 4.31: Some of the known π -conjugated NN biradical derivatives based on pyridine units, with their calculated intermolecular through-space interactions (Φ).

The molecule **i** represented the only other known example of NN biradical in the terpyridine system. The intramolecular interactions between the radical moieties was excluded, but it exhibited only weak intermolecular and antiferromagnetic contributions in the bulk with $\Phi = -2.2$ K [45]. These analyses of the electronic and magnetic properties, did not allow us to clearly compare our findings with such reference data. In all the new biradical systems reported in this work, we provided either the zero-field splitting parameters and always, although weak, the forbidden half-field transitions were observed. Our terpyridine NN system **12** showed in contrast with **i** a fairly large ferromagnetic through-bond interaction ($2J / k_b \sim 22$ K), that was decreasing in the IN system **13** ($2J / k_b \sim 12.5$ K). For that reason, not only the through-bond interactions between the radical units were present, could be observed and clearly defined, but they were really large compared with those, for example, estimated in **a** and **b** (see Figure 4.30), where there is only one aromatic ring connecting the radical units. Our results accounted for a very efficient propagation of the spin polarization through the coupler, besides theoretical predictions, and therefore those would constitute unprecedented

findings. Our clear attribution of the electronic ground-state made it possible to visualize the variation of the ΔE_{ST} in the π -conjugated systems **12**, **13**, **26**, **28**, **33** and **34** (see Figure 4.32). This illustrates experimentally the weight of the five-member (pyrazole) ring in slightly hampering but unexpectedly not quenching the through-bond exchange interaction, due to the

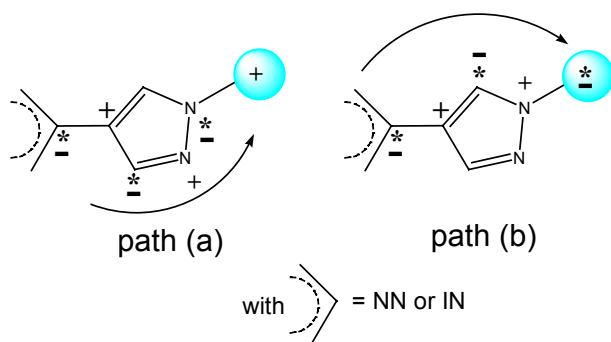
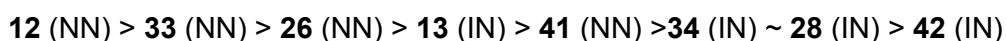


Figure 4.32

presence of two different pathways for the spin-polarization (Figure 4.32).

Under the assumption that in the imino nitroxide biradicals the coupling unit core would be as planar as those observed in the X-ray structures of **12**, **26** and **34** (all nitronyl nitroxides, NN, see Chapter 5), no dominant geometrical factors seemed responsible for modulating the observed different singlet-triplet stabilities.

Noteworthy, the averaged intramolecular radical distances in the terpyridine systems **12** and **13** are larger than in **26**, **28**, **33** and **34** (see Table 4.3) being accompanied with small *zfs*. However, their exchange couplings are the strongest one. Even though in **41** a decrease in the magnitude of *J* is expected, overall the trends in *J* experimentally obtained would be hard to acquire quantitatively by other means (e.g. with the aid of theoretical predictions). Therefore the following efficiency in the coupling unit series could be drawn, according to the radical type and size of *J* estimated.



One note of criticism we might furthermore add, upon comparison with the other class of relatively stable and much more studied nitroxide radical systems [45]: the very common assumption [44] that the nitronyl nitroxide should exhibit much weaker coupling with respect to the nitroxide moiety (Figure 4.33), need to be reconsidered in view of these recent findings.

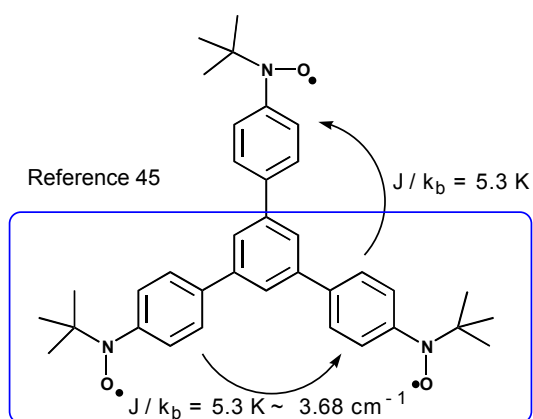


Figure 4.33

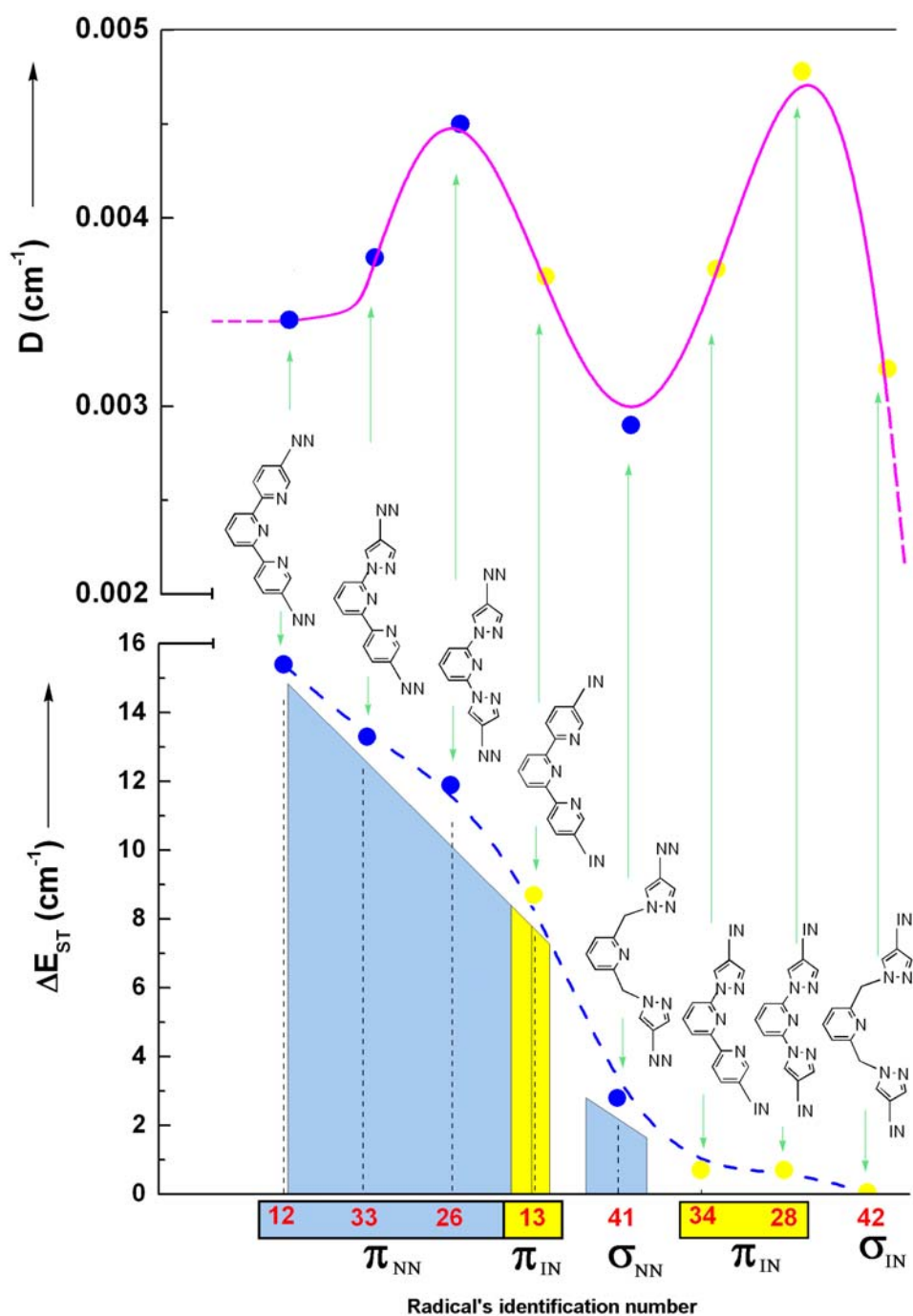


Figure 4.32: Comparison among the observed zfs (D , upper figure) with the singlet-triplet energy gap ($\Delta E_{ST} = 2J/k_b$, lower figure,) in the synthesized biradical systems.

References

- [1] (a) Gerson F., Huber W., *Electron Spin Resonance Spectroscopy of Organic Radicals*, 2004, Wiley-VCH. (b) Barth U., Hedin L., "A Local Exchange –correlation Potential for Spin Polarized case: I". *J. Phys. C: Solid State Phys.*, 5, **1972**, 1629. (c) Gerson, F. and Huber, W., *Electron Spin Resonance spectroscopy of Organic Radicals*, Wiley-VCH, 2003.(d) Bales, B.L.; Peric, M.; Dragutan, I., *J. Phys. Chem. A*, 107, **2003**, 9086.
- [2] (a) Catala L., Feher R., Amabilino D.B., Wurst K., Veciana J., *Polyhedron*, 20, **2001**, 1563. (b) Vasilevsky S.F., Tretyakov E.V., Usov O.M., Molin Y. N., Fokin S.V., Shwedenkov Y.G., Ikorskii V.N., Romanenko V.G., Sagdeev R.Z., Ovcharenko V.I., *Mendeleev Commun.*, **1998**, 216. (c) Cirujeda J., Hernández-Gasiò E., Rovira C., Stanger J-L., Turek P., Veciana J., *J. Mat. Chem.*, 5, **1995**, 243. (d) Nagashima H., Inoue H., Yoshioka N., *Polyhedron*, 22, **2003**, 1823. (e) Takui T., Miura Y., Inui K., Teki Y., Makoto I., Ito H K., *Mol. Cryst. Liq. Cryst.*, 271, **1995**, 55. (f) Davis M.S., Morokuma K., Kreilick R.W., *J. Am. Chem. Soc.* 94, **1972**, 5588. See also "Electron Carbon Couplings of Aryl Nitronyl Nitroxide Radicals" Neely J.W., Hatch G.F., Kreilick R.W., *J. Am. Chem. Soc.*, 96, **1974**, 652.
- [3] Heisenberg W., *Z. Phys.*, 49, **1928**, 168.
- [4] Dirac P.A.M., *The principles of Quantum Mechanics*, 3rd Ed., Clarendon, Oxford.
- [5] Anderson P.W., *Solid State Phys.*, 14, **1963**, 99.
- [6] (a) Löwdin P.O., *Phys. Rev.* 97, **1955**, 1509. (b) *Rev. Mod. Phys.* 34, **1962**, 80.
- [7] (a) Nesbet R. K., *Ann. Phys. (Leipzig)* 3, 1958, 397. (b) Nesbet R. K., *Ann. Phys. (Leipzig)*, 4, 1958, 87. (c) Nesbet R. K., *Phys. Rev.* 122, **1961**, 1497. (d) Nesbet R. K., *Phys. Rev.* 135, **1964**, A460.
- [8] Hay P.J., Thibeault J.C., Hoffmann R. *J. Am. Chem. Soc.*, 97, **1975**, 4884.
- [9] (a) Kahn O., Briat B., *J. Chem. Soc. Faraday Trans.*, 72, **1976**, 268. (b) Kahn O. *Molecular Magnetism*, Wiley-VCH, New York, **1993**, Chapter 8.
- [10] Noodleman L., *J. Chem. Phys.*, 74, **1981**, 5737.
- [11] Noodleman L., Davidson E.R., *Chem. Phys.*, 109, **1986**, 131.
- [12] Schleyer P.V., Allinger N.L., Clark T., Gasteiger J. Kollman P.A., Schaefer H.F. III, Schreiner P.R. (Eds.) *Encyclopedia of Computational Chemistry*, **1998**, Wiley, Chichester.
- [13] Bauschlicher C.W. Jr., Langhoff S.R., Taylor P.R., *Adv. Chem. Phys.* 77, **1990**, 103.
- [14] Roos B.O. (Ed.), *Lecture Notes in Quantum Chemistry; Lecture Notes in Chemistry*, Vols 58 and 59, **1992**, Springer, Berlin-Heidelberg, New York.
- [15] Parr R.J., Yang W., *Density Functional Theory of atoms and Molecules*, **1989**, Oxford University Press, New York.
- [16] Dreizler R.M., Gross E.K.U., *Density Functional Theory: An approach to the Quantum Many Body Problem*, **1990**, Springer, Berlin Heidelberg New York.

- [17] (a) Seminario J.M., Politzer P. (Eds), *Modern Density Functional Theory: a tool for chemistry*, Vol.2, **1995**, Elsevier, Amsterdam. (b) Illas F. and Martin R., *J. Chem. Phys.*, **7**, **2001**, 2887.
- [18] Illas F., Moreira I. de P.R., Graaf de C., Barone V., Magnetic Coupling in Biradicals, Binuclear Complexes and wide-gap insulator: a survey of ab initio wave function and density functional theory approaches, *Theor. Chem. Acc.*, **104**, 2000, 265.
- [19] White R.M. *Quantum Theory of Magnetism. Springer Series in Solid-State Sciences*, Vol 32, **1983**, Springer, Berlin Heidelberg New York.
- [20] O. Kahn, *Magnetism: A Supramolecular Function*, Eds., Kluwer, Dordrecht, **1996**.
- [21] Casper W.J. *Spin Systems*, **1989**, World Scientific, Singapore.
- [22] (a) Yoshida K, *Theory of Magnetism*, **1998**, Springer, Berlin Heidelberg New York. (b) J. E. Wertz, J. R. Bolton, *Electron Spin Resonance, Elementary Theory and Practical Applications*, **1986**, Chapman & Hall. (c) Mabbs F.E., Collins D., *Electron Paramagnetic resonance of Transition Metal Compounds*, Elsevier, **1992**. (d) De Groot, M.S. and van der Waals J. H., *Physica*, **29**, **1963**, 1128. (e) Grivet, J. –Ph. and Mispelter J., *Mol. Phys.* **27**, **1974**, 15.
- [23] McConnell H. M., *J. Chem. Phys.* **33**, **1960**, pp.115-121.
- [24] McLachlan A. D. in “Self-consistent field theory of the electron spin distribution in π -electron radicals” *Mol.Phys.* **3**, **1960**, pp.233-252.
- [25] (a) Salem L., *The molecular orbital theory of conjugated systems*, Benjamin, New York, NY, 1965. (b) J. E. Wertz, J. R. Bolton, *Electron Spin Resonance, Elementary Theory and Practical Applications*, **1986**, Chapman & Hall, p.254.
- [26] (a) Fang S., M-S. Lee, Hrovat D.A., Borden W.T., *J. Am. Chem. Soc.*, **117**, **1995**, 6727. (b) Chiarelli R., Gambarelli S., Rassat A. “Exchange interactions in nitroxide biradicals”, *Mol.Cryst. Liq. Cryst.*, **305**, **1997**, 455.
- [27] Kobori Y., Takeda K., Tsuji K., Kawai A., Obi K., *J. Phys. Chem. A*, **102**, **1998**, 5160 (in particular page 5166) and references cited therein.
- [28] (a) Anderson P.W., *Phys. Rev.*, **115**, **1959**, pp.2-13. (b) J. E. Wertz, J. R. Bolton, *Electron Spin Resonance, Elementary Theory and Practical Applications*, **1986**, Chapman & Hall, pp153-154.
- [29] Bales L.B., Peric M., Dragutan I., *J. Phys. Chem. A*, **107**, **2003**, 9086.
- [30] Kanaya T., Shiomi D., Sato K., Takui T., *Polyhedron*, **20**, **2001**, 1397.
- [31] Tretyakov E.V., Samoilova R.I., Ivanov Y.V., Plyusnin V.F., Pashchenko S.V., Vasilevsky S.F., *Mendeleev Commun.*, **1999**, 92.
- [32] (a) M. Tinkham, M. W. P. Strandberg, *Phys. Rev.* **1966**, **97**, 937. (b) K. Mukai, T. Tamaki, *Bull. Chem. Soc. Jpn.* **1977**, **50**, 1239.
- [33] E. F. Ullman, J. H. Osiecki, D.G.B.Boocock, *J. Am. Chem. Soc.* **1972**, **94**, 7049.

- [34] (a) B. Bleaney, K. Bowers, *Proc. R. Soc. London* **1952**, A214, 451. (b) Mukai K., Tamaki T., *Bull Chem. Soc. Jpn.*, **50**, **1977**, 1239. (c) Mukai K., Sakamoto J., *J. Chem. Phys.*, **68**, **1978**, 1432.
- [35] C. Stroh, R. Ziessel, *Tetrahedron Lett.* **40**, **1999**, 4543.
- [36] Portis A.M. *Phys. Rev.* **91**, **1953**, 1071-1078.
- [37] Castner T.J. Jr. *Phys. Rev.* **115**, **1959**, 1506-1515.
- [38] (a) Hase S., Shiomi D., Sato K., Takui T., *J Mat. Chem.* **11**, **2001**, 756. (b) Izuoka A., Fukada M., Sugawara T., *Mol. Cryst. Liq. Cryst.*, **232**, **1993**, 103.
- [39] Shiomi D., Tamura M., Sawa H., Kato R., Kinoshita M., *J. Phys. Soc. Jpn.*, **62**, **1993**, 289.
- [40] Caneschi A., David L., Gatteschi D., Sessoli R., *Inorg. Chem.*, **32**, **1993**, 1445.
- [41] Catala L., LeMoigne J., Kyritsakas N., Rey P., Novoa J. J., Turek P., *Chem. Eur. J.*, **7**, **2001**, 2466.
- [42] (a) Ziessel R., Ulrich G., lawson R.C., Echegoyen L., *J. Mat. Chem.*, **9**, **1999**, 1435. (b) Ulrich G., Ziessel R., *Tetrahedron Lett.*, **35**, 1994, 1215. (c) Romero F. M., Ziessel R., *Tetrahedron Lett.*, **40**, **1999**, 1895. see also the short review R. Ziessel, *Mol. Cryst. Liq. Cryst.*, **273**, **1995**, 101.
- [43] Shiomi D., Ito K., Nishizawa M., sato K., takui T., Itoh K., *Synthetic Metals*, **103**, **1999**, 2271.
- [44] (a) Joe A. Crayston, John N. Devine and John C. Walton, Conceptual and Synthetic Strategies for the Preparation of Organic Magnets, *Tetrahedron*, **56**, **40**, **2000**, 7829. (b) Nakatsuji S., Kiroyuki A., *J. Mat. Chem.* **7**, **1997**, 2161.
- [45] Kanno F., Inoue K., Koga N., Iwamura H., *J. Phys. Chem.*, **97**, **1993**, 13267. For other examples of nitroxides biradicals see also: Matsumoto T., Ishida T., Koga N., Iwamura H., *J. Am. Chem. Soc.*, **114**, **1992**, 9952.

Chapter 5 – Crystal Structures of the Radicals

Experimentally the mechanism of through-bond spin coupling can be elucidated only by understanding the phenomenological relationships among spin delocalisation, spin polarisation, molecular conformations, radical separation distances, and hetero-ring substitutions. The spin delocalization/polarization effects and the studies of molecular conformations in solution for all the radicals synthesized have been discussed in details in Chapter 4. In this chapter the central point is devoted to the analyses of the structural factors that characterize three nitronyl nitroxide biradicals (namely **12**, **26** and **33**). It is also reported the structure of the nitronyl nitroxide monoradical **8** since it disclosed in the EPR solution studies (Chapter 4) evidence of spin polarization from the radical moiety to the protons of the neighbour pyridine ring. Regardless of several attempts, unfortunately, no suitable crystals for **41** and all the correspondent imino nitroxides were obtained. The three systems **12**, **26** and **33** shared nearly planar arrangements of the coupling-core. Rather small torsions between the imidazolyl and the pyridyl/pyrazolyl rings were observed. Therefore the geometrical prerequisites to enable excellent conjugation between the radical moieties through the coupler were ensured. Such structural findings further enhance the potential advantages that similar hetero-ring cores present with respect to those based on phenylene moieties, since the larger torsions between adjacent benzene rings ($> 30^\circ$) in turn would induce far less efficient radical conjugation.

5.1. The crystal structure of **12** and the supramolecular π -stacking chain formation.

Crystals with the $P2_1/c$ (No. 14) symmetry for the nitronyl nitroxide biradical based on terpyridine **12** were grown in a solution of acetone upon slow diffusion of hexane at 4°C within few days. The structure is shown in Figure 5.1. Details of the structural refinements are given in Table 1 at the end of this chapter. The torsional angles ϕ_1 , ϕ_2 , ϕ_3 , and ϕ_4 are meaningful parameters for the transmission of effective π -conjugation between the two spin carriers through the spacer, because very strong torsions would hamper or even cancel the conjugation effect through the coupler. The ϕ_1 angle (N5-C18-C5-C4) is $\sim -0.7^\circ$ and the ϕ_2 angle (N2-C6-C1-C2) is -4.0° thus the overall terpyridine backbone is fairly planar. The torsional angle ϕ_3 between the imidazolyl and one of the pyridyl-moiety (N6-C23-C21-C20) is $\sim -30.1^\circ$; this large torsion arises from the interaction between the imidazolyl oxygen O3 involved in hydrogen bonding with one of the two water molecules (O11) found in the crystals. Similarly, the ϕ_4 angle (N3-C11-C9-C8) follows the same trend, with 31.9° , since again the O1 oxygen interacts *via* hydrogen bonding with the second water molecule O12.

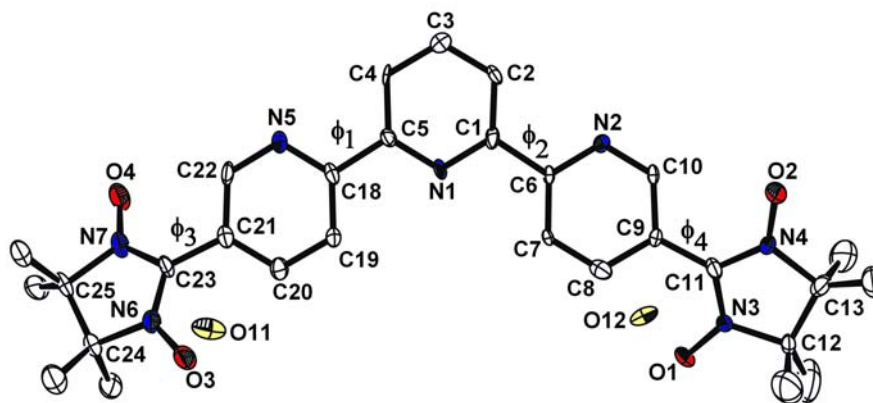


Figure 5.1. Crystal structure of **12** with ORTEP drawn at the 50% of probability level. The hydrogen atoms have been omitted for clarity.

The intraring-torsional angles of the imidazolyl rings are $\sim -19.3^\circ$ (C23-N7-C25-C24), -19.1° (C23-N6-C24-C25), -13.7° (C11-N4-C13-C12), and -14.8° (C11-N3-C12-C13). The intramolecular (O3-O1) distance between the oxygens is 11.24 Å. The intramolecular distances between the two ONĈNO groups (C23-C11) is $d = 12.11$ Å, while that between the pyridyl carbons (C9-C21) is $d = 9.52$ Å. Two of the N-O bond distances, are slightly longer than the others, and those in fact are associated with hydrogen bonding between the radical oxygen and the water molecules (N3-O1, $d = 1.29$ Å and N6-O3, $d = 1.29$ Å), while the other two have $d = 1.26$ Å (N7-O4) and $d = 1.28$ Å (N4-O2). The crystal packing of **12** is shown in Figure 5.2. The stacking among the terpyridine moieties is gated by these two bridging water molecules, allowing the formation of an infinite chain with 180° rotated units in top to each other. The Figure 5.3 shows a section of the chain (trimer A-B-C) where the nitrogen of the pyridine **A** (N5) is connected with the water molecules O12 ($d_{\text{N5-O12}} = 2.92$ Å) and hydrogen bonded with the radical oxygen (O1) of the molecule **B** ($d_{\text{O12-O2}} = 2.92$ Å). Then, the nitrogen of the pyridine **B** (N2) is connected with the water molecules O11 ($d_{\text{N2-O11}} = 2.93$ Å) and hydrogen bonded with

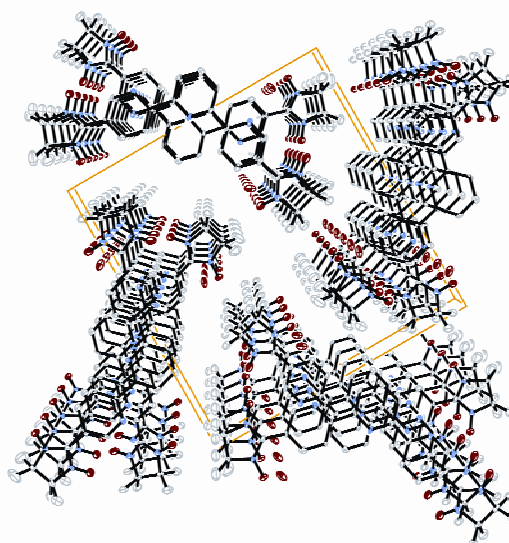


Figure 5.2. ORTEP sketch for the crystal packing of **12** (nitrogen ●, oxygen ●, carbon ●). The unit cell is depicted as thin yellow solid line.

the radical oxygen (O3) of the molecule **C** ($d_{O11-O3} = 2.82 \text{ \AA}$). This allows a stacking motif with distances C6(A)-C18(B) of 3.28 \AA and C18(B)-C6(C) of 3.29 \AA as repeating unit for the chain.

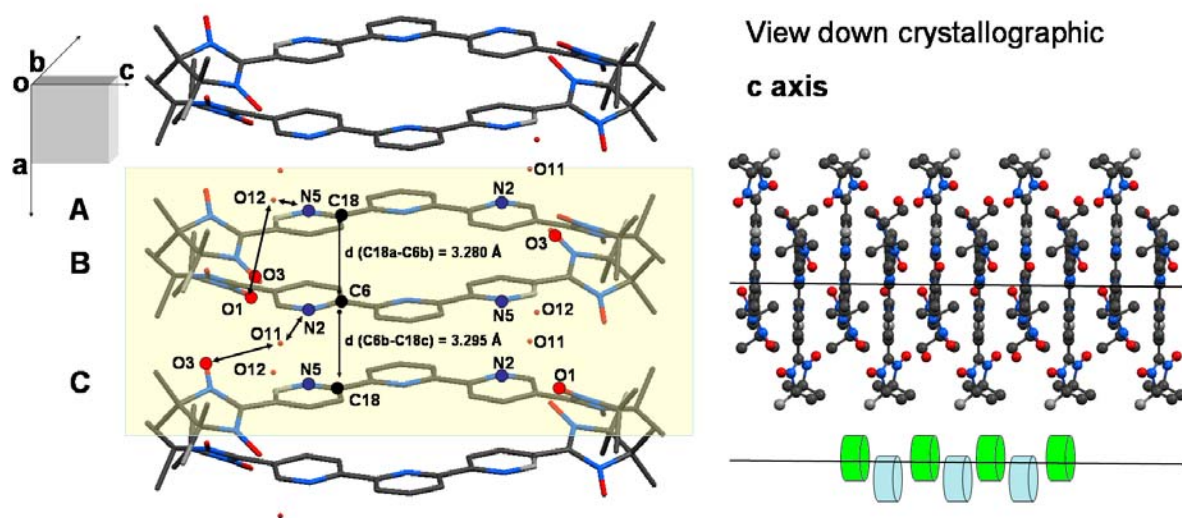


Figure 5.3. Capped stick sketch of the molecular packing in **12** with a perspective of the chain section.

Such appealing supramolecular organisation found in **12** gave an unprecedented model for probing the bulk magnetic properties of the material. The static magnetic susceptibility was therefore measured down to cryogenic temperature with a Faraday balance. This experiment was performed by Dr. K. Falk (Prof. W. Haase Group, TU Darmstadt). As shown in the Figure 5.4, the effective magnetic moment is $2.37\mu_B$ hence slightly smaller than the expected $2.43\mu_B$ for two uncorrelated spins. This value appears almost constant down to 50 K. Then below 20 K the magnetic moment decreases. Nevertheless a small increase is observed in the range 40-20 K, which is consistent with the intramolecular singlet-triplet gap of $15.4 \pm 2.0 \text{ cm}^{-1}$ obtained from the EPR studies. Presumably, the sharp decrease of μ_{eff} below 20 K arises from dominating inter-chain antiferromagnetic interactions; however the full evaluation of these data is still under examinations. This is due to the large numbers of intermolecular interactions (J_{inter} , see Figure 5.5), and a suitable model for their parameterization has not been developed yet. This observation underlines once more the better suitability of the EPR technique for evaluating at least the through-bond exchange interaction, because by working with magnetically dilute samples, it allows minimizing intermolecular contributions. Although **12** did not show bulk ferromagnetic properties, still it represents a unique example in the terpyridine family, where only rather strong antiferromagnetic interactions in the bulk are found, with negligible through-bond interaction, as observed for the other one example reported so far in literature (see Figure 5.4 B).

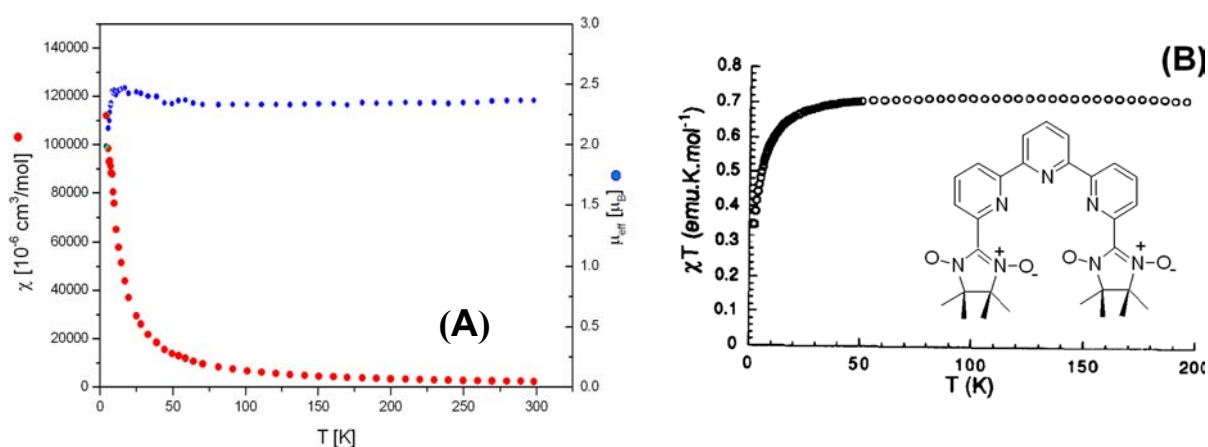


Figure 5.4. (A) The static magnetic susceptibility χ (red circles, ●) and the effective magnetic moment μ_{eff} (blue circles, ●) for the π -stacking of the polycrystalline biradical **12** showing the dominant contribution arising from the weak intermolecular antiferromagnetic interactions below $T = 20$ K. (B) The product $\chi \cdot T$ (open circles, ○) in the other known NN biradical based on the terpyridine system, measured on polycrystalline powder (taken from Stroh C., R. Ziessel, *Tetrahedron Lett.*, 40, **1999**, 4543.)

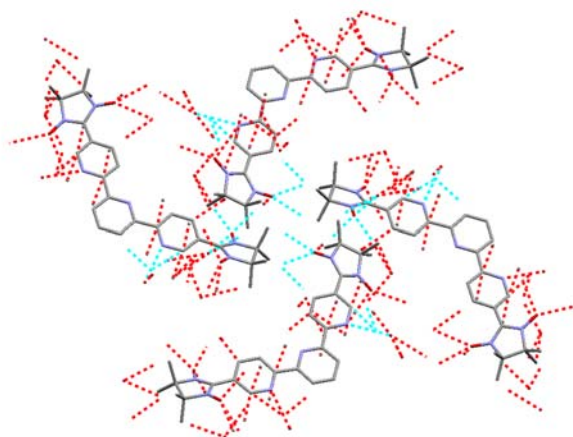


Figure 5.5. Perspective of the short (< 3.5 Å) magnetic contacts (red dotted lines) and the H-bonding (light blue dotted lines) found in the crystals of **12**.

5.2. The crystal structure of **26** and the zig-zag chain formation.

Diffusion of hexane into a CHCl_3 solution of radical **26** within 2 days allowed the formation of a blue crystalline material that was structurally characterized by X-ray diffraction (Figure 5.6). Since the molecules are located on a twofold rotation axis ($C2/c$, $N^\circ 15$), the torsional angles ϕ_1 and ϕ_2 are identical for each half-molecule. The ϕ_1 (C6-N2-C1-N1) angle is 4.6° and the torsional angle (C6-N2-N3-C4) is $\sim 0.3^\circ$ thus the two pyrazolyl-rings and the pyridyl central-core are nearly coplanar. The torsional angle ϕ_2 between the imidazolidyl and

pyrazolyl-moiety (N5-C7-C5-C6) falls in very similar range with 4.2° hence, the overall planar structure of **26** (more planar than **12**), satisfies in the crystals the geometrical prerequisite for

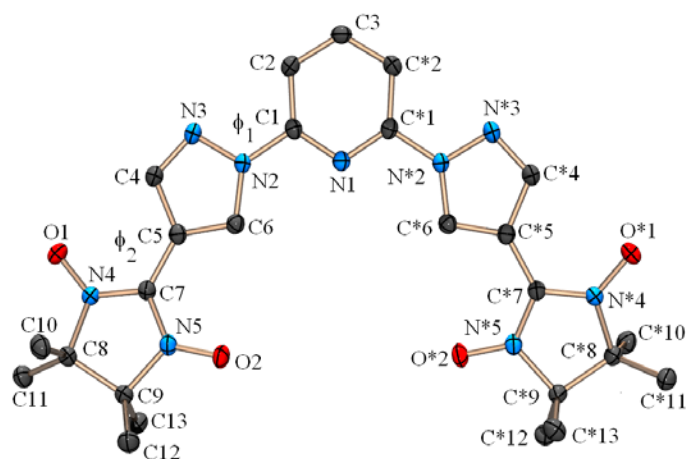


Figure 5.6. Crystal structure of **26** with ORTEP drawn at the 50% of probability level. The hydrogen atoms were omitted for clarity.

effective π -conjugation between the two radical fragments.

The intraring torsion of the imidazolyl rings are respectively -18.9° (C8-C9-N5-C7) and -22.6° (C9-C8-N4-C7). The intramolecular (O2-O*2) and the shortest intermolecular through-space distances between the oxygens are 5.64 Å and 4.74 Å. The intramolecular distances between the two ONĈNO groups (C7-C*7), where most of the radical-spin densities is about are located is about 9.13 Å, while that one

between the pyrazolyl-carbons (C5-C*5) is 7.71 Å. The N-O bond distances are both 1.28 Å for O2-N5 and for O1-N4. The Figure 5.7 shows the zig-zag chain motif found in the crystals, in which the units are rotated by 180° , running along the b-axis. Such motif arises by short electrostatic contacts, (shorter than the sum of the van der Waalls radii minus 0.1 Å) between the imidazolyl-oxygens and the methyl groups of the neighbouring radicals.

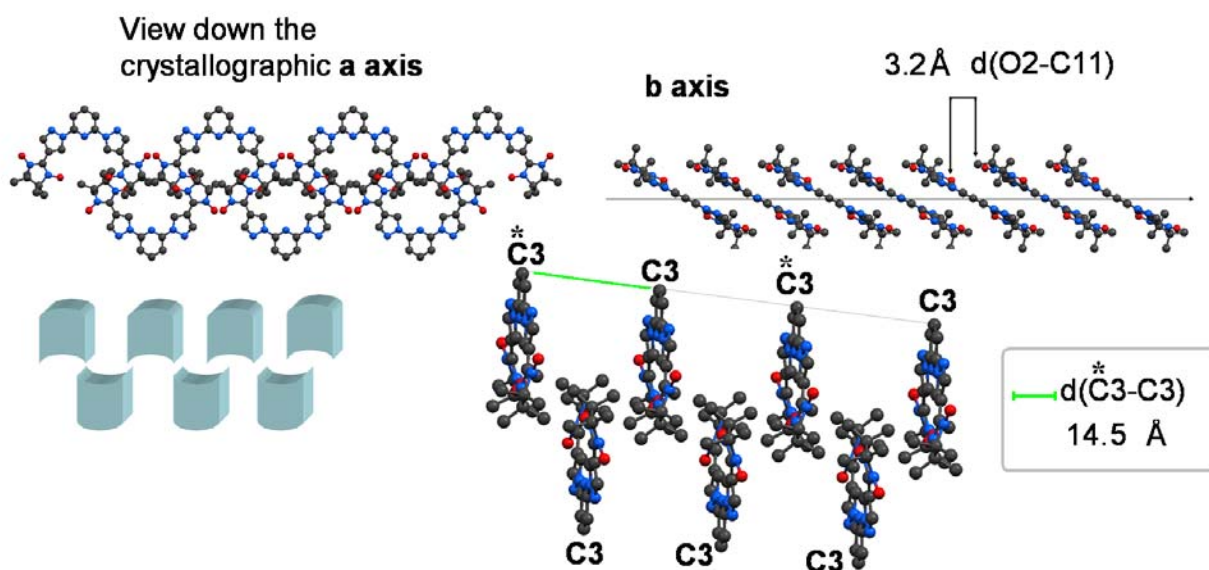


Figure 5.7. The representation of the molecular packing in **26** drawn with ORTEP32.

5.3. The structure of **33** and the dimers formation.

After diffusion of ether into a CHCl_3 solution of the radical **33**, a blue crystalline material was obtained in the $P-1$ (No.2) symmetry. Two molecules for the biradical plus two solvent molecules (CHCl_3) were found per unit cell. In Figure 5.8 is reported the structure of the isolated **33**.

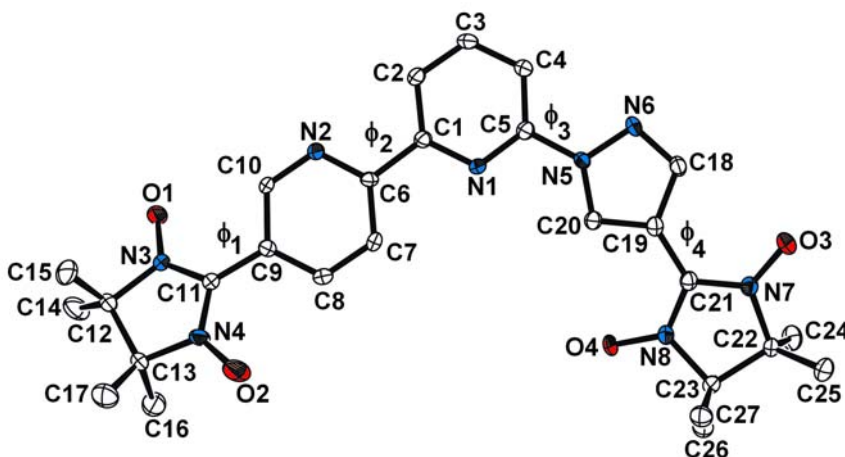


Figure 5.8. Crystal structure of **33** with ORTEP drawn at the 50% of probability level. The hydrogen atoms were omitted for clarity.

The ϕ_2 angle (C10-C9-C11-N3) is $\sim -3.2^\circ$ and the ϕ_3 angle (C20-N5-C5-N1) falls in the similar range (-4.3°), thus the bispyridyl-pyrazolyl rings, are nearly coplanar. The large torsional angle ϕ_1 between the imidazolyl and pyridyl-moiety (N3-C11-C9-C10) accounts for -27.8° . Similarly, the ϕ_4 angle between imidazolyl and pyrazolyl residue (N7-C21-C19-C18) is -14° . The overall structure of **33** is more planar with respect to **12** but less than **26** (see Figure 5.1 and 5.6). The intraring torsional angles of the imidazolyl rings are -8.4° (N7-C21-N8-C23), -21.9° (C21-N7-C22-C23), $\sim -8.3^\circ$ (N4-C11-N3-C12), and 16.7° (C11-N4-C13-C12). The presence of two solvent molecules allows the formation of dimeric structures (Figure 5.7) with units rotated 180° in top of each other. This feature is similar to those observed in the radicals **12** and **26**.

The intramolecular (O4-O2) and the shortest intermolecular through-space distances between the imidazolyl-oxygens (short magnetic contacts) are respectively 8.5 \AA and 4.3 \AA . The later is associated with the distance between oxygen in the dimer. The intramolecular distances between the two ONCNO groups, where most of the radical-spin densities are located, is $d(\text{C21-C11}) = 10.64 \text{ \AA}$, and that between the pyrazolyl-pyridyl carbons (C9-C19) is $d = 8.64 \text{ \AA}$. The intradimer distance between two ONCNO groups (C21-C11, $d = 4.668 \text{ \AA}$) is indeed far more close (Figure 5.10).

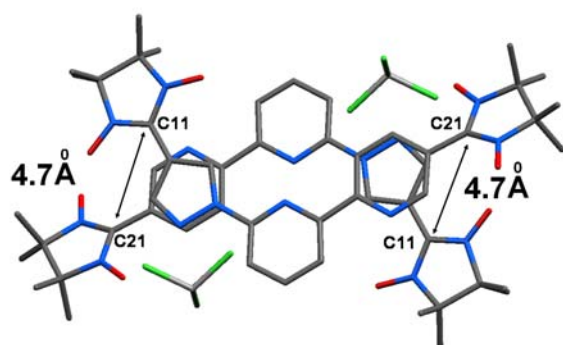


Figure 5.9. The view of the dimeric form of (**33**) found in the crystals. The two CHCl_3 molecules are drawn in green.

The N-O bond distances are 1.27 Å for O2-N4 and 1.29 Å for O4-N8. As previously found in **12**, also for **33** there are short interdimer contacts. Those arise from the interaction between the imidazolyl-oxygens and the methyl groups of the neighbouring radicals as schematically depicted in the Figure 5.10 (B, red lines).

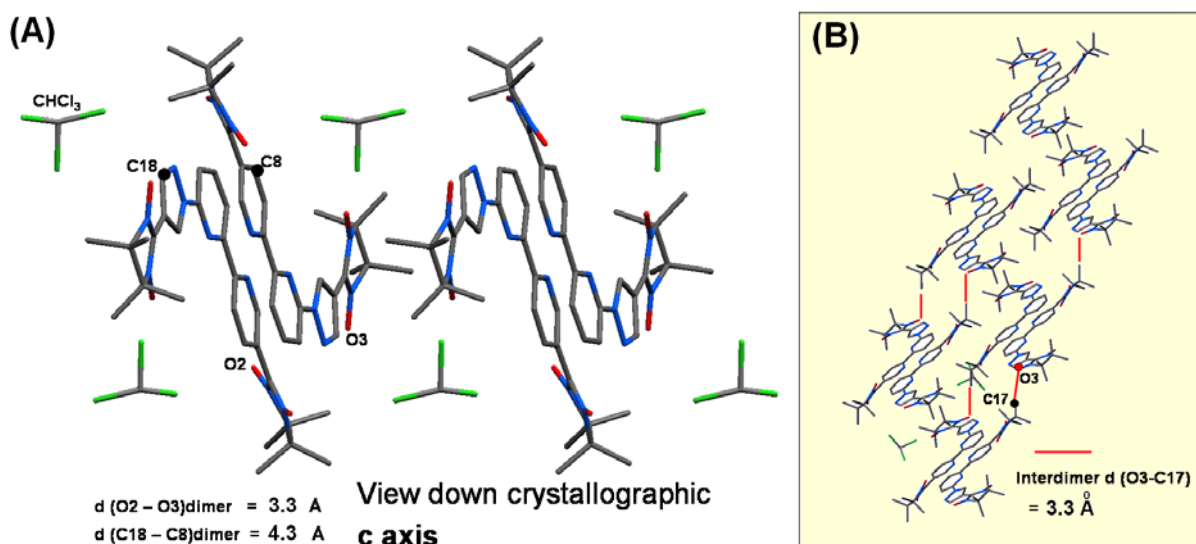


Figure 5.10. The molecular packing of **33**.

5.4. The structure of **8** and the dimers formation.

Suitable crystals for the bipyridine based monoradical **8** were grown in a solution of acetone upon slow diffusion of ether within one day, in the $P-2_1/n$ (No.14) symmetry. Structurally, as shown in Figure 5.11, the two pyridine-rings are nearly coplanar with a torsional angle of -2.80° (N2-C6-C5-C4). However, the torsion between the imidazolyl and the pyridyl ring (N4-C11-C9-C8) is large, accounting for -35.4° . In addition, also the

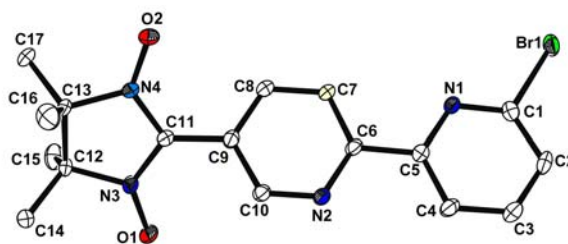


Figure 5.11. Crystal structure of **8** with ORTEP drawn at the 50% of probability level. The hydrogen atoms were omitted for clarity.

intraring torsion for the imidazolyl moiety is large, with $\sim 21.7^\circ$ (N4-C13-C12-N3) and $\sim 5.0^\circ$ (C12-N3-C11-N4). The shortest intermolecular through-space distances between the radical-oxygens (short magnetic contact) is 4.25 Å. The N-O bond distances for N3-O1 and N4-O2 are both 1.28 Å, and no solvent molecules were found to fill the unit cell.

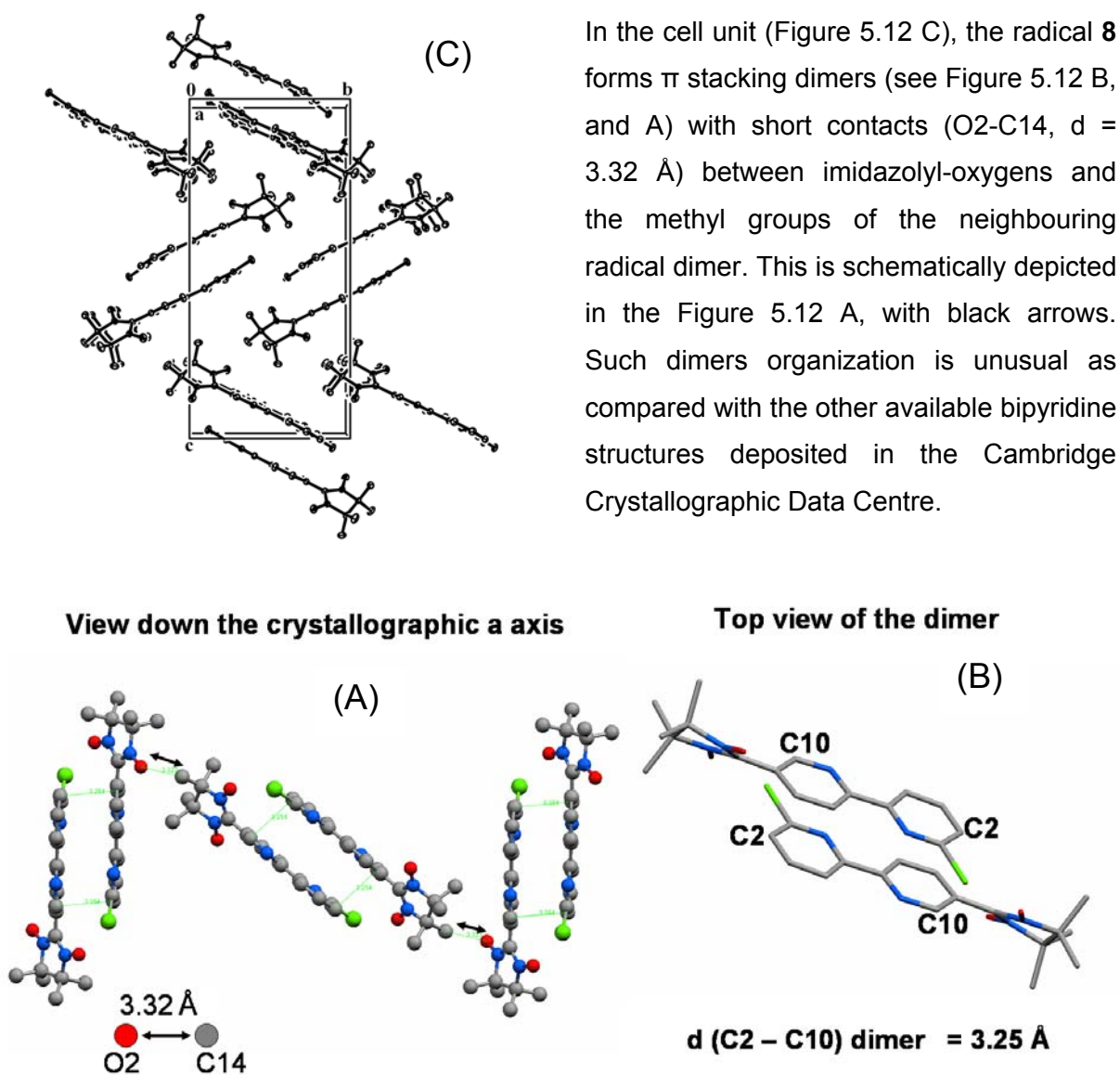


Figure 5.12. (A), (B) and (C) show the molecular packing for the monoradical **8**.

5.5. Conclusion.

In the present chapter the crystal structures of three nitronyl nitroxide biradical systems were presented, together with one example of monoradical. The structural analyses showed that the small torsions between radical moieties and coupling unit core (bispyrazolyl-pyridine, terpyridine and pyrazolyl-bispyridine) favour significant through-bond exchange

interaction, despite the large through-space radical distances. Such arrangement of the molecular units underlined the advantage on using nitrogen-containing heterocycles with respect to the more often used benzene cores. Other than the greater proclivity to adopt planar conformations, these radical systems offer in addition various coordination sites for metal chelation, a further advantage in order to extend the magnetic structures.

Table 5.1. X-ray data: experimental details, structure solutions and refinements.

Compound	12	26	33	8
CCDC number	234179	217301	229003	229004
Formula	C ₂₉ H ₃₇ N ₇ O ₆	C ₂₅ H ₃₁ N ₉ O ₄	C ₂₈ H ₃₃ Cl ₃ N ₈ O ₄	C ₁₇ H ₁₈ BrN ₄ O ₂
Formula Weight <i>M</i>	579.66	521.57	651.98	390.25
Crystal System	Monoclinic	Monoclinic	Triclinic	Monoclinic
Space group	<i>P</i> 2 ₁ / <i>c</i> (N° 14)	<i>C</i> 2/ <i>c</i> (N° 15)	<i>P</i> 1 (N° 2)	<i>P</i> -2 ₁ / <i>n</i> (N° 14)
<i>a</i> (Å)	6.5690	18.5194(7)	11.5796(4)	6.6600(4)
<i>b</i> (Å)	21.5610	9.6934(5)	12.3160(5)	10.9300(5)
<i>c</i> (Å)	20.6620	14.4537(6)	12.7410(5)	23.1570(7)
α (°)	90	90	69.9597(13)	90
β (°)	90.8	103.4960(10)	65.7760(145)	96.3620(13)
γ (°)	90	90	88.9354(12)	90
<i>V</i> (Å ³)	2926.16	2522.92(19)	1540.85(11)	1675.31(14)
<i>Z</i>	4	4	2	4
ρ_{calc} (g×cm ⁻³)	1.316	1.373	1.405	1.547
μ (MoK α) (mm ⁻¹)	0.094	0.085	0.346	2.471
<i>F</i> (000)	1232	548	680	796
Crystal Size (mm)	0.09×0.14×0.42	0.43×0.26×0.18	0.09×0.21×0.38	0.08×0.15×0.41
Colour	Blue	Blue	Blue	Blue
Shape	Prism	Needles	Prism	Needles
Temperature (K)	120	120	120	120
Radiation, λ (Å)	MoK α ,0.71073	MoK α ,0.71073	MoK α ,0.71073	MoK α ,0.71073
θ Min-Max (°)	4.1-27.4	4.1-27.5	4.0-29.0	4.0-29.5
Total data	5870	3057	31506	19655
Unique data	1924	2889	8016	4621
<i>R</i> _{int}	0.060	0.060	0.060	0.000
Observed data	1911	1895	3793	2764
<i>N</i> _{ref}	1911	1895	3793	2764
<i>N</i> _{par}	379	175	388	217
<i>S</i> (GooF)	1.07	1.05	1.07	1.08
^a <i>R</i> ₁	0.0645	0.0385	0.0512	0.0405
^b <i>wR</i> ₂	0.0666	0.0453	0.0571	0.0448

$$^a R_1 = \sum ||F_o| - |F_c|| / \sum |F_o|$$

$$^b wR_2 = \{ \sum w(|F_o| - |F_c|)^2 / \sum w|F_o|^2 \}^{1/2}$$

The **CCDC** code corresponds to the deposition number provided by the Cambridge Crystallographic Data Centre, 12 Union Road, Cambridge CB2 1EZ, UK.

Chapter 6 - Summary and Outlook

Eight novel potential high spin ligands based on terpyridine, bispyrazolylpyridine and pyrazolylbipyridine cores decorated with nitronyl nitroxide (NN) and imino nitroxide (IN) radicals were synthesized, together with four monoradical molecules. The preparation of the radicals involved several types of reactions (bromination, iodination, N- and carbaldehyde protecting groups, Stille coupling, Grignard reaction, etc.) in order to assemble the mono and the bis-carbaldehyde hetero-derivatives as key precursors for the radical systems. Such intermediates were subjected to condensation reaction with 2,3-dimethyl-2,3-bis(hydroxylamino)-butane (generally in dioxane under argon for ~ 7 days), followed by oxidation of the bis-hydroxylimidazolyn precursor under phase transfer conditions ($\text{NaIO}_4/\text{H}_2\text{O}$). The use of other oxidants (e.g. PbO_2) was found to be far less effective in the oxidation step for all the presented systems. The structures of these radicals are given in Figure 6.1.

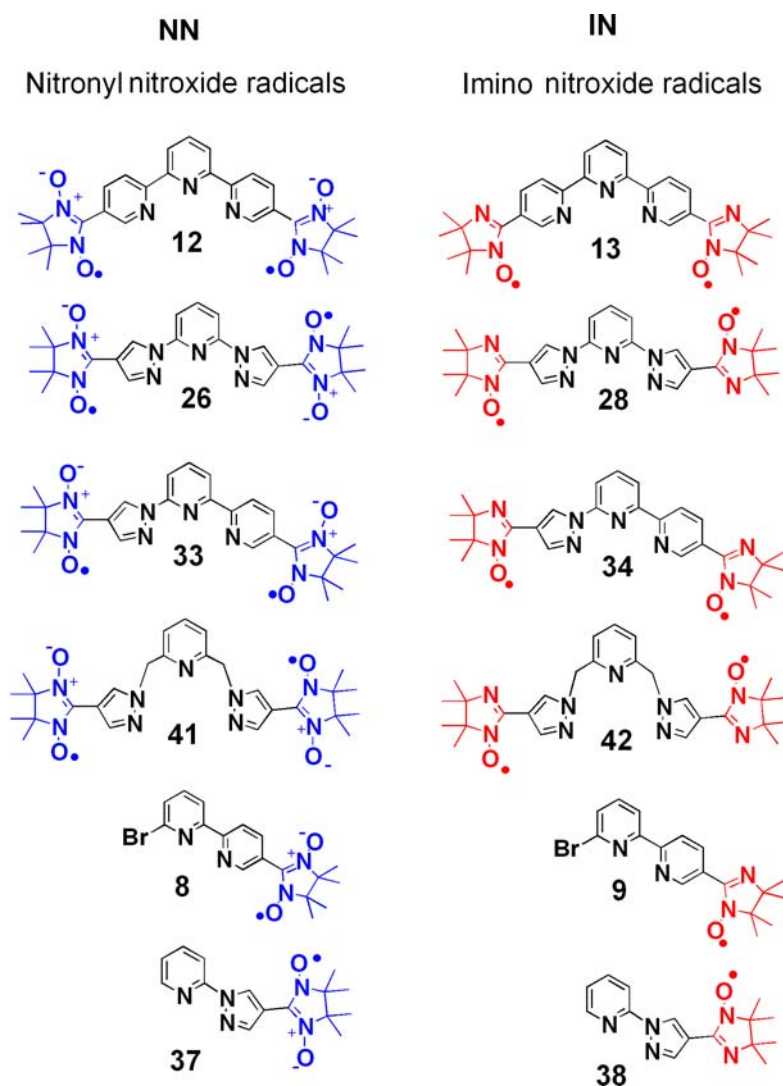


Figure 6.1: The novel mono and biradical systems synthesised based on nitronyl (NN, drawn in blue) and imino nitroxide (IN, drawn in red) moieties.

The nitronyl nitroxide radicals were always obtained in lower yields with respect to the imino nitroxides. This was explained by the difficulties in controlling the over oxidation/dehydration of the hydroxylimidazolyn-derivatives, even upon working under stoichiometric conditions of oxidizing agent, and with argon saturated solutions. In particular, those based on pyridine were much more sensitive towards the dehydration processes than the others attached to the pyrazole.

UV/Vis solution of the radicals witnessed no specific interaction between solvent and radical systems, in a broad range of solvent polarities. However the radical stabilities strongly decreased in protic solvents, especially in THF and MeOH, where they could not be stored even for few days under argon. In toluene solutions they were all very stable (up to a year), and those based on pyrazole could be even heated up to 60°C for few hours without any decomposition, providing that the medium was maintained free of oxygen.

Nitronyl nitroxides gave blue colour solutions, with two characteristic absorption bands: one defined as $n \rightarrow \pi^*$ transition related to the aminoxyl-oxide residue that occurs around 600 nm with several vibronic components, and a second one with a much higher intensity in the UV region ($\pi \rightarrow \pi^*$, ~ 390 nm).

These bands were strongly dependent for both intensity and position on the type of hetero-ring to which the radical units were connected. The radicals based on pyrazole exhibited enhanced optical properties in the visible ($\epsilon \geq 1000 \text{ M}^{-1} \times \text{cm}^{-1}$) and a relatively strong blue-shift of the $\pi \rightarrow \pi^*$ absorption (< 390 nm), while those grafted to pyridine rings showed hampered optical properties on the visible ($\epsilon \leq 500 \text{ M}^{-1} \times \text{cm}^{-1}$) and a red shift for the $\pi \rightarrow \pi^*$ absorption (≥ 390 nm). These findings were consistent with the enhanced aromatic character of the systems. The imino nitroxide radicals provided orange-red solutions, with a broad absorption band around 470 nm ($n \rightarrow \pi^*$), while the second transition ($\pi \rightarrow \pi^*$) of the amino-oxyl moiety appeared embedded into the organic backbone absorptions, and could not be discriminated.

The trends observed previously in the NN radicals were followed also in the IN radicals, in which the radical molar extinction in the visible decreased in the pyridine ($\epsilon \ll 1000 \text{ M}^{-1} \times \text{cm}^{-1}$) and increased when connected to pyrazoles ($\epsilon \geq 1000 \text{ M}^{-1} \times \text{cm}^{-1}$).

The UV/Vis transitions for three biradical systems (namely **12**, **13**, and **26**) were simulated, after geometry optimization, using ROHF/AM1/CIS (20,20) in order to assign the type of the experimentally observed absorptions. Although the calculated transitions corresponded fairly well with the observed ones, their relative intensities did not reproduce the trends experimentally found for ϵ (pyridine hampered and pyrazole enhanced).

The FTIR absorption spectra of the bis-hydroxylimidazolidyn precursors always showed a characteristic broad absorption (ν_{OH} , 3100 - 3400 cm^{-1}) that was lost upon oxidation. The NN radicals exhibited a strong band around 1350 cm^{-1} ($\nu_{\text{N-OH}}$), while for the IN radicals

such transition were both shifted to longer wavenumbers and much less intense ($\sim 1370\text{ cm}^{-1}$). The room temperature X-band EPR studies in solution for the mono and biradical NN systems gave respectively five and nine lines pattern, while the correspondent IN mono- and biradicals showed seven and thirteen lines. All the radicals did not witness line-width dependency upon changing solvent polarities (from hexane to MeOH), in agreement with the UV/Vis findings. However, they were all instable in protic solvents. This was corroborated by monitoring the decrease of their double integrated signal intensities *versus* time. On the other hand, 2-propanol constituted an exception; here the radicals were fairly high stables, but only those based on pyrazoles showed a slight increase in the observed nitrogen hyperfine interaction, (where a_N , raises from $\sim 0.75\text{ mT}$ to $\sim 0.77\text{ mT}$) without any substantial variation in the UV/Vis envelopes.

The observed g_{iso} for the NN radicals directly attached on pyridine moieties were centred at 2.0066(1) and 2.0061(1) for the NN. The slight shift at $g_{\text{iso}} = 2.0065(1)$ (NN) and 2.0060(1) (IN) were found for the radicals attached on pyrazoles. The biradical systems featured half of the spacing between the lines, as compared with the monoradicals (e.g. $a_N/2 \sim 0.374\text{ mT}$ for the nitronyl nitroxide biradicals where $a_N = 0.748\text{ mT}$ for the monoradicals, and $a_{N1}/2 \sim 0.430\text{ mT}$, $a_{N2}/2 \sim 0.225\text{ mT}$ for the imino nitroxide biradicals with $a_{N1} = 0.885\text{ mT}$, $a_{N2} = 0.430\text{ mT}$ for the related monoradicals, all recorded in toluene). These findings revealed that the radical moieties were strongly exchange coupled (J) within the EPR limit.

Estimation of the lower limit for J were obtained by fitting the EPR isotropic spectra, yielding in all cases $|J/a| \geq 40$, i.e. $2J = \Delta E_{\text{ST}} > 0.056\text{ cm}^{-1}$. For the monoradical **8** (NN), in addition to the major five lines, the high resolution spectra showed a more complex pattern with at least 13 visible additional splittings overlapped on each N *hfc*, originating from the presence of additional couplings of the single unpaired electron ($S = 1/2$) with twelve hydrogen nuclei ($I=1/2$), of the four methyl groups ($a_H = 0.022\text{ mT}$), the 6' ($a_H = 0.041\text{ mT}$) and 4' hydrogens ($a_H = 0.044\text{ mT}$) of the pyridyl moiety. Such finding experimentally demonstrates that non "zero spin density" resides also in the pyridine ring. The very similar resolved pattern occurred also in the case of monoradical **37**, where the spin carrier (nitronyl nitroxide) is connected to the pyrazole ring. The solution EPR studies did not show any appreciable broadening in line-width upon cooling for all the monoradical systems; in addition they followed nicely the Curie-law in dilute system with $[C] < 7 \times 10^{-3}\text{ M}$, making them suitable standards for the biradicals spin concentration.

Some of the coupled systems (e.g. **12**, **13**, **26**, **28**) did not feature a strong temperature dependence of the EPR line-width upon cooling. However, in the cases of **33**, **34**, **41**, and **42** the EPR spectra in solution witnessed strong temperature dependency. For **33** and **34**, such alternating line-width were explained by assuming the out-of-phase rotation of the radicals attached to the pyridine unit versus that one attached to the pyrazole moiety, in the EPR time

scale. In the biradicals **41** and **42**, where two CH₂ σ bonding are present, conformational interconversions in solution (rotamers) more easily allowed strong torsions between the radical moieties and the coupling unit core, leading to a fraction of uncoupled biradicals (~ 35%, with $J \ll a_N$).

The molecules **12**, **13**, **26**, **28**, **33**, **34**, **41** and **42**, encompassed ~ 2.0 uncorrelated spins in solution (down to 210 K), once their double integrated spectra were compared with monoradical standards, recorded under identical conditions. Such findings undoubtedly confirmed that thermally activated spin states were present in the high temperature regime. The EPR spectra for the frozen state solution of the monoradical systems showed patterns typical for axial systems, while the biradicals give zero-field-splitting (zfs). The monoradical impurities in some of the biradical systems did not exceed ~ 3-6% of the total spectral absorption lines (**26** and **28**) and were recognised easily, since they exhibited different saturation trends upon increasing microwave power (saturation behaviour). By comparing such saturation trends, the pure zfs parameters, D , for the biradical **41** was obtained.

Enhancement of the averaged radical distances led to a decrease in the magnitude of zfs, with the smaller value observed for the nitronyl nitroxide biradical **41** ($|D/hc| \sim 2.90 \times 10^{-3} \text{ cm}^{-1}$) (in **42** the close value of $|D/hc| \sim 3.18 \times 10^{-3} \text{ cm}^{-1}$ is extracted) and the largest for the imino nitroxide biradical **28** ($|D/hc| \sim 4.78 \times 10^{-3} \text{ cm}^{-1}$). In the biradicals, in addition to the zfs, the forbidden half-field transition ($\Delta m_s = 2$) were recorded, even at 120 K and in dilute (10^{-3} M) solutions. However, also at this temperature, the spin concentration accounted for only 2.0 (± 0.2) uncorrelated spins. Such knowledge provided the lower and upper limit for the singlet-triplet energy gap, ΔE_{ST} , of $0.056 \text{ cm}^{-1} \leq |2J| \leq 69.5 \text{ cm}^{-1}$, without however gaining the sign of J .

In order to determine their ground spin state multiplicity, the $\Delta m_s = 2$ transitions were followed down to cryogenic (~ 4K) temperature. The fitting of their double integrated signal intensities times temperature ($DI \times T$) versus temperature, according to the Bleaney-Bowers model for two interacting spin systems, gave both a more precise estimation and also the sign of the intramolecular exchange interactions, and thus their singlet-triplet energy gap (ΔE_{ST}).

These results are collected together in Figure 6.2. The NN biradicals showed greater proclivity to adopt high spin ground state with respect to the IN systems. Furthermore, by comparing their ΔE_{ST} trends, one could illustrate the effect of the five membered ring (pyrazole) on slightly hampering but not quenching the through-bond exchange interaction. This was due to the presence of two competitive pathways for the propagation of the spin polarization through the coupler. No comparison could unfortunately be made with references data, since for similar biradical systems based on pyridine moieties, no $\Delta M_s = 1$ transition envelopes were ever reported, no estimation of the zero-field splitting terms, D and E , were ever made, nor any $\Delta M_s = 2$ transition were ever observed. Furthermore, from the literature, always very weak

or negligible through-bond antiferromagnetic interactions were observed in pyridine based biradicals. Therefore the presented results would constitute unprecedented findings.

Our work underlined the opportunity *via* synthetic chemistry to fine tune the through-bond exchange interaction among closely related π -conjugated hetero-systems, in which the S=1 ground state were preferentially adopted.

The resolved X-ray structures for three biradicals were successfully obtained. The terpyridine NN **12** featured an unprecedented supramolecular π -stacking motif with units 180° rotated on top of each other. Such arrangement was mediated by bridging water molecules, leading to the formation of infinite chains. Although the stacking motif should give ferromagnetic interaction, according to the McConnell (through-space) model I, there were dominant inter-chain antiferromagnetic contributions, and the effective moment in the bulk sharply decreased below 20 K. The biradical **26** formed a zig-zag chain developing along the crystallographic b axis, while the biradical **33** gave dimers, due to the presence of solvent molecules (CHCl₃) that hindered supramolecular organization.

The future development of this work will be naturally directed towards the use of these molecular units in extended magnetic structures, using either the chelating properties of the coupling unit backbone and/or the NO radical moieties. Such approach is promising, especially for the NN type, in which the S=1 state in **12**, **26** and **33** show fairly large singlet-triplet energy gap. In addition to that, some metal complexes of Fe(II) and Co(II) coordinated on terpyridine and dipyrzoly-pyridine cores are known to exhibit spin-crossover behaviour, but no metal-complexes of these ligands in presence of stable radical units were synthesised. In this perspective, Fe (II) and Co (II) metal complexes on either the biradical systems **12**, **26** and **33** and their carbaldehyde precursors, might constitute the base for future studies on spin-crossover phenomena. These molecules can provide valuable model systems to test:

(A) The effect of the ligand field strength in the stabilisation of the high or low spin state of the metal (inductive effect due to the presence of substituents on the ligand moieties and the effect of the different donor properties of the nitrogen cores).

(B) The modulation of the metal spin state induced by their different metal binding-site size (steric constraint), because the metal-to-ligand distances represent one of the factors that provoke the spin-crossover phenomenon.

(C) How the presence of additional spins ferromagnetically interacting through the organic core might tune the energy difference between the lowest vibronic levels of the high-spin and low –spin states of the metals.

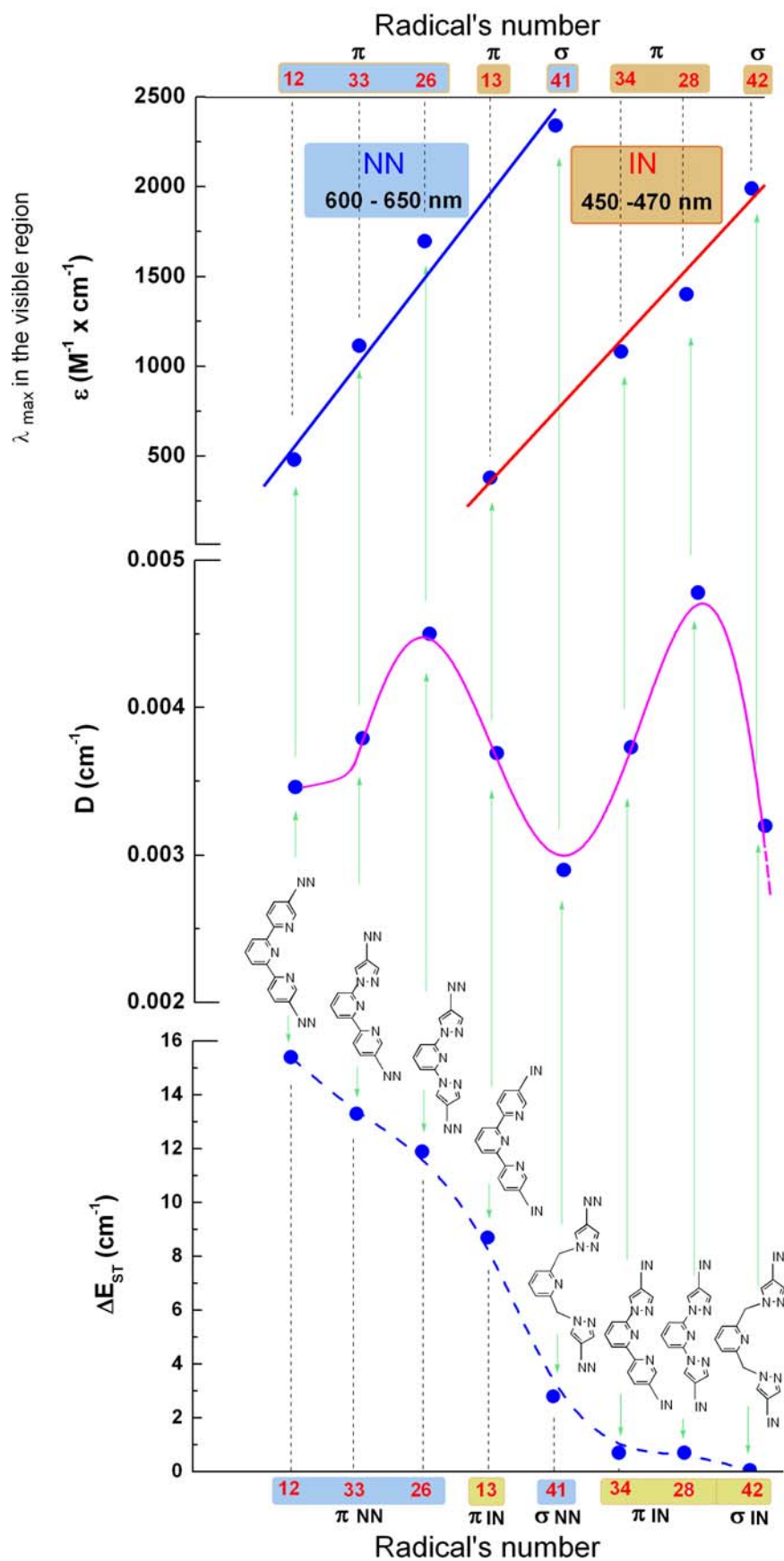
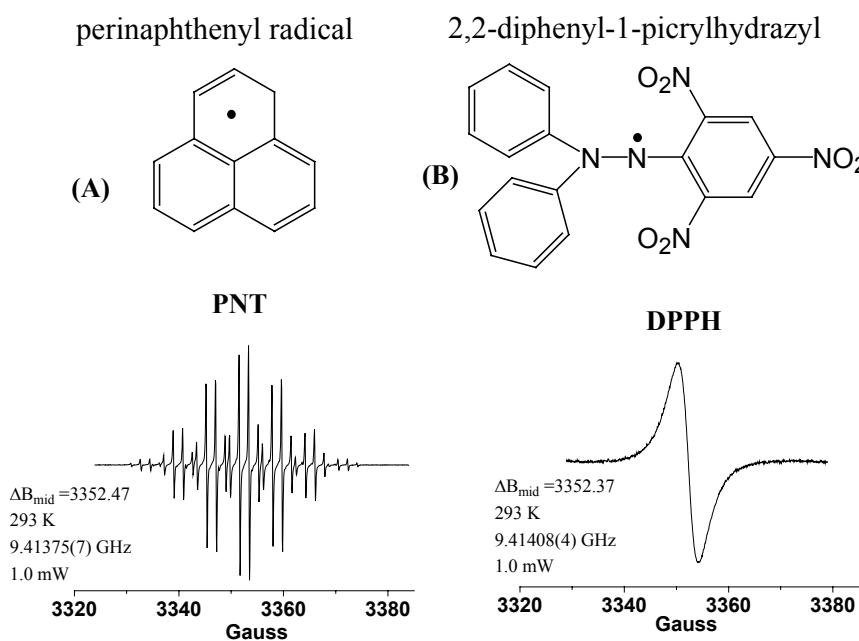


Figure 6.2: Overview of the optical properties, zero-field splitting (D) parameters, and singlet-triplet energy gap ($2J/k_b = \Delta E_{ST}$) in the biradical systems.

Chapter 7 - Experimental Session

7.1. Materials and Methods

Solvents were distilled before use and kept dry over molecular sieves; in particular diethylether and toluene were dried over sodium/benzophenone and distilled under Argon. All the reagents were used as received. ESR spectra were recorded in diluted and oxygen-free solutions of toluene with the concentration of $10^{-4} \text{ mol} \times \text{dm}^{-3}$ unless otherwise stated by using a Bruker X-band spectrometer ESP300 E, equipped with an NMR gaussmeter (Bruker ER035), a frequency counter (Bruker ER 041 XK) and a variable temperature control continuous flow N_2 cryostat (Bruker B-VT 2000) or with Oxford system (ESR 910) helium continuous flow cryostat. The g-factor corrections were obtained by using either PNT radical ($g = 2.0026$) (A) or DPPH ($g = 2.0037$) (B) as EPR standards.



UV/Vis spectra were recorded in toluene solutions with Perkin Elmer Spectrometer (UV/Vis/NIR Lambda 900) by using 1 cm optical-path quartz cell at room temperature. ^1H - and ^{13}C -NMR spectra were recorded on Bruker AMX 250 spectrometer. IR spectra were recorded in KBr pellet (Nicolet 730 FT-IR Spectrometer) at room temperature. Mass spectra were obtained on FD-MS, VG Instruments ZAB-2 mass spectrometer. Elemental analyses were performed at the University of Mainz, Faculty of Chemistry and Pharmacy on Foss Heraeus Varieo EL. Melting points were measured on Büchi B-545 apparatus (uncorrected) using open-ended capillaries. The X-ray crystallographic data were collected on Nonius Kappa CCD (Mo-K α) diffractometer equipped with graphite monochromator. The structures were solved by direct method and refined by a full-matrix least-squares procedure. The crystallographic

structures were drawn using the upgraded shared version of Mercury 1.2.1 and EnCIFER 1.0 (from the Cambridge Crystallographic Data Centre). The Mercury program was used for the search of non bonding, and bonding contacts. The structural analyses were also carried out on ORTEP-3 (v.1.0.3) kindly provided to G.Z. by Prof. L. J. Farrugia, University of Glasgow (UK). Compounds **1** [1], **2** [2], and **3** [2] are known, but no procedures were provided in the published communications. Compound **10** is also known [3] but it was prepared *via* a completely novel synthetic strategy. Compounds **14** [4] and **15** [5] (Method A) were prepared from the very brief literature procedures, with substantial modifications. Several different procedures were provided over the years for **6** [6] starting from 2,3-dimethyl-2,3-dinitrobutane. The compound **6** was prepared following the procedures reported in reference 6a. Compounds **16** [7], **17** [7] and **20** [8] were prepared with minor modifications with respect to previous reports.

References

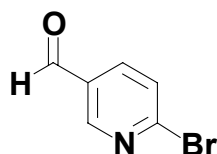
- [1] X. Wang, P. Rabbat, P. O`Shea, R. Tiller, E. J. J. Grabowski, P. J. Reider *Tetrahedron Lett.*, 41, **2000**, 4335.
- [2] F. J. Romero-Salguero, J.-M. Lehn *Tetrahedron Lett.*, 40, **1999**, 859.
- [3] (a) Sasaki I., Daran J.C., Balavoine G.G.A., *Synthesis*, 5, **1999**, 815. (b) Goral V., Nelen M.I., Eliseev A.V., Lehn J.-M., *PNAS*, 98 (4), **2001**, 1347.
- [4] Z. Arnold Z., *Coll. Czech. Chem. Commun.* 26, **1961**, 3051.
- [5] Takagi K., Bajnati A., Hubert-Habart M., *Bull. Soc. Chim. Fr.*, 127, **1990**, 660.
- [6] (a) Ovcharenko V.I., Fokin S.V., Rey P., *Mol. Cryst. Liq. Cryst.*, 334, **1999**, 109. (b) Ovcharenko V.I., Fokin S.V., Romanenko V., Korobkov I.V., Rey P., *Russ. Chem. Bull.*, 48, **1999**, 1519. (c) Hirel C., Vostrikova K.E., Pécaut J., Ovcharenko V.I., Rey P., *Chem. Eur. J.*, 7, **2001**, 2007.
- [7] Vasilevsky S.F., Klyatskaya S.V., Tretyakov E.V., Elguero J., *Heterocycles*, 60 (4), **2003**, 879.
- [8] Jameson L. D., Goldsby K.A., *J. Org. Chem.*, 55, **1990**, 4992.

7.2. Data treatment

The determination of the spin concentrations were carried out by EPR spectroscopy on diluted and degassed solutions (10^{-4} M); for the biradicals systems the double integrated signal intensities were compared against the monoradicals **8**, **9**, **37**, and **38**, recorded under identical conditions (modulation amplitude, receiver gain, power, sweep time, temperature) using the same EPR tube, and by careful control of the filling factors. In particular, prior the measurements, the sample temperatures were allowed to equilibrate for over 10 min in the

cavity cell-holder. The simulation of the solution EPR lines were obtained by numerical diagonalisation of the correspondent spin-Hamiltonian with the software WinEPR-SimFonia (v. 1.25, Bruker) or *BiRad* written by Dr. Dariush Hinderberger and P.D. Dr. Gunnar Jeschke (Prof. Dr. Hans W. Spiess Group, Max Planck Institute für Polymerforschung, Mainz) run on MatLab platform (v. 6.5). The EPR temperature dependence of the signal intensities for the mono and biradical systems were analyzed using least-square method procedures using the software Origin 6.0, and based on the Curie and Bleaney-Bowers equations. Constraint equations were home-made. The semi-empirical (ROHF/AM1) approach with extended configuration interaction (CAS) was used for assessing the spin-state ordering of biradicals **12** and **13**. The active space involved mixing of 8 electrons in 8 MOs, i.e. CAS [8,8]. This CAS choice was largely dictated by the nature of the frontier MOs; whereas the next-larger MO active space is not admissible due to orbital degeneracy, further extensions are already impracticable from a computational perspective. The CAS method provides the only size-consistent treatment of the lowest spin-dependent states. In the computation of local spin densities however, we expand substantially the MO basis at the expense of dropping the CAS requirement. Namely, we use the single-excited CI approach for 20 electrons in 20 MOs, or CIS [20,20]. The semi-empirical computations were performed with an upgraded version of MOPAC.

7.2.1 Synthesis of 6-bromo-3-pyridinecarbaldehyde (**1**)

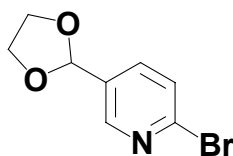


2,5-Dibromopyridine (5g, 21.1 mmol) was charged into a flask, evacuated and kept under argon. Dry diethylether (130 mL) was added from a syringe under stirring and the solution was cooled to $-78\text{ }^{\circ}\text{C}$ in dry ice/ acetone bath. The yellowish solution was very dense due to the low solubility of 2,5-dibromopyridine in diethyl ether at this concentration (0.144 M). Then *n*-BuLi (1.6 M in hexane, 16 mL, 25.3 mmol) was added drop-wise from a syringe within 10 min. As soon as the addition was completed, the color of the dense solution turned into red. The reaction mixture was stirred for 35 min under continuous cooling, then dry DMF (2.3 mL, 29.5 mmol, $d = 0.94\text{ g/mL}$) was added drop-wise within 5 min. The solution became deep clear red. The temperature ($-78\text{ }^{\circ}\text{C}$) was maintained further for 90 min and after that raised slowly till $-35\text{ }^{\circ}\text{C}$ and kept for additional 30 min at this temperature. Then the solution was warmed to room temperature. A saturated solution of ammonium chloride (50 mL) was added and the mixture was shaken vigorously in a separator funnel. The phases were separated and the

aqueous layer was extracted with dichloromethane (CH_2Cl_2 , 3×30 mL). The combined organic layers were collected and the solvent evaporated under reduced pressure to a small volume. The crude oily mixture was then separated by column chromatography (silica gel, dichloromethane/hexane, 3/2). The main isolated product was 6-bromo-3-pyridinecarbaldehyde **1** ($R_f = 0.26$) as pale yellow powder. The product was finally washed with small cold portions of light petroleum ether (low boiling point 30°C - 40°C) (3×15 ml) and it was collected as highly pure white crystalline powder (2.63 g, 67 %). Starting from 10 g of 2,5-dibromopyridine we obtain 4.32 g of pure product (yield 55%).

M.p. $97 - 98^\circ\text{C}$. **$^1\text{H-NMR}$** (CDCl_3 , 250 MHz, 298 K, 16 scan) 10.03δ (s, 1H, -CHO), 8.77δ (s, 1H, H-6), 7.94δ (d, 1H, $^3J = 8.2$ Hz, H-4), 7.62δ (d, 1H, $^3J = 8.1$ Hz, H-3). **$^{13}\text{C-NMR}$** (CDCl_3 , 63 MHz, 298 K, 10000 scan) δ ppm: 189.85, 152.88, 148.66, 137.87, 130.95, 129.38. **MS-FD** (70 eV, CH_2Cl_2) 187.2 (100%) (MW+H calculated 187.01). **UV/Vis**, λ/nm (CHCl_3 , $\epsilon \text{ M}^{-1} \times \text{cm}^{-1}$) 282 nm (24560), 310 nm (2860), 321 nm (2060). **Elemental analyses**, found C 38.46, H 2.25, N 7.35%. $\text{C}_6\text{H}_4\text{BrNO}$ (186.01) required C 38.74, H 2.17, N 7.53%.

7.2.2. Synthesis of 2-bromo-5-[1,3]dioxolan-2-yl-pyridine (**2**)

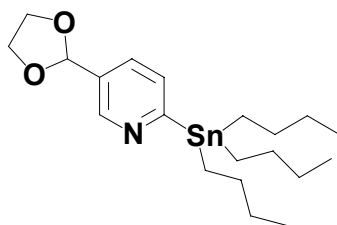


6-Bromo-3-pyridinecarbaldehyde **1** (1 g, 5.37 mmol) was charged into a round flask together with benzene (30 mL), ethyleneglycol (0.54 mL, 9.7 mmol) and *p*-toluenesulfonic acid as catalyst (0.08 g, 0.42 mmol, 8% with respect to the 6-bromo-3-pyridinecarbaldehyde). The solution was heated to reflux and stirred for one day. Then it was neutralized with diluted aqueous potassium carbonate (K_2CO_3) till pH 8-9 and the phases were separated. The aqueous layer was extracted with small portions of benzene (3×10 ml) and the combined organic layers were collected, dried over MgSO_4 and filtered. The benzene solution was evaporated under reduced pressure and the resulting oil was dried in vacuum overnight at 40°C . Totally 1.086 g (4.7 mmol) of 2-bromo-5-[1,3]dioxolan-2-yl-pyridine **2** as pale yellow oil was obtained (yield 87%).

B.p. $> 200^\circ\text{C}$ (760 mbar). **$^1\text{H NMR}$** (CDCl_3 , 250 MHz, 298 K, 16 scan) 8.43δ (s, 1H, H-6), 7.62δ (dd, 1H, $^3J = 2.2, 7.9$ Hz, H-3), 7.49δ (d, 1H, $^3J = 8.2$ Hz, H-4), 5.80δ (s, 1H, -CH), 4.32δ (m, 4H, $-\text{CH}_2$). **$^{13}\text{C NMR}$** (CDCl_3 , 63 MHz, 298 K, 9000 scan) δ (ppm): 147.7, 141.8, 135.7,

132.1, 126.8, 100.2, 64.4. **MS-FD** (70 eV, CHCl₃) 230.1 (100%, M⁺), MW calculated (C₈H₈BrNO₂) 230.06.

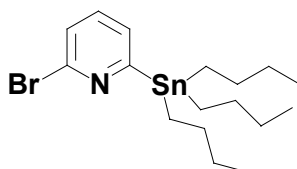
7.2.3. Synthesis of 2-tributylstannyl-5-[1,3]dioxolan-2-yl-pyridine (**3**)



2-Bromo-5-[1,3]dioxolan-2-yl-pyridine **2** (1.086 g, 4.7 mmol) was charged into a round flask together with freshly distilled diethylether (40 mL), and kept under argon. The solution was cooled to -78°C using dry ice/acetone bath and n-BuLi (1.6 M in hexane, 3.5 ml, 5.7 mmol) was added slowly within 10 min. The mixture was kept for 90 min at this temperature under stirring and rigorous argon atmosphere. Initially, after the complete addition of n-BuLi the solution appeared deep-green and after 90 min turned black.

Tributyltin-chloride (Bu₃SnCl, 97%) (1.66 mL, 6.2 mmol) was added within 5 min. The solution slowly turned into deep-red. The low temperature (-78°C) was maintained for 120 min and after that the mixture was allowed to warm slowly to room temperature overnight. The oily solution was filtered from the inorganic salts and the solvent evaporated under reduced pressure. Finally 3.8 mL of bright orange oil ($\rho = 1.05 \text{ g/mL}$) of **3** were obtained and used for the Stille coupling reaction without purification. (Note that a part from the known toxicity of the stannyl-compounds, the product decomposes either on silica or alumina columns.)

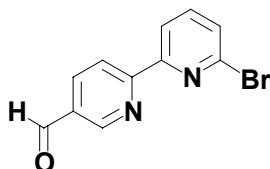
7.2.4. Synthesis of 2-tributylstannyl-6-bromopyridine (**4**)



2,6-Dibromopyridine (1 g, 4.22 mmol) was charged into a flask, evacuated and put under argon. Dry diethylether (70 mL) was added from a syringe under stirring and the solution was cooled to -50°C in dry ice/acetone bath. The white solution was very dense due to the low solubility of 2,6-dibromopyridine in diethylether. Then excess of n-BuLi (1.6 M in hexane, 5.6 mL, 8.96 mmol) was added dropwise from a syringe within 3 min. As soon as the addition was completed the mixture turned deep green. The reaction mixture was stirred for 30 min under

continuous cooling (-50 °C) then the temperature was lowered till – 60 °C. Tributylstannylchloride (Bu_3SnCl , 97%) (2.72 mL, 10.1 mmol) was added from a syringe within 5 min. When half of the addition was completed the solution became pale green and very limpid. The temperature was maintained for 60 min, then lowered till – 78 °C and kept for an additional hour. Finally the mixture was allowed to warm slowly overnight till room temperature. The solution was filtered from the white inorganic salts and dry toluene (2 mL) was added. The organic solution was collected and the diethylether was evaporated under reduced pressure avoiding heating to afford 3.7 mL of 2-tributylstannyl-6-bromopyridine **4** as pale yellowish oil ($\rho = 1.134 \text{ g/mL}$) which was used for the Stille coupling reaction without purification (the product decomposes either in silica or alumina columns.)

7.2.5. Synthesis of 6'-bromo-[2,2']-dipyridinyl-5'-carbaldehyde (**5**)



The crude oily **3** (3.7 mL, 4.22 mmol) was transferred into a two-necked round bottomed flask together with an excess of 6-bromo-3-pyridinecarbaldehyde (1.8 g, 9.7 mmol). The mixture was degassed and kept under argon. Then dry and degassed toluene (70 mL) was added with a syringe together with dichlorobis(triphenylphosphine)-palladium(II) (148 mg, 0.21 mmol, 5% with respect to **3** and triphenylphosphine (110 mg, 0.42 mmol) as catalyst. The solution was then heated to reflux, in argon under stirring, for 72 hours. During the reaction the initially light-yellow solution became very dark after 72 hours. The solvent was evaporated under reduced pressure and then dichloromethane (50 ml) together with a saturated solution ammonium-chloride (30 mL) and a solution of EDTA (5%, 10 ml) was added to the resulting black-slurry. The mixture was shaken vigorously in a separator funnel and the phases were separated. The aqueous layer was extracted with portions of dichloromethane (2 × 30 mL). The combined organic layers were collected and the solvent evaporated under reduced pressure till small volume. The crude oily mixture was subjected to column chromatography (silica gel, ethyl-acetate/dichloromethane/hexane, 1/3/4). The main fraction eluted was 6'-bromo-[2,2']-bipyridinyl-5-carbaldehyde ($R_f = 0.65$) as pale yellow powder. The product **5** was further washed with small cold portions of light petroleum ether (2 × 5 mL) (b.p. 30 - 40°C) and it was collected as highly pure white crystalline powder (750 mg, 68%). The second clear fraction collected was found to consist of [2,2']-bipyridinyl-5-5'-dicarboxaldehyde ($R_f = 0.25$, 90 mg) as homocoupled product of **3**. Starting from 8.44 mmol (7.4 mL) of 2-tributylstannyl-6-

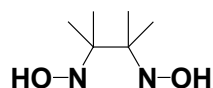
bromopyridine and 3.6 g of 6-bromo-3-pyridinecarbaldehyde (19.4 mmol) was obtained 1.29 g of 6'-bromo-[2,2']-bipyridinyl-5-carbaldehyde (yield 58%).

[2,2']-Bipyridinyl-5-5'-dicarboxaldehyde: $^1\text{H-NMR}$ (DMSO- d_6 , 250 MHz, 298 K, 32 scan) δ (ppm): 10.26 δ (s, 2H), 9.31 δ (s, 2H), 8.75 δ (d, $^3J = 8.2$ Hz, 2H), 8.52 δ (dd, $^3J = 2.0, 8.0$ Hz, 2H). **MS-FD** (70eV, CH_2Cl_2) 212.30 (M-H, 100%), MW calculated (MW+H) 213.30. **Elemental analyses**, found C 68.11, H 3.65, N 13.30 %, C/N = 5.12. $\text{C}_{12}\text{H}_8\text{N}_2\text{O}_2$ required C 67.92, H 3.80, N 13.20 %, C/N = 5.14.

Procedure for the homocoupling: 6-bromo-3-pyridinecarbaldehyde (300 mg, 1.6 mmol) dissolved in dry xylene (20 mL) was added tributyltin-chloride (Bu_3SnCl) (0.13 mL, 0.16 mmol), dichlorobis(triphenylphosphine)-palladium(II) (24.4 mg) and triphenylphosphine (18.2 mg) and heated to reflux under argon for 60 hours. The work up followed the same procedure as reported above (204 mg, yield 60%).

6'-Bromo-[2,2']-bipyridinyl-5-carbaldehyde:M.p. 176 – 177 °C. $^1\text{H NMR}$ (CDCl_3 , 250 MHz, 298 K, 64 scan) δ (ppm): 10.15 (s, 1H, -CHO), 9.09 (s, 1H, H-6'), 8.57 (d, $^3J = 8.5$ Hz, 1H, H-3), 8.45 (d, $^3J = 7.7$ Hz, 1H, H-3'), 8.28 (d, $^3J = 8.3$ Hz, 1H, H-4'), 7.70 (t, $^3J = 7.8$ Hz, 1H, H-4), 7.56 (d, $^3J = 7.8$ Hz, 1H, H-5). $^{13}\text{C NMR}$ (CDCl_3 , 63 MHz, 298 K, 8000 scan) δ (ppm): 188.7, 157.2, 154.2, 149.8, 140.2, 137.7, 135.4, 129.7, 127.4, 119.9, 119.2. **MS-FD** (70eV, CH_2Cl_2) 264.1 (M-H, 100%), MW calculated (MW+H) 264.1. UV-Vis (CHCl_3) λ/nm (ϵ , $\text{mol}^{-1} \times \text{cm}^{-1}$) 321 nm (21380), 310 nm (25850), 260 nm (12030). **FT-IR** (KBr pellet, $\nu \text{ cm}^{-1}$) 3042 (w, $\nu_{\text{C-H}}$), 2962 (w, $\nu_{\text{C-H}}$), 2883 (w, $\nu_{\text{C-H}}$), 1682 (s, $\nu_{\text{C=O}}$), 1592 (s, pyr), 1546 (s, pyr), 1435(m, pyr), 1369 (m), 1263 (m, pyr), 1209 (m, pyr). **Elemental analyses**, found C 47.20, H 3.30, N 10.01%, C/N = 4.72. $\text{C}_{11}\text{H}_7\text{N}_2\text{O} \times \text{H}_2\text{O}$ required C 47.00, H 3.20, N 9.97 %, C/N = 4.71.

7.2.6. Synthesis of 2,3-dimethyl-2,3-bis(hydroxylamino)-butane (6)

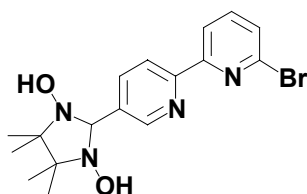


A suspension of 2,3-dimethyl-2,3-bis(hydroxylamino)-butane sulfate salt (85%, $\text{C}_6\text{H}_{16}\text{N}_2\text{O}_2 \times \text{H}_2\text{SO}_4$, MW 264.30, 5 g, 18.92 mmol) in THF (70 mL) was kept cold with an ice bath and a solution of NaOH (1.56 g, 39 mmol, dissolved in 10 mL H_2O) was added drop by drop while stirring within 10 min. The suspension became limpid after the addition of the base was completed. Then the resulting mixture was left under stirring at 4°C for further 10 min. A white solid slowly precipitated that consisted of Na_2SO_4 . The salt was filtered off and the filtrate was slowly evaporated under air stream in a crystallizing disk. A white powder very hygroscopic was left, and it was further washed with cold hexane and dried under vacuum. In case that this

powder slowly became pale rose, it was indicative for decomposition of the product into oxyme. Thus, the powder was washed first with cold and degassed water, followed by hexane. A white solid consisting of 2,3-dimethyl-2,3-bis(hydroxylamino)-butane (free base) was collected and stored at -10°C in a closed bottle (1.4 g, MW 148.20, yield 50%).

M.p. 160-161 $^{\circ}\text{C}$. **FT-IR** (KBr) ν/cm^{-1} : 3257 (vs and broad, ν_{OH}), 2987 (vs, $\nu_{\text{C-H}}$), 1479-1374 (vs, several bands), 1261 (s), 1178 (vs), 1145 (vs), 1080 (s), 1035 (vs), 989 (m), 952 (vs), 904 (vs), 852 (m), 790 (m), 690 (m). **$^1\text{H NMR}$** (D_2O , 250 MHz, 298 K, 16 scan) δ (ppm): 1.25 (s, - CH_3). **$^{13}\text{C NMR}$** (D_2O , 63 MHz, 298 K, 256 scan) δ (ppm): 21.5 (CH_3), 63.3 (CH_3 -C- CH_3).

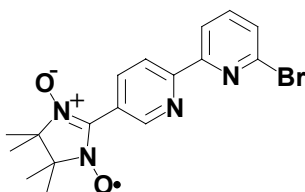
7.2.7. Synthesis of 6-bromo-5'[1,3-dihydroxy-4,4,5,5-tetramethylimidazolidin-2-yl]-2,2'-bipyridine (7)



6'-Bromo-[2,2']-dipyridinyl-5'-carbaldehyde **5** (280 mg, 1.06 mmol) and 2,3-bis(hydroxylamino)-2,3-dimethylbutane **6** (444 mg, 3.0 mmol) were dissolved in 30 mL of dioxane and CH_2Cl_2 (1/1) and stirred under argon for four days until a fine white precipitate was formed. The solvent was removed by slow evaporation at room temperature and the solid product was collected, washed with a small amount of cold methanol/water mixture (1/1), and air dried to give crude **7** (354 mg, crude yield 85 %) that was subjected to the oxidation step without further purification.

It decomposes before melting (from white powder to bright red powder) at 166-167 $^{\circ}\text{C}$ (from methanol). **FT-IR** (KBr pellet, ν/cm^{-1}) 3251 (s and very broad, -OH), 2983 (s, $\nu_{\text{C-H}}$), 2920 (s, $\nu_{\text{C-H}}$), 1570 (m), 1548 (m), 1431 (s), 1378 (s), 1255 (w), 1155 (s), 1124 (s), 875 (s) 790 (s). **$^1\text{H NMR}$** (DMSO-d_6 , 250 MHz) δ (ppm) 8.65 (s, 1H, -CH), 8.31 (d, $^3J = 7.53$ Hz, -CH), 8.18 (d, $^3J = 8.17$, 1H, -CH), 7.96-7.92 (dd, $^3J = 8.16$ Hz, 1.9 Hz, 1H, -CH), 7.87 (s, 1H, -OH), 7.82 (t, $^3J = 7.85$ Hz, 1H, -CH), 7.62 (d, $^3J = 7.54$ Hz, 1H, -CH), 4.56 (s, 1H, - CH_{imid}), 1.00 (d, $^3J = 7.84$ Hz, 12 H, 4- CH_3). **$^{13}\text{C NMR}$** (63 MHz, DMSO-d_6) δ (ppm) 156.7, 152.7, 149.7, 149.4, 141.0, 140.6, 138.3, 137.2, 128.2, 119.7, 87.8, 66.3, 24.2, 17.2. **Elemental analyses**, found C 47.76, H 5.75, N, 12.81%. $\text{C}_{17}\text{H}_{21}\text{BrN}_4\text{O}_2 \times 2 \text{H}_2\text{O}$ (429.31) required C 47.56, H 5.87, N 13.05.

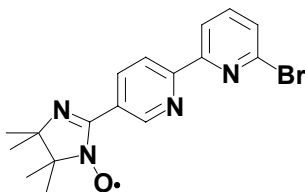
7.2.8. Synthesis of 6-bromo-5'[3-oxide-1-oxyl-4,4,5,5-tetramethylimidazolidin-2-yl]-2,2'-bipyridine (8)



6-Bromo-5'[1,3-dihydroxy-4,4,5,5-tetramethylimidazolidin-2-yl]-2,2'-bipyridine **7** (250 mg, 0.58 mmol) was oxidized under phase transfer conditions in water/chloroform mixture (30mL, 1/3) using NaIO_4 (186 mg, 0.87 mmol) for 30 min; during this period of time the solution gradually became blue-greenish. The phases were separated and the aqueous layer was extracted with chloroform (3×15 mL). The organic phases were collected and evaporated under air. The green-blue solid was dissolved in the minimum amount of acetone and chromatographed on neutral alumina using as eluents a mixture of acetone/petroleum-ether (low boiling point, 1/3). The first blue fraction eluted was collected and the solvent was removed under reduced pressure to afford pure 6-bromo-5'[3-oxide-1-oxyl-4,4,5,5-tetramethylimidazolidin-2-yl]-2,2'-bipyridine **8** (56 mg, yield 25 %) was obtained as deep blue powder.

M.p. 165 – 166 °C (from acetone, upon melting changes from deep-blue to bright orange). **FT-IR** (KBr pellet, ν/cm^{-1}) 3112 (w, $\nu_{\text{C-H}}$), 2981 (s, $\nu_{\text{C-H}}$), 2933 (s, $\nu_{\text{C-H}}$), 2875 (s, $\nu_{\text{C-H}}$), 1583 (m), 1548 (m), 1454 (s), 1430 (s), 1413 (s), 1352 (s, N-O), 1213 (m), 1124 (m) (pyridine and pyrazolyl- moieties). **UV/Vis**, λ/nm (toluene), (ϵ , $\text{M}^{-1} \times \text{cm}^{-1}$): 316 (23270), 327 (24480), 342 (20235), 377 (5580), 394 (8960), 468 (84), 498 (71), 537 (115), 574 (187), 620 (259), 669 (221), 746 (65). **Elemental analyses**, found C 47.76, H 5.45, N 12.90%. $\text{C}_{17}\text{H}_{18}\text{BrN}_4\text{O}_2 \times 2\text{H}_2\text{O}$ (425.08) required C 47.90, H 5.20, N 13.14%. **EPR** (298 K, 9.399870 GHz, 7×10^{-5} M in toluene): five lines, $g_{\text{iso}} = 2.0066(1)$, $a_{\text{N}} = 0.748$ mT, $a_{\text{H}} = 0.022$ mT (12 H, $-\text{CH}_3$), $a_{\text{H}} = 0.044$ mT and 0.041 mT (2H, 6' and 4').

7.2.9. Synthesis of 6-bromo-5'[1-oxyl-4,4,5,5-tetramethylimidazolidin-2-yl]-2,2'-bipyridine (9)

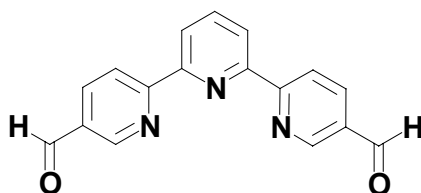


6-Bromo-5'[1,3-dihydroxy-4,4,5,5-tetramethylimidazolidin-2-yl]-2,2'-bipyridine **7** (100 mg, 0.23 mmol) was oxidized under phase transfer conditions in water/chloroform mixture (20mL, 1/3)

using excess of NaIO_4 (242 mg, 1.63 mmol), previously dissolved in 15 mL of water, for 60 min and upon warming the reaction mixture up to 40°C . During this period of time the organic phase became bright red. The phases were separated and the aqueous layer was extracted with chloroform (3 x 20 mL). The organic phases were collected and evaporated under reduced pressure. The crude red solid was dissolved in acetone and purified by chromatographic separation on neutral alumina, using as eluents acetone /petroleum ether (low boiling point, 1/3) mixture. The red fraction eluted ($R_f = 0.67$) was collected and upon drying it gave pure 6-bromo-5-[1-oxyl-4,4,5,5-tetramethylimidazolidin-2-yl]-2,2'-bipyridine **9** (24 mg, yield 28 %) as bright red solid very hygroscopic.

M.p. 147 – 148°C (from acetone). **FT-IR** (KBr pellet, ν/cm^{-1}) 3072 (w, $\nu_{\text{C-H}}$), 2964 (s, $\nu_{\text{C-Hal}}$), 2923 (s, $\nu_{\text{C-H}}$), 2855 (s, $\nu_{\text{C-H}}$), 1594 (m), 1544 (s), 1455 (m), 1428 (s), 1373 (s, N-O), 1261 (m), 1155 (s), 1124 (s) (pyridine and pyrazolyl- moieties). **UV/Vis**, λ/nm (toluene) (ϵ , $\text{M}^{-1} \times \text{cm}^{-1}$) 308 (19086), 343 (3222), 392 (282), 438 (278), 464 (321), 493 (287), 534 (157). **Elemental analyses**, found C 47.43, H 5.85, N, 13.00%. $\text{C}_{17}\text{H}_{18}\text{BrN}_4\text{O} \times 3 \text{H}_2\text{O}$ (428.30) required C 47.67, H 5.65, N 13.08. **EPR** (298 K, 9.399947 GHz, 10^{-4} M in toluene): seven lines, $g_{\text{iso}} = 2.0061(1)$, $a_{\text{N1}} = 0.885$ mT, $a_{\text{N2}} = 0.430$ mT.

7.2.10. Synthesis of 5, 5''-diformyl-2,2':6',2'' terpyridine (10)

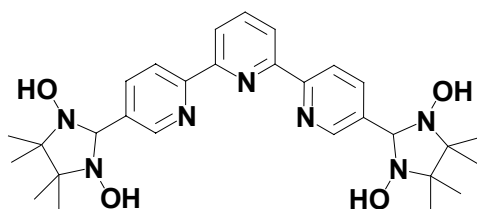


2-Tributylstannyl-5-[1,3]dioxolan-2-yl-pyridine **3** (3.8 mL, 4.7 mmol) was placed in a two-necked round bottomed flask together with the 6'-bromo-[2,2']-bipyridinyl-5-carbaldehyde **5** (900 mg, 3.4 mmol). The mixture was degassed and kept under rigorous argon atmosphere. Then dry and degassed toluene (50 ml) was added with a syringe together with dichlorobis(triphenylphosphine)-palladium(II) (165 mg, 0.235 mmol) and triphenylphosphine (123 mg, 0.47 mmol) as catalyst. The solution was heated to reflux in argon under stirring for 60 hours. The resulting dark solution was washed with a saturated solution of ammonium-chloride (20 ml). The mixture was shaken vigorously in a separator funnel. The phases were separated and the aqueous layer was extracted with toluene (2 x 15 mL). The combined dark yellow organic layers were collected and the solvent evaporated under reduced pressure. The oily solution was then treated with HCl (20 mL, 6N) and was heated to reflux for 6 hours under stirring. This ensures for the complete hydrolysis of the dioxolane. The mixture was treated

with CH_2Cl_2 (10 mL) and the aqueous phase was collected. Basification with a saturated solution of K_2CO_3 shows the formation of a white flocculate at pH 7-8 that consists mainly of 5,5"-diformyl-2,2':6',2"-terpyridine. The crude product was extracted with dichloromethane (3 × 40 ml). The organic layers were collected and the solvent evaporated till small volume under reduced pressure. The mixture was separated by column chromatography (silica gel, ethyl-acetate/dichloromethane/hexane, 1/4/4). The fraction eluted (colorless) was 5,5"-diformyl-2,2':6',2"-terpyridine ($R_f = 0.2$) as pale yellow powder. The product was further washed with small portions of light petroleum ether (2 × 10 mL) (b.p. 30 - 40°C) and it was collected as highly pure white crystalline powder (720 mg, 73 %).

M.p. 246-247 °C. **FT-IR** (KBr) ν/cm^{-1} : 3036 (w, $\nu_{\text{C-H}}$), 2961 (w, $\nu_{\text{C-H}}$), 2877 ($\nu_{\text{C-H}}$), 1693 (s, $\nu_{\text{C=O}}$), 1591(s, pyr), 1560 (s, pyr), 1482 (w, pyr), 1450 (w, pyr), 1371 (s), 1264 (m, pyr), 1205 (m, pyr). **$^1\text{H NMR}$** (DMSO d_6 , 250 MHz, 298 K, 64 scan) δ (ppm): 10.19 (s, 2H, -CHO), 9.22 (s, 2H, H-6, H-6"), 8.84 (d, $J = 8.2$ Hz, 2H, H-3, H-3"), 8.62 (d, $^3J = 7.9$ Hz, 2H, H-3', H-5'), 8.44 (dd, $^3J = 2.2, 8.2$ Hz, 2H, H-4, H-4"), 8.24 (t, $^3J = 7.9$ Hz, 1H, H-4'). **$^{13}\text{C-NMR}$** (DMSO- d_6 , 63 MHz, 298 K, 10000 scan), δ (ppm): 192.5, 159.3, 154.3, 151.9, 139.5, 137.7, 131.7, 123.2, 121.5. **MS-FD** (70eV, CH_2Cl_2) 290.4 (100%), (MW+H calc 290.4). **UV/Vis** (CHCl_3) λ/nm (ϵ , $\text{mol}^{-1} \times \text{cm}^{-1}$) 321 nm (31800), 312 nm (30870), 256 nm (23020). **Elemental analyses**, found C 70.42, H 3.92, N 14.40%. $\text{C}_{17}\text{H}_{11}\text{N}_3\text{O}_2$ (289.29) required C 70.58, H 3.83, N 14.53 %.

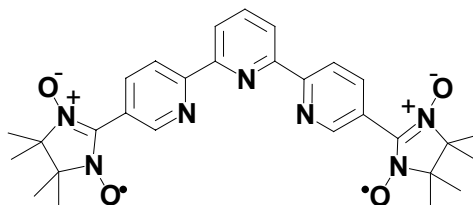
7.2.11. Synthesis of 5,5"-bis(1,3-dihydroxy-4,4,5,5-tetramethylimidazolidin-2-yl)2,2':6',2"-terpyridine (11)



5,5"-Diformyl-2,2':6',2"-terpyridine **10** (590 mg, 2.04 mmol) was placed in a round bottomed flask together with 2,3-bis-hydroxylamino-2,3-dimethylbutane **6** (906 mg, 6.12 mmol). A mixture of 1,4-dioxane, trichloromethane (CHCl_3) and methanol (20 mL /15 mL /15 mL) was used as reaction solvents due to the low solubility of the diformyl-derivative. The mixture was then stirred for 7 days under argon at room temperature. The white precipitate 5,5"-bis(1,3-dihydroxy-4,4,5,5-tetramethylimidazolidin-2-yl)2,2':6',2"-terpyridine was filtered, washed with small portions of cold methanol/acetone (4/1, 3 × 5 mL) and dried in high-vacuum. The radical precursor was then recovered as fine white powder, and was used without further purification (960 mg, yield 86%).

It decomposes before melting at 186 – 187 °C. **¹H NMR** (DMSO *d*₆, 250 MHz, 298 K, 64 scan) δ (ppm): 8.76 (s, 2H, H-6, H-6''), 8.57 (d, ³*J* = 7.8 Hz, 2H, H-3, H-3''), 8.40 (d, ³*J* = 7.5 Hz, 2H, H-3', H-5'), 8.05 (m, ³*J* = 7.8, 8.2, 6.7 Hz, 3H, H-4, H-4', H-4''), 7.94 (s, 4H, OH), 4.66 (s, 2H, -CH), 1.09 (d, ³*J* = 6.6 Hz, 24H, -CH₃). **¹³C NMR** (DMSO- *d*₆, 63 MHz, 298 K, 8000 scan) δ (ppm): 154.5, 153.9, 148.9, 137.2, 136.6, 129.1, 120.0, 119.4, 87.5, 65.8, 23.9, 16.8. MS-FAB (NBA matrix) *m/z* 549.4 (100%)(M+H)⁺, calculated (MW) 549.66. **UV/Vis** (DMSO) λ /nm (ϵ , mol⁻¹ × cm⁻¹) 290 nm (11900). **FT-IR** (KBr) ν /cm⁻¹ = 3252 (s, broad, ν_{OH}), 2988 (s, ν_{C-H}), 2930 (s, ν_{C-H}), 1596 (m, pyr), 1560 (m, pyr), 1374 (s), 1262 (s, pyr). **Elemental analyses**, found C 59.40, H 7.55, N 16.63%, C/N = 3.57. C₂₉H₃₉N₇O₄ × 2H₂O required C 59.50, H 7.35, N 16.75%, C/N = 3.55.

7.2.12. Synthesis of 5,5''-bis(1-oxyl-3-oxo-4,4,5,5-tetramethylimidazolidin-2-yl)2,2':6',2''-terpyridine (12)

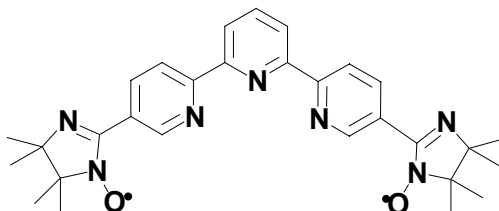


Compound **11** (217 mg, 0.39 mmol) was charged into a small flask together with 20 mL of CHCl₃ and CH₂Cl₂ (4/1). Then it was degassed and kept under argon while stirring at room temperature. Separately, a solution of NaIO₄ (211 mg, 0.987 mmol) dissolved in 10 mL of H₂O was first degassed and saturated by argon exchange; then it was added to the solution of the radical precursor by using a syringe under argon. After 30 min a deep green solution was obtained. The organic layer was extracted by using portions of CHCl₃ (3 × 10 mL) until the aqueous phase was almost colorless. The organic solution was evaporated by continuous argon bubbling until a small volume of solvent was left (~2 mL). The mixture was separated by column chromatography (Aluminium oxide, acetone/light petroleum ether, 3/7). The 5,5''-bis(1-oxyl-3-oxo-4,4,5,5-tetramethylimidazolidin-2-yl)2,2':6',2''-terpyridine **12** (*R_f* = 0.23) was obtained after solvent evaporation (by argon bubbling) as deep green powder (35 mg, yield 16 %).

FT-IR (KBr) ν /cm⁻¹ = 3066 (w, ν_{C-H}), 2990 (m, ν_{C-H}), 2924 (m, ν_{C-H}), 2853 (m, ν_{C-H}), 1591 (m, pyr), 1482 (m, pyr), 1452 (m, pyr), 1387 (m), 1351 (s, ν_{N-O}), 1216 (m, pyr). **MS-FAB** (NBA matrix) *m/z* 544.6 (100%) [M+H]⁺, calculated (MW+H, 544.66). **UV/Vis** (CHCl₃) λ /nm (ϵ , mol⁻¹ × cm⁻¹) 718 (145), 650 (425), 605 nm (480), 562 (350), 387 nm (13100), 342 nm (28300), 328 nm (33400), 282 nm (31550). **Elemental analyses**, found C 59.96, H 6.50, N 16.82%.

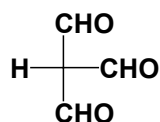
$C_{29}H_{33}N_7O_4$ (543.62) \times 2 H_2O required C 60.09, H 6.43, N 16.91%. **EPR** (260 K, 9.400220 GHz, toluene 10^{-4} M): 9 lines, $g_{iso} = 2.0066(1)$, $a_N = 0.374$ mT.

7.2.13. Synthesis **5,5''-bis(1-oxyl-4,4,5,5-tetramethylimidazolidin-2-yl)2,2':6',2''-terpyridine (13)**



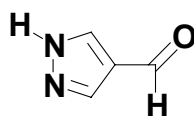
Compound **11** (240 mg, 0.44 mmol) was charged into a small flask together with 20 mL of a mixture of $CHCl_3$ and CH_2Cl_2 (4/1), under stirring at room temperature. A solution of $NaIO_4$ (377 mg, 1.76 mmol, 10 mL H_2O) was slowly added to the solution of the radical precursor and then the mixture was slightly warmed at 40 °C. After 30 min an orange-red solution was obtained. The organic layer was extracted by using portions of $CHCl_3$ (3×10 mL). The organic solution was evaporated under reduced pressure up to small volume (1 mL). The mixture was separated by column chromatography (Aluminium oxide, acetone/light petroleum-ether low boiling point, 3/7). The 5,5''-bis(1-oxyl-4,4,5,5-tetramethylimidazolidin-2-yl)2,2':6',2''-terpyridine **13** ($R_f = 0.25$) was obtained after solvent evaporation as orange powder (63 mg, yield 28 %).

M.p. 139-140 decompose by changing color from bright red to pale yellow and melt to dark mass at 239-240°C. **FT-IR** (KBR) $\nu/cm^{-1} = 3070$ (w, ν_{C-H}), 2957 (s, ν_{C-H}), 2924 (s, ν_{C-H}), 2870 (m, ν_{C-H}), 1596 (m, pyr), 1554 (s, C=N), 1469 (s, pyr), 1448 (s, pyr) 1425 (s), 1378 (s, ν_{N-O}), 1262 (s, pyr), 1216 (s, pyr). **MS-FAB** (NBA matrix) m/z 512.2 (100%) $[M+H]^+$, calculated MW 511.6. **UV/Vis** ($CHCl_3$) λ/nm (ϵ , $mol^{-1} \times cm^{-1}$) 528 (170), 490 (315), 459 nm (380), 300 nm (16200), 257 nm (24100). **Elemental analyses**, found C 63.36, H 6.91, N 17.74%. $C_{29}H_{33}N_7O_2$ (511.62) \times 2 H_2O required C 63.60, H 6.81, N 17.90%. **EPR** (260 K, 9.402404 GHz, toluene 10^{-4} M): 13 lines, $g_{iso} = 2.0061(1)$, $a_{N1} = 0.430$ mT, $a_{N2} = 0.225$ mT.

7.2.14. Synthesis of triformylmethane (14)

To a cooled solution of DMF ($\text{C}_3\text{H}_7\text{NO}$, 40 mL, 0.518 mol, at $\sim 0^\circ\text{C}$), POCl_3 (13.8 mL, 0.147 mol) was added drop wise over a period of 1 hour keeping the temperature below 5°C . The solution appeared initially greenish and turned at the end of the addition into pale orange. Then the ice-bath was removed and the dense mixture was left under stirring at room temperature for one hour. The bromoacetic acid was added in small portions (7.15 g, 0.051 mol) and the mixture was heated for 24 hours at 70°C . The brownish mixture was decomposed with ice/water (200 mL) and solid Na_2CO_3 was carefully added in excess (till pH ~ 8). To this dense solution, absolute ethanol was added (2 L) and the inorganic salts were filtered off. The organic filtrate was evaporated slowly and the pale yellowish residue left was neutralized with H_2SO_4 (50%, 10 mL), extracted with CHCl_3 (3×200 mL) and dried over MgSO_4 . After solvent removal, the triformylmethane was obtained as yellowish crystals that were further purified by sublimation (2.3 g, yield 45% calculated based on bromoacetic acid).

M.p. $102\text{-}103^\circ\text{C}$ (lit. M.p, 101°C). **FT-IR** (KBr) ν/cm^{-1} : 2828 (w, $\nu_{\text{C-H}}$), 2731 (m, $\nu_{\text{C-H}}$), 1699 (s, C=O), 1599(s), 1566 (s), 1561 (m), 1207 (s), 1166 (m), 826 (s), 723 (m). **$^1\text{H NMR}$** (CDCl_3 , 250 MHz, 298 K, 32 scan) δ (ppm): 9.92 (s, 1H, -CHO), 8.13 (s, 2H). **Elemental analyses**, found C 48.25, H 4.11%; $\text{C}_4\text{H}_4\text{O}_3$ (MW 100.07) required C 48.01, H 4.03%.

7.2.15. Synthesis of 4-formyl-1(H)-pyrazole (Method A) (15)

To a mixture of hydrazine-monohydrate (0.33 g, 6.6 mmol) dissolved in methanol (20 mL) a solution of HCl was added (6N, 3 mL). Separately a solution of triformylmethane **14** (0.6 g, 6 mmol) dissolved in methanol (20 mL) was prepared, and then the acidified methanolic solution of hydrazine was added drop wise very slowly over 3 hours. The solution was stirred at room temperature for other 20 hours and then was air dried. The yellowish residue dissolved in water (20 mL) was neutralised with solid NaHCO_3 . Then the crude product was extracted with ethylacetate (3×20 mL). The organic phase was collected and the solvent extracted under reduced pressure. The crude mixture was chromatographed over silica (hexane/ethylacetate

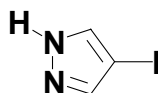
mixture, 2/1). The 4-Formyl-1(H)-pyrazole (**15**) (MW 96.09) was collected ($R_f = 0.2$) and upon drying, it gave 0.58 g of pure compounds in the form of yellowish powder very hygroscopic (yield 52%).

M.p. 83-84°C (from ethylacetate). $^1\text{H NMR}$ (250 MHz, CDCl_3 , 298 K, 16 scan) δ (ppm): 9.92 (s, 1H, 1-CHO), 8.13 (s, 2H, -CH). $^1\text{H NMR}$ (250 MHz, DMSO-d_6 , 298 K, 16 scan): δ (ppm): 13.56 (broad, s, -NH), 9.83 (s, 1H, 1-CHO), 8.47 (s, broad, 1H, -CH), 7.99 (s, broad, 1H, -CH). $^{13}\text{C NMR}$ (DMSO-d_6 , 63 MHz, 298 K, 256 scan) δ (ppm), 185.4, 139.6, 134.1, 123.8. $^{13}\text{C NMR}$ (CDCl_3 , 63 MHz, 298 K, 2000 scan) δ (ppm), 182.8, 134.6, 122.21. **FT-IR** (KBr) ν/cm^{-1} : 3176 - 2790 (strong and broad band with several components), 1689 (vs, C=O), 1650 (s), 1558(s), 1509 (s), 1413 (s), 1386 (s), 1213 - 609 (several strong absorptions). **Elemental analyses**, found C 49.96, H 4.33, N 29.00. $\text{C}_4\text{H}_4\text{N}_2\text{O}$ (96.09) required C 50.00, H 4.20, N 29.15%.

7.2.16. Synthesis of 4-formyl-1(H)-pyrazole (Method B)

The following methodology represents an alternative route to the synthesis of 4-formyl-1(H)-pyrazole. It relies on three synthetic steps: iodination of pyrazole, N-H protection, Grignard reaction followed by N-H deprotection.

Synthesis of 4-iodo-pyrazole (**16**):

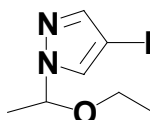


Pyrazole (3.4 g, 50 mmol) was dissolved in acetic acid (30 mL) and left under stirring. Separately, a solution containing HIO_3 (1.8 g, 10 mmol), I_2 (5.1 g, 20 mmol), H_2SO_4 (2 mL, 30%) and acetic acid (15 mL) was prepared, leading to a deep red-violet mixture. The pyrazole solution was heated up to 60°C under argon, and then the iodine mixture was slowly added, taking care that before any further addition, all the iodine was consumed. When half of the addition was completed, the rest of the iodine was dropped fully, and the pyrazole solution was left to react for 60 min. Then, a saturated solution of NaHCO_3 (15 mL) was added in order to smoothly start the quenching of the acetic acid. A saturated solution of Na_2CO_3 was finally added slowly until no evolution of CO_2 was observed and a fine white flocculate was formed. The flocculate was extracted with CHCl_3 (3 × 30 mL), the organic layer dried over MgSO_4 , filtered and left to crystallise under air. Finally 8.6 g as white needles of 4-iodo-pyrazole have been obtained (yield 88%).

M.p. 107-108°C (from CHCl_3) (literature M.p. 108.5°C). $^1\text{H NMR}$ (250 MHz, CDCl_3 , 298 K, 16 scan), δ (ppm): 9.51 (s, broad, 1H, -NH), 7.62 (s, asymmetric, 2H, 2-CH). $^1\text{H NMR}$ (250 MHz,

DMSO- d_6 , 298 K, 16 scan), δ (ppm): 13.20 (s, broad, 1H, -NH), 7.90 (s, broad, 1H, -CH), 7.62 (s, broad, 1H, -CH). ^{13}C NMR (DMSO- d_6 , 63 MHz, 256 scan), δ (ppm): 56.9, 133.6, 143.8. **FT-IR** (KBr): ν/cm^{-1} = 3114 – 2788 (m, several broad vibronic band), 1624 (m), 1537 (m), 1475 (m), 1452 (m), 1365 (s), 1328 (m), 1267 (m), 1178 (m), 1141 (m), 1033 (s), 954 (s), 937 (vs), 871 (s), 810 (vs), 609 (vs). **FD-MS** (8 kV, CHCl_3) m/z : found 194.1 (100%), requires for $\text{C}_9\text{H}_7\text{BrN}_3\text{O}$ ($\text{MW}+\text{H}^+$) 193.97. **Elemental analyses**, found C 18.40, H 1.62, N 14.32. $\text{C}_3\text{H}_3\text{N}_2\text{I}$ (193.97) required C 18.58, H 1.56, N 14.44%.

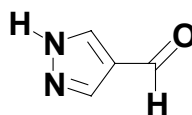
7.2.17. Synthesis of 1-(1-ethoxyethyl)-4-iodo-pyrazole (17) (Method B):



Into a 4-iodo-pyrazole **16** (3.0 g, 15.47 mmol, 1 eq.) solution, previously dissolved in 20 mL of benzene, were added 3 drops of HCl (33%) and ethylvinylether (ethoxyethene, 2.0 mL, $d = 0.754$ g/mL, 21 mmol, 1.36 eq.) and left under stirring for 6 hours at 45-50°C. A bright yellow-orange solution was slowly formed. The solution was cooled to room temperature and neutralised with a saturated solution of NaHCO_3 in water. Then the organic phase was separated and the water phase extracted with portions of benzene (3×10 mL). The collected organic portions were dried over MgSO_4 and reduced to small volume. The crude mixture was chromatographed on Al_2O_3 column using a mixture of hexane/ CHCl_3 /ethylacetate (2/4/1). The first fraction eluted ($R_f = 0.75$) was concentrated under reduced pressure (60°C, 20 mbar) and 1-(1-ethoxyethyl)-4-iodo-pyrazole (**17**) was collected highly pure (3.9 g, 4.2 mL, 3.49 mmol/mL, yield 94.7 %) as very pale yellowish oil.

^1H NMR (250 MHz, CDCl_3 , 298 K, 16 scan), δ (ppm): 7.61 (s, 1H, -CH), 7.47 (s, 1H, -CH), 5.49-5.42 (q, $^3J = 6$ Hz, 2H, -CH), 3.48-3.23 (m, 2H, - CH_2), 1.60 (d, $^3J = 6$ Hz, 3H, - CH_3), 1.11 (t, $^3J = 7$ Hz, 3H, - CH_3). ^{13}C NMR (CDCl_3 , 63 MHz, 298 K, 256 scan), δ (ppm): 14.7, 22.1, 57.3, 64.2, 87.9, 130.6, 143.7. **FD-MS** (8 kV, CH_2Cl_2) m/z : found 266.1 (100%), requires for $\text{C}_7\text{H}_{11}\text{IN}_2\text{O}$ ($\text{MW}+\text{H}^+$) 266.08.

7.2.18. Synthesis of 4-formyl-1(H)-pyrazole (18) (Method B)

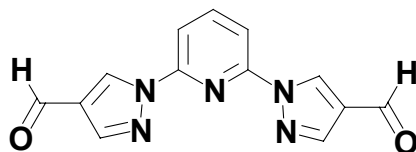


In a small round bottomed flask (20 mL) closed at the top with a rubber cup, it was placed 1-(1-ethoxyethyl)-4-iodo-pyrazole (1.5 mL, 5.2 mmol) and THF (6 mL), then the solution was cooled in ice bath (0-4°C), carefully evacuated and kept under argon. A cold solution of EtMgBr (Grignard reagent, CH₃CH₂MgBr, 1.9 mL, 5.7 mmol) was slowly added drop by drop with a syringe through the rubber septum into the cold solution of iodo-pyrazole within 5 min. A milky solution that became a solid paste was slowly formed due to the low solubility of the pyrazolyl-magnesiante derivative. The solution was then aged under stirring for 60 min. Dry DMF (0.5 mL, $\rho = 0.946$ g/mL, 6.5 mmol) was added drop by drop while keeping the temperature below 4°C, and left under stirring for 60 min. Then the ice bath was removed and left at room temperature for 30 min.

A pale yellowish solution very dense was formed. A saturated solution of NH₄Cl (5 mL) was added, left under stirring for 20 min, and the organic layer collected, while the water phase was extracted with portions of CHCl₃ (3 × 10 mL). The organic phases were collected and allowed to dry under stream of air affording a pale yellowish oil. This oil, that contained the aldehyde still protected with the ethoxyethyl-group (TLC SiO₂, ethylacetate/CHCl₃/ hexane, 1/4/2, $R_f = 0.5-0.7$), was placed in a flask together with dioxane (10 mL) and HCl (10 mL, 20% in water) and left under stirring at 60 °C overnight. The solution was neutralised with a saturated solution of K₂CO₃ in water, and the water phase extracted with ethylacetate (3 × 10 mL).

The organic phases were collected, reduced to a small volume and chromatographed over a small SiO₂ column (ethylacetate/ hexane, 1/2), and pure 4-formyl-1(H)-pyrazole **18** ($R_f = 0.2$) as been collected as very sticky yellowish powder (0.4 g, yield 80%).

7.2.19. Synthesis of 2,6-bis(4'-formylpyrazol-1'-yl)-pyridine (**19**)



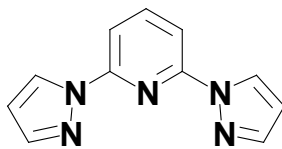
To a solution of 4-formylpyrazole **18** (1 g, 10 mmol) dissolved in dry diglyme (30 mL, b.p. 162 °C), potassium metal was added (0.4 g, 10 mmol) then the mixture was heated under argon at 70 °C under stirring until all of the potassium was reacted to form the pyrazolate-derivative. Then, 2,6-dibromopyridine (1.18 g, 5 mmol) was added in portions, and the reaction mixture was heated at 110 °C for further 72 h under argon. The solid product formed upon cooling to room temperature the reaction mixture was filtered off, washed first with cold water, and then with small portions of ethanol. Finally the residue was air dried. Recrystallisation from toluene

afforded 2,6-bis(4'-formylpyrazol-1'-yl)-pyridine **19** (0.6 g, yield 45%) as pale yellowish crystals.

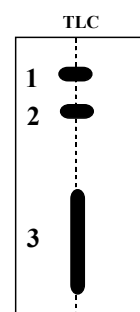
M.p. 283-284°C (from toluene). **FT-IR** (KBr): ν/cm^{-1} = 3129 (w, $\nu_{\text{C-H}}$, aromatic), 3097 (w, $\nu_{\text{C-H}}$, aromatic), 2857 (w, $\nu_{\text{C-H}}$), 1682 (s, $\nu_{\text{C=O}}$), 1610 (m), 1583 (m), 1552 (s), 1473 (s), 1409 (m), 1336 (w), 1290 (w), 1217 (m) (pyridinyl- and pyrazolyl- moieties). **$^1\text{H NMR}$** (250 MHz, DMSO- d_6 , 298 K, 32 scan): δ = 9.97 (s, 2H, 2-CHO), 9.73 (s, 2H, 2-CH), 8.34 (s, 2H, 2-CH), 8.25 (t, 1H, 3J = 7.2 Hz, -CH), 7.95 (d, 2H, 3J = 7.9 Hz, 2-CH). **$^{13}\text{C NMR}$** (63 MHz, DMSO- d_6 , 298 K, 8000 scan): δ = 185.3, 148.9, 143.0, 142.4, 133.1, 125.8, 111.3. **FD-MS** (8 kV, CH_2Cl_2): m/z (%) = found 266.90 (100%), calculated for $\text{C}_{13}\text{H}_9\text{N}_5\text{O}_2$ (267.24). **Elemental analyses**, found C 58.28, H 3.56, N, 26.10%. $\text{C}_{13}\text{H}_9\text{N}_5\text{O}_2$ (267.24) required C 58.43, H 3.39, N 26.21.

Bispyrazolylpyridine derivatives

7.2.20. Synthesis of 2,6-bis-pyrazol-1-yl-pyridine (**20**)



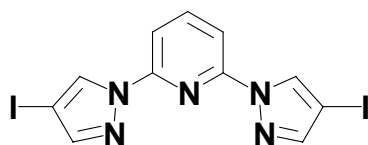
Pyrazole (5.5 g, 0.081 mol) dissolved in dry diethylene glycol dimethyl ether (diglyme, 100 mL) was stirred under argon with potassium metal (3 g, 0.0765 mol) and heated up to 50°C until all the potassium was consumed. Then, 2,6-dibromopyridine (5.9 g, 0.0248 mol) was added with a cannula and the reaction mixture heated at 140 °C for four days, keeping rigorous argon atmosphere. The mixture was cooled to room temperature and the solvent evaporated under air stream. The pale yellowish residue was pored into cold water (4°C) and stirred for 10 min and filtered. The residue left consisted of the product, the monocoupled 2-bromo-6-pyrazol-1-yl-pyridine and unreacted 2,6-di-bromopyridine. The crude mixture was purified by column chromatography using a mixture of CHCl_3 /hexane/ethylacetate (6/2/1). The 2,6-di-bromopyridine (**1**) was eluted first, then 2-bromo-6-pyrazol-1-yl-pyridine (**2**) (R_f = 0.8), and finally 2,6-bis-pyrazol-1-yl-pyridine (**3**) (R_f range 0.1 - 0.5) was collected (see TLC, SiO_2). After solvent removal and recrystallisation from methanol/ethylacetate (1/1), 2.6 g of the product were obtained as white crystalline plates (yield 49.6%, M.p. 137-138°C). The monocoupled 2-bromo-6-pyrazol-1-yl-pyridine (2.2 g, yield 39%) was recrystallised from CHCl_3 as white crystalline needles.



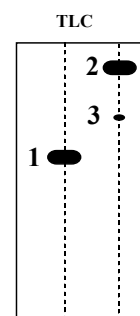
2-Bromo-6-pyrazol-1-yl-pyridine : $^1\text{H-NMR}$ (250 MHz, CDCl_3 , 298 K, 16 scan), δ (ppm): 8.52-8.50 (dd, $^3J = 3$ Hz, 0.7 Hz, 1H, -CH), 7.92-7.88 (dd, $^3J = 8.5$ Hz, 1 Hz, 1H, -CH), 7.71 (d, $^3J = 1$ Hz, 1 H, -CH), 7.63 (t, $^3J = 7.9$ Hz, 1H, -CH), 7.35-7.31 (dd, $^3J = 6.9$ Hz, 0.7 Hz, 1H, -CH), 6.45-6.43 (m, 1H, -CH). **FT-IR** (KBr): $\nu/\text{cm}^{-1} = 3160$ (w), 3082 (w), 3048 (w), 2923 (w), 2852 (w), 1588 (s), 1565 (s), 1465 (s), 1398 (s), 1208 (s), 1116 (vs), 1035 (s), 985 (s), 940 (vs), 795 (vs), 759 (vs), 651 (s), 621 (s). **FD-MS** (70 eV, CHCl_3): $m/z = 224.1$ (100%), calculated MW 224.06. **Elemental analyses**, found C 43.00, H 2.85, N 18.60%. $\text{C}_8\text{H}_6\text{N}_3\text{Br}$ (224.06) required C 42.88, H 2.70, N 18.75%.

2,6-Bis-pyrazol-1-yl-pyridine: $^1\text{H-NMR}$ (250 MHz, CDCl_3 , 298 K, 64 scan) δ (ppm): 8.55 (s, 2H, -CH), 7.95 – 7.81 (m, 3H, -CH), 7.74 (s, 2H, -CH), 6.49 – 6.47 (dd, $^3J = 1.90$ Hz, 0.95 Hz, 2H, -CH). $^{13}\text{C-NMR}$ (CDCl_3 , 63 MHz, 298 K, 256 scan), δ (ppm): 148.7, 141.1, 140.1, 125.7, 108.1, 106.7. **FT-IR** (KBr): $\nu/\text{cm}^{-1} = 3162$ (w), 3103 (w), 1607 (s), 1582 (s), 1526 (s), 1480 (vs), 1459 (s), 1391 (vs), 1334 (m), 1216 (m), 1153 (m), 1127 (m), 1127 (m), 1072 (m), 1035 (vs), 950 (s), 935 (vs), 807 (vs), 758 (vs), 607 (m). **MS-FD** (70 eV, CH_2Cl_2): $m/z = 211.3$ (100%), calculated MW 211.22. **UV/Vis**, λ_{max} (CH_2Cl_2)/ nm (ϵ , $\text{mol}^{-1} \times \text{cm}^{-1}$): 312 (7830), 272 (6600). **Elemental analyses**, found C 62.25, H 4.40, N 32.92%. $\text{C}_{11}\text{H}_9\text{N}_5$ (211.22) required C 62.55, H 4.29, N 33.16%.

7.2.21. Synthesis of 2,6-bis-(4-iodo-pyrazol-1-yl)-pyridine (21)



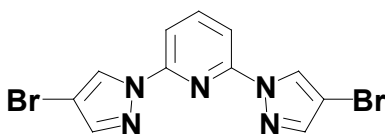
2,6-Bis-pyrazol-1-yl-pyridine **20** (0.3 g, 1.42 mmol) was charged in a round bottomed flask with acetic acid (4 mL), H_2SO_4 (30% in water, 0.5 mL) and heated up to 60°C under argon. Separately, a deep CH_3COOH solution (10 mL) containing HIO_3 (0.1 g, 0.57 mmol), I_2 (0.29 g, 1.14 mmol) and two drops of concentrated H_2SO_4 was slowly added into the 2,6-bis-pyrazol-1-yl-pyridine solution in such way that the iodine was consumed before adding the next drop. Only when half of this solution (5 mL) was added, the remaining 5 mL were dropped into the reaction mixture that appeared heterogeneous due to the presence of a white flocculate. Then, the solution was left at 60°C for further 3h under argon. After cooling to room temperature, $\text{Na}_2\text{S}_2\text{O}_3$ was added just in enough amounts to quench the pale rose solution. A $\text{NaHCO}_3/\text{Na}_2\text{CO}_3$ (1/1) water solution was added until the pH reached neutrality (pH 7-8) and the product 2,6-bis-(4-iodo-pyrazol-1-yl)-pyridine **21** was extracted with portions of CHCl_3 , air dried and recrystallised from benzene to afford white crystalline



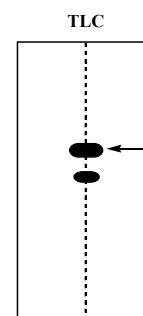
needles (0.64 g, yield 97%). The product obtained was controlled by TLC using a mixture of CHCl_3 /hexane/ethylacetate (4/2/1) as shown in the figure, where **1** represents the starting material ($R_f = 0.6$), **2** the bis-iodo derivative, and **3** a very small amount of, presumably, mono-iodo derivative since it has R_f exactly in-between with respect to **1** and **2**. When the TLC was run in presence of 5% of Et_3N , **3** was not found, therefore part of the bis-iodo-derivative seemed to decompose on silica. No starting material was left in the collected crystals. The reaction can be scaled up, upon working in more diluted solution using the following proportions: 2,6-Bis-pyrazol-1-yl-pyridine (1.2 g, 5.68 mmol) dissolved in acetic acid/ H_2O / H_2SO_4 (16 mL / 2 mL / 2 mL 30%), then HIO_3 / I_2 (0.408 g, 1.16 g) dissolved in acetic acid/ H_2SO_4 (60 mL / 2 drops) and heated at 70°C for 1 h. The yield is however lower (2.2 g, 82%).

M.p. 188 – 189°C. **MS-FD** (CHCl_3 , 70 eV) $m/z = 463.1$ (100%), calculated MW 463.02. **FT-IR** (KBr): $\nu/\text{cm}^{-1} = 3149$ (w), 3096 (w), 2874 (w), 1611 (m), 1586 (s), 1514 (m), 1466 (vs), 1422 (m), 1372 (s), 1314 (m), 1198 (m), 1145 (m), 963 (m), 950 (s), 801 (s), 601 (s). **$^1\text{H-NMR}$** (250 MHz, CDCl_3 , 298 K, 16 scan) δ (ppm): 8.57 (s, 2H, -CH), 7.96 – 7.90 (dd, $^3J = 6.95$ Hz, 1.90 Hz, 1H, -CH), 7.81 – 7.78 ($d_{\text{asymmetric}}$, $^3J = 7.27$ Hz, 2H, -CH), 7.72 (s, 2H, -CH). **$^{13}\text{C-NMR}$** (CDCl_3 , 63 MHz, 298 K, 256 scan), δ (ppm): 150.0, 148.1, 142.7, 132.4, 110.4, 61.2. **UV/Vis**, λ_{max} (CH_2Cl_2)/ nm (ϵ , $\text{mol}^{-1} \times \text{cm}^{-1}$): 262 (17020), 279 (sh, 13250), 286 (14590), 314 (23650). **Elemental analyses**, found C 28.74, H 1.65, N 14.98%. $\text{C}_{11}\text{H}_7\text{I}_2\text{N}_5$ (463.02) required C 28.53, H 1.52, N 15.13%.

7.2.22. Synthesis of 2,6-bis-(4-bromo-pyrazol-1-yl)-pyridine (**22**)



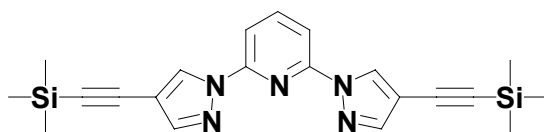
2,6-Bis-pyrazol-1-yl-pyridine **20** (1.0 g, 4.73 mmol) was charged in a round bottomed flask with acetic acid (15 mL), H_2SO_4 (10% in water, 2.0 mL) and heated up to 60°C . Separately, a solution of Br_2 ($d = 3.11$ g/mL, MW 159.82, 0.364 mL, 7.102 mmol) dissolved in acetic acid (10 mL) was slowly added into the 2,6-bis-pyrazol-1-yl-pyridine solution drop by drop. When half of this solution (5 mL) was added, a dense orange-yellowish solution was formed, showing the presence of a white flocculate. Then, the Br_2 solution was added faster, and the temperature rose up to 85°C . The mixture left under stirring for 1 h. After cooling to room temperature the mixture was quenched with NaHCO_3 and then Na_2CO_3 water



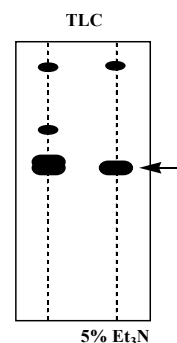
solutions until pH ~ 9 was reached. $\text{Na}_2\text{S}_2\text{O}_3$ was added just in enough amounts to destroy the Bromine left. The white precipitate formed was extracted with CHCl_3 and the solvent evaporated under reduced pressure. The 2,6-bis-(4-bromo-pyrazol-1-yl)-pyridine **22** was purified by column chromatography (SiO_2) using a mixture of ethylacetate/ CHCl_3 /hexane (1/1/6) ($R_f = 0.6$). Recrystallisation from ethylacetate/hexane mixture (1/1) afforded 1.0 g of pure product (yield 57%).

FT-IR (KBr): $\nu/\text{cm}^{-1} = 3157$ (w), 3097 (w), 2954 (w), 2923 (ws, ν_{CH} aliphatic), 2852 (w), 1735 (m), 1612 (vs), 1587 (vs), 1525 (m), 1471 (vs), 1428 (s), 1378 (vs), 1325 (s), 1273 (m), 1198 (ms), 1145 (s), 1032 (ms), 958 (vs), 848 (ms), 796 (vs), 775 (ms), 646 (m), 598 (s). **$^1\text{H-NMR}$** (250 MHz, CDCl_3 , 298 K, 16 scan) δ (ppm): 8.55 (s, 2H, -CH), 7.98 – 7.91 (dd, $^3J = 6.95$ Hz, 2.21 Hz, 1H, -CH), 7.84 – 7.80 ($d_{\text{asymmetric}}$, $^3J = 8.53$ Hz, 2H, -CH), 7.68 (s, 2H, -CH). **$^{13}\text{C-NMR}$** (CDCl_3 , 63 MHz, 298 K, 256 scan), δ (ppm): 147.6, 141.3, 140.1, 125.5, 107.8, 95.2. **MS-FD** (CHCl_3 , 70 eV) $m/z = 369.2$ (100%), calculated MW 369.01. **Elemental analyses**, found C 35.64, H 2.02, N 18.74%. $\text{C}_{11}\text{H}_7\text{Br}_2\text{N}_5$ (369.01) required C 35.80, H 1.91, N 18.98%.

7.2.23. Synthesis of 2,6-bis-(4-trimethylsilamylethynyl-pyrazol-1-yl)-pyridine (**23**)



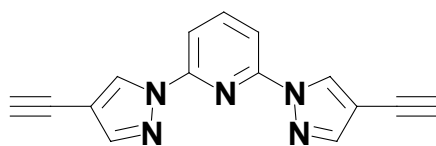
2,6-Bis-(4-iodo-pyrazol-1-yl)-pyridine **21** (0.36 g, 0.78 mmol) was charged in a round bottomed flask with anhydrous triethylamine (Et_3N , 10 mL) and dioxane (2 mL), together with dichlorobis(triphenylphosphine)-palladium(II) (55 mg, MW 701.89, 0.078 mmol), triphenylphosphine (41 mg, MW 262.28, 0.156 mmol) and CuI (20 mg, 0.1 mmol) as catalyst. The solution was further evacuated and left under argon. A solution of trimethylsilylacetylene (0.71 g/mL, MW 98.22, 0.33 mL, 2.35 mmol) was added with a syringe under argon, and the resulting mixture was heated up to 80°C for 30 min until it became dark green/black. Then, the mixture was cooled at room temperature and left further under stirring for an additional hour. The solution was partially neutralized with HCl (20% in water) (the pH > 7) and the product extracted with portions of CH_2Cl_2 (3×20 mL). The orange-yellow organic phase was collected, and it was washed further with a saturated solution of NH_4Cl . The organic phase was collected for the second time, dried over MgSO_4 , filtered from the inorganic salt and the CH_2Cl_2 evaporated under air stream affording a pale yellowish powder. The product 2,6-bis-(4-trimethylsilamylethynyl-pyrazol-1-yl)-pyridine was purified on silica column (SiO_2) using a



mixture of CHCl_3 /hexane (5/3) in presence of Et_3N (5%) ($R_f = 0.55$) since showed some hint of decomposition due to the acidity of the silica gel. After collection of the fractions containing the product (see TLC) and recrystallization from Et_2O , the 2,6-bis-(4-trimethylsilamylethynyl-pyrazol-1-yl)-pyridine **23** was obtained as fine yellowish powder (285 mg, yield 91 %). The product can be stored at room temperature for long time without decomposition.

M.p. 132 – 133°C (decompose before melting from yellow to dark brown powder). **FT-IR** (KBr): $\nu/\text{cm}^{-1} = 3139$ (w), 3056 (w), 2958 (s, ν_{CH} aliphatic), 2896 (w), 2164 (vs, $\text{C}\equiv\text{C}-\text{Si}[\text{CH}_3]_3$), 1608 (s), 1582 (s), 1554 (m), 1471 (vs), 1435 (s), 1402 (s), 1348 (m), 1249 (s), 1180 (m), 1010 (vs), 966 (m), 952 (m), 858 (vs), 800 (s), 759 (m), 657 (m). **$^1\text{H-NMR}$** (250 MHz, DMSO-d_6 , 298 K, 16 scan) δ (ppm): 9.47 (s, 2H, -CH), 8.16 (t, $^3J = 8.2$ Hz, 1H, -CH), 8.04 (s, 2H, -CH), 7.83 – 7.80 (d, $^3J = 7.9$ Hz, 2H, -CH), 0.23 (s, 18 H, $-\text{CH}_3$). **$^{13}\text{C-NMR}$** (DMSO-d_6 , 298 K, 1024 scan), δ (ppm): 148.7, 144.7, 143.0, 131.4, 128.7, 109.7, 105.1, 96.4, -0.1. **Elemental analyses** found C 62.16, H 6.42, N 17.10%. $\text{C}_{21}\text{H}_{25}\text{Si}_2\text{N}_5$ (403.63) required C 62.49, H 6.24, N 17.35%.

7.2.24. Synthesis of 2,6-bis-(4-ethynyl-pyrazol-1-yl)-pyridine (**24**)



2,6-Bis-(4-trimethylsilamylethynyl-pyrazol-1-yl)-pyridine **23** (150 mg, 0.372 mmol) was initially dissolved in MeOH (99 % dry)/ THF (5mL/5mL) and kept under argon. Then solid K_2CO_3 (52 mg, 0.376 mmol) was added, and the mixture was left under stirring in argon for 3 hours at room temperature. Initially the solution appeared bright yellow that became very dark at the end of the reaction. The organic solution was evaporated under air stream, and the brown-yellowish residue was dissolved in CH_2Cl_2 (10 mL). A saturated solution of NaHCO_3 (5 mL) was added and the organic phase extracted using portions of CH_2Cl_2 (2 × 10 mL). Collection of the organic phase followed by drying over MgSO_4 and solvent evaporation, afforded a pale yellowish residue containing the product. The residue was dissolved in the minimum amount of CH_2Cl_2 and chromatographed on alumina column (CH_2Cl_2 /hexane/ethylacetate, 3/2/0.5). The first fraction eluted contained the 2,6-bis-(4-trimethylsilamylethynyl-pyrazol-1-yl)-pyridine **24** as pale yellowish powder that was further recrystallised from ethylacetate (92 mg, yield 95%).

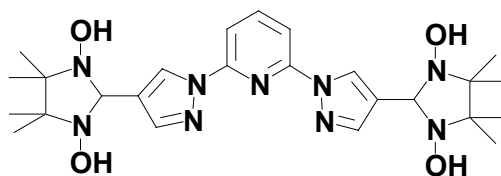
M.p. > 390°C. **FT-IR** (KBr): $\nu/\text{cm}^{-1} = 3280$ (s, $\nu \text{C}\equiv\text{C}-\text{H}$), 3157 (w), 3097 (w), 2962 (w, ν_{CH} aliphatic), 2921 (w), 1604 (s), 1581 (m), 1552 (m), 1479 (vs), 1434 (m), 1400 (m), 1346 (w),

1261 (m), 1207 (mw), 1095 (m), 1005 (s), 952 (s), 871 (m), 798 (vs), 671 (m). $^1\text{H-NMR}$ (250 MHz, DMSO- d_6 , 298 K, 16 scan) δ (ppm): 9.41 (s, 2H, -CH), 8.16 (t, $^3J = 8.2$ Hz, 1H, -CH), 8.04 (s, 2H, -CH), 7.84 – 7.81 (d, $^3J = 8.2$ Hz, 2H, -CH), 4.23 (s, 2H, $\equiv\text{-CH}$). $^{13}\text{C-NMR}$ (DMSO- d_6 , 298 K, 1024 scan), δ (ppm): 149.1, 145.2, 143.4, 132.1, 110.0, 104.8, 83.3, 75.1. **UV/Vis**, λ_{max} (CH_2Cl_2)/ nm (ϵ , $\text{mol}^{-1} \times \text{cm}^{-1}$): 263 (9810), 279 (sh, 9080), 286 (9570), 319 (12480), 351 (sh, 4100), 379 (broad, 850). **Elemental analyses** found C 69.62, H 3.66, N 26.88%. $\text{C}_{15}\text{H}_9\text{N}_5$ (259.27) required C 69.49, H 3.50, N 27.01%.

Synthesis of 2,6-bis(4'-formylpyrazol-1'-yl)-pyridine by Grignard reaction (see also 19.)

2,6-Bis-(4-iodo-pyrazol-1-yl)-pyridine (300 mg, MW 463.02, 0.648 mmol) was placed in a round bottomed Schlenk with dry THF (15 mL) evacuated and kept under argon while stirring. The solution was cooled using an ice bath (0 - 4°C). Through the rubber septum, a cold solution of Grignard reagent (EtMgBr in diethylether, 1.43 mmol, 0.47 mL) was slowly added within 10 min through with a syringe under argon. Upon addition of the Grignard reagent, the reaction mixture became slowly milky and pale rose after aging for 90 min (temperature should not rise above 4°C). Then, dry DMF (0.12 mL, 1.6 mmol) was added, and left for 60 min at 4°C. The ice bath was removed and the solution was left to warm up to room temperature. A creamy solution was obtained showing the presence of a fine precipitate. The solvent (THF) was removed and the residue washed with a solution of EDTA in water (10 %) and filtered. The pale yellowish residue left that was further washed, first with cold portions of acetone (2 × 2 mL) and then CH_2Cl_2 (2 × 2 mL). A fine yellowish powder of 2,6-bis(4'-formylpyrazol-1'-yl)-pyridine was finally obtained (125 mg, yield 72 %).

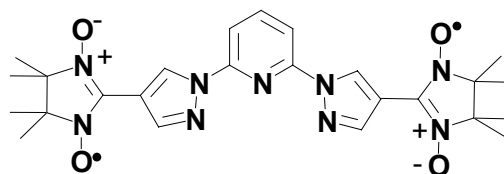
7.2.25. Synthesis of 2,6-bis[4'-(1,3-dihydroxy-4,4,5,5-tetramethylimidazolidin-2-yl)pyrazol-1'-yl]-pyridine (25)



A mixture of 2,6-bis(4'-formylpyrazol-1'-yl)-pyridine **19** (300 mg, 1.12 mmol) and 2,3-bis(hydroxylamino)-2,3-dimethylbutane **6** (600 mg, 4 mmol) in dioxan (40 mL) was stirred under argon for 10 days. The solvent was removed under reduced pressure and the solid product was collected, washed with water, ethanol and air dried to afford 265 mg of crude 2,6-bis[4'-(1,3-dihydroxy-4,4,5,5-tetramethylimidazolidin-2-yl)pyrazol-1'-yl]-pyridine **26** that was subjected to the oxidation step without further purification (yield of the crude 42%).

M.p. 253-254°C (from ethanol). **FT-IR** (KBr): ν/cm^{-1} = 3215 (s, broad, ν_{OH}), 3121 (s, $\nu_{\text{C-H}}$, aromatic), 2977 (s, $\nu_{\text{C-H}}$), 2932 (s, $\nu_{\text{C-H}}$), 1620 (s), 1472 (s), 1405 (s), 1320 (m), 1207 (m) (pyridinyl- and pyrazolyl- moieties). **$^1\text{H NMR}$** (250 MHz, DMSO- d_6 , 298 K, 32 scan): δ = 8.85 (s, 2H, 2-CH), 8.17 (t, 3J = 2.8 Hz, 1H, -CH), 8.0 (s, 4H, 4-OH), 7.86 (s, 2H, 2-CH), 7.82 (d, 3J = 8.2 Hz, 2H, 2-CH), 4.75 (s, 2H, 2-CH imidazolidyn), 1.15 (d, 3J = 8.4 Hz, 24H, 8- CH_3). **$^{13}\text{C NMR}$** (63 MHz, DMSO- d_6 , 298 K, 6000 scan) δ = 149.8, 142.7, 141.5, 126.7, 126.0, 108.5, 83.1, 66.2, 24.0, 17.5. **Elemental analyses**, found C 52.96, H 7.44, N 22.10%. $\text{C}_{25}\text{H}_{37}\text{N}_9\text{O}_4 \times 2 \text{H}_2\text{O}$ (563.65) required C 53.27, H 7.33, N 22.37.

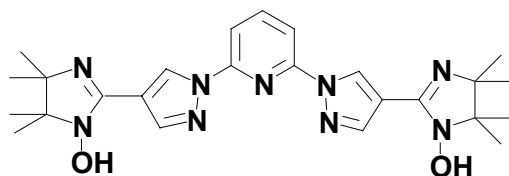
7.2.26. Synthesis of 2,6-bis[4'-(3-oxide-1-oxyl-4,4,5,5-tetramethylimidazolin-2-yl)pyrazol-1'-yl]-pyridine (26)



The compound **26** (200 mg, 0.38 mmol) dissolved in chloroform (30 mL) was oxidized under phase transfer conditions with NaIO_4 (400 mg, 1.85 mmol), previously dissolved in water (20 mL), during 30 min to afford finally a deep blue organic solution. The organic phase was collected and evaporated under air. The bluish residue was dissolved in acetone (3 mL) and chromatographed on SiO_2 column using mixture of acetone/petroleum ether (2/8) as eluents to afford the biradical product **27** as blue solid (R_f = 0.34) that was further recrystallised from CHCl_3 (54 mg, yield 27 %).

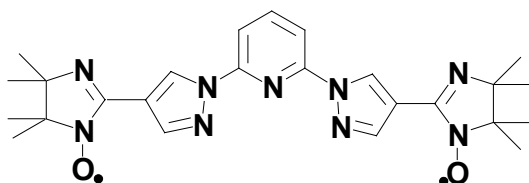
M.p. 220-221 °C (from CHCl_3). **FT-IR** (KBr): ν/cm^{-1} = 3164 (w, $\nu_{\text{C-H}}$, aromatic), 2984 (w, $\nu_{\text{C-H}}$), 2936 (w, $\nu_{\text{C-H}}$), 1596 (s), 1470 (s), 1429 (s), 1403 (s), 1359 (s, $\nu_{\text{N-O}}$), 1312 (m), 1190 (m) (pyridinyl- and pyrazolyl- moieties). **UV/Vis** (toluene): λ_{max} nm (ϵ , $\text{M}^{-1} \times \text{cm}^{-1}$) 668 (1460), 610 (1696) 563 (930), 518 (328), 375 (16960), 328 (24850), 323 (31220). **FAB-MS** (NBA matrix): m/z (%) = found 521.30 (100%) $[\text{M}+\text{H}]^+$, calculated for $\text{C}_{25}\text{H}_{31}\text{N}_9\text{O}_4$ (521.57). **Elemental analysis**, found C 57.34, H 5.72, N, 23.94%. $\text{C}_{25}\text{H}_{31}\text{N}_9\text{O}_4$ (521.57) required C 57.57, H 5.99, N 24.17%. **EPR** (298 K, 9.403341GHz, 10^{-4} M toluene): 9 lines, g_{iso} = 2.0065(1), $a_{\text{N}}/2$ = 0.380 mT.

7.2.27. Synthesis of 2,6-bis[4-(1-hydroxy-4,4,5,5-tetramethylimidazolin-2-yl)pyrazolyl]-pyridine (27)



A mixture of 2,6-bis-(4'-formylpyrazol-1'-yl)pyridine **19** (260 mg, 1 mmol) and 2,3-bis(hydroxylamino)-2,3-dimethylbutane **6** (300 mg, 2.02 mmol) in dioxan (40 mL) was heated at 60 °C under argon for 7 days. The solvent was removed under reduced pressure, and the solid product was collected, washed with water, ethanol and dried under nitrogen stream to give the highly air sensitive compound 2,6-bis[4-(1-hydroxy-4,4,5,5-tetramethylimidazolin-2-yl)pyrazolyl]pyridine **28** (225 mg, crude yield 46 %) that was subjected for the next step without further purification. **FT-IR** (KBr): ν/cm^{-1} = 3225 (broad, -OH), 3121 (s, $\nu_{\text{C-H}}$, aromatic), 2977 (s, $\nu_{\text{C-H}}$), 2932 (s, $\nu_{\text{C-H}}$), 1620 (s), 1472 (s), 1405 (s), 1320 (s), 1207 (m) (pyridinyl- and pyrazolyl- moieties). **Elemental analyses**, found C 60.78, H 6.52, N 25.34%. $\text{C}_{25}\text{H}_{33}\text{N}_9\text{O}_2$ (491.59) required C 61.08, H 6.77, N 25.64%.

7.2.28. Synthesis of 2,6-bis[4-(1-oxyl-3-4,4,5,5-tetramethylimidazolin-2-yl)pyrazolyl]pyridine (**28**)

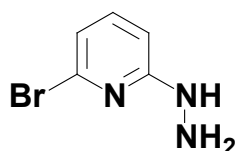


Compound **28** (200 mg, 0.41 mmol) was oxidized under phase transfer condition (H_2O / CHCl_3 , 20/40 mL) mixture using NaIO_4 (400 mg, 1.87 mmol) for 30 min; within this period of time, the color of the organic layer gradually turned to deep orange. The organic phase was collected and evaporated under reduced pressure then the residue was dissolved in 5 mL of acetone and chromatographed over SiO_2 column using acetone and petroleum ether as eluents (2/8, low boiling point, 30-40°C, R_f = 0.46). After solvent removal, pure 2,6-bis[4-(1-oxyl-3-4,4,5,5-tetramethylimidazolin-2-yl)pyrazolyl]pyridine **29** was collected as orange hygroscopic solid (105 mg, yield 51%). The solid was then recrystallised from CH_2Cl_2 .

M.p. 254-255 °C (from CH_2Cl_2). **FT-IR** (KBr): ν/cm^{-1} = 3142 (w, $\nu_{\text{C-H}}$, aromatic), 2976 (m, $\nu_{\text{C-H}}$), 2926 (w, $\nu_{\text{C-H}}$), 1599 (s, $\nu_{\text{C=N}}$), 1585 (m), 1470 (s), 1439 (m), 1405 (m), 1289 (w), 1257 (w), 1198 (w) (pyridinyl- and pyrazolyl- moieties). **UV/Vis** (toluene): λ_{max} nm (ϵ , $\text{M}^{-1} \times \text{cm}^{-1}$) = 552 (90), 500 (850), 468 (1400), 442 (1285), 415 (910), 315 (23850). **Elemental analyses**, found C 58.96, H 6.66, N 24.68%. $\text{C}_{25}\text{H}_{31}\text{N}_9\text{O}_2 \times \text{H}_2\text{O}$ (507.59) required C 59.16, H 6.55, N 24.84%.

EPR (298 K, 9.402690 GHz, 10^{-4} M toluene): 13 lines, $g_{\text{iso}} = 2.0060(1)$, $a_{\text{N}1}/2 = 0.450$ m, $a_{\text{N}2}/2 = 0.210$ mT.

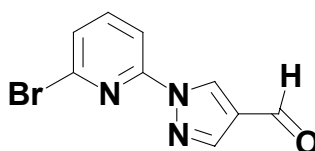
7.2.29. Synthesis of 2-bromo-6-hydrazinopyridine (29)



2,6-Dibromopyridine (1.44 g, 6.1 mmol) was charged in a round-bottomed flask together with an excess of hydrazine-monohydrate (1.61 g, 32.2 mmol) and butanol (100 mL) and the mixture was stirred under reflux for 5 hours. Then, the solvent was evaporated slowly under air and yellowish crystals were obtained. The crystals were initially washed with small portions of cold water (3×10 mL) then the solid was dissolved in CHCl_3 . The solution was chromatographed on SiO_2 column ($\text{CHCl}_3/\text{Hexane}$, 1/2). The unreacted 2,6-dibromopyridine was eluted first ($R_f = 0.41$) then ethylacetate (EtOAc) was added, and pure 2-bromo-6-hydrazinopyridine was collected as pale yellowish needles after solvent evaporation (0.72 g, yield 63%). Starting from 3 g of 2,6-dibromopyridine (12.66 mmol) and 3.35 g of hydrazine monohydrate (66.92 mmol) it was obtained 1.36 g of 2-bromo-6-hydrazinopyridine **30** (7.23 mmol, yield 57%).

M.p. 117-118°C (from ethylacetate). **FT-IR** (KBr pellet, ν/cm^{-1}): 3307 (m), 3104 (w), 3029 (m), 1564 (s), 1546 (s), 1513 (s), 1385 (s), 1167 (s), 1134 (s), 1093 (s), 980 (s), 787 (s), 742 (s), 650 (s). **MS-FD** (8 kV, CH_2Cl_2) m/z : found 188.1 (100%), $\text{C}_5\text{H}_6\text{BrN}_3$ requires MW 188.03. **^1H NMR** (250 MHz, CDCl_3 , 298 K, 32 scan) δ (ppm): 7.20 (m, -CH), 6.74 (d, $^3J = 7.58$ Hz, -CH), 6.61 (d, $^3J = 8.2$ Hz, -CH), 6.42 (s, br, -NH-), 3.47 (s, br, - NH_2). **^{13}C NMR** (DMSO-d_6 , 63 MHz, 298 K, 1024 scan) δ (ppm): 162.3, 139.6, 139.2, 114.4, 104.5. **UV/vis**, λ_{max} (CH_2Cl_2)/ nm (ϵ , $\text{mol}^{-1} \times \text{cm}^{-1}$): 278 (4740), 284 (sh, 3715). **Elemental analyses**, found C 31.77, H 3.32, N, 22.21%. $\text{C}_5\text{H}_6\text{BrN}_3$ required C 31.94, H 3.22, N 22.35%.

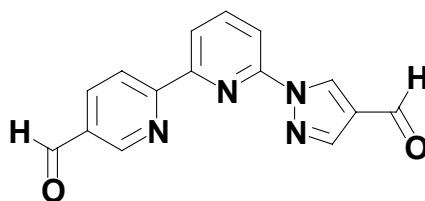
7.2.30. Synthesis of 6-bromo-2-[4'-formylpyrazol-1'-yl]-pyridine (30)



To a mixture of 2-bromo-6-hydrazinopyridine **30** (2.0 g, 10.6 mmol) and triformyl methane **14** (1.06 g, 10.6 mmol) in methanol (60 ml), a solution of HCl (3.0 mL, 6 N) was added, and then stirred for 1 day at room temperature. The solvent was removed under reduced pressure and the residue was neutralized with aqueous Na₂CO₃ solution. The yellowish solid product was filtered off and dissolved in CHCl₃. The mixture was chromatographed on silica gel using mixture of CHCl₃/Hexane/Ethylacetate (1/3/1). The yellowish fraction eluted (*R_f* = 0.67) was collected and upon air-drying it gave pure 6-bromo-2-[4'-formylpyrazol-1'-yl]-pyridine **31** (1.87 g, yield 70%) as pale yellowish powder that strongly retains water.

M.p. 141-142°C. **FT-IR** (KBr pellet, v/cm⁻¹) 3110 (w, ν_{C-H}), 2865 (m, ν_{C-Hal}), 1668 (s, C=O), 1583(s), 1566 (s), 1544 (s), 1454 (s), 1363 (s), 1211 (s) (pyridine- and pyrazolyl- moieties). **¹H NMR** (DMSO-d₆, 250 MHz, 298 K, 16 scan) δ (ppm), 9.96 (s, 1H, -CHO), 9.26 (s, 1H, -CH), 8.31 δ (s, 1H, -CH), 7.98 δ (m, 2H, 2-CH), 7.73 δ (m, 1H, -CH). **¹³C NMR** (DMSO-d₆, 63 MHz, 298 K, 1024 scan) δ (ppm), 185.4, 149.9, 142.8, 141.5, 139.5, 133.0, 127.1, 125.6, 112.0. **FD-MS** (8 kV, CH₂Cl₂) m/z: found 253.1 (100%), required for C₉H₇BrN₃O (MW+H⁺) 253.08. **UV/Vis**, λ_{max} (CH₂Cl₂)/ nm (ε, mol⁻¹ × cm⁻¹): 261 (sh, 11340), 265 (11730), 299 (16350), 338 (broad, 685). **Elemental analyses**, found C 39.82, H 3.30, N 15.20. C₉H₆BrN₃O × H₂O required C 40.02, H 2.99, N 15.50%.

7.2.31. Synthesis of 6'-(4-formyl-pyrazol-1-yl)-[2,2']-bipyridinyl-5-carbaldehyde (**31**)

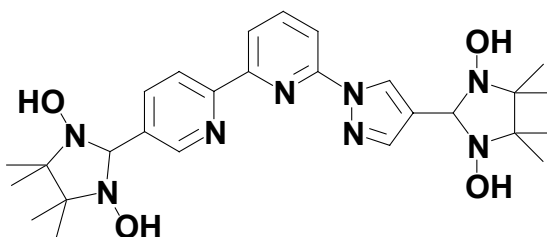


2-Tributylstannyl-5-[1,3]dioxolan-2-yl-pyridine **3** (3.8 ml, 4.7 mmol) was placed in a two-necked round bottomed flask together with the 6-bromo-2-[4'-formylpyrazol-1'-yl]pyridine **30** (720 mg, 2.8 mmol). The mixture was degassed and kept under rigorous argon atmosphere. Then dry and degassed toluene (30 mL) was added with a syringe together with dichlorobis(triphenylphosphine)-palladium(II) (296 mg, 0.42 mmol), triphenylphosphine (220 mg, 0.84 mmol) and catalytically amount of CuI (20 mg, 0.1 mmol). The solution was then heated to reflux in argon atmosphere under stirring for 60 hours. A dark solution was formed and it was filtered from the inorganic salts, collected and washed with a saturated solution of ammonium-chloride (20 mL). The organic mixture was shaken vigorously in a separator funnel. The aqueous layer was extracted with toluene (2 × 15 mL) and the combined dark

organic layers were collected and the solvent evaporated under reduced pressure. The oily solution was treated with HCl (20 mL, 6N) and heated to reflux for 8 hours under stirring; this procedure ensured for the complete hydrolysis of the dioxolane. Basification with saturated solution of potassium carbonate K_2CO_3 afforded the formation of a yellowish flocculate at pH 8 that consists of the product **31**. The product was extracted with dichloromethane (3 × 20 mL). The organic layers were collected and the solvent evaporated to small volume under reduced pressure to afford a yellowish powder. The product was further washed with small portions of light petroleum ether (2 × 10 ml) (b.p. 30 - 40°C) and 4'',5'-diformyl-6-(pyrazol-1''-yl)-2,2'-bipyridine **31** was collected analytically pure as yellowish powder that strongly retains water (360 mg, yield 46 %).

M.p. 221-222°C. **FT-IR** (KBr pellet, ν/cm^{-1}) 3128 (w, ν_{C-H}), 2946 (w, ν_{C-H}), 2915 (w, ν_{C-H}), 2848 (w, ν_{C-H}), 1689 (s and asymmetric, C=O), 1592(s), 1546 (s), 1463 (s), 1454 (s), 1363 (s), 1211 (s) (pyridine- and pyrazolyl- moieties). **1H NMR** (DMSO- d_6 , 250 MHz, 298 K, 64 scan) δ (ppm), 10.20 (s, 1H, -CHO), 10.01 (s, 1H, -CHO), 9.70 (s, 1H, -CH), 9.22 (s, 1H, CH), 8.88 (d, $^3J = 8.16$ Hz, 1H, -CH), 8.47 (m, 2H, 2-CH), 8.36 (s, 1H, -CH), 8.26 (t, $^3J = 7.85$ Hz, 1H, -CH), 8.11 (d, $^3J = 7.84$ Hz, 1H, -CH). **^{13}C NMR** (DMSO- d_6 , 63 MHz, 298 K, 8000scan) δ (ppm): 192.1, 185.3, 158.0, 153.1, 151.4, 149.7, 141.6, 141.4, 137.40, 132.6, 131.5, 125.5, 121.4, 120.6, 114.0. **MS-FD** (8 kV, CH_2Cl_2) m/z: found 278.30 (100%), $C_{15}H_{10}N_4O_2$ required (MW. 278.27). **Elemental analyses**, found C 60.50; H, 4.23; N, 18.67%. $C_{15}H_{10}N_4O_2 \times H_2O$ required C 60.81, H 4.08, N 18.91%. **UV/Vis** (DMSO) λ_{max} (ϵ , $mol^{-1} \times cm^{-1}$) 320 nm (17230).

7.2.32. Synthesis of 4'',5'-bis[1,3-dihydroxy-4,4,5,5-tetramethylimidazolidin-2-yl]-6-(pyrazol-1''-yl)-2,2'-bipyridine (**32**)

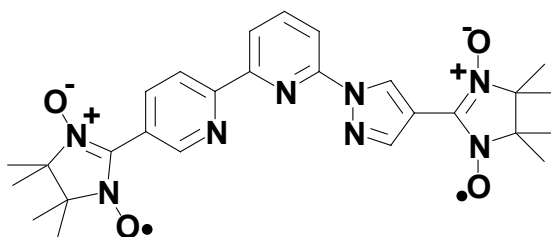


4'',5'-Diformyl-6-(pyrazol-1''-yl)-2,2'-bipyridine (**31**, 180 mg, 0.65 mmol) was placed in a round bottomed flask together with 2,3-bis-hydroxylamino-2,3-dimethylbutane **6** (337 mg, 2.27 mmol). A mixture of 1,4-dioxane and trichloromethane (10 mL/10 mL) was used as reaction solvents due to the low solubility of **31**. The mixture was then stirred for 7 days under argon at room temperature. The solution appeared yellowish-orange with no hint of precipitate formation. Afterwards the mixture was dried under air and a pale brownish powder was obtained. This powder was washed on filter paper with small portions of cold water (2 × 5 mL)

and cold light petroleum ether (2 × 5 mL). Finally 255 mg of light brown powder consisting on crude 4'',5'-bis[1,3-dihydroxy-4,4,5,5-tetramethylimidazolidin-2-yl]-6-(pyrazol-1''-yl)-2,2'-bipyridine **32** was obtained (yield of the crude 73%). A complex ¹H-NMR (250 MHz, DMSO-*d*₆) indicated that the residue was a mixture of the desired product **32**, plus the excess of 2,3-bis-hydroxylamino-2,3-dimethylbutane and its decomposition products (oxime), nevertheless, it was judged adequate for the next oxidation step.

M.p. 213-214°C. **FT-IR** (KBr pellet, ν/cm^{-1}) 3257 (s, broad, -OH), 2977 (s, $\nu_{\text{C-Hal}}$), 2925 (s, $\nu_{\text{C-Hal}}$), 2859 (s, $\nu_{\text{C-Hal}}$), 1594 (s), 1563 (m), 1465 (s) (pyridyl and pyrazolyl-moieties), 1386 (s), 1141 (s and wide).

7.2.33. Synthesis of 4'',5'-bis[3-oxide-1-oxyl-4,4,5,5-tetramethylimidazolin-2-yl]-6-(pyrazol-1''-yl)-2,2'-bipyridine (**33**)

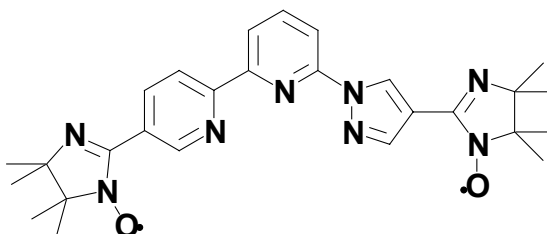


The crude 4'',5'-bis[1,3-dihydroxy-4,4,5,5-tetramethylimidazolidin-2-yl]-6-(pyrazol-1''-yl)-2,2'-bipyridine **32** (130 mg, 0.24 mmol) was charged into a small flask together with CHCl_3 (15 mL), degassed and kept under argon while stirring at room temperature. Separately, a solution of NaIO_4 (128 mg, 0.6 mmol) dissolved in water (15 mL) was degassed and saturated by argon exchange; then it was added to the solution of the radical precursor by using a syringe under argon. After 20 min a deep blue-violet solution was obtained. The organic layer was extracted by using portions of CHCl_3 (3 × 10 mL). The organic solution was evaporated by continuous argon bubbling to a small volume. The mixture was separated by column chromatography (Al_2O_3 , acetone/light petroleum ether, 1/3). The 4'',5'-bis[3-oxide-1-oxyl-4,4,5,5-tetramethylimidazolin-2-yl]-6-(pyrazol-1''-yl)-2,2'-bipyridine **33** ($R_f = 0.37$) was obtained after solvent evaporation as deep blue powder in poor yield (12 mg, yield 9 %).

M.p. 209 – 210°C (from acetone). **FT-IR** (KBr pellet, ν/cm^{-1}): 3174 (w, $\nu_{\text{C-H}}$), 3097 (w, $\nu_{\text{C-H}}$), 2983 (m, $\nu_{\text{C-H}}$), 2937 (w, $\nu_{\text{C-H}}$), 2869 (w, $\nu_{\text{C-H}}$), 1592 (s), 1548 (m), 1462 (s), 1423 (m), 1387 (m), 1352 (s, N-O), 1217 (m). **UV/Vis**, λ_{max} (toluene)/ nm (ϵ , $\text{mol}^{-1} \times \text{cm}^{-1}$): 321 (33624), 336 (35017), 350 (31867), 373 (17510), 392 (10685), 470 (163), 518 (260), 564 (634), 610 (1114), 666 (1004), 746 (70). **Elemental analyses**, found C 60.64, H 6.01, N 20.84 (%). $\text{C}_{27}\text{H}_{32}\text{N}_8\text{O}_4$

(532.59 MW) required C 60.89, H 6.06, N 21.04%. **EPR** (298 K, 9.400200 GHz, 10^{-4} M toluene): 9 lines, $g_{\text{iso}} = 2.0066(1)$, $a_{\text{N}} = 0.37$ mT.

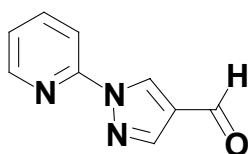
7.2.34. Synthesis of 4'',5'-bis[1-oxyl-4,4,5,5-tetramethylimidazolin-2-yl]-6-(pyrazol-1''-yl)-2,2'-bipyridine (**34**)



The compound **33** (125 mg, 0.23 mmol) was charged into a small flask and dissolved in CHCl_3 (15 mL). Then a solution of NaIO_4 (197 mg, 0.92 mmol) dissolved in water (15 mL) was added. After 40 min a deep orange-red solution was obtained. The organic layer was extracted by using portions of CHCl_3 (3×10 mL). The organic solution was evaporated under reduced pressure till small volume (~ 1 mL). The mixture was separated by column chromatography (Al_2O_3 , acetone/hexane, 2/3) and 4'',5'-bis[1-oxyl-4,4,5,5-tetramethylimidazolin-2-yl]-6-(pyrazol-1''-yl)-2,2'-bipyridine **34** ($R_f = 0.42$) was obtained after solvent evaporation as fine orange-red powder, that was further recrystallised from CHCl_3 (21 mg, yield 18%).

M.p. 205 – 206°C (from CHCl_3). **FT-IR** (KBr pellet, v/cm^{-1}): 3160 (w, $\text{v}_{\text{C-H}}$), 3104 (w, $\text{v}_{\text{C-H}}$), 2977 (m, $\text{v}_{\text{C-H}}$), 2929 (m, $\text{v}_{\text{C-H}}$), 2865 (m, $\text{v}_{\text{C-H}}$), 1595 (s), 1458 (vs), 1409 (m), 1371 (s, N-O), 1267 (m) 1157 (m) (pyridine and pyrazolyl moieties). **UV/Vis**, λ_{max} (toluene)/nm (ϵ , $\text{mol}^{-1} \times \text{cm}^{-1}$): 321 (26100), 417 (791), 442 (997), 467 (1082), 496 (773), 536 (284). **Elemental analyses**, found C 61.74, H 6.10, N 20.97%. $\text{C}_{27}\text{H}_{32}\text{N}_8\text{O}_4 \times \frac{1}{3} \text{CHCl}_3$ required C 62.07, H 6.23, N 21.19. **EPR** (298 K, 9.400210 GHz, 10^{-4} M toluene): 13 lines, $g_{\text{iso}} = 2.0061(1)$, $a_{\text{N}1} = 0.45$ mT, $a_{\text{N}2} = 0.21$ mT.

7.2.35. Synthesis of 2-(4-formylpyrazolyl)pyridine (**35**)

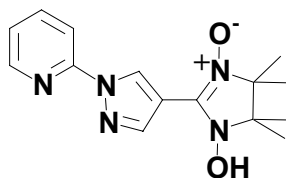


To a mixture of 2-hydrazinopyridine (0.55 g, 5 mmol) and triformyl methane **14** (0.5 g, 5 mmol) in methanol (50 mL), it was added HCl (1 mL, 6 N) and then stirred for 22 hours at room

temperature. The solvent was removed under reduced pressure and the residue was neutralised with aqueous NaHCO_3 solution. The solid product **35** was filtered off and recrystallised from ethanol to afford pale yellow crystals (0.66 g, yield 76%).

M.p 96-97 °C (from ethanol). **FT-IR**(KBr) ν/cm^{-1} = 3105 (w), 3062 (w), 2855 (w), 1672 (s, $\nu_{\text{C=O}}$) 1596 (s), 1549 (s), 1476 (s), 1455 (s), 1396 (m), 1207 (s), 1056 (m), 950 (s), 885 (m), 776 (s), 749 (s), 719 (m), 655 (m), 611 (m). **^1H NMR** (CDCl_3 , 250 MHz) δ (ppm): 7.2-7.26 (m, 1H, CH), 7.82-7.85 (m, 1H, -CH), 7.9-7.95 (d, 1H, J = 8.2 Hz, -CH), 8.1 (s, 1H, CH), 8.39-8.41(d, 1H, J =4.7 Hz, -CH), 9.0 (s, 1H, -CH), 9.93 (s, 1H, -CHO). **^{13}C NMR** (DMSO-d_6 , 63 MHz) δ (ppm): 113.3, 123.1, 125.8, 131.3, 139.4, 141.8, 148.7, 150.8, 184.5 **Elemental analyses**, found C 56.23, H 4.86, N 21.77%. $\text{C}_9\text{H}_7\text{N}_3\text{O} \times \text{H}_2\text{O}$ required C 56.54, H 4.74, N 21.98%.

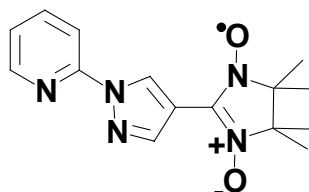
7.2.36. Synthesis of 2[4-(1-hydroxy-3-oxyl-4,4,5,5-tetramethylimidazolin-2-yl)pyrazolyl]-pyridine (**36**)



A mixture of **35** (0.5 g, 3 mmol) and 2,3-bis(hydroxylamino)- 2,3-dimethylbutane **6** (0.45 g, 3 mmol) was dissolved in methanol/chloroform mixture (3/1, 40 mL) and heated at 60 °C under argon for 48 hours. The precipitated product was filtered off, washed several times with methanol and air dried to afford 270 mg (yield 30 %) of the yellowish product which was identified as the highly air sensitive derivative **36**.

M.p. 195-196 °C (from methanol, before melting the colour changes to red-brown). **FT-IR** (KBr), ν/cm^{-1} = 3160 (broad, ν_{OH}), 3091(m), 3056 (m), 2991 (m), 2935 (m), 2632 (broad), 2505 (m), 1618 (m), 1595 (s), 1575 (s), 1527 (s), 1475 (s), 1457 (s), 1407 (m), 1384 (m), 1292 (s), 1230 (s), 1207 (s), 1132 (s), 1054 (m), 1020 (s), 998 (s), 954 (s), 879 (m), 846 (w), 782 (s). **^1H NMR** (DMSO-d_6 , 250 MHz) δ (ppm): 1.25- 1.3 (d, 12H, 4- CH_3), 7.4-7.5(m, 1H, -CH), 8.0-8.15 (m, 2H, 2-CH), 8.6-8.63 (d, 1H, -CH), 9.45 (s, 1H, -OH), 9.65 (s, 1H, -CH). **Elemental analyses**, found C 59.40, H 6.55, N 22.93%. $\text{C}_{15}\text{H}_{19}\text{N}_5\text{O}_2$ (301.34) required C 59.79, H 6.36, N 23.24%.

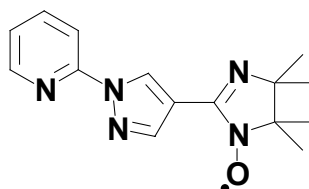
7.2.37. Synthesis of 2[4-(1-oxide-3-oxyl-4,4,5,5-tetramethylimidazolin-2-yl)pyrazolyl]-pyridine (37)



Compound **36** (200 mg, 0.66 mmol) was oxidized under phase transfer condition with NaIO_4 (150 mg, 1 mmol) using water/chloroform mixture (1/1) during 30 min. The organic phase became deep blue. After separation and evaporation of the organic phase, the product was chromatographed on SiO_2 using a mixture of acetone /petroleum ether (30-40 °C, 3/7, $R_f = 0.6$) as eluents to finally afford the radical product **37** as blue solid (120 mg, yield 60%).

M.p. 132-133 °C (from acetone). **FT-IR** (KBr) $\nu/\text{cm}^{-1} = 3170$ (w), 3128 (w), 3064 (w), 2991 (m), 2929 (w), 1593 (s), 1577 ($\nu_{\text{C}=\text{N}}$, s), 1462 (s), 1431 (m), 1415 (m), 1392 (w), 1357 ($\nu_{\text{N}=\text{O}}$, s); 1325 (m), 1267 (w), 1219 (w), 1182 (s), 1136 (m), 1093 (w), 1051 (w), 1007 (m), 955 (m), 870 (w), 777 (m), 667 (m). **UV/Vis** (toluene) λ_{max} (ϵ , $\text{M}^{-1} \times \text{cm}^{-1}$) 295 (18970), 312 (sh, 13470), 351 (6580), 368 (11100), 513 (152), 558 (460), 607 (870), 664 (785). **Elemental analyses**, found C 53.62, H 6.60, N 20.78%. $\text{C}_{15}\text{H}_{18}\text{N}_5\text{O}_2$ (300.34) $\times 2 \text{H}_2\text{O}$ required C 53.56, H 6.59, N 20.82%. **EPR** (298 K, 9.399628 GHz, toluene, 10^{-4}M): 5 lines, $g_{\text{iso}} = 2.0065(1)$, $a_{\text{N}} = 0.750 \text{ mT}$, L/G = 1/3.

7.2.38. Synthesis of 2[4-(1-oxyl-4,4,5,5-tetramethylimidazolin-2-yl)pyrazolyl]-pyridine (38)

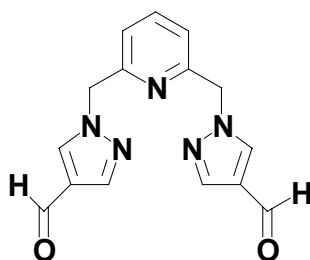


Despite the sensitivity of compound **36** (the powder gets bluish on air exposition) it appeared surprisingly hard to over-oxidize the radical **37** into the imino nitroxide monoradical **38** (with NaIO_4). Therefore as oxidizing agent it was used a solution of NaNO_2 (20 mg, 0.29 mmol) dissolved in acidified water solution (10 mL H_2O , 3 drops of HCl 33%). The compound **37** (70 mg, 0.23 mmol) was initially dissolved in chloroform (10 mL) and the oxidising reagent was

added under stirring. The organic phase became reddish very fast (~ 1 min). After separation and evaporation of the organic phase, the product was chromatographed on SiO₂ using a mixture of acetone /petroleum ether (30-40 °C, 1/2, *R_f* = 0.8) as eluents, to finally afford the radical product **38** as orange solid (33 mg, yield 50%).

FT-IR (KBr) ν/cm^{-1} = 3074 (w), 2968 (ms), 2923 (m), 2860 (m), 1594 (m), 1546 (s), 1431 (vs), 1371 ($\nu_{\text{N-O}}$, s) 1294 (s), 1126 (s), 1024 (w), 858 (w), 802 (s), 765 (m). **UV/Vis** (toluene) λ_{max} (ϵ , $\text{M}^{-1} \times \text{cm}^{-1}$) 321 (sh, 2550), 415 (487), 442 (705), 469 (768), 500 (467), 552 (50). **Elemental analyses**, found C 63.01, H 6.11, N 24.32%. C₁₅H₁₈N₅O (284.34) required C 63.36, H 6.38, N 24.63%. **EPR** (298 K, 9.400113 GHz, toluene, 10⁻⁴ M): 7 lines, $g_{\text{iso}} = 2.0060(1)$, $a_{\text{N1}} = 0.440$ mT and $a_{\text{N2}} = 0.885$ mT, Lorentzian line.

7.2.39. Synthesis of 2,6-bis(4-formylpyrazolylmethyl)pyridine (**39**)

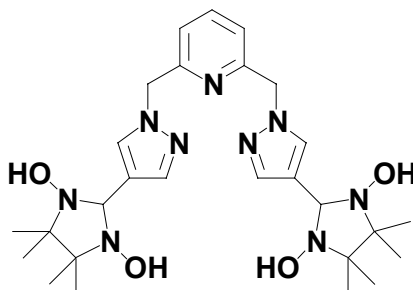


To a solution of 4-formylpyrazole **15** (1 g, 10.4 mmol) in 30 mL dry THF, NaH was added (0.24 g, 10 mmol), then the mixture was heated under Argon at 50 °C while stirring for 20 min. Then 1.32 g (5 mmol) of 2,6-dibromomethylpyridine were added and the reaction mixture was heated up to 60 °C for 3 h. The reaction mixture was cooled to room temperature and the solvent was removed under reduced pressure. The pale yellowish residue was poured into water/ice mixture. All the inorganic salts were solubilized in the water phase and a white solid was collected. Recrystallization from ethanol/water solution (1/1) afforded 0.8 g of 2,6-bis(4-formylpyrazolylmethyl)pyridine **39** (yield 54 %).

M.p. 106 –107 °C (from water). **FT-IR** (KBr) ν/cm^{-1} = 3108 (m), 3061 (w), 2969 (w), 2845 (w), 2789 (w), 1683 ($\nu_{\text{C=O}}$, s), 1595 (m), 1573 (m), 1544 (s), 1456 (m), 1420 (m), 1324 (m), 1197 (s), 1162 (s), 1091 (m), 997 (s), 985 (w), 967 (w), 894 (m), 872 (m), 761 (s), 631 (s). **¹H NMR** (CDCl₃, 250 MHz, 298 K, 16 scan) δ (ppm): 5.4 (s, 4H, 2-CH₂), 7.11-7.14 (d, 2H, $^3J = 8.0$ Hz, 2-CH), 7.66-7.73 (t, 1H, $^3J = 8.0$, CH), 7.96 (s, 2H, 2-CH), 8.05 (s, 2H, 2-CH), 9.83(s, 2H, 2-CHO). **¹³C NMR** (CDCl₃, 63 MHz, 298 K, 1024 scan) δ (ppm): 57.6, 121.6, 124.7, 133.6, 138.4, 141.0, 154.8, 183.9. **FD-MS** (70 eV, CHCl₃): $m/z = 295.1$ (100%). **Elemental analyses**,

found C 57.30, H 4.94, N 22.24%. $C_{15}H_{13}N_5O_2$ (295.30) \times H_2O required C 57.50, H 4.83, N 22.35%.

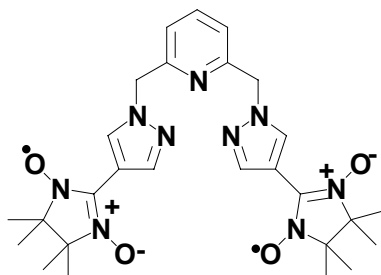
7.2.40. Synthesis of 2,6-bis[4-(1,3-dihydroxy-4,4,5,5-tetramethylimidazolidin-2-yl)pyrazolyl-methyl]-pyridine (40)



2,6-Bis(4-formylpyrazolylmethyl)pyridine **39** (590 mg, 2 mmol) and 2,3-bis(hydroxylamino)-2,3-dimethylbutane **6** (600 mg, 4 mmol) were charged into a small flask with methanol (40 mL), and stirred under argon for 48 h. The white solid product was filtered off, washed with water, ethanol and air dried to give 690 mg of 2,6-bis[4-(1,3-dihydroxy-4,4,5,5-tetramethylimidazolidin-2-yl)pyrazolyl-methyl]-pyridine **40** (yield 62 %) that was judged adequately pure for the oxidation step without further purification.

M.p. 148-149 °C (from water, it decomposes before melting by changing colour to deep red). **FT-IR** (KBr) ν/cm^{-1} = 3238 (broad, ν_{OH}) 2976 (s), 2929 (s), 1599 (m), 1575 (s), 1459 (s), 1421 (s), 1363 (s), 1311 (w), 1209 (w), 1174 (s), 1145 (s), 1093 (w), 1022 (m), 999 (s), 964 (w), 935 (w), 912 (m), 843 (m), 802 (m), 762 (s), 695 (w), 665 (w). **1H NMR** (DMSO- d_6 , 250 MHz, 298 K, 64 scan) δ (ppm): 0.65- 0.74 (dd, 24H, 4- CH_3), 4.34 (s, 2H, 2-CH), 5.07 (s, 4H, 2- CH_2), 6.50-6.53 (d, 2H, $J=8.0$ Hz, 2-CH), 7.15 (s, 2H, 2-CH), 7.30-7.34 (t, 1H, $J=7.0$ Hz, -CH), 7.37 (s, 2H, -CH), 7.53 (s, 4H, 4-OH), **^{13}C NMR** (DMSO- d_6 , 63 MHz, 298 K, 1024 scan) δ (ppm): 16.8, 23.4, 56.0, 65.4, 78.7, 82.9, 119.9, 122.6, 129.6, 138.6, 156.3. **Elemental analyses**, found C 58.04, H 7.66, N 22.36%. $C_{27}H_{41}N_9O_4$ (555.67) required C 58.36, H 7.44, N 22.69%.

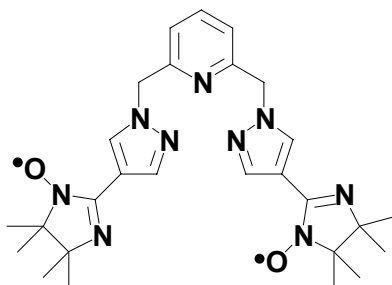
7.2.41. Synthesis of 2,6-bis[4-(1-oxyl-3-oxide-4,4,5,5-tetramethylimidazolin-2-yl)pyrazolylmethyl] pyridine (41)



The compound **40** (555 mg, 1 mmol) was oxidised with NaIO₄ (540 mg, 2.5 mmol) by working under phase transfer condition in water/chloroform mixture (1/1), during 60 min. The organic phase became deep blue. After collection and evaporation of the organic phase, the product was chromatographed on SiO₂ using a mixture of acetone/petroleum ether (low boiling point, 4/6) as eluents ($R_f = 0.28$) to give 355 mg of the radical product **41** as blue solid (yield 64%).

M.p. 169-170°C (from acetone). **FT-IR** (KBr) $\nu/\text{cm}^{-1} = 3145$ (w), 2977 (s), 2987 (m), 2931 (m), 1672 (w), 1598 (m), 1573 (w), 1541 (w), 1460 (s), 1427 (m), 1403 (m), 1365 (s, $\nu\text{N-O}$), 1317 (m), 1219 (w), 1196 (m), 1174 (m), 1138 (m), 1016 (m), 993 (d), 868 (m), 813 (w), 773 (m) 659 (m). **UV/Vis** (toluene) λ/nm (ϵ , $\text{M}^{-1} \times \text{cm}^{-1}$) 651 (2340), 596 (2155), 550 (1000), 352 (44060), 336 (18660). **FAB-MS** (NBA matrix) 550.3 $[\text{M}+\text{H}]^+$. **Elemental analyses**, found C 58.73, H 7.50, N 22.78%. C₂₇H₃₅N₉O₄ (549.63) required C 59.00, H 6.42, N 22.94%. **EPR** (293 K, 9.400086 GHz, toluene 10⁻⁴ M) 9 lines, $g_{\text{iso}} = 2.0065(1)$, $a_{\text{N}} = 0.374$ mT.

7.2.42. Synthesis of 2,6-bis[4-(1-oxyl-4,4,5,5-tetramethylimidazolin-2-yl)pyrazolylmethyl]pyridine (**42**)



The compound **41** (45 mg, 0.09 mmol) dissolved in CHCl₃ (15 mL) was oxidised with NaNO₂ (24.8 mg, 0.36 mmol) dissolved in HCl/H₂O mixture (5%, 5 mL) by working under phase transfer condition during ~ 2 min until the organic phase became deep red. After collection and evaporation of the solvent from the organic phase, the product was chromatographed on SiO₂ using a mixture of acetone/petroleum ether (low boiling point, 4/6) as eluents ($R_f = 0.42$) to give 35 mg of the radical product **42** as orange-red solid (yield 75 %).

M.p. 190 – 191°C (from acetone). **FT-IR** (KBr) $\nu/\text{cm}^{-1} = 3149$ (m), 2977 (s), 2929 (s), 1614 (s), 1575 (s), 1548 (w), 1527 (w), 1458 (s), 1425 (m), 1387 (s), 1375 (s), 1244 (s), 1213 (m), 1142 (s), 1116 (m), 1016 (m), 997 (m), 953 (m), 875 (m), 823 (m), 762 (m) 692 (s). **UV/Vis** (toluene), λ/nm (ϵ , $\text{M}^{-1} \times \text{cm}^{-1}$) 552 (156), 504 (1177), 470 (1990), 444 (1830), 414 (sh, 1245), 353 (80). **Elemental analyses**, found C 62.30, H 7.00, N 24.02%. C₂₇H₃₅N₉O₂ (517.63) required C 62.65, H 6.82, N 24.35%. **EPR** (293 K, 9.402404 GHz, toluene 10⁻⁴ M) 13 lines with strong temperature dependencies, $g_{\text{iso}} = 2.0060(1)$, $a_{\text{N}1}/2 = 0.450$ mT, $a_{\text{N}2}/2 = 0.220$ mT.

Acknowledgements

I would like to thank the following persons for the constant support within these years at MPIP:

The supervisors of the present work: P.D. Dr. Martin Baumgarten for giving the opportunity to pursue a PhD in the exciting field of Molecular Magnetism. I am indebted to him for his continuous support, the outstanding guidance, and the in-depth discussions. Without his driving passion on sharing his knowledge and curiosity with a beginner as I was, this work would never be completed. I will keep his teaching not only in my mind but also in my heart. I extend my sincere thanks to Prof. Dr. Klaus Müllen, for accepting me as a part of his prestigious group. I am grateful for his countless advices, suggestions and for carefully monitoring the progresses of this work. His tireless enthusiasm for Science is undoubtedly a source of inspiration for all of us.

I had the opportunity to meet wonderful and unique people here at MPIP, both from the scientific and personal point. Although some of them left the Institute, they will remain forever in my thoughts. Because "*verba volant scripta manent*" I would like to fully acknowledge them here. Dr. Anela Ivanova [University of Sofia] for her Quantum Mechanical Computational work for the high spin molecules, for being so patient in teaching the theoretical basis of QMC, but above all to be the best friend I ever had. Prof. Dr. A. Geies [University of Assiut, Egypt] for teaching me the beauty "hidden" in the heterocyclic chemistry, for his sense of humor combined with a great heart. Another special thank I wish to address to three extraordinary friends: Dr. Chris Clark, for all the precious discussions we had about scientific and non scientific issues, and for valuable advices on writing part of this work, Erhan Ergen, and Krasimir Vasilev (Prof. Knoll Group), for the joy, the optimism and sense of humor that are able to inspire. Thank to have been there when I needed most. I acknowledge all the people in the Prof. K. Müllen Group and particularly: the Group Leaders, Dr. Andrew Grimdale, Dr. Manfred Wagner, Dr. Andreas Herrmann, Dr. Markus Klapper, Dr. Hans Joachim Räder, personnel and most close colleagues, Lileta Gherghel, Dr. Gueorgui Mihov, Moustafa Abdulla, Al-Hussaini Aymann, Dr. W. Wu [Prof. Knoll Group], Roland Bauer, Zeljco Tomovic, Luke Oldridge, R. S. Prabakaran, N.R. Kundu, Dr. Josemon Jacob, A. K. Mishra, Dr. P. Sonar and Dr. J. Sakamoto (ETHZ, Switzerland), Dr. Ingo Lieberwirth, Dr. Volker Enkelmann for solving the crystal structures of the biradicals presented in this work and Dr. R. Kita (Prof. Wegner Group), Yutta Schenee for all the help in the laboratory, and last but not least the wonderful people of the ChemLager Marcus Thull and Willi Lutz.

C.V.
Giorgio Zoppellaro

Personal informations:

Marital status: single.

Italian citizenship. Born on 22.12.1967.

e-mail: zoppella@mpip-mainz.mpg.de, giorgio_zoppellaro@yahoo.com,
giorgio.zoppellaro@int.fzk.de

Academic Records:

Laurea in Industrial Chemistry from The University of the Studies of Milan, Italy, Faculty of Industrial Chemistry on date 31/10/1997 (96 months). Research work on enzyme biomimics. Thesis title (work in Italian): “Uno Studio sui Complessi Binucleari e Trinucleari derivati da un Legante Octadentato Misto contenente donatori Azotati Aminici e Benzimidazolici”, pp. 1 – 131. Final result expressed in 110th base was 101.

Research assistant at the CNR (National Research Council), Department of Analytical Chemistry, University of the Studies of Milan, Italy, till February 1998 (3 months). Research work: “Spectroscopic characterization of Ascorbate Oxidase”.

Master in Pharmaceutical Sciences from The Graduate School of Natural Sciences and Technology, Kanazawa University, Japan on 22/03/2000 (24 months). Thesis title (work in English): “The Tetraelectronic Reduction of Dioxygen into Water by Laccase”, pp. 1 - 82. Final Result expressed on 30th base was 30. This work is available through the Library Collection of the Max Planck Society; Location MPIP Polymer Research, Mainz, Call number Dr-00, 6084-10.

Research assistant at The Royal Veterinary and Agricultural University (KVL), Department of Mathematics and Physics, Copenhagen, Denmark till December 2000. Research work: “Perturbed Angular Correlation Spectroscopy (PAC) applied on mononuclear copper proteins: electron transfer processes mediated by Plastocyanin and Mavicyanin” (3 months).

Research assistant at the University of Oslo, Department of Biochemistry, till 15th November 2001 in the laboratory of K. K. Andersson (8 months).

Ph.D. (Phys-Org. Chemistry) at the Max Planck Institute for Polymer Research, Mainz (Germany) obtained on 19th November 2004, with a work in the field of Organic-based Molecular Magnets. (36 months).

Thesis title (work in English): “A Study of Nitronyl and Imino Nitroxide Radicals Attached to Heterocyclic Cores. High Spin Building Blocks Towards Organic Magnets” pp. 1- 161. Final

result : Magna Cum Laude. This work is available through the Library Collection of the Max Planck Society; Location MPIP Polymer Research, Mainz, Call number Dr-20/4,8068.

Awards:

Year 1995- Honorary Diploma from the Ministry of the Italian Defence (Military Service).

Year 1998 - Monbusho prize from the Ministry of Education, Sport and Culture of Japan.

Year 2000- Monbusho prize from the Ministry of Education, Sport and Culture of Japan (3 months research grant).

Year 2003 - Young Scientist Award, from the European Material Research Society.

Others:

1991-1993

Teaching postion for the courses of Inorganic and Physical Chemistry at the Higher School Institute IPSIA, 21013 Gallarate (Varese) and for Mathematics and Physics at the Institute Cavallotti, 21013 Gallarate (Varese) Italy.

1994-1995

Military Service in the Italian Army at 7° RGT "Cuneo", Spaccamela Street N.128, Udine, Italy.

1999

Italian language's Teacher at the Berlitz School Centre. Address: Berlitz Language Centre, 2-35, Takaoka-machi, Kanazawa City, 920-0864 Japan.

Teaching-assistant in the laboratory of Analytical Chemistry for undergraduate students, Kanazawa University, Division of Life Sciences, Kanazawa, Japan.

2003

Teaching-assistant (two semesters) in the laboratory of Organic and Analytical Chemistry for Biologists (72 students) at the University of Mainz.

General Skills

EPR (Models Varian, Bruker, Jeol) X and Q-band (9-33GHz) from cryogenic to room temperature with Oxford System;

SQUID (Quantum Design, MPMS-5);

CD-MCD (Jasco J 500C);

UV-Vis/stopped-flow (Otsuka-Denshi RA, HP, Jasco) under aerobic/anaerobic conditions;

FT-IR;

Atomic Absorption. NMR (Bruker AMX, 250 MHz, 300 MHz);

FD-MS, MALDI-TOF (the later applied especially for the analysis of biomolecules);

Electrochemical apparatus;

Languages

English, Italian.

International Publications and Contributions

1. One Low Temperature EPR and Mössbauer Spectroscopic analysis of two cytochromes with His-Met axial coordination exhibiting HALS signals.
Zoppellaro G., Teschner T., Benda R., Harbitz E., Karlsen S., Schünemann V., Arciero D. M., Ciurli S., Trautwein A.X., Hooper A. B., Andersson K.K. Submitted 2005.
2. One step synthesis of symmetrically substituted 4,4"-2,6-bis(pyrazol-1-yl)pyridine systems.
Zoppellaro G. and Baumgarten M., *Eur. J. Org. Chem.* 14 (2005), 2888.
3. 2,6-Bis(pyrazolylpyridine) functionalised with two nitronylnitroxide and iminonitroxide radicals.
Zoppellaro G., Geies A., Enkelmann V., Baumgarten M., *Eur. J. Org. Chem.* 11 (2004), 2367.
4. Models for biological trinuclear copper clusters. Characterization and enantioselective catalytic oxidation of catechols by the copper (II) complexes of a chiral ligand derived from (S)-(-)-1,1'-binaphthyl-2,2'-diamine.
Mimmi M.C., Gullotti M., Santagostini L., Battaini G., Monzani E., Pagliarin R., **Zoppellaro G.**, Casella L., *Dalton Trans.* (2004), 2192.
5. A multifunctional high-spin biradical pyrazolylbipyridine-bisnitronylnitroxide.
Zoppellaro G., Volker Enkelmann V., Geies A. and Baumgarten M., *Org. Letters*, 6 (2004), 4929.
6. The reversible change in the redox state of type I Cu in *Myrothecium verrucaria* bilirubin oxidase depending on pH
Zoppellaro G., Sakurai N, Kataoka K, Takeshi Sakurai
BIOSCIENCE BIOTECHNOLOGY AND BIOCHEMISTRY 68 (2004)1998.
7. Synthesis, magnetic properties and theoretical calculations of novel nitronylnitroxide and iminonitroxide diradicals grafted on terpyridine moiety.
Zoppellaro G., Ivanova A., Enkelmann V., Geies A. and Baumgarten M., *Polyhedron*, 22 (2003), 2099.
8. Spectroscopical studies of cytochrome cs, some exhibiting HALS EPR signals.
Harbitz E., **Zoppellaro G.**, Teschner T, Fauchald S, Katterle B, Schunemann V, Trautwein AX, Arciero D, Hooper A, Ciurli S, Andersson KK. *J. Inorg. Biochem.*, 86 (2001), 249.
9. Kinetic studies on the reaction of the fully reduced laccase with dioxygen.
Zoppellaro G., Huang HW., Sakurai T., *Inorg. Reac. Mech.*, 2 (2000), 79.
10. Spectroscopic and kinetic studies on the oxygen-centered radical formed during the four-electron reduction process of dioxygen by *Rhus-vernificera* laccase.
Huang HW., **Zoppellaro G.**, Sakurai T., *J. Biol. Chem.* 274 (1999), 32718.
11. Four electron reduction of dioxygen by *Rhus vernificera* laccase.
Huang HW., **Zoppellaro G.**, Sakurai T. *J. Inorg. Biochem.* 74 (1999), 169.

-
12. A novel mixed valence form of dioxygen by *Rhus-vernificera* laccase and its reaction with dioxygen to give a peroxide intermediate bound to the trinuclear center.
Zoppellaro G., Sakurai T., Huang HW., *J. Biochem.*, 129 (2001), 949.
 13. Synthetic models for biological trinuclear copper clusters. Trinuclear and binuclear complexes derived from an octadentate tetraamine-tetrabenzimidazole ligand.
Monzani E., Casella L., **Zoppellaro G.** et al. *Inorg. Chim. Acta*, 282 (1998), 180.
 14. The 48th Symposium on Coordination Chemistry of Japan, Kouchi 1998, Japan (Oral contribution) Magnetic Properties in the Intermediate Detected in the Four-electron Reduction Process of Dioxygen in Laccase.
 15. ICBIC IX Poster Section, Minneapolis 1999, USA (Poster section). The Four-electron Reduction Process of Dioxygen in Multicopper Oxidases.
 16. The 26th International Conference on Solution Chemistry, Section S6, Fukuoka 1999, Japan (Oral contribution). The Four-electron Reduction Process of Dioxygen in Laccase.
 17. The 49th Symposium on Coordination Chemistry of Japan, Sapporo 1999, Japan (Oral contribution). Dioxygen Reduction by Multicopper-Oxidases and their Derivatives and Metastabilization of Activated Oxygen.
 18. The Annual Meeting of the Iron-Oxygen protein Network, Les Arcs, 2001 France. Copper proteins and copper enzymes (Oral contribution).
 19. The International Conference of Biological Inorganic Chemistry, ICBIC X 2001 Florence, Italy (Poster session).
 20. The Fπ5 International Conference, Functional π Electron System, Ulm, 2002, Germany (Poster session).
 21. The EUROBIC VI, 29 July-03 August, Copenhagen, Denmark (Poster session).
 22. The International Conference on Molecule Based Magnets, ICMM 2002, Valencia, Spain (Poster session and oral contribution).
 23. E-MRS Spring Meeting, Strasbourg, France, 2003 (Poster Session).
 24. The International Conference on Molecule Based Magnets, ICMM 2004, Japan (Poster Session).